RESEARCH INTO A NEW FAULT GENERATED NOISE DISTRIBUTION SYSTEM FAULT LOCATOR

BY

MEHDI EL-HAMI

Thesis submitted to City University for the Degree of Doctor of philosophy

June 1990

Electrical Power and Energy Systems
Research Centre
Department of Electrical, Electronic and Information Engineering

City University
Northampton Square
London EC1V 0HB

This thesis is dedicated to my mother

and my beloved late father.

LIST OF CONTENTS

SYNOPSIS

The problems associated with detection and clearing of faults on overhead distribution systems, particularly in interconnected networks, are still of great concern. Most utilities employ reclosing relays with circuit breakers to handle transient faults. Permanent faults, however, require a location of the faulty line section, isolation and possibly rescheduling of the network, before normal power delivery may be resumed.

This work is mainly concerned with the design of a new directional fault locator, suitable for use on overhead power distribution systems operating typically at 11kV. It is possible to design a protective scheme based upon a variety of operating principles, but the operating principle of the new equipment and the scheme developed are based upon detection of fault generated noise. In the past, schemes based upon this operating principle have relied on use of a communication link to locate a fault. However, the new scheme developed in this work does not require the presence of such a communication link.

The electronics that interface with the new equipment enable it to determine the direction of a fault, i.e, distinguish between upstream and downstream faults. The means by which directional fault finding is achieved are fully discussed. Moreover, with further signal processing of fault generated signals, the usefulness of the new scheme has been extended and, in addition to being directional, it is also capable of locating the faulty line section of an overhead distribution system, i.e, distinguish between in-zone and out-of-zone faults.

The effect of fault resistance, fault inception angle, fault position, source capacity and the effect of type of fault on the performance of the new equipment have been studied and relevant simulation results are presented. Finally the behaviour of a number of new directional fault locators on a radial overhead system has been evaluated using the Electromagnetic Transients Program, EMTP.

ACKNOWLEDGEMENTS

The author wishes to express his sincere thanks to Professor A. T. Johns, D.Sc., Ph.D., B.Sc., C.Eng., FIEE, SMIEEE, FRSA, for his guidance, encouragement and his invaluable advice throughout the course of this work.

He would like to thank Mr D. J. Daruvala and Dr L. L. Lai for very useful technical discussions and their contributions towards this work.

Thanks are also due to my wife, whose patience, encouragement and support inspires me in every aspect of my life.

He is grateful to City University, London, for provision of facilities and British Technology Group (BTG), London, for supporting this work.

He would like to thank everyone at the Electrical Power and Energy Systems Research Centre, for their support and friendship. Especial thanks to Mr S. H. Lewis and Mr M. Gasparro for their extremely helpful contributions to the preparation of this thesis.

COPYRIGHT DECLARATION

I grant powers of discretion to the University librarian to allow this thesis, (RESEARCH INTO A NEW FAULT GENERATED NOISE DISTRIBUTION SYSTEM FAULT LOCATOR), to be copied in whole or in part without further reference to me. This covers only single copies made for study purposes, subject to normal conditions of acknowledgement.

June, 1990

LIST OF PRINCIPAL SYMBOLS

$\bar{V}$ = Voltage transform

Z = Series impedance matrix per unit length

Y = Shunt admittance matrix per unit length

$\bar{V}_i$ = Incident voltage transform

$\bar{V}_r$ = Reflected voltage transform

Q = Voltage eigenvector matrix

Γ = Propagation constant matrix

Φ = $Q.\Gamma.Q^{-1}$

$\bar{V}_S$ = Sending end voltage transform

$\bar{V}_R$ = Receiving end voltage transform

$\bar{I}_S$ = Sending end current transform

$\bar{I}_R$ = Receiving end current transform

A1,B1,C1,D1 = Matrices defining line section up to point of fault

A2,B2,C2,D2 = Matrices defining line section beyond point of fault

Af,Bf,Cf,Df = Matrices defining fault discontinuity

A_S, B_S, C_S, D_S = Matrices defining the line between sending and receiving ends before the fault

$\bar{V}_{ff}, \bar{E}_{ff}$ = Transform of superimposed voltages at point of fault

$\bar{V}_{fs}$ = Transform of prefault voltages at point of fault

$\bar{I}_{fS}$, $\bar{I}_{fR}$ = Transform of currents at point of fault

$\bar{E}_{fS}$, $\bar{E}_{fR}$ = Transform of voltages at point of fault

$\bar{V}_{SS}$ = Transform of prefault voltages at sending end of line

$\bar{I}_{SS}$ = Transform of prefault currents at sending end of line

$\bar{V}_{RS}$ = Transform of prefault voltages at receiving end of line

$\bar{I}_{RS}$ = Transform of prefault currents at receiving end of line

$\bar{V}_{Rf}$ = Transform of superimposed voltage at receiving end of line

$\bar{I}_{Rf}$ = Transform of superimposed current at receiving end of line

$\bar{V}_{Sf}$ = Transform of superimposed voltage at sending end of line

$\bar{I}_{Sf}$ = Transform of superimposed current at sending end of line

w = Angular frequency

R_f = Fault resistance matrix

Z_{SS} = Sending end source impedance matrix

$\bar{I}_{fSf}$, $\bar{I}_{fRf}$ = Transform of superimposed currents at point of fault

a,b,c = Phases a, b and c

f(w) = Fourier transform of f(t)

α = Frequency shift constant

$f(w - j\alpha)$ = Modified Fourier transform

f = Truncation frequency

f_c = Centre frequency

THL = Threshold level

X = Ratio of the effective impedance of the line trap circuit, ZT, to the surge impedance of the line Ro at centre frequency f_c

Ro = Surge impedance of the line

U, [U] = Unit matrix

CHAPTER (1)

INTRODUCTION AND LITERATURE SURVEY

1.1 LITERATURE SURVEY

There is an increasing demand for determination of faults in power transmission and distribution systems. Distribution line fault clearing is commonly performed by an overcurrent sensing device such as an overcurrent relay/circuit breaker combination, a recloser or a fuse. While these devices must interrupt fault currents they must also carry normal and emergency load currents as well as transient overcurrents caused by inrush or load pick-up surges. These operating requirements impose a compromise in choosing the level of current at which a device will operate.

The compromise involves a tradeoff between the desire to clear all low grade faults and the desire to minimise the number of occurrences of unnecessary customer outages due to tripping load on normal switching operations. The current which flows during a fault depends upon a number of variables, one of which is the impedance of the fault itself. In some instances, a faulted distribution primary may exhibit a very low fault current. Such faults are usually called high impedance faults and a solid return path for current is not clearly established in the case of such faults.

An example of such a fault is the case of an energised conductor coming into close proximity with an object at a much lower potential than itself, without making solid contact with that object. The high potential difference that exists between them causes the air gap to break down and arcing occurs between the conductor and the object. The fault current is limited by the arc resistance combined with the ground resistance.

In some cases, the action of the arcing may cause a solid fault path to be eventually established and the fault may be cleared by overcurrent protection. In many instances, fault resistance remains high and the arcing fault persists indefinitely. Common arcing faults include a broken conductor which has fallen on earth, or a conductor in contact with a grounded object such as a tree or pole crossarm. There is a very strong desire in the utility industry to have the ability to detect such faults.

It is not easy to protect overhead distribution systems against such faults using existing overcurrent protection devices and schemes. Figure (1.1), provides an indication of the approximate coverage for different types of fault detection devices on a typical distribution feeder, [15]. The diagram shows the range of fault currents which could be observed for different faults on

this feeder, indicating which devices may be expected to detect a fault with a given fault current. The coverage regions are marked for the existing electromechanical substation overcurrent relay (marked "SUB. RELAY") and the existing downstream protection on the feeder (fuses and line reclosers). The region marked "NEW" represents the approximate coverage region of the substation-based detecting devices which are currently being researched. The designation of the region of very low fault currents with a question mark means that, at present no commercial or developmental equipment is available which can reliably and securely detect faults with only a few amperes of current under all conditions.

The nature of high impedance faults has been intensively investigated and considerable interest in solving the problem associated with such faults has resulted in the development of certain schemes and equipments for the detection of these faults.

Balser [1], suggested a technique that is based on statistical hypothesis tests made on normalised sequence currents at the fundamental, third harmonic and fifth harmonic frequencies. Based on these tests the technique would identify the presence of a high impedance fault due to separated conductor incidents when levels of interrupted load current are roughly 5 percent or greater, with a 90 percent probability of detection. Arcing faults

due to downed conductors were identified for arcing faults of roughly 10 amperes or greater, again with a 90 percent detection probability. The algorithm inhibits identification of a high impedance fault if a high current fault has been detected. The level of detection can be adjusted to avoid false alarms due to significant normal load changes.

Aucoin [2], has described the development of a microprocessor based feeder protection and monitoring system (FPMS), at Texas A&M university. The feeder protection and monitoring system indicates an overcurrent relay to provide overcurrent protection for distribution feeders and it includes an arcing fault detector which identifies some low current faults which are not cleared by overcurrent protection. A prototype ratio ground relay was developed at PP&L [3]. The relay has an operating element responsive to zero sequence current and a restraining element responsive to load level. This results in a pick-up value that varies with load level which allows the detection of many broken conductors and high impedance faults.

Phadke [4], has suggested a microprocessor based digital relaying scheme in which changes in the positive, negative and zero sequence components of the fundamental power frequency are monitored continuously in real time. Changes in the ratio of the symmetrical components are

used to detect presence of a high impedance fault.

Graham [5], has suggested monitoring the distribution feeder input impedance at high frequencies in the range of 50kHz to 100kHz. Tests on this impedance monitoring technique have shown that, broken conductor faults offer large changes in input impedance and should be the easiest to detect. The system is applicable to high transformer density lines as well as to residential area lines. The entire electronic system can be fabricated onto a single integrated circuit for minimal cost and ease of serviceability.

Russell [6], has examined the high impedance fault problem from the perspective of system protection. He also presented a fault detection theory which utilised a fault-generated increase in the range of 2kHz to 10kHz component of feeder current for fault detection. Aucoin and Russell [7], suggested that, arcing causes burst noise signals which manifest a wide band of frequencies which can also be identified at frequencies near 60Hz. Analysis of data from staged fault tests indicated that frequencies sufficiently below 60Hz or midway between harmonics provided improved detection of low grade faults. In this paper it was also suggested that, while arcing faults produced only subtle changes in the fundamental current, they caused substantial amplitude changes in off-harmonic frequency components.

A statistical algorithm was developed by power technology, Inc [8], for the detection of high impedance faults based on changes in sequence current unbalance. A fault detector was also designed by researchers at Texas A&M university [9] for the detection of those faults which include ground and which include arc. This detector identifies the burst noise caused by arcing faults at high frequency, specifically 2kHz to 10kHz components. This arcing fault detector operates on an increase in the wide band frequency components of current generated by arc burst noise.

Digital fault investigations on six PP&L 12kV distribution feeder have led to the development of a prototype ratio ground relay to theoretically provide better detection of broken conductors faults, reference [10]. The ratio ground relay concept as implemented in the prototype relay, relies on tripping when the ratio of $3I_0$, the zero sequence current, to I_1, positive sequence current exceeds a certain pre-set level. This concept is implemented using an induction disc type relay with two windings.

Russell [11], further investigated the significance of the low frequency components as indicators of the presence of faults on distribution primary lines. Two frequencies, 180Hz and 210Hz were selected for study due

to strong magnitude variations associated with arcing faults. A hierarchical algorithm with adaptive characteristics is presented along with the performance results when applied at these low frequencies. The algorithm can be implemented inexpensively in a microprocessor based architecture and can be integrated with other detection schemes for more secure fault identification.

Don Russell [12], has described how signal processing hardware and software can be used to significantly improve the detection of certain power system faults using computer relays. By using a knowledge based system, it is possible to dynamically adjust protection weighting factors and improve protection performance within the relay itself. Additional advantages of the proposed design include the ability to interface with higher level protection systems, the ability to provide detailed fault and feeder evaluation information, and the ability to implement sophisticated protection routines without hardware changes.

The behaviour of several low frequency spectra between 30Hz and 360Hz were investigated for arcing faults and normal switching events, reference [13]. It was observed that the in-between harmonic frequencies can be used to distinguish arcing faults from capacitor bank switching operations. There was a marked increase in the

magnitude of the harmonic frequencies during arcing fault conditions. However, they are not immune to switching and capacitor bank operations. It was also found that the magnitude of in-between harmonics depends on burst duration and soil condition. The arcing bursts were mostly of short duration separated by short intervals of inactivity on wet soil, of medium duration separated by similar intervals of inactivity on dry soil and of long duration separated by long intervals of inactivity on sandy soil.

Using polymeric materials technology, a sensor has been built for the measurement of voltage and current on system voltages up to 36kV [14]. The sensor is constructed using polymeric materials applied to an aluminium tube, the whole forming a concentric cylinder capacitor with suitable terminations. The electronic circuits built to interface with this device can provide directional fault finding and phase angle information as well as economic voltage and current monitoring.

It is clearly seen that, a number of promising detection schemes and techniques have been developed and tested over the years and although all these schemes offer a potential solution to the problem of detecting high impedance faults on power distribution feeders, none to date has proven to be the ideal solution.

1.2 THE MAIN OBJECTIVES OF THE THESIS

The increasing complexity of the rural distribution networks demands higher performance of protection and better control equipment. As already explained, it is difficult to detect the full range of possible faults on overhead power distribution systems using the existing overcurrent protection devices. Moreover, most faults require the location of the faulty line section, isolation and possibly the rescheduling of the network before normal power delivery may be resumed. Non-directional fault indicators are available both for short circuit and earth fault current detection [14]. However, if a network is interconnected, then a non-directional detector becomes less useful and often a directional fault locator is required to locate the faulty line section. Therefore the main objective of this work is to investigate and design a new directional fault locator scheme for overhead power distribution feeders.

It is possible to design a protective scheme based upon a variety of operating principles, but the scheme used here in this work is based upon the detection of the fault induced high frequency components introduced into the line by a fault. In the past, all schemes based upon this operating principle have relied upon the use of a communication link in order to pin-point the location of a fault. In the case of interconnected overhead distribution

systems, the use of such a communication link for purposes of fault detection and location would be highly uneconomical.

The main advantage of the scheme developed in this work over the other schemes used so far is that it does not require the presence of a communication link for fault detection and location. The new equipment is particularly, but not exclusively, useful for overhead distribution networks operating at typically 11kV.

1.3 CONSTRUCTION OF THE THESIS

This thesis consists of nine chapters. In this section a brief synopsis of each chapter is provided.

1.3.1 CHAPTER (1) SYNOPSIS

This chapter consists of a literature survey of previous works plus the main introduction to this thesis. It also includes a discussion on the construction of the thesis.

1.3.2 CHAPTER (2) SYNOPSIS

The development of the new locator, which has been the main objective of this work, from its first and simplest form to its final arrangement or design is

discussed in Chapter (2). The representation of the locator using matrix notation plus the degree of attenuation provided by the equipment in the case of a fault situation are also covered in this chapter.

1.3.3 CHAPTER (3) SYNOPSIS

In this chapter, the operating principle of the new scheme and the new locator developed have been explained. The means by which the new equipment can distinguish between in-zone and out-of-zone faults as well as the direction of a fault on a given overhead power distribution system are discussed.

1.3.4 CHAPTER (4) SYNOPSIS

This chapter covers the digital computer simulation of the system network used for the design of the new directional fault locator. Simulation of the locator itself is also included. Finally the details of other interface programs used as the second part of the simulation, which is concerned with the signal processing of voltages and currents of interest, are provided.

1.3.5 CHAPTER (5) SYNOPSIS

In this chapter, simulation results to illustrate the performance of the proposed arrangement for directional

fault finding are presented. Also sensitivity analysis including the effect of fault positions, fault inception angle, fault resistance, type of fault and the effect of source capacities on the directionality of the locator are presented. Finally in Chapter (5), the maximisation of the discrimination margin which is used to determine the direction of a fault is discussed.

1.3.6 CHAPTER (6) SYNOPSIS

Further simulation results and sensitivity analysis to illustrate the capability of the locator to distinguish between in-zone and out-of-zone faults are provided in this chapter. The sensitivity analysis carried out includes effects of the type of fault, fault resistance, fault inception angle and the effect of source capacity.

1.3.7 CHAPTER (7) SYNOPSIS

The Electromagnetic Transients Program (EMTP), was used to simulate a more realistic radial overhead distribution system. The system included five such locators and their behaviour in the case of a fault was illustrated by using further simulation results.

1.3.8 CHAPTER (8) SYNOPSIS

The results obtained are summarised in this chapter

and their significance is critically evaluated. Some proposals for future work are discussed.

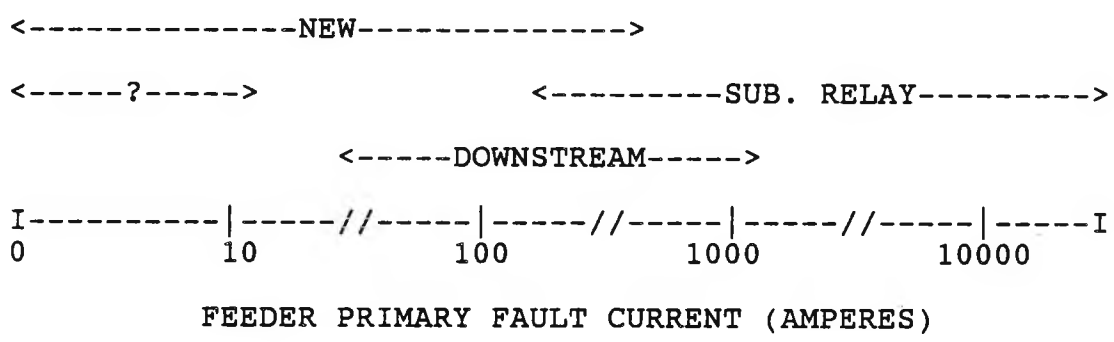

Fig (1.1), COVERAGE REGIONS OF FEEDER FAULT DETECTORS

CHAPTER (2)

DEVELOPMENT OF A NEW DIRECTIONAL FAULT LOCATOR

2.1 INTRODUCTION

As previously described in Chapter (1), the problems associated with detection and clearing of faults on overhead distribution feeders are still of great concern. Utilities and equipment manufacturers have been investigating and developing automated systems for power distribution for the last 10 years. A fully developed system would reduce the amount of primary plant needed, and would also cut down operating costs. Immediate detection and isolation of faulted distribution feeders would reduce the time required for fault location and restoration of supplies. Studies in the US and Japan have shown that substantial savings are possible [17,18].

In this chapter, the development of a new equipment, (a new directional fault locator) from its first and simplest form to its final arrangement for use on overhead distribution networks operating typically at 11kV is discussed. The main feature of this new directional fault locator is that, it would not only detect the high frequency components travelling on the line due to a fault, but would also attenuate them in their passage through it.

The representation of the locator on a three phase system for simulation purposes, using matrix notation is also explained in this chapter. Finally the degree of the attenuation provided by this locator in the case of a fault situation is discussed.

2.2 DESIGN OF THE NEW LOCATOR

Considering the basic performance expected from this new locator, as briefly mentioned in the introduction, it is clear that, the development of this equipment basically hinges upon design and combination of two different circuit configurations as outlined below:

(i) A circuit to attenuate the high frequency components injected into the line due to a fault, i.e, a line trap circuit.

(ii) A circuit to perform the observation of these h.f components, i.e, a stack tuner.

When a fault occurs, it causes h.f components to be introduced into the line which propagate from the fault point along the line in both directions towards the ends of the line. Therefore it is decided that the attenuation is to be performed by inserting a circuit of some form in series with the line itself. And the observation of these signals can be achieved using another circuit connected

between the line and the ground. It should be noted that, these components involve frequencies below and well above the power frequency, therefore the circuits to attenuate and observe these frequency components must be in the form of tuned circuits.

Therefore Figure (2.1) shows the simplest arrangement possible for the locator . In Figure (2.1), L1 and C1 represent a so called line trap circuit, LP1, Cs and LP2, Cs will be referred to as stack tuners. It should be appreciated that, for signal discrimination purposes (described in Chapter 3), two of such series tuned circuits or stack tuners are needed, one on each side of the parallel tuned circuit or the line trap circuit.

Considering the basic task of the line trap circuit of the locator, the introduction of deliberate damping into it became essential. By this means the impedance of the line trap circuit could be set to a relatively high value within a narrow band of frequencies around the centre frequency f_c to which the circuit was tuned. This in turn would provide a high degree of attenuation. The additional damping could have been introduced in the form of series resistance in the inductance or shunt resistance. The former was impracticable because the 50Hz losses would be considerably increased and therefore Shunt damping was used. In practice, however, it is advantageous to add another series resonant circuit tuned to the same

centre frequency f_c as well as the damping resistance as shown in Figure (2.2). With this arrangement the impedance of the line trap circuit is more uniform over the bandwidth of interest. The value of the inductor L1 is set to a very low value (typically 0.1mH) so that the line trap circuit of Figure (2.2) operates virtually as a short circuit at very low frequencies (power-frequency) and does not affect or influence the 50Hz steady-state performance of the system in which the locator is included. Figure (2.3) shows the variation of the impedance of the line trap circuit of Figure (2.2) against frequency from 0 to 140 kHz. It is clearly evident from Figure (2.3) that, the impedance of the line trap circuit at 50Hz is almost zero due to the low value of inductor L1 and reaches a maximum value equal to R1 at the centre frequency f_c to which the line trap circuit of the locator is tuned.

Since the operating principle of this new digital fault locator is based upon observing high frequency components (travelling-wave signals), it is necessary to introduce an additional damping resistor. This is simply to damp down the unwanted oscillation due to the elements L1 and C1 being connected in parallel in the line trap circuit. This is basically due to the fact that, this unwanted oscillation would influence the actual high frequency components on the line arising from a fault. The introduction of this damping resistor in series with the inductor L1 would, as previously described, increase the

50Hz losses on the line, therefore it was placed in series with the capacitor C1 in the line trap circuit. Finally Rc, placed in series with L1, represents the resistance of the inductor L1 at high frequencies due to the skin effect; at very high frequencies axial current flow in a solid cylindrical conductor is essentially concentrated in a thin layer or skin near the surface. Appendix 2A shows that the expression for resistance of the inductor L1 at high frequencies is as given below [27].

$$Rc = R_{h.f} = \frac{\left[\frac{\pi . f . \mu}{\tau}\right]^{\frac{1}{2}}}{2 . \pi . r_o} \text{ ohms/meter} \qquad (2.1)$$

where f is frequency, μ is permeability, τ is conductivity and r_o is the radius of the wire.

The final arrangement of the line trap circuit is therefore, as shown in Figure (2.4). The total impedance of this circuit at centre frequency f_c is equal to ZT as given below.

$$ZT(jw) = \frac{Z1(jw) \; . \; Z2(jw) \; . \; Z3(jw)}{[Z1(jw) \; . \; Z2(jw)] + [Z1(jw) + Z2(jw)] \; . \; Z3(jw)} \; \Omega \qquad (2.2)$$

Where

$$Z1(jw) = Rc + jwL1 \; \Omega \qquad (2.3)$$

$$Z2(jw) = Rd + 1/jwC1\ \Omega \qquad (2.4)$$

$$Z3(jw) = R1 + jwL2 + 1/jwC2\ \Omega \qquad (2.5)$$

where,

$$w = 2\pi f_c$$

and

$$f_c = 90.0\ kHz$$

Figure (2.5) shows the variation of the impedance of the line trap circuit of Figure (2.4) against frequency from 0 to 140 kHz. The bandwidth and the cut-off frequencies for the line trap circuit used are as given below.

$$(\Theta f)_{Trap} = (f_2 - f_1)_{Trap} = 5000\ Hz \qquad (2.6)$$

where,

f_2 = Upper cut-off frequency = 92.5 kHz

and

f_1 = Lower cut-off frequency = 87.5 kHz

Appendix 2B outlines the definition of the bandwidth and the cut-off frequencies used.

The stack tuners shown in Figure (2.1) are used to observe travelling-wave signals or high frequency components on the line and provide us with outputs which can be used for further processing in fault detection and

location. It should be appreciated that at most distribution system voltages it is possible to form the stack tuning capacitors, marked Cs in Figure (2.1), using a directly connected capacitor or as a concentric capacitor separated from the h.v conductors by a suitable insulating dielectric, e.g, polymeric insulating material [14].

The inductors LP1 and LP2 are physically added to the circuit for tuning purposes. The stack tuners shown in Figure (2.1), each would have a zero impedance at the centre frequency f_c to which they are tuned. Since this new locator has been designed to be placed between each phase of a three phase system and the ground, a zero impedance by either of the stack tuners employed on each side of the locator would mean, in the case of a fault, a short circuit between the faulty phase and the earth at the tuned frequency at a point where a locator is placed. Consequently, at the centre frequency f_c, this would short to ground all the high frequency components, travelling on the line and hence completely destroy the operating principle of the locator for discrimination purposes. For this reason a linear resistor was added in series with each stack tuner as shown in Figure (2.6). This in turn would allow us to achieve the following:

(i) Match the effective impedance of each stack tuner to the characteristic impedance of the line at

the centre frequency f_c.

(ii) Allow us to set the value of the effective impedance of each stack tuner in such a way that the locator would correctly terminate the line when there is a fault.

With this new arrangement each stack tuner can have a very high impedance, so as not to let any current flow through it at low frequencies (power-frequency) and an effective impedance equal to the value of each resistor at the centre frequency f_c to which each is tuned. The variation of the impedance of each stack tuner against frequency from 0 to 140 kHz is shown in Figure (2.7).

For production of the best possible discrimination between the signals observed at both ends of the locator, the high frequency components that pass through the line trap circuit of the locator should be attenuated at the same centre frequency as that of the stack tuners. Therefore for the locator network the relationship given below exists.

$$Cs.LP1 = Cs.LP2 = C1.L1 = C2.L2 \qquad (2.7)$$

Furthermore, for more accurate results the bandwidth of the stack tuners must be equal to each other as given below.

$$(\theta f)_{\text{Stack tuners}} = (f_2 - f_1)_{S1} = (f_2 - f_1)_{S2}$$

$$= 5000 \text{ Hz} \qquad (2.8)$$

where S1 and S2 correspond to stack tuners 1 and 2 respectively,

f_2 = Upper cut-off frequency = 92.5 kHz

and

f_1 = Lower cut-off frequency = 87.5 kHz

The bandwidth and the cut-off frequencies are defined in Appendix 2B.

As previously mentioned, the effective impedance of each stack tuner at centre frequency f_c to which they are tuned, should match the surge impedance of the line. Therefore the value of the resistors RP1 and RP2 in stack tuners S1 and S2 respectively were chosen to be 500.0 Ω each. That is to say,

$$RP1 = RP2 = Ro$$

$$= \text{Surge impedance of the line.}$$

$$= 500.0\ \Omega \qquad (2.9)$$

Knowing the values for RP1 and RP2 plus the centre frequency and the bandwidth of interest, the values for inductors LP1 and LP2 and capacitors Cs were calculated using the fundamental equations given below.

$$LP1 = LP2 = \frac{RP1}{2.\pi.\theta f} \qquad (2.10)$$

and

$$Cs = \frac{1}{(\ 2\pi f_c\ )^2 .\ LP1} \qquad (2.11)$$

Further simulations showed that, for the largest discrimination margin between the two sides of the locator, the values of the two damping resistors R1 and Rd in the line trap circuit should be equal to 10000.0 Ω and 2.0 Ω respectively. Finally, knowing the values for R1, f_c, L1 and the bandwidth of interest, the rest of the elements in the line trap circuit were evaluated using fundamental equations for series and parallel L-C-R resonant networks.

The list of parameter values of the locator is provided in Appendix 2C.

2.3 REPRESENTATION OF THE LOCATOR

The representation of the locator on the line for the purposes of fault calculation was next considered and two-port transfer matrices were used. The voltages and currents, V1, I1, V2 and I2, on both sides of the locator, as illustrated in Figure (2.8), are related to each other by the equation given below.

$$\begin{bmatrix} V1 \\ I1 \end{bmatrix} = \begin{bmatrix} A & B \\ C & D \end{bmatrix} \begin{bmatrix} V2 \\ I2 \end{bmatrix} \qquad (2.12)$$

$$X = Y \cdot Z$$

where the elements A, B, C and D are matrix elements representing the locator and are outlined in Appendix 2D. When representing the locator on all three phases as shown in Figure (2.9), X and Z in Equation (2.12) take the form of a (6 x 1) matrix and Y takes the form of a (6 x 6) matrix as given by Equation (2.13) below and outlined in Appendix 2D.

$$\begin{bmatrix} V1_a \\ V1_b \\ V1_c \\ I1_a \\ I1_b \\ I1_c \end{bmatrix} = \begin{bmatrix} A_a & 0 & 0 & B_a & 0 & 0 \\ 0 & A_b & 0 & 0 & B_b & 0 \\ 0 & 0 & A_c & 0 & 0 & B_c \\ C_a & 0 & 0 & D_a & 0 & 0 \\ 0 & C_b & 0 & 0 & D_b & 0 \\ 0 & 0 & C_c & 0 & 0 & D_c \end{bmatrix} \begin{bmatrix} V2_a \\ V2_b \\ V2_c \\ I2_a \\ I2_b \\ I2_c \end{bmatrix} \qquad (2.13)$$

In Equation (2.13),

$$\left.\begin{aligned} A_a &= A_b = A_c \\ B_a &= B_b = B_c \\ C_a &= C_b = C_c \\ D_a &= D_b = D_c \end{aligned}\right] \qquad (2.14)$$

The elements in Equation (2.14) are also given in Appendix 2D.

From the Equations (2.13) and (2.14), it is clearly seen that the elements A, B, C and D in Equation (2.12) become diagonal (3 x 3) submatrices. This is due to the fact that the mutual effect between the locators placed on three phases is zero. This is a useful feature of the new scheme since ,from the construction point of view, it would be much better and more convenient not to have any connections from one locator to another.

2.4 ATTENUATION OF THE LOCATOR

In the locator network, the effective impedance of each stack tuner at the centre frequency f_c to which it is tuned, matches the line earth mode surge impedance. Therefore the equivalent circuit of the locator at centre frequency f_c can be represented as shown in Figure (2.10). Appendix 2E shows that, the degree of attenuation provided by the locator at f_c is given by the expression below.

$$\frac{VX}{VY} \approx \frac{1}{(2X + 1)} \qquad (2.15)$$

In the above equation, X is the ratio of the effective impedance of the line trap circuit of the locator network at centre frequency f_c to the surge impedance of the line, as given below.

$$X = \frac{ZT}{Ro} \qquad (2.16)$$

The magnitude frequency response of the locator near the band of frequencies around the centre frequency f_c is typically shown in Figure (2.11). Due to the coupling effect between the two stack tuners and the line trap circuit of the locator which are tuned to the same centre frequency and bandwidth, the 3dB bandwidth of this curve is 6200 Hz as given below.

$$(\theta f)|Vout/Vin| = (f'_2 - f'_1)|Vout/Vin| = 6200 \text{ Hz} \qquad (2.17)$$

where,

f'_2 = Upper cut-off frequency on attenuation curve
= 93.1 kHz

and

f'_1 = Lower cut-off frequency on attenuation curve
= 86.9 kHz

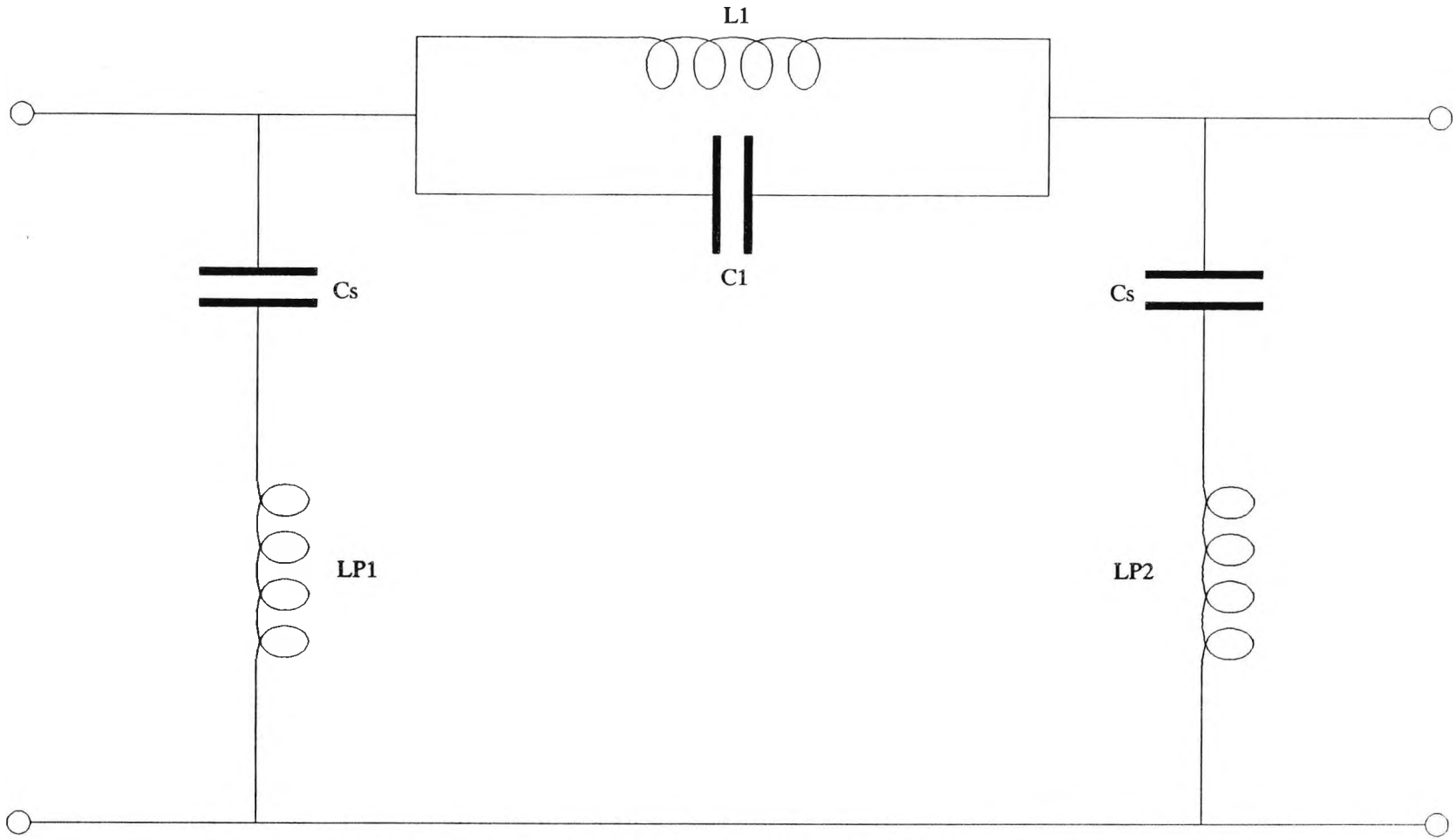

FIG(2.1), THE SIMPLEST ARRANGEMENT OF THE LOCATOR.

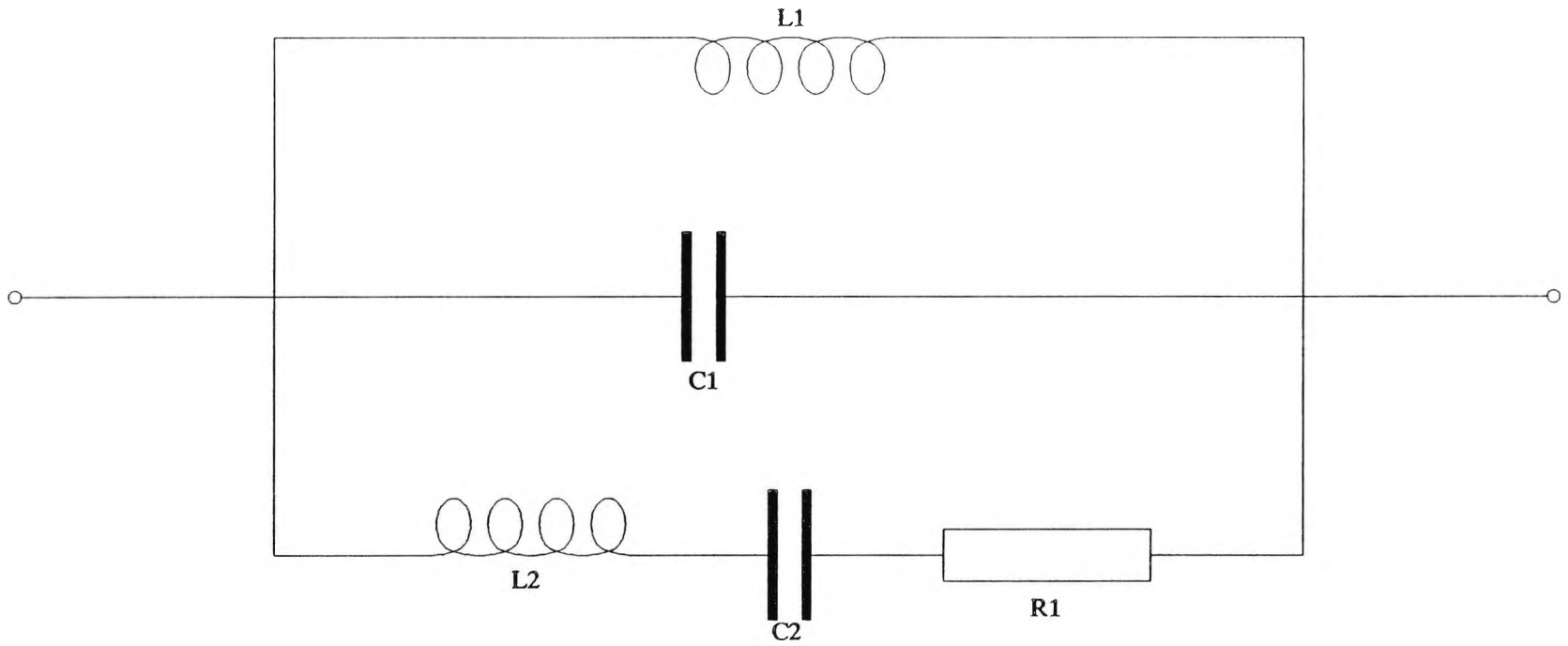

FIG(2.2), THE MODIFIED LINE TRAP CIRCUIT OF THE LOCATOR.

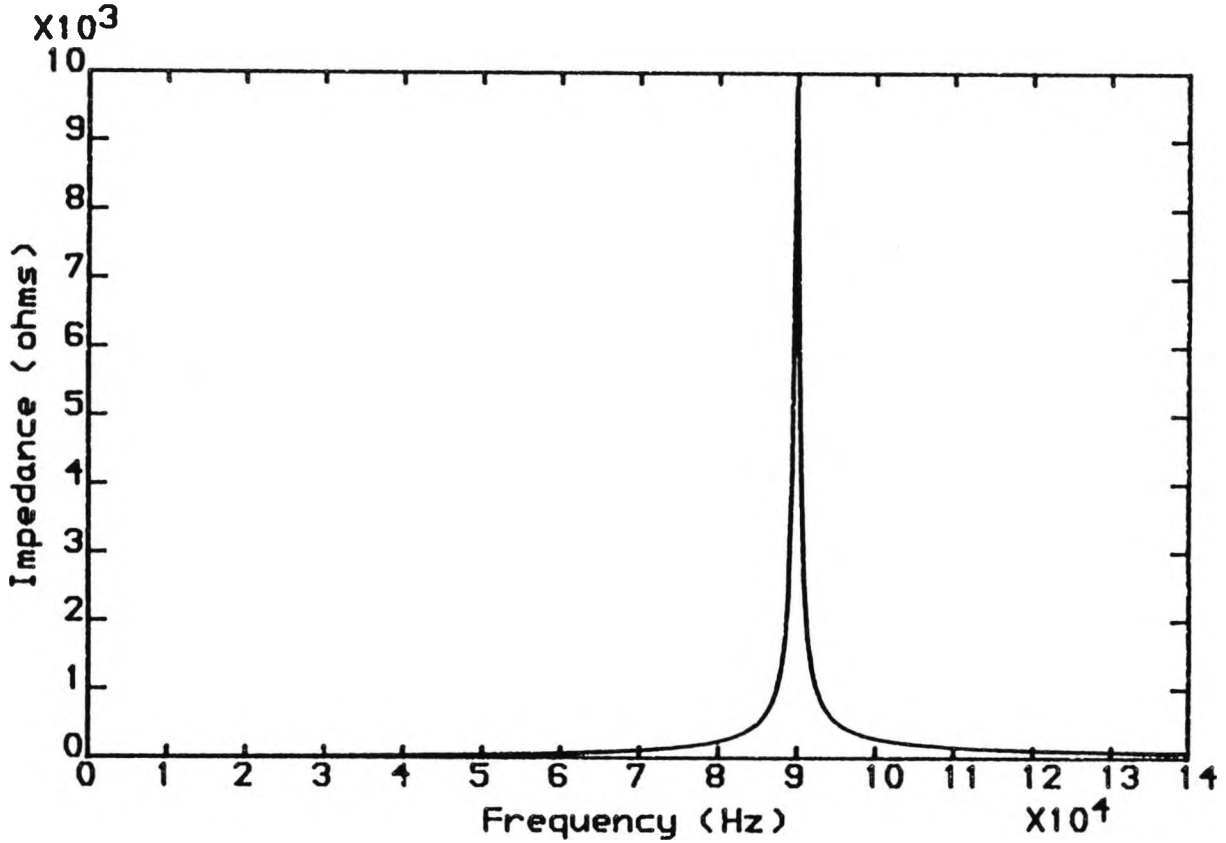

FIG(2.3), THE VARIATION OF THE LINE TRAP CIRCUIT IMPEDANCE AGAINST FREQUENCY.

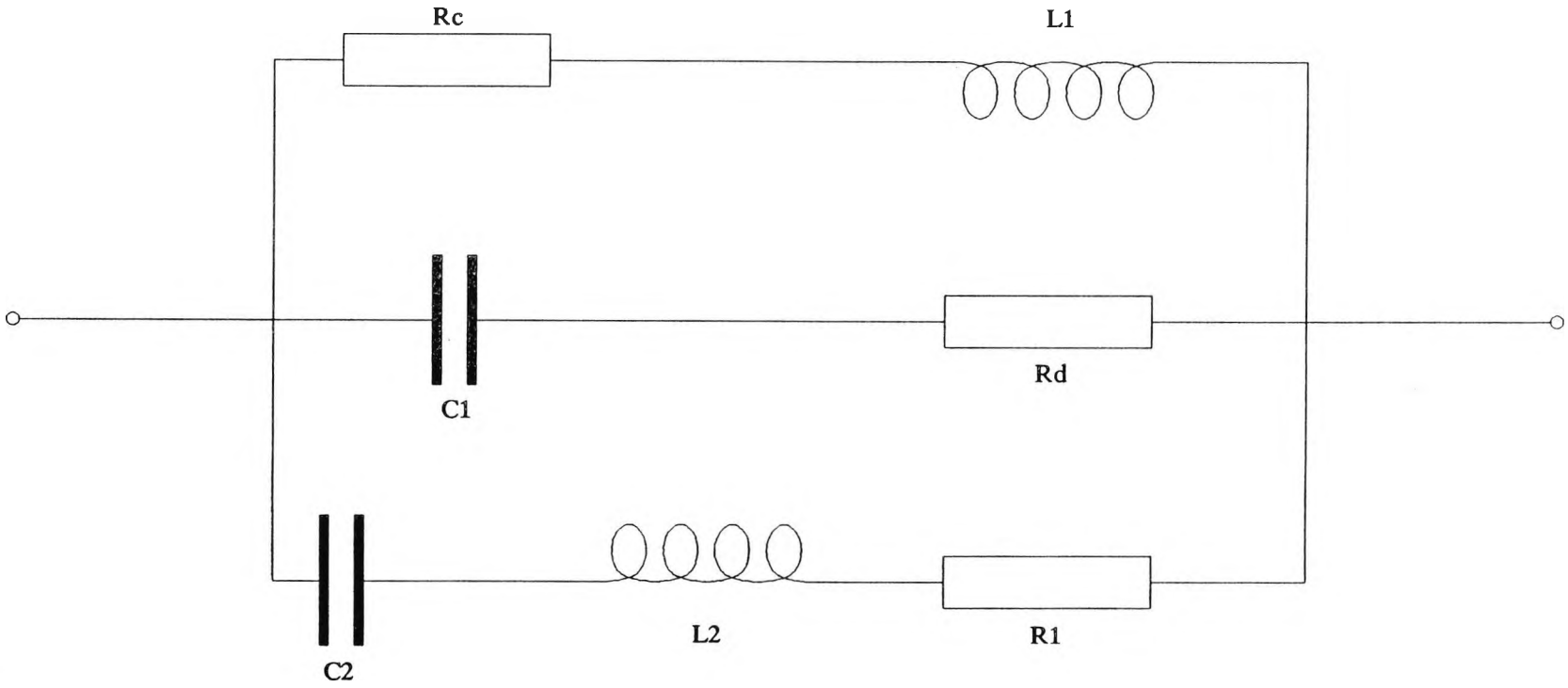

FIG(2.4), THE FINAL ARRANGEMENT OF THE LINE TRAP CIRCUIT OF THE LOCATOR.

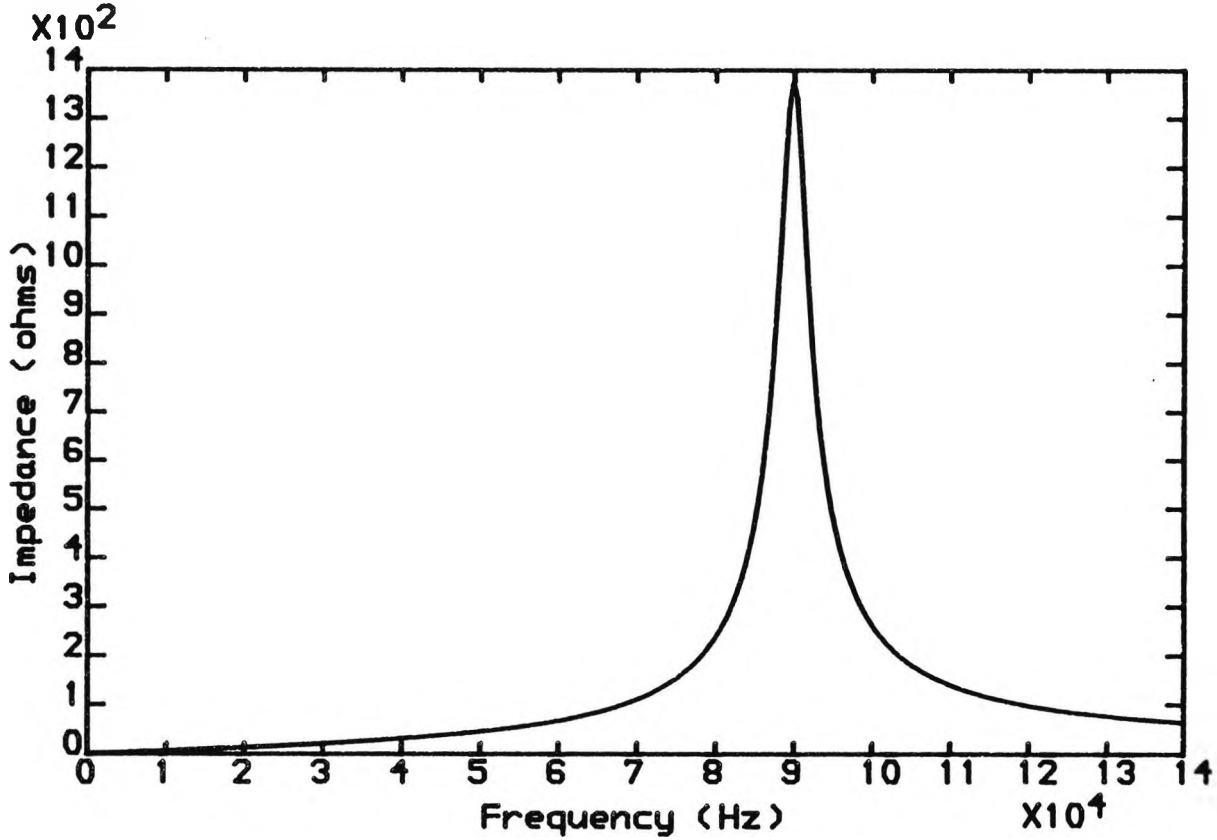

FIG(2.5), THE VARIATION OF THE FINAL LINE TRAP CIRCUIT IMPEDANCE AGAINST FREQUENCY.

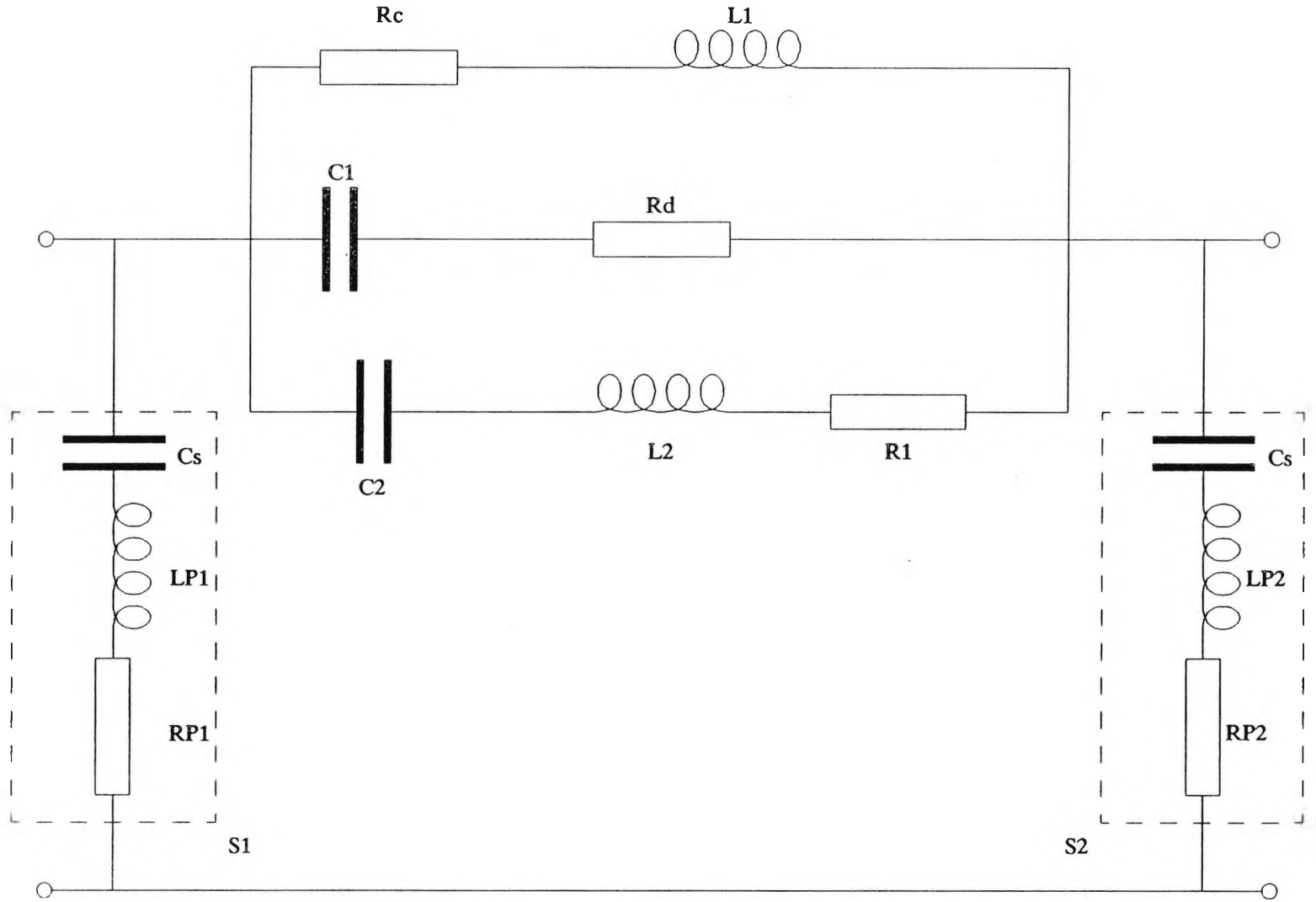

FIG(2.6), THE FINAL CIRCUIT TOPOLOGY OF THE NEW LOCATOR.

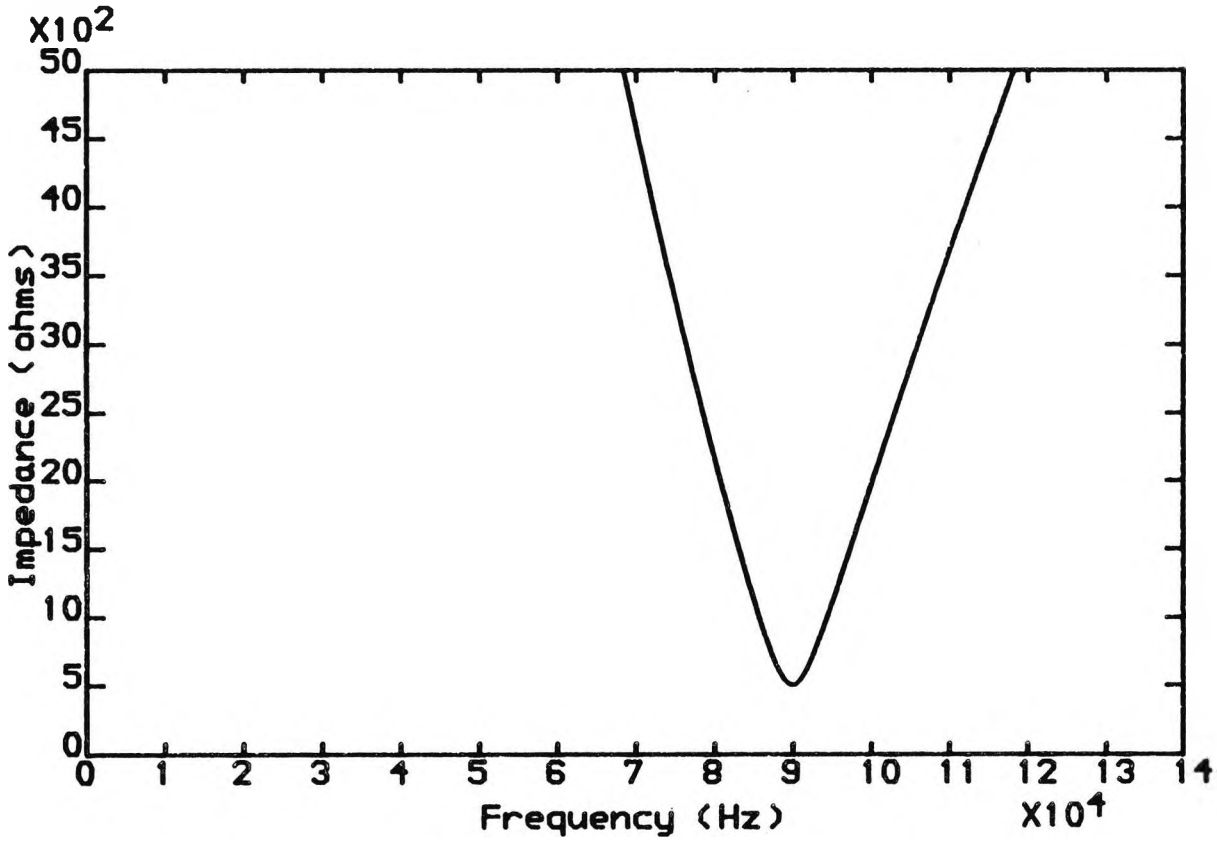

FIG(2.7), THE VARIATION OF IMPEDANCE OF EACH STACK TUNER AGAINST FREQUENCY.

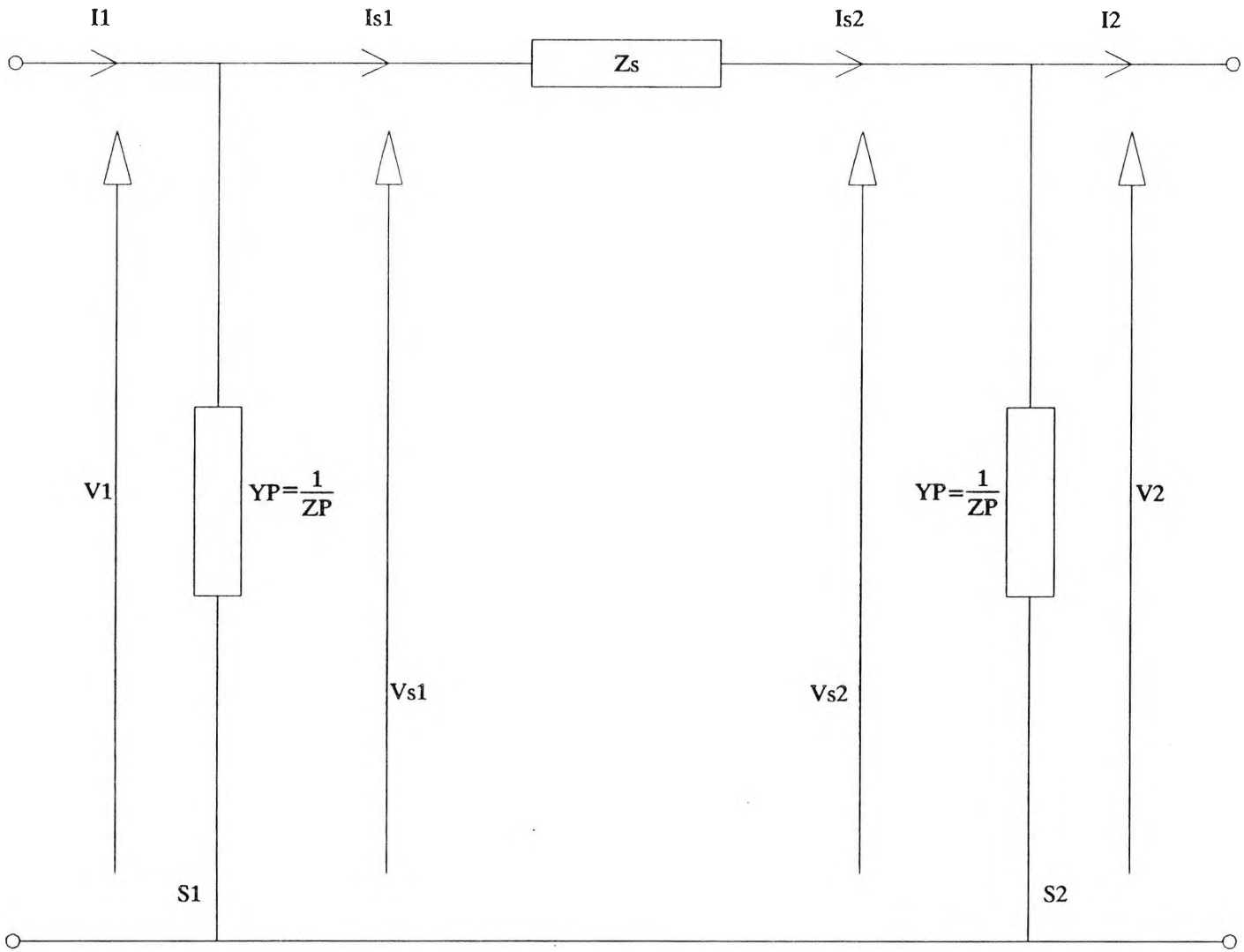

FIG(2.8), A SCHEMATIC BLOCK DIAGRAM OF THE LOCATOR.

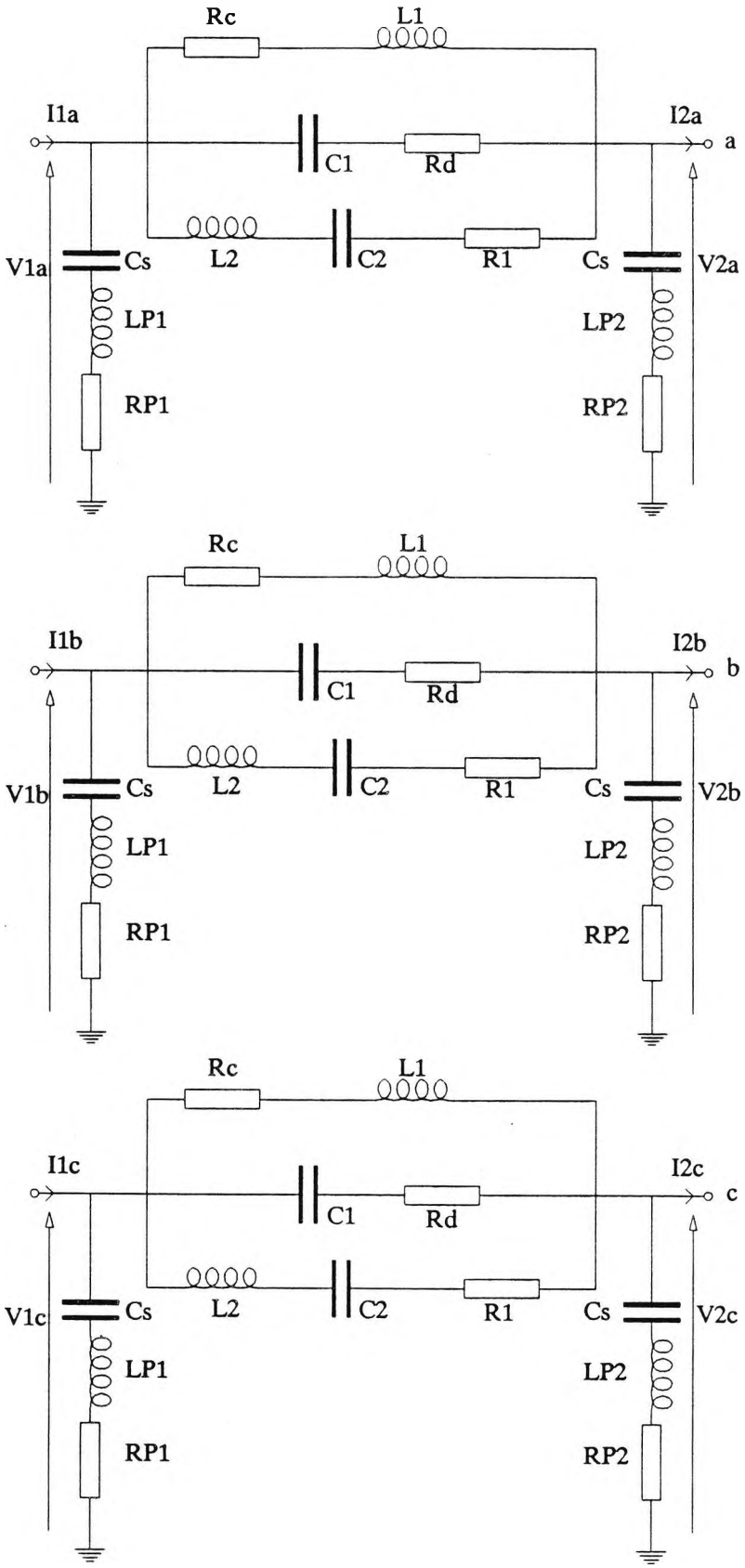

FIG(2.9), REPRESENTATION OF LOCATORS ON THREE PHASES OF A THREE PHASE SYSTEM.

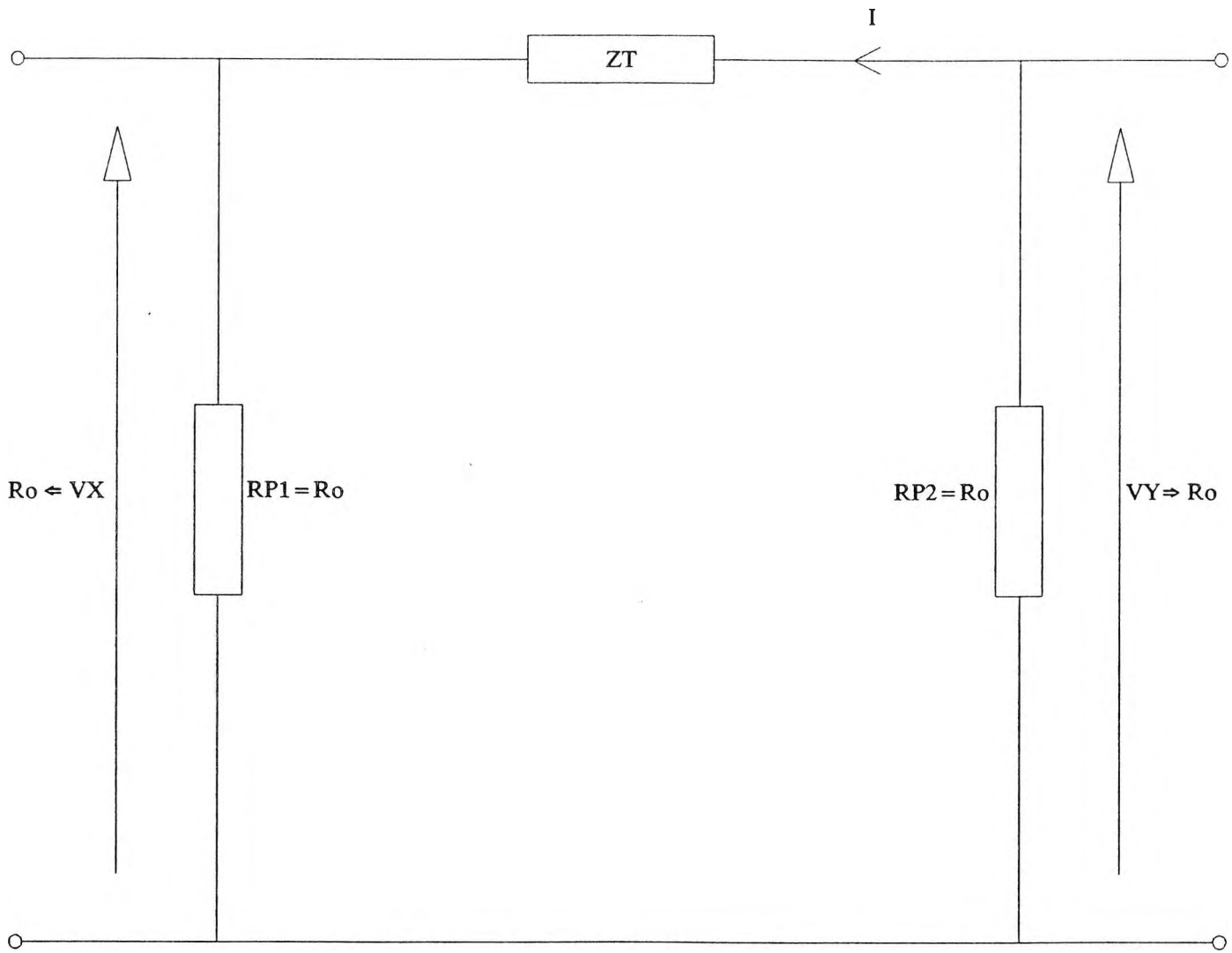

FIG(2.10), THE EQUIVALENT CIRCUIT OF THE LOCATOR AT CENTRE FREQUENCY f_c.

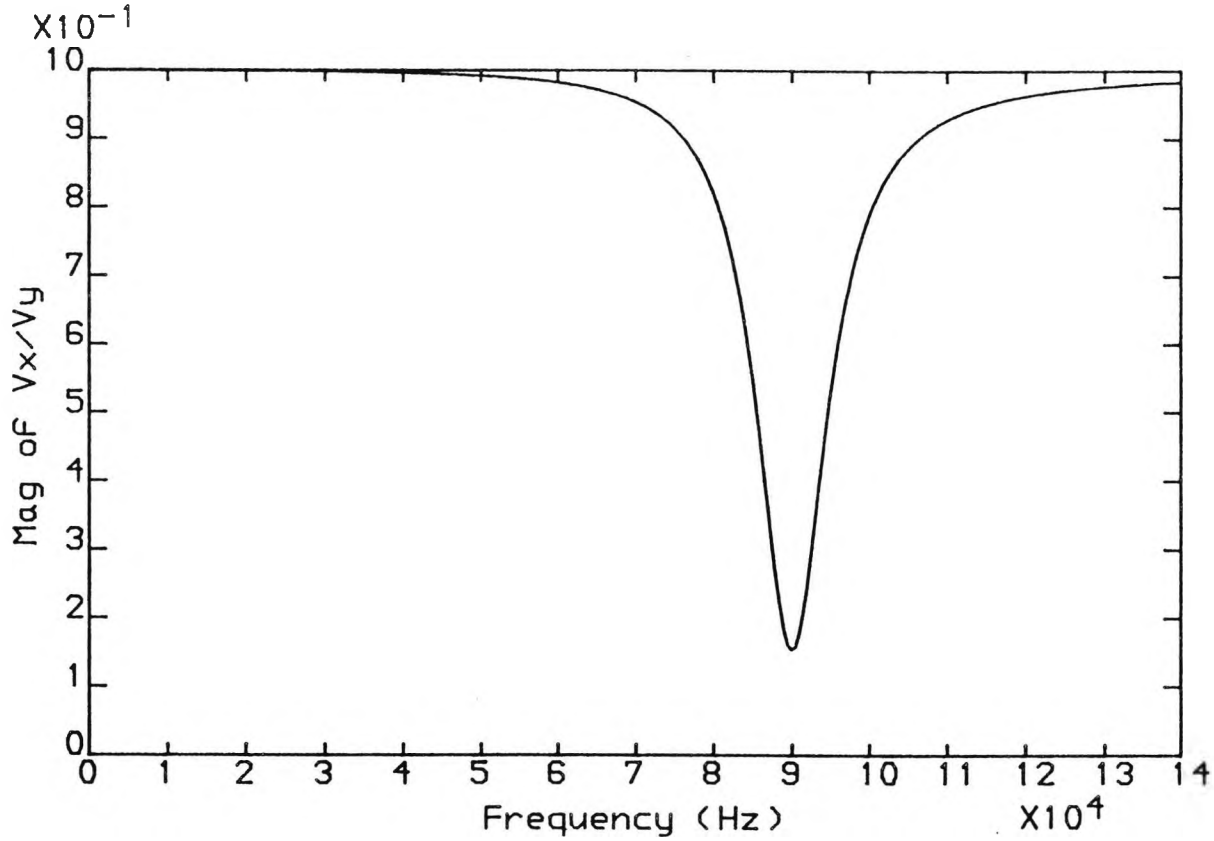

FIG(2.11), THE MAGNITUDE-FREQUENCY RESPONSE OF THE LOCATOR NETWORK.

CHAPTER (3)

THE OPERATING PRINCIPLE OF THE LOCATOR AND THE NEW SCHEME

3.1 INTRODUCTION

Distribution systems can be damaged or disrupted in many ways by faults due to lightning, flashovers, vegetation, etc. It is therefore essential to design protective schemes to ensure a reliable supply of energy to the consumers with the highest possible continuity. It is possible to design a protection scheme based upon a variety of operating principles. The scheme used here is based upon the detection of the fault induced high frequency components in the line.

In the past, protection schemes based upon this operating principle have relied on the use of communication links to pin-point the location of a fault. In the case of interconnected overhead distribution systems the cost of such a communication network becomes very high. However, the scheme used here does not require the presence of such a communication network.

3.2 THE NEW PROPOSED TECHNIQUE

The new fault locators (described in Chapter 2) are inserted at convenient intervals and at strategic points along an overhead distribution line dividing it into

several zones as shown in Figure (3.1). With this arrangement each locator determines:

(i) Whether the fault is upstream or downstream (see Figure (3.1)).

(ii) Whether, or not, the fault is in one of the Zones adjacent to that locator or is in a zone remote from it beyond the next locator.

In Figure (3.1), $(LOC)_n$, (n = 1, 2, ... , n) are the "locators" referred to above and $(o/p)_n$, (n =1, 2, ... ,n) are the output signals from each locator which are then used to sense the direction and location of a fault. This information would then be used to effect the opening of the relevant circuit breakers. A flow chart to indicate the logic incorporated in the detection and location algorithm with the locator $(LOC)_n$ arbitrarily chosen for this purpose is shown in Figure (3.2).

The scheme would operate as follows:
the locator $(LOC)_n$, after observing the fault induced noise voltages, would first determine whether the fault is in-zone or out-of-zone. If the fault is out-of-zone, no action would be taken and no trip signal produced. However if the fault is identified to be in-zone, the locator $(LOC)_n$ would then decide whether the fault has occurred in its upstream adjacent zone or downstream adjacent zone,

and in either case a trip signal would be produced. Note, Figure (3.1) shows only a single line diagram in which for a three phase line one locator is placed between each phase and the earth.

3.3 THE OPERATING PRINCIPLE OF THE NEW SCHEME AND THE LOCATOR

The occurrence of a fault on a transmission or distribution system can be considered as equivalent to superimposing a voltage at the point of fault which is equal and opposite to the pre-fault voltage. The post-fault voltage and current components can be considered as made up of the pre-fault steady-state components and the fault injected components as given below:

$$v_{post} = v_{pre} + v_{fault}$$
$$= v_{pre} + (v)_{steady\text{-}state} + (v)_{transient}. \quad (3.1)$$

$$i_{post} = i_{pre} + i_{fault}$$
$$= i_{pre} + (i)_{steady\text{-}state} + (i)_{transient}. \quad (3.2)$$

The detection of the fault injected components representing the travelling-waves of interest is the basis upon which the operating principle of this new equipment and the scheme, is based.

In Chapter (2) it was described how the new locator was developed to its final stage which is shown here again in Figure (3.3) for convenience. Figure (3.4) shows part of the line in Figure (3.1) with the effective and equivalent circuits of locators $(LOC)_n$ and $(LOC)_{n+1}$ per phase at the centre frequency f_c to which the stack tuners and the line trap circuit of each locator are tuned. In order to understand the operating principle of the new scheme, first let us consider an out-of-zone fault at F2, which as described previously, would cause a wideband noise to be impressed on the line at F2. All frequency components generated by this fault in a narrow band of frequencies (±2.5kHz) around f_c would be attenuated in their passage through the locator $(LOC)_{n+1}$ in Figure (3.4).

It will be seen that, the in-band signal level at point X_{n+1} is, as described in Chapter (2), approximately (1/(2X + 1)) times the in-band signal level that appears at the point Y_{n+1}. X is the ratio of the effective impedance of the line trap circuit of the locator network at centre frequency f_c to the surge impedance of the line. Consequently the output voltages $(VX_{n+1})_{F2}$ and $(VY_{n+1})_{F2}$ would have the relationship given below:

$$\frac{(VX_{n+1})_{F2}}{(VY_{n+1})_{F2}} \approx \frac{1}{(2X + 1)} \qquad (3.3)$$

The locator $(LOC)_{n+1}$ thus greatly reduces the in-band

signals impressed on the line by F2, passing through it. Due to this fact the in-band signal level observed by locator $(LOC)_n$ is relatively low.

Now let us consider a fault at F1. In this case the whole of the in-band noise is absorbed by both locators $(LOC)_n$ and $(LOC)_{n+1}$ at points Y_n and X_{n+1} respectively. $(VY_n)_{F1}$ and $(VX_{n+1})_{F1}$, which are respectively the signals received at Y_n and X_{n+1} due to the fault at F1, are approximately (2X + 1) times higher than that of their corresponding fault noise generated for the previously considered fault at F2. This would yield the equations given below:

$$\frac{(VY_n)_{F2}}{(VY_n)_{F1}} \approx \frac{1}{(2X + 1)} \qquad (3.4)$$

$$\frac{(VX_{n+1})_{F2}}{(VX_{n+1})_{F1}} \approx \frac{1}{(2X + 1)} \qquad (3.5)$$

The subscript F2 refers to the signals produced by the fault at F2. Also a fault at F1 would yield the following equations:

$$\frac{(VX_n)_{F1}}{(VY_n)_{F1}} \approx \frac{1}{(2X + 1)} \qquad (3.6)$$

and

$$\frac{(VY_{n+1})_{F1}}{(VX_{n+1})_{F1}} \approx \frac{1}{(2X + 1)} \qquad (3.7)$$

However, on comparing the signals received at points X_n and Y_n of locator $(LOC)_n$ due to an out-of-zone fault at F2, a completely different relationship between those signals appears as outlined below:

$$(VX_n)_{F2} \approx (VY_n)_{F2} \qquad (3.8)$$

This is due to the fact that, since all locators $(LOC)_n$, (n = 1, 2, ... ,n) are tuned to the same centre frequency and bandwidth, when the fault induced high frequency disturbance passes through locator $(LOC)_{n+1}$, components in a certain part of the frequency spectrum are removed. Consequently the in-band signals received on both sides of any locator situated beyond the locator closest to a fault are almost equal. It is also evident that the in-band signals received by the two locators connected on each side of a faulty section of a line are much higher than those connected elsewhere.

In any scheme, such as this one, which relies for its operation on the pick-up of unwanted fault generated noise signals, it is important to use a detection scheme which incorporates a cancellation feature for any common mode signals. Such signals may be induced in the power lines from remote sources such as radio transmitters or from sources of large r.f. interference in the vicinity. The

use of the aerial mode component of propagation makes it possible to achieve this.

The three output voltages across the resistors of the stack tuners of the three phases are then fed to a summation circuit as shown in Figure (3.5) where they will be added together according to the mode distribution matrix equation given below:

Modal Phasor

$$\begin{bmatrix} V_1' \\ V_2' \\ V_3' \end{bmatrix} = \begin{bmatrix} 1 & 1 & 1 \\ 1 & 0 & 1 \\ 1 & -2 & 1 \end{bmatrix} \begin{bmatrix} V_a \\ V_b \\ V_c \end{bmatrix} \qquad (3.9)$$

The three output voltages can be added together using the aerial mode [1 0 -1] or they can be combined using the aerial mode [1 -2 1]. The combination [1 -2 1] is particularly convenient and has been used here because it causes any common mode signals induced in the power lines from a remote source to be cancelled.

The summation circuit then produces output voltages, say, $SVY_{(n)}$ and $SVX_{(n)}$, (n = 1, 2, ..., n) which are fed into a narrow band pass filter that is tuned to the band of frequencies (typically ±1 kHz) around the centre frequency f_c, to which the stack tuners and the line trap circuit of each locator are tuned. The filter, (see Section 3.4), whose bandwidth corresponds to the 3dB

bandwidth of the locator band-stop network, produces output signals, $FSVY_{(n)}$ and $FSVX_{(n)}$, (n = 1, 2, ..., n). These output voltages are next squared and integrated with respect to time, t, according to the equation given below:

$$E = \int_0^t V^2 \, . \, dt \qquad (3.10)$$

producing an output which is proportional to the energy extracted from the filtered waveforms.

From Equations (3.3), (3.6) and (3.7), it can be seen that, If EVX_C and EVY_C are respectively the energy levels obtained by squaring and integrating the filtered voltages across the resistors of stack tuners situated at sides X and Y of the closest locator to a fault, it should be appreciated that for a downstream fault, see Figure (3.4),

$$EVY_C > EVX_C \qquad (3.11)$$

and conversely for an upstream fault,

$$EVY_C < EVX_C \qquad (3.12)$$

The direction decision logic check, shown in Figure (3.5) thus determines the fault direction by producing high or low logic signal outputs, V_{DD} and V_{DU} according to the direction of the fault. These signals can be used as

fault direction indicators and are fed to a fault zone decision logic as shown.

From Equation (3.8), it is clear that, if EVY_A and EVX_A are respectively, the energy levels obtained by squaring and integrating the filtered voltages across the resistors of stack tuners situated at sides Y and X of any locator placed beyond the closest locator to a fault, for both downstream and upstream faults,

$$EVY_A \approx EVX_A \tag{3.13}$$

It is evident that, the magnitude of the energy level difference E_C between the two sides of the closest locator to a fault is always at a much higher level than its corresponding E_A for any other locator placed beyond the closest locator to a fault. Hence for both downstream and upstream faults, it is true to say that,

$$E_C > E_A \tag{3.14}$$

where,

$$E_C = | EVY_C - EVX_C | \tag{3.15}$$

and

$$E_A = | EVY_A - EVX_A | \tag{3.16}$$

Therefore the best and maximum possible discrimination margin between an in-zone and out-of-zone

fault is achieved by comparing the magnitude of the energy level difference E_{loc}, between the two sides of any locator with a predefined threshold level THL in the level detection circuits shown in Figure (3.5). The expression for E_{loc} corresponding to any locator is given by the Equation (3.17).

$$E_{loc} = | EVY_{loc} - EVX_{loc} | \qquad (3.17)$$

The threshold level THL, depends on the various circuit gains and it can be set to control the basic sensitivity to faults.

Hence for a locator seeing a fault to be in-zone,

$$E_{loc} > THL \qquad (3.18)$$

and for the same locator seeing a fault to be out-of-zone,

$$E_{loc} < THL \qquad (3.19)$$

From Figure (3.5) it can be seen that the outputs of the directional logic check and the level detectors are next fed into the fault zone decision logic, which would decide whether or not to produce a trip signal. The waveforms of Figures (3.6) and (3.7) further illustrate the principle of operation of the equipment for faults at points F1 and F2 respectively as shown in Figure (3.4).

With reference to Figure 3.6(a), the locator $(LOC)_{n-1}$ determines the fault to be an out-of-zone fault in accordance with the previously defined threshold level on the level detectors within the locator $(LOC)_{n-1}$, that is to say:

$$(E_{n-1})_{F1} = | (EVY_{n-1})_{F1} - (EVX_{n-1})_{F1} |$$

$$< THL \qquad (3.20)$$

therefore no trip signal is produced.

With reference to Figure 3.6(b), locator $(LOC)_n$ identifies the fault to be an in-zone fault, because the energy level difference $(E_n)_{F1}$ between its two sides exceeds the threshold level on the level detectors within the locator $(LOC)_n$, this is to say that,

$$(E_n)_{F1} = | (EVY_n)_{F1} - (EVX_n)_{F1} |$$

$$> THL \qquad (3.21)$$

but in this case the locator $(LOC)_n$ would also determine the fault as downstream in accordance with the previously defined directional check, (Equation (3.11)), as outlined below:

$$(EVY_n)_{F1} > (EVX_n)_{F1} \qquad (3.22)$$

therefore a trip signal is produced to indicate that the fault is between locators $(LOC)_n$ and $(LOC)_{n+1}$. The locator $(LOC)_{n+1}$, Figure 3.6(c), likewise identifies the fault as being in-zone between locators $(LOC)_{n+1}$ and $(LOC)_n$, because,

$$(E_{n+1})_{F1} = | (EVY_{n+1})_{F1} - (EVX_{n+1})_{F1} |$$

$$> THL \qquad (3.23)$$

but in this case the locator $(LOC)_{n+1}$ sees the fault as upstream due to the fact that,

$$(EVX_{n+1})_{F1} > (EVY_{n+1})_{F1} \qquad (3.24)$$

therefore a trip signal is produced.

Figure (3.7) shows the corresponding response for a fault at F2 in Figure (3.4). In this case the in-band noise generated by F2 is attenuated by locator $(LOC)_{n+1}$. With reference to Figure 3.7(a), the locator $(LOC)_{n-1}$ identifies the fault to be out-of-zone fault in accordance with the fact that,

$$(E_{n-1})_{F2} = | (EVY_{n-1})_{F2} - (EVX_{n-1})_{F2} |$$

$$< THL \qquad (3.25)$$

hence no trip signal is produced.

Similarly with reference to Figure 3.7(b), and on the account of

$$(E_n)_{F2} = | (EVY_n)_{F2} - (EVX_n)_{F2} |$$

$$< THL \qquad (3.26)$$

by virtue of signal attenuation by locator $(LOC)_{n+1}$ the fault is again correctly identified as out-of-zone by locator $(LOC)_n$ and hence produces no trip signal.

With reference to Figure 3.7(c), and due to the fact that there is no locator and hence high attenuation between locator $(LOC)_{n+1}$ and the fault, the energy difference level $(E_{n+1})_{F2}$ is above the threshold level on the values set on the level detector as given below:

$$(E_{n+1})_{F2} = | (EVY_{n+1})_{F2} - (EVX_{n+1})_{F2} |$$

$$> THL \qquad (3.27)$$

and since,

$$(EVY_{n+1})_{F2} > (EVX_{n+1})_{F2} \qquad (3.28)$$

the locator $(LOC)_{n+1}$ identifies the fault to be in-zone and downstream between it and the next locator downstream (not shown in Figure (3.4)), and therefore produces a trip signal.

3.4 DESIGN OF THE FILTER USED IN DECISION LOGIC UNIT

The filter used (which forms an essential part of the decision logic check unit) is a band-pass Butterworth filter. The design procedure described by Weinberg [29,30], was followed. In this section a brief description of how this filter was designed and how element values were calculated is provided.

Figure (3.8), shows the magnitude frequency response for a band-pass Butterworth filter. In Figure (3.8), w_1 and w_2 are the lower and upper angular cut-off frequencies respectively, at which the attenuation is -3dB. For the magnitude frequency response curve shown, the 3dB bandwidth is $(w_2 - w_1)$ and the relationship between w_2 and w_1 is given by Equation (3.29).

$$w_o^2 = w_1 \cdot w_2 \qquad (3.29)$$

The first step to design the band-pass filter was to design a Butterworth low-pass prototype filter with a 3dB cut-off frequency of $(w_2 - w_1)$. For Butterworth characteristics the attenuation in the stop-band is 6dB per octave per section.

Hence, the larger the number of sections the steeper the transition region of the filter. A 9-section filter was chosen as this would provide an attenuation of 54dB per octave. This was deemed to be a sufficiently steep transition region. Knowing the number of sections required and that the filter is to be fed with a voltage source, the general form of the filter would be of the form shown in Figure (3.9). The general form of a low-pass ladder network varies depending upon whether it is fed from a voltage source or a current source, and also upon whether it contains an even number of sections or an odd number of sections. For simplicity the ratio of the source resistance to the load resistance was taken to be 1, i.e,

$$r = \frac{R_n}{R_1} = 1 \qquad (3.30)$$

Next the element values for the required filter with n = 9, where n is the number of sections, and r = 1, are read from Table (1). It should be noted that these element values are for a normalised filter: one for which the cut-off frequency is 1 rad/sec and the load impedance is 1.0 Ω.

The frequency normalisation is removed by dividing the value of every inductance and capacitance by the required value of the cut-off frequency and leaving the resistances unchanged. Having removed the frequency

normalisation, the required band-pass filter was then formed. For each inductance, in the low-pass filter, of L Henrys a capacitance of value (1 / w_o^2.L) Farads was added in series with it and for each capacitance of C Farads, an inductance of value (1 / w_o^2.C) Henry was added in parallel with it, leaving the resistors unchanged. It should be noted that, each added element always resonates with the original element at the frequency w_o.

However, the band-pass filter obtained is still normalised for load resistance, R_1 = 1Ω. This normalisation is simply removed by multiplying the values of all resistances and inductances by the desired value of the load impedance (R_1), and dividing the value of all capacitances by the same quantity. Figure (3.10) shows the completed 9-section band-pass filter used and its elements values are listed in Appendix 3A.

The magnitude frequency response of the actual band-pass filter used is shown in Figure (3.11).

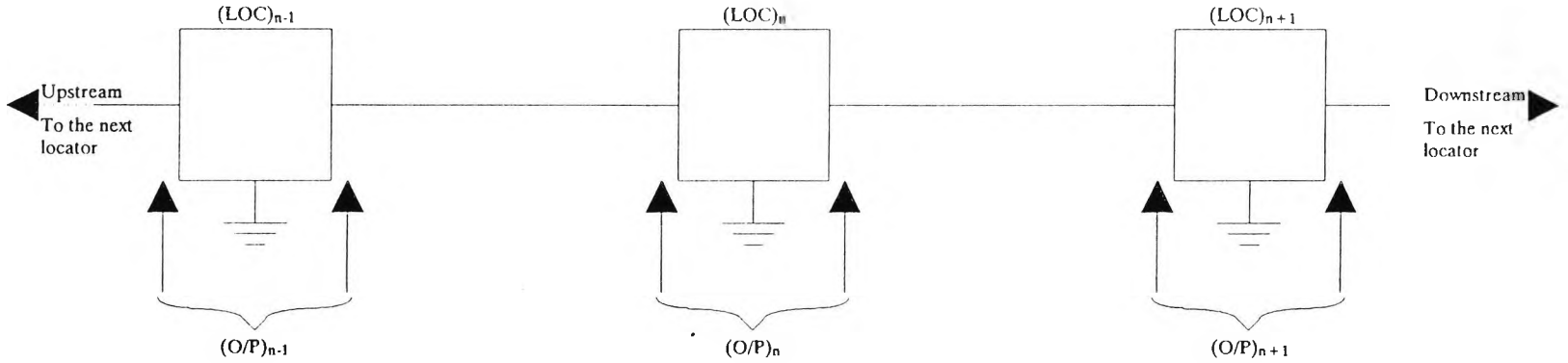

FIG(3.1), SCHEMATIC DIAGRAM OF PART OF AN OVERHEAD LINE WITH THREE LOCATORS.

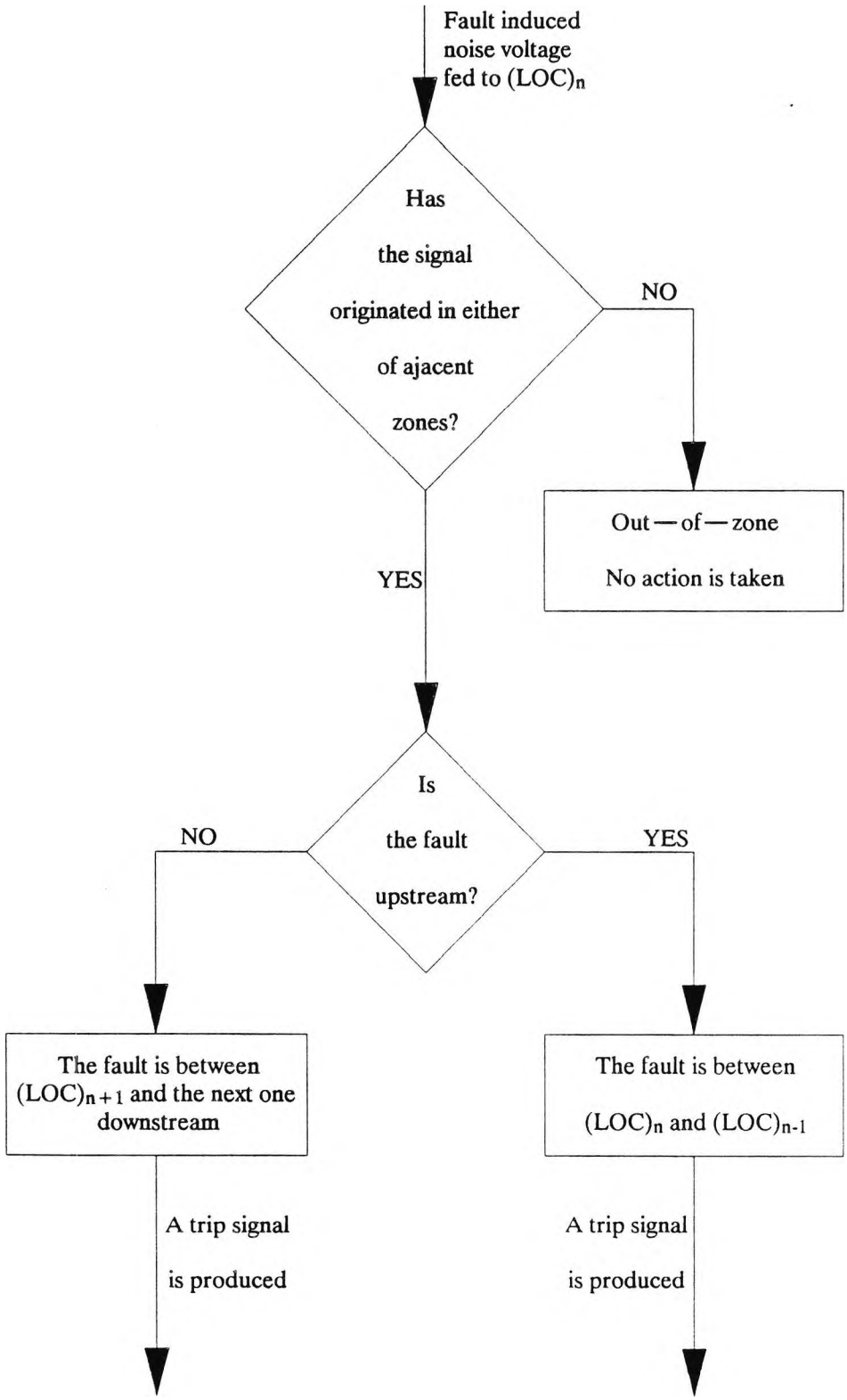

FIG(3.2), A FLOW CHART OF THE NEW PROPOSED TECHNIQUE.

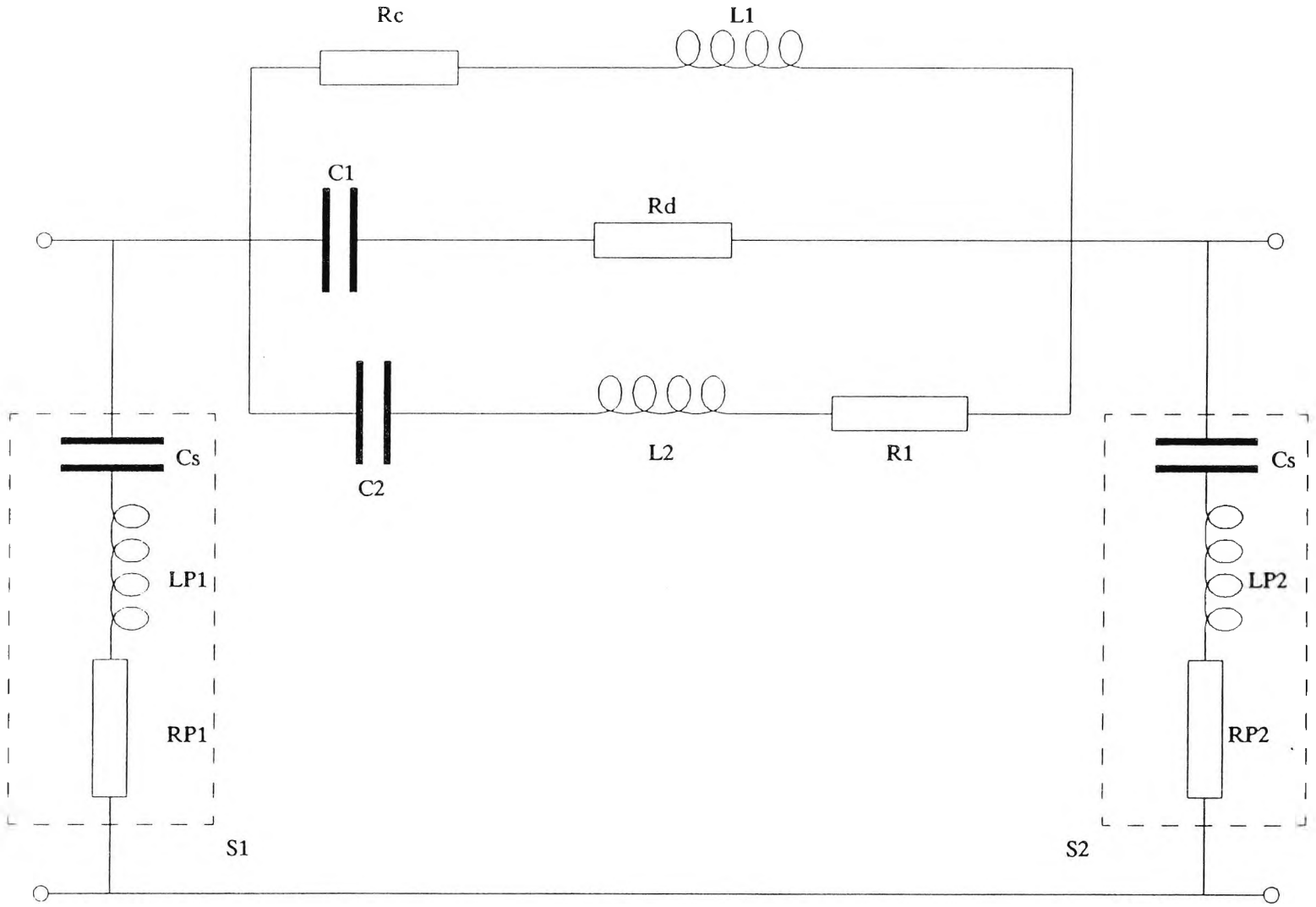

FIG(3.3), THE FINAL ARRANGEMENT OF THE NEW LOCATOR.

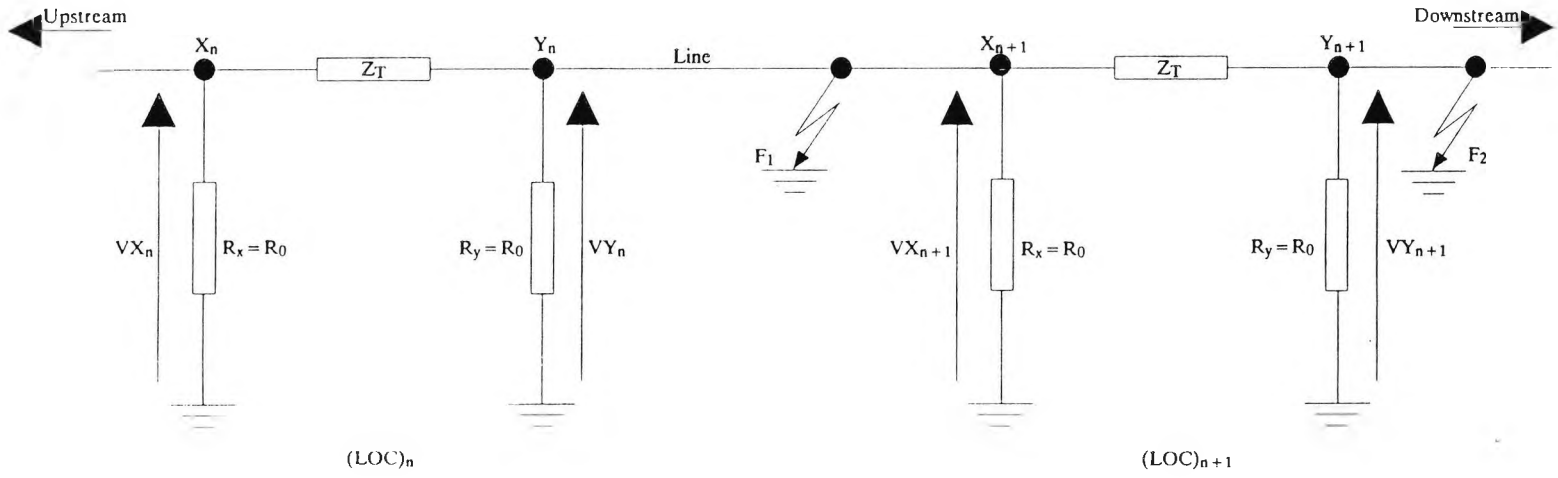

FIG(3.4), THE EQUIVALENT CIRCUITS OF $(LOC)_n$ AND $(LOC)_{n+1}$ PER PHASE AT CENTRE FREQUENCY f_c.

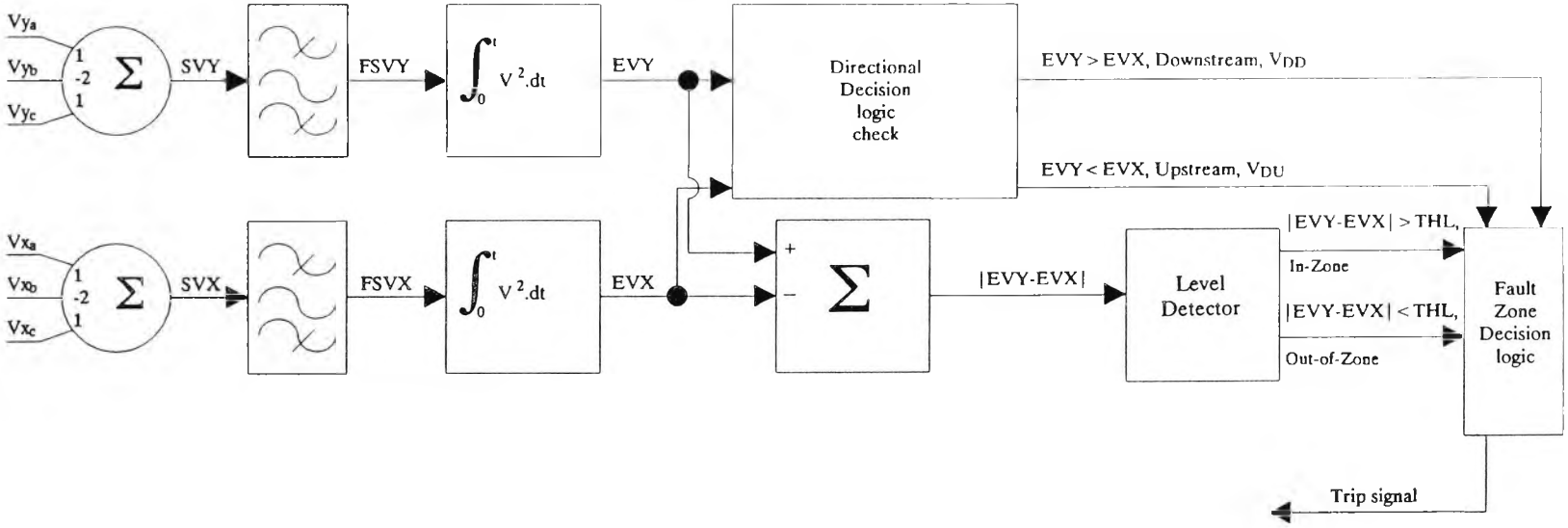

FIG(3.5), DECISION MAKING REPRESENTATION.

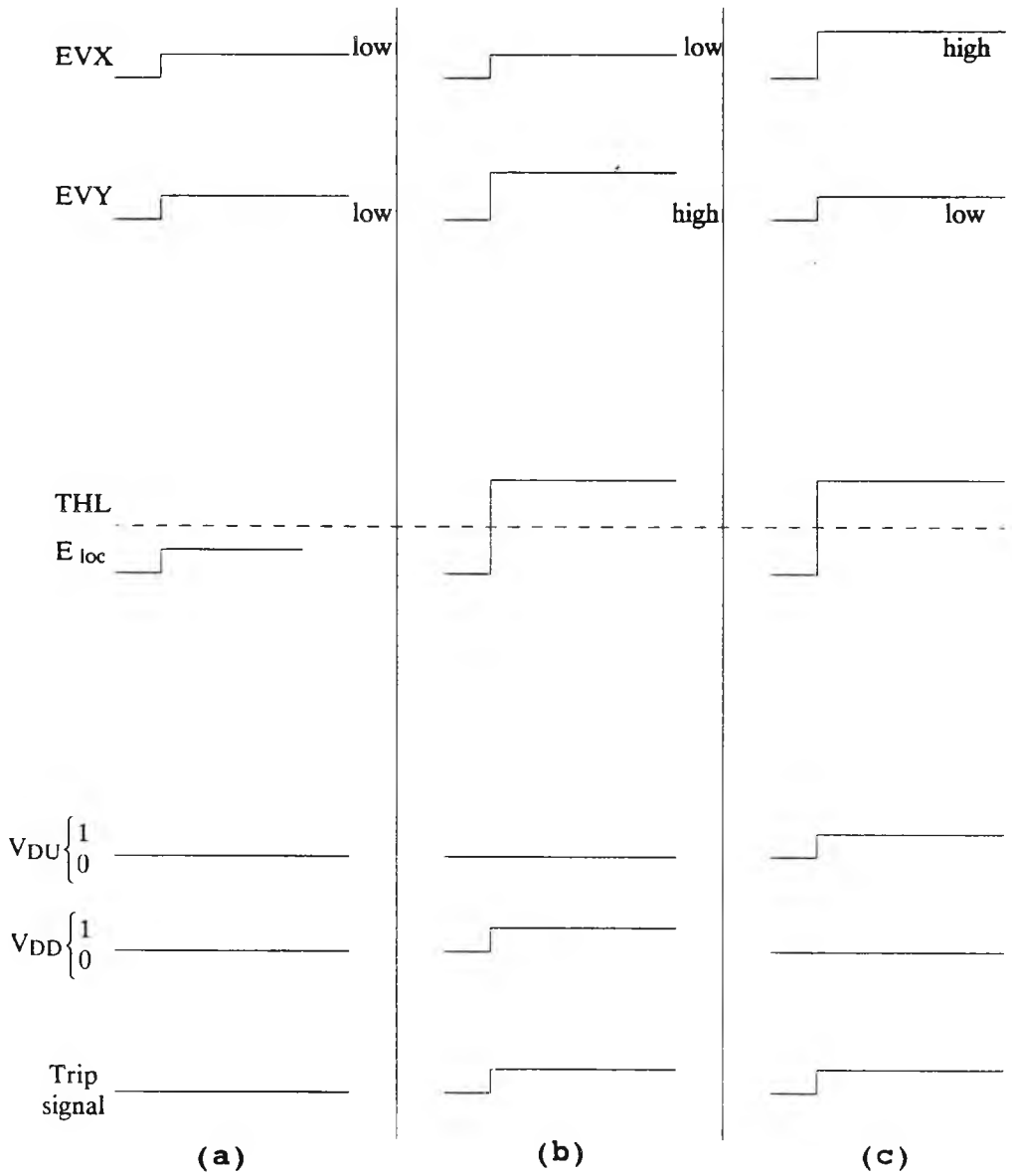

FIG(3.6), THE BEHAVIOUR OF LOCATORS IN FIG(3.1) DUE TO A FAULT AT F1.

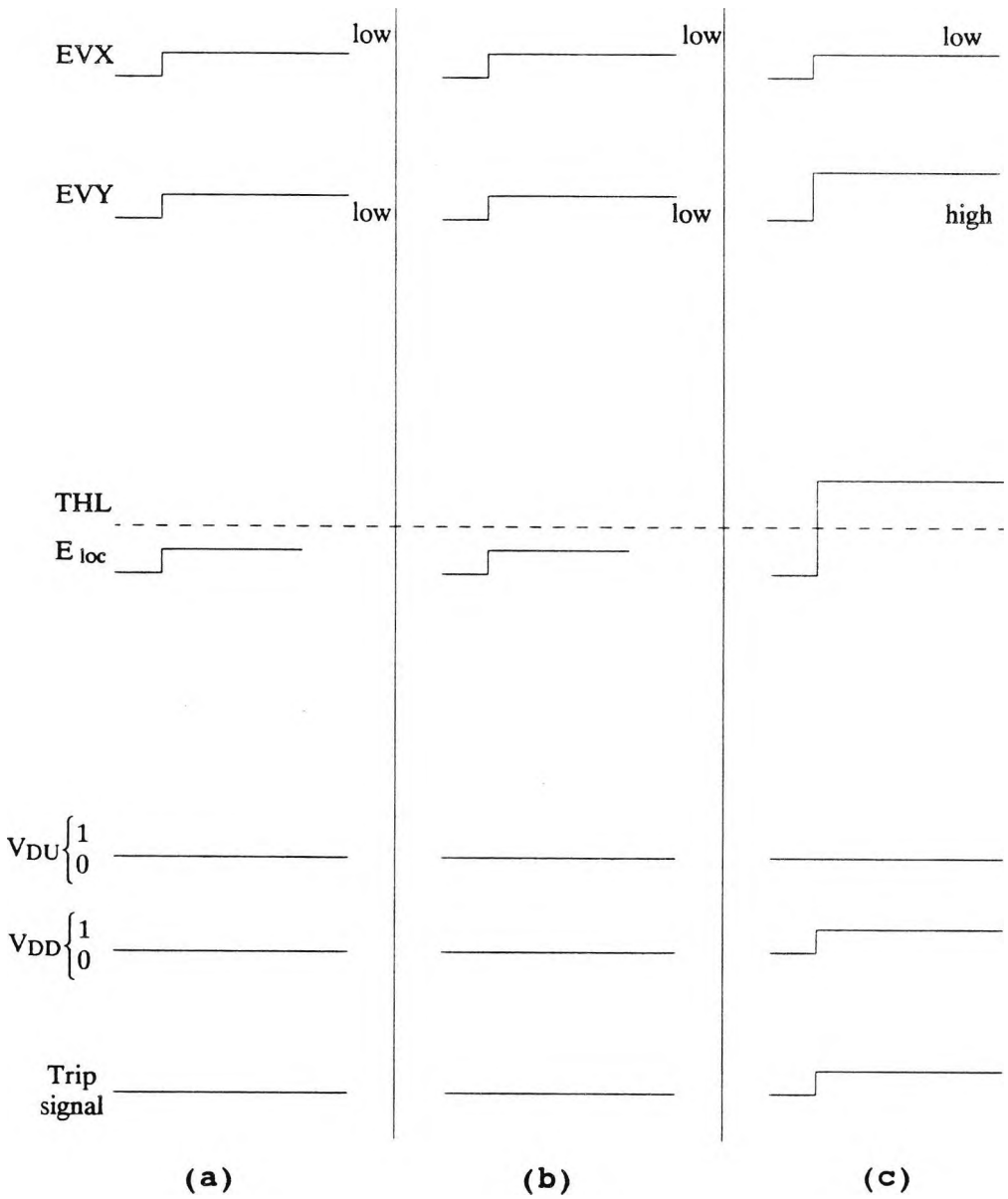

FIG(3.7), THE BEHAVIOUR OF LOCATORS IN FIG(3.1) DUE TO A FAULT AT F2.

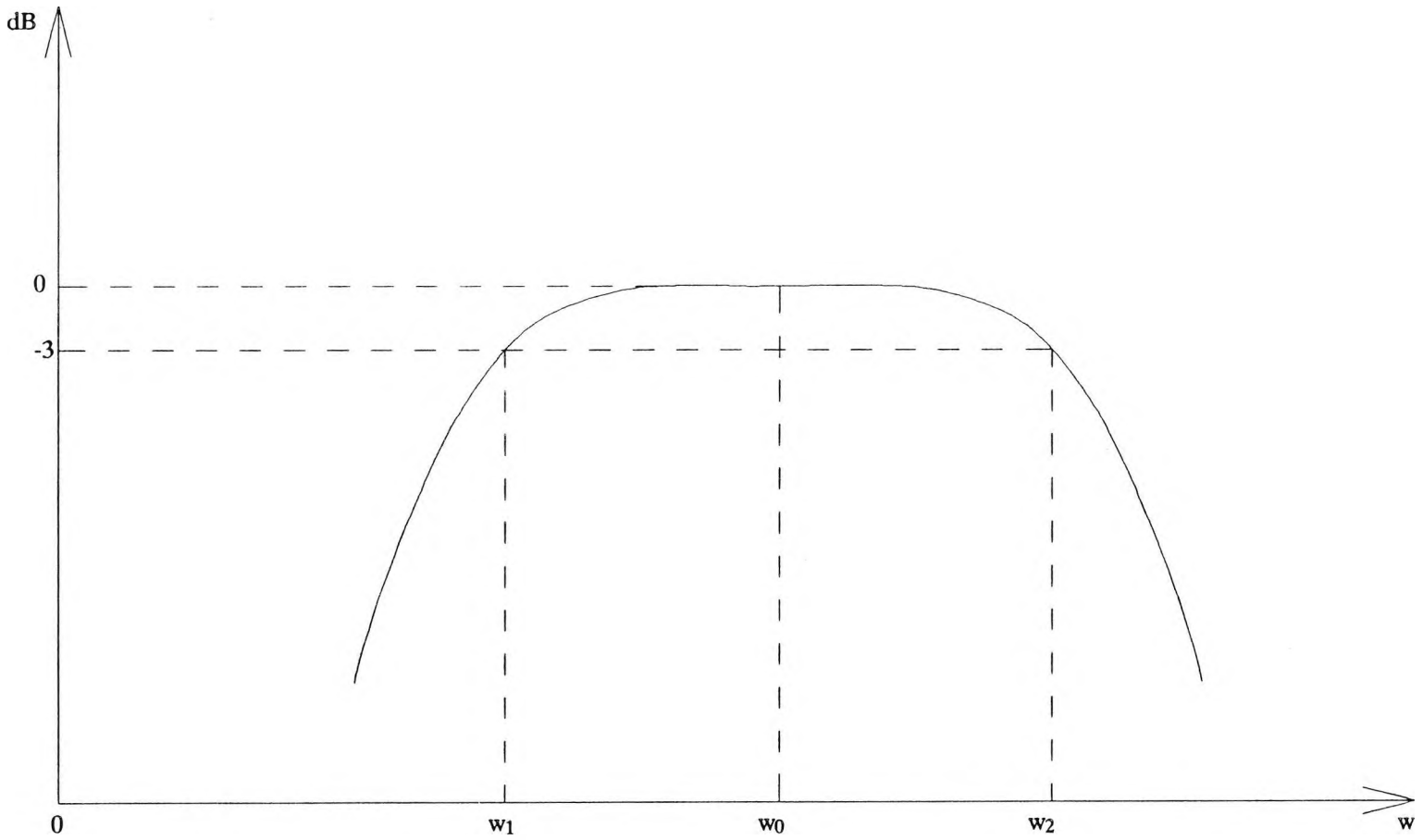

FIG(3.8), MAGNITUDE FREQUENCY RESPONSE OF A BAND-PASS FILTER.

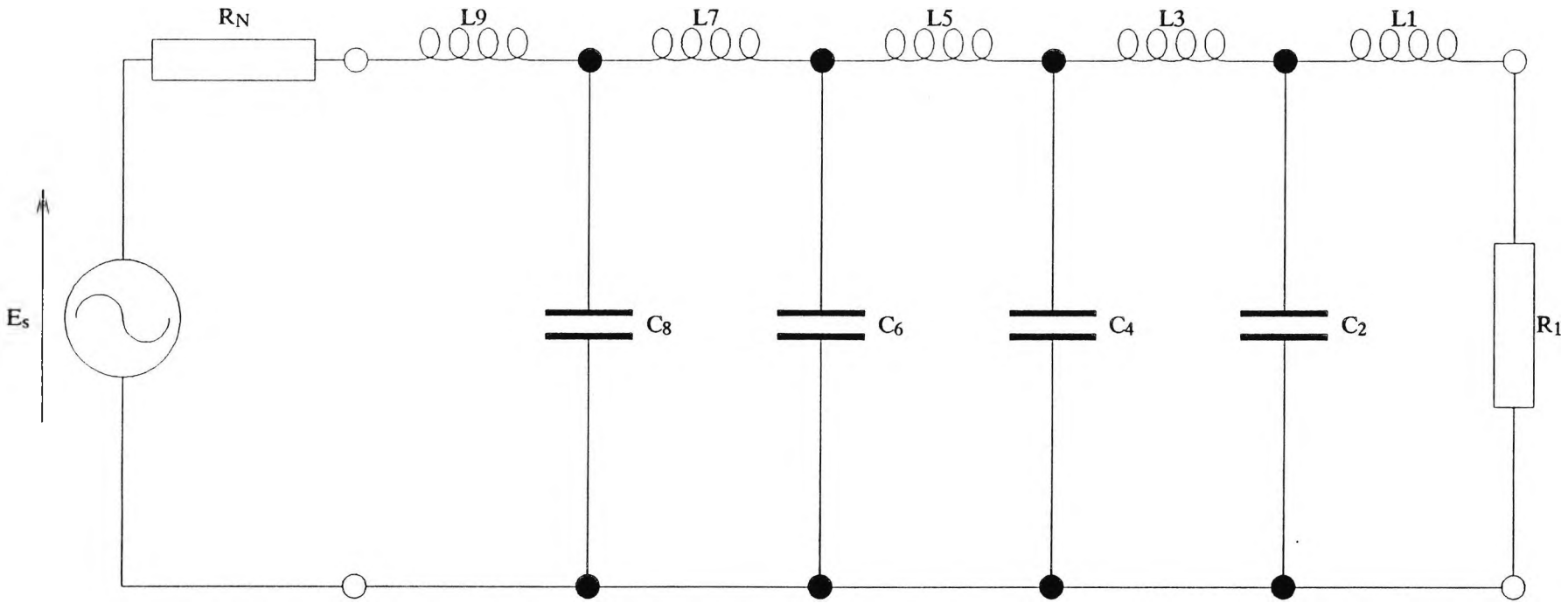

FIG(3.9), GENERAL FORM OF THE REQUIRED LOW-PASS PROTOTYPE FILTER.

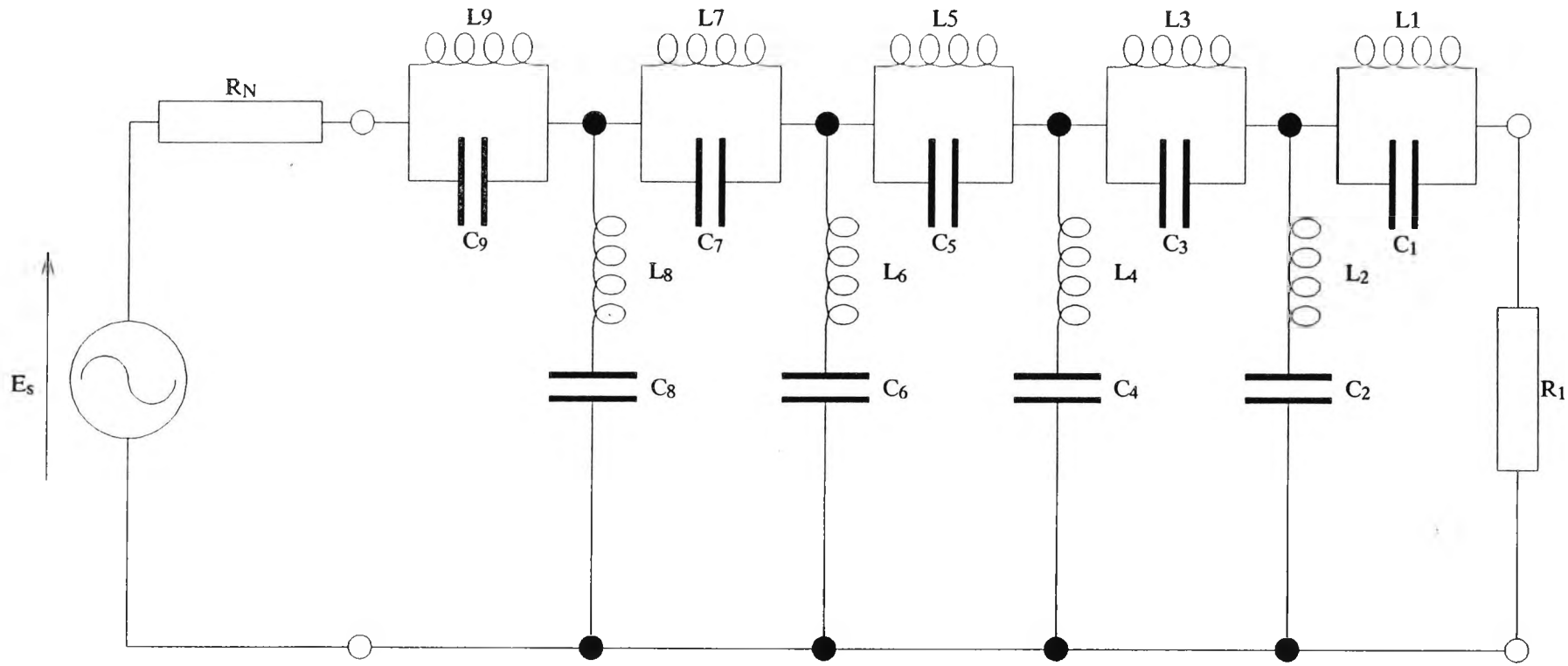

FIG(3.10), THE REQUIRED BAND-PASS FILTER.

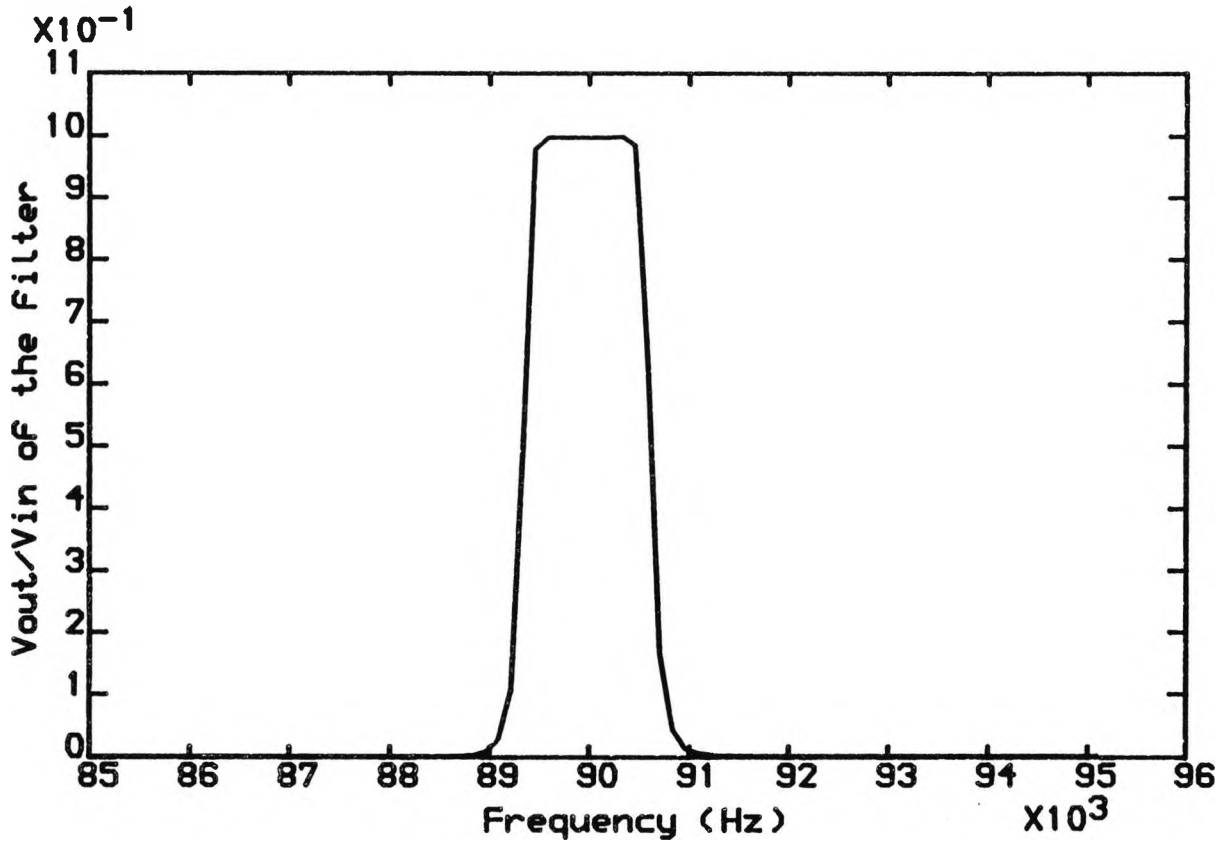

FIG(3.11), MAGNITUDE FREQUENCY RESPONSE OF THE BAND-PASS FILTER USED.

TABLE (1)

Element Values (in ohms, henrys, farads) for a Normalized Butterworth Filter.

Value of n	C_1 or L_1'	L_1 or C_1'	C_2 or L_2'	L_2 or C_2'	C_3 or L_3'	L_3 or C_3'	C_4 or L_4'	L_4 or C_4'	C_5 or L_5'	L_{10} or C_{10}'
a) r = 0										
1	1.0000									
2	0.7071	1.4142								
3	0.5000	1.3333	1.5000							
4	0.3827	1.0824	1.5772	1.5307						
5	0.3090	0.8944	1.3820	1.6944	1.5451					
6	0.2588	0.7579	1.2016	1.5529	1.7593	1.5529				
7	0.2225	0.6560	1.0550	1.3972	1.6588	1.7988	1.5576			
8	0.1951	0.5776	0.9370	1.2588	1.5283	1.7287	1.8246	1.5607		
9	0.1736	0.5155	0.8414	1.1408	1.4037	1.6202	1.7772	1.8424	1.5628	
10	0.1564	0.4654	0.7626	1.0406	1.2921	1.5100	1.6869	1.8121	1.8552	1.5643
b) r = 1/8										
1	9.0000									
2	11.9764	0.0939								
3	12.4442	0.1735	4.1674							
4	12.5605	0.2032	8.9296	0.0493						
5	12.6076	0.2169	11.3305	0.1146	2.5343					
6	12.6190	0.2243	12.6794	0.1533	6.1898	0.0330				
7	12.6199	0.2287	13.5040	0.1778	8.5607	0.0835	1.8121			
8	12.6166	0.2314	14.0417	0.1940	10.2279	0.1190	4.6929	0.0248		
9	12.6117	0.2333	14.4102	0.2053	11.3856	0.1446	6.8248	0.0653	1.4086	
10	12.6064	0.2346	14.6730	0.2135	12.2305	0.1635	8.4293	0.0965	3.7699	0.0198
c) r = 1/4										
1	5.0000									
2	6.2741	0.1992								
3	6.3870	0.3608	2.1699							
4	6.3840	0.4180	4.6024	0.1018						
5	6.3636	0.4435	5.8036	0.2350	1.2992					
6	6.3425	0.4567	6.4673	0.3130	3.1601	0.0675				
7	6.3238	0.4641	6.8671	0.3618	4.3727	0.1700	0.9225			
8	6.3078	0.4687	7.1244	0.3940	5.1943	0.2417	2.3838	0.0503		
9	6.2941	0.4716	7.2984	0.4162	5.7720	0.2932	3.4607	0.1325	0.7143	
10	6.2825	0.4739	7.4209	0.4321	6.1916	0.3312	4.2683	0.1955	1.9091	0.0401
d) r = 1/3										
1	4.0000									
2	4.8284	0.2761								
3	4.8473	0.4934	1.6725							
4	4.8105	0.5676	3.5233	0.1386						
5	4.7743	0.5997	4.4239	0.3186	0.9912					
6	4.7446	0.6156	4.9155	0.4233	2.4042	0.0913				
7	4.7206	0.6244	5.2085	0.4882	3.3200	0.2294	0.7006			
8	4.7012	0.6295	5.3950	0.5308	3.9376	0.3258	1.8075	0.0678		
9	4.6853	0.6326	5.5200	0.5601	4.3762	0.3948	2.6209	0.1785	0.5410	
10	4.6720	0.6346	5.6071	0.5809	4.6833	0.4454	3.2293	0.2630	1.4445	0.0540
e) r = 1/2										
1	3.0000									
2	3.3461	0.4483								
3	3.2612	0.7789	1.1811							
4	3.1868	0.8826	2.4524	0.2175						
5	3.1331	0.9237	3.0510	0.4955	0.6857					
6	3.0938	0.9423	3.3687	0.6542	1.6531	0.1412				
7	3.0640	0.9513	3.5532	0.7512	2.2726	0.3536	0.4799			
8	3.0408	0.9558	3.6678	0.8139	2.6863	0.5003	1.2341	0.1042		
9	3.0223	0.9579	3.7436	0.8565	2.9734	0.6046	1.7846	0.2735	0.3685	
10	3.0072	0.9588	3.7934	0.8864	3.1795	0.6808	2.1943	0.4021	0.9818	0.0825
f) r = 1										
1	2.0000									
2	1.4142	1.4142								
3	1.0000	2.0000	1.0000							
4	0.7654	1.8478	1.8478	0.7654						
5	0.6180	1.6180	2.0000	1.6180	0.6180					
6	0.5176	1.4142	1.9319	1.9319	1.4142	0.5176				
7	0.4450	1.2470	1.8019	2.0000	1.8019	1.2470	0.4450			
8	0.3902	1.1111	1.6629	1.9616	1.9616	1.6629	1.1111	0.3902		
9	0.3473	1.0000	1.5321	1.8794	2.0000	1.8794	1.5321	1.0000	0.3473	
10	0.3129	0.9080	1.4142	1.7820	1.9754	1.9754	1.7820	1.4142	0.9080	0.3129

Journal of The Franklin Institute, 264, p12, July 1957.

CHAPTER (4)

THE SIMULATION OF THE TEST NETWORK

4.1 INTRODUCTION

The simulation of the network used for developing the new directional fault locator described in Chapter (2), is based upon a standard fortran program. This program carries out a frequency domain analysis on a given section of a HV distribution network and then gives, as its outputs, the values of the required voltages and currents in the time domain via a Fourier transform algorithm [19,20,21,22]. The types of faults that can be simulated using this program are, three phase-to-earth, two phase-to-earth, single phase-to-earth and phase-to-phase.

It is discussed in this chapter, how the voltages and currents of interest are obtained. Details are also provided of other interface programs which are used as the second part of the simulation. This latter part of the simulation is concerned with the signal processing of these voltages and currents.

4.2 SIMULATED TEST CIRCUIT

The system used for simulation is schematically shown in Figure (4.1), which is a simple radial 11kV overhead

distribution line including three locators and an open end. Note, Figure (4.1) shows only a single line diagram in which for a three phase line one locator is placed between each phase and the earth.

Figure (4.2) shows the line configuration which is a horizontally constructed line with no earth wire. The line data [23,24] used for simulation are outlined in Appendix 4A.

4.3 CALCULATION OF VOLTAGES AND CURRENTS OF INTEREST

A multiconductor line is defined by its series-impedance matrix Z and its shunt-admittance matrix Y per unit length. Each element of Z varies with frequency and is determined by the conductor types, their physical geometry and the nature of the earth plane. The admittance matrix Y is a function only of the physical geometry of the conductors relative to the earth plane. Reference [19], details the calculation of these matrices from basic line data. Reference [22], shows how the system voltage steady-state equations, given by Equation (4.1) can be transformed into a series of independent differential equations of the form given in Equation (4.2).

$$\frac{d^2\bar{V}}{dx^2} = P\bar{V} \qquad (4.1)$$

$$\bar{V} = \exp(-\Phi x)\bar{V}_i + \exp(\Phi x)\bar{V}_r \qquad (4.2)$$

where,

$$P = Z.Y \tag{4.3}$$

$\bar{V}$ is voltage transform, $\bar{V}_i$ and $\bar{V}_r$ are the incident and reflected voltage transforms and Φ is given by Equation (4.4).

$$\Phi = Q.\Gamma.Q^{-1} \tag{4.4}$$

where

Q = Voltage eigenvector matrix

and

Γ = Propagation constant matrix

Matrix function theory permits easy evaluation of the hyperbolic functions, the poly phase surge impedance and surge admittance [19]. These are given in Equations (4.5) and (4.6).

$$Z_o = Q.\Gamma^{-1}.Q^{-1}.Z \tag{4.5}$$

and

$$Y_o = Y.Q.\Gamma^{-1}.Q^{-1} \tag{4.6}$$

With reference to Figure (4.1), the voltages of interest are the voltages across the resistors of stack tuners of each locator, when there is a disturbance on the line. The following sections detail the calculation of

these voltages.

4.3.1 TRANSFER-MATRIX FUNCTIONS

The system shown in Figure (4.1), with a fault at point F, essentially consists of a network of cascade sections as shown in Figure (4.3). Two-port transfer matrices are useful in the solution of such problems.

The relationship between the currents and voltages at either end of the line is given by Equation (4.7),

$$\begin{bmatrix} \bar{V}_S \\ \bar{I}_S \end{bmatrix} = \begin{bmatrix} A1 & B1 \\ C1 & D1 \end{bmatrix} \begin{bmatrix} Af & Bf \\ Cf & Df \end{bmatrix} \begin{bmatrix} A2 & B2 \\ C2 & D2 \end{bmatrix} \begin{bmatrix} \bar{V}_R \\ \bar{I}_R \end{bmatrix} \tag{4.7}$$

where A1, B1, C1 and D1 are the matrices defining the line section up to the point of fault, A2, B2, C2 and D2 are the matrices defining the line section beyond point of fault and the fault discontinuity is defined by the matrices Af, Bf, Cf and Df. In Equation (4.7),

$$\begin{bmatrix} A1 & B1 \\ C1 & D1 \end{bmatrix} = \begin{bmatrix} A_{S1} & B_{S1} \\ C_{S1} & D_{S1} \end{bmatrix} \begin{bmatrix} A_{L1} & B_{L1} \\ C_{L1} & D_{L1} \end{bmatrix} \begin{bmatrix} A_{S2} & B_{S2} \\ C_{S2} & D_{S2} \end{bmatrix} \tag{4.8}$$

and

$$\begin{bmatrix} A2 & B2 \\ C2 & D2 \end{bmatrix} = \begin{bmatrix} A_{L2} & B_{L2} \\ C_{L2} & D_{L2} \end{bmatrix} \begin{bmatrix} A_{S3} & B_{S3} \\ C_{S3} & D_{S3} \end{bmatrix} \cdot \begin{bmatrix} A_{L3} & B_{L3} \\ C_{L3} & D_{L3} \end{bmatrix} \begin{bmatrix} A_{S4} & B_{S4} \\ C_{S4} & D_{S4} \end{bmatrix} \quad (4.9)$$

From Equations (4.8) and (4.9), it can be seen that, the line sections S1, S2, S3 and S4 in Figure (4.1) are all represented by ABCD parameters with subscripts S1, S2, S3 and S4 respectively and locators $(LOC)_{L1}$, $(LOC)_{L2}$ and $(LOC)_{L3}$ are represented by ABCD parameters with subscripts L1, L2 and L3 respectively. In Equation (4.8),

$$A_{S1} = \cosh(\Phi X1) \quad (4.10)$$

$$B_{S1} = \sinh(\Phi X1).Zo \quad (4.11)$$

$$C_{S1} = Yo.\sinh(\Phi X1) \quad (4.12)$$

and

$$D_{S1} = Yo.\cosh(\Phi X1).Zo \quad (4.13)$$

where

X1 = Distance between sending end source and the first locator $(LOC)_{L1}$.

The matrices defining the transfer matrix representing sections S2, S3 and S4 of the line are similarly found by substituting the distances X2, X3 and X4 respectively for X1. The elements A_{L1}, A_{L2}, A_{L3} and A_{L4} in the matrix defining the first locator $(LOC)_{L1}$ have already been defined in Chapter (2). The matrices defining the transfer matrices of the second and third locators, $(LOC)_{L2}$ and $(LOC)_{L3}$ are calculated in the same way, since all the locators are identical. Finally the matrices defining the fault discontinuity are formulated according to the type of fault.

The equations given so far provide a solution to the steady-state response of the system. However, when a fault occurs on the line, the disturbance is propagated away from the fault towards both ends of the line. A proportion of this disturbance is reflected from the terminating busbars and from within each source network, to constitute a series of travelling waves which are ultimately damped by the system as a whole [20]. Such phenomena represent variations in frequency over a wide range and it is therefore, necessary to evaluate the system equations over the entire frequency spectrum of the disturbance in order to obtain the complete transient response.

4.3.2 FAULT TRANSIENT MODEL

The transient solution is a computation of the

voltages and currents in the system following the application of a superimposed generator at the fault point. The basis of the method hinges upon representing the voltage at the fault point by the sum of two voltages $\bar{V}_{fs}$ and $\bar{V}_{ff}$ as shown in Figure (4.4). $\bar{V}_{fs}$ is sinusoidal and is arranged to be equal to the steady-state voltage at the point of fault before the disturbance. $\bar{V}_{ff}$ is a suddenly applied voltage which when added to $\bar{V}_{fs}$, represents the postfault voltage. A solution may thus be obtained by performing two separate calculations in which the desired voltages and currents are evaluated when $\bar{V}_{fs}$ is applied to the energised system and the superimposed voltage $\bar{V}_{ff}$ is applied to the line with all source voltages set to zero.

The method is essentially one of superposition and it should be noted that the steady-state voltage vector $\bar{V}_{fs}$ can be evaluated from a knowledge of the pre-fault voltages and currents at the terminating ends of the line. In fact, the vector $\bar{V}_{fs}$ is only needed in so far as it enables the value $\bar{V}_{ff}$ to be evaluated as a prerequisite to the second part of the computational process.

A pre-fault calculation is performed to provide the steady-state voltage and current at the source and also to determine the fault point voltage $\bar{V}_{fs}$, at the fault point F1. The pre-fault calculation is determined at power frequency, since it is assumed that the system is in a

steady-state condition before the occurrence of any disturbance on the system. Appendix 4B details the evaluation of $\bar{V}_{fs}$ which is given by Equation (4.14).

$$\bar{V}_{fs} = A2.A_s^{-1}.\bar{V}_{SS} \qquad (4.14)$$

where,

$$A_s = \left[A1.A2 + B1.C2 \right]$$

It should also be noted that, it is necessary to establish the response of the unenergised circuit to the superimposed voltage transform $\bar{V}_{ff}$, both for the faulted and healthy phases. In the case of the faulted phase or phases, no difficulty exists, for example, if we consider a single phase to earth fault on phase a, $\bar{V}_{ffa}$ is the transform of a suddenly applied voltage of the form,

$$\bar{V}_{ffa} = - \bar{V}_{fsa}.\sin(w_o t + \beta)h(t) \qquad (4.15)$$

where w_o is nominal system angular frequency and h(t) is unit step function.

The superimposed voltage is simply equal and opposite to the pre-fault voltage at the point of fault. Unfortunately for healthy conductors, there is no such direct means of knowing the appropriate value of the superimposed voltages. It is shown in Appendix 4C that, the currents due to the application of the superimposed

voltages are related by Equation (4.16).

$$\bar{V}_{ff} = -\left[\left[M\right]^{-1} + Rf\right]\left[\bar{I}_{fSf} - \bar{I}_{fRf}\right] \qquad (4.16)$$

where, $\bar{I}_{fRf}$ and $\bar{I}_{fSf}$ are the transform of superimposed currents at fault point, Rf represents the fault resistance matrix and,

$$\left[M\right] = \left[\left[C1 + D1.Z_{SS}^{-1}\right]\left[A1 + B1.Z_{SS}^{-1}\right]^{-1} + \left[C2.A2^{-1}\right]\right] \qquad (4.17)$$

It is evident from the foregoing, that the analysis requires the source impedance matrix over the range of frequency of interest. For the purpose of confirming the digital simulation which is used here, a general source model based upon arbitrarily defined Short-Circuit Levels at the terminating busbars has been used. The evaluation of this source impedance matrix, Z_{SS}, which is given by Equation (4.18) is outlined in Appendix 4D.

$$Z_{SS} = \begin{bmatrix} Z_{se} & Z_{mu} & Z_{mu} \\ Z_{mu} & Z_{se} & Z_{mu} \\ Z_{mu} & Z_{mu} & Z_{se} \end{bmatrix} \qquad (4.18)$$

where, the source self impedance Z_{se} is given by Equation (4.19),

$$Z_{se} = Z_{s1} + \frac{1}{3} (Z_{so} - Z_{s1}) \qquad (4.19)$$

and the source mutual impedance is given by Equation (4.20).

$$Z_{mu} = \frac{1}{3} (Z_{so} - Z_{s1}) \qquad (4.20)$$

In Equations (4.19) and (4.20) Z_{so} and Z_{s1} are the zero and positive phase sequence source impedances respectively.

The vector of transposed superimposed voltages from each conductor to earth, $\bar{E}_{ff}$ is obtained from Equation (4.21) given below.

$$\bar{E}_{ff} = \bar{V}_{ff} + R_f \cdot \left[\bar{I}_{fSf} - \bar{I}_{fRf} \right] \qquad (4.21)$$

Equation (4.16) involves (3 x 3) matrices for single circuit configuration and for simplicity it takes of the

form given in Equation (4.22).

$$\begin{bmatrix} \bar{V}_{ffa} \\ \bar{V}_{ffb} \\ \bar{V}_{ffc} \end{bmatrix} = \begin{bmatrix} Z_{aa} & Z_{ab} & Z_{ac} \\ Z_{ba} & Z_{bb} & Z_{bc} \\ Z_{ca} & Z_{cb} & Z_{cc} \end{bmatrix} \begin{bmatrix} (\bar{I}_{fSf} - \bar{I}_{fRf})_a \\ (\bar{I}_{fSf} - \bar{I}_{fRf})_b \\ (\bar{I}_{fSf} - \bar{I}_{fRf})_c \end{bmatrix} \tag{4.22}$$

For example, for single phase-to-earth fault, (a-e), Equation (4.22) takes the form given in Equation (4.23).

$$\begin{bmatrix} \bar{V}_{ffa} \\ \bar{V}_{ffb} \\ \bar{V}_{ffc} \end{bmatrix} = \begin{bmatrix} Z_{aa} \\ Z_{ba} \\ Z_{ca} \end{bmatrix} \left[\left(\bar{I}_{fSf} - \bar{I}_{fRf} \right)_a \right] \tag{4.23}$$

This is because the currents $\bar{I}_{fSf}$ and $\bar{I}_{fRf}$ are equal in the healthy b and c phases. The voltage transform $\bar{V}_{ffa}$ is known, therefore $\bar{V}_{ffb}$ and $\bar{V}_{ffc}$ can easily be evaluated as shown below.

From Equation (4.23),

$$\bar{V}_{ffa} = Z_{aa} \cdot \left[\left(\bar{I}_{fSf} - \bar{I}_{fRf} \right)_a \right] \tag{4.24}$$

from which,

$$\left[\left(\bar{I}_{fSf} - \bar{I}_{fRf} \right)_a \right] = Z_{aa}^{-1} \cdot \bar{V}_{ffa} \tag{4.25}$$

therefore,

$$\bar{V}_{ffb} = Z_{ba} \cdot \left[Z_{aa}^{-1} \cdot \bar{V}_{ffa} \right] \qquad (4.26)$$

and,

$$\bar{V}_{ffc} = Z_{ca} \cdot \left[Z_{aa}^{-1} \cdot \bar{V}_{ffa} \right] \qquad (4.27)$$

The final step in the process involves computing the spectrum of the voltages and currents of interest. The transformed superimposed voltages and currents at the sending end of the line were evaluated in order to find the transformed superimposed voltages and currents at either side of each locator along the line. Appendix 4E, shows that the transformed superimposed voltage on the left hand side of the first locator in Figure (4.1) is given by the Equation (4.28).

$$\bar{V}1 = \left[U - C_{S1}^{-1}.D_{S1}.B_{S1}^{-1}.A_{S1} \right]^{-1} \cdot C_{S1}^{-1}.\bar{I}_{Sf} -$$

$$\left[U - C_{S1}^{-1}.D_{S1}.B_{S1}^{-1}.A_{S1} \right]^{-1} \cdot$$

$$\left[C_{S1}^{-1}.D_{S1}.B_{S1}^{-1} \right] \cdot \bar{V}_{Sf} \qquad (4.28)$$

where U is a unit matrix.

Appendix 4E also shows that,

$$\bar{I}1 = B_{S1}^{-1} \cdot \left[\bar{V}_{sf} - A_{S1} \cdot \bar{V}1 \right] \qquad (4.29)$$

where, $\bar{I}1$ is the transformed superimposed current on the left hand side of the first locator in Figure (4.1).

Finally putting Equation (4.28) in Equation (4.29) would give the current $\bar{I}1$. Similarly the transformed superimposed voltage, $\bar{V}2$ and current, $\bar{I}2$ on the right hand side of the first locator in Figure (4.1) are found using Equation (4.30).

$$\begin{bmatrix} \bar{V}1 \\ \bar{I}1 \end{bmatrix} = \begin{bmatrix} A_{L1} & B_{L1} \\ C_{L1} & D_{L1} \end{bmatrix} \begin{bmatrix} \bar{V}2 \\ \bar{I}2 \end{bmatrix} \qquad (4.30)$$

From Equation (4.30), $\bar{V}2$ is evaluated in exactly the same way as $\bar{V}1$, which was outlined in Appendix 4E. $\bar{V}2$ is therefore given by Equation (4.31).

$$\bar{V}2 = \left[U - C_{L1}^{-1} \cdot D_{L1} \cdot B_{L1}^{-1} \cdot A_{L1} \right]^{-1} \cdot C_{L1}^{-1} \cdot \bar{I}1 -$$

$$\left[U - C_{L1}^{-1} \cdot D_{L1} \cdot B_{L1}^{-1} \cdot A_{L1} \right]^{-1} \cdot$$

$$\left[C_{L1}^{-1} \cdot D_{L1} \cdot B_{L1}^{-1} \right] \cdot \bar{V}1 \qquad (4.31)$$

It should be noted that, $\bar{V}1$ and $\bar{V}2$ are the total voltages across stack tuners on both sides of the locator,

(see Figure (4.5)), and each take the form of a (3 x 1) matrix. However, for programming purposes these voltages are formed as (3 x 3) diagonal matrices as given below.

$$\bar{V}1 = \begin{bmatrix} \bar{V}1_a & 0 & 0 \\ 0 & \bar{V}1_b & 0 \\ 0 & 0 & \bar{V}1_c \end{bmatrix} \qquad (4.32)$$

and

$$\bar{V}2 = \begin{bmatrix} \bar{V}2_a & 0 & 0 \\ 0 & \bar{V}2_b & 0 \\ 0 & 0 & \bar{V}2_c \end{bmatrix} \qquad (4.33)$$

The transformed superimposed voltages of interest are the voltages across the resistors of stack tuners. Knowing the voltages $\bar{V}1$ and $\bar{V}2$ and the admittance of the stack tuners, the voltages across the resistors of the stack tuners S1 and S2 of the corresponding three phases are obtained using Equations (4.34) and (4.35) respectively.

$$\begin{bmatrix} \bar{V}_{RP1a} \\ \bar{V}_{RP1b} \\ \bar{V}_{RP1c} \end{bmatrix} = \begin{bmatrix} \bar{V}1_a & 0 & 0 \\ 0 & \bar{V}1_b & 0 \\ 0 & 0 & \bar{V}1_c \end{bmatrix} \cdot \begin{bmatrix} YS1_a & 0 & 0 \\ 0 & YS1_b & 0 \\ 0 & 0 & YS1_c \end{bmatrix}$$

$$\begin{bmatrix} RP1_a \\ RP1_b \\ RP1_c \end{bmatrix} \qquad (4.34)$$

where

$$YS1_a = YS1_b = YS1_c$$

= Admittance of stack tuner S1

and

$$RP1_a = RP1_b = RP1_c$$

= Resistance of stack tuner S1

$$\begin{bmatrix} \bar{V}_{RP2a} \\ \bar{V}_{RP2b} \\ \bar{V}_{RP2c} \end{bmatrix} = \begin{bmatrix} \bar{V}2_a & 0 & 0 \\ 0 & \bar{V}2_b & 0 \\ 0 & 0 & \bar{V}2_c \end{bmatrix} \cdot \begin{bmatrix} YS2_a & 0 & 0 \\ 0 & YS2_b & 0 \\ 0 & 0 & YS2_c \end{bmatrix}$$

$$\begin{bmatrix} RP2_a \\ RP2_b \\ RP2_c \end{bmatrix} \qquad (4.35)$$

where

$$YS2_a = YS2_b = YS2_c$$

= Admittance of stack tuner S2

and

$$RP2_a = RP2_b = RP2_c$$

= Resistance of stack tuner S2

The inverse Fourier transform given in Equation (4.36) forms the basis of the method by which the frequency spectrum is used to determine the corresponding time variation of any voltage and current of interest.

$$f(t) = \frac{1}{2\pi} \int_{-\infty}^{\infty} f(w).\exp(jwt).dw \qquad (4.36)$$

References [21,22] have developed and successfully used a modified halfrange form of the basic Fourier integral as given in Equation (4.37).

$$f(t) = \mathrm{Re}\ \frac{\exp(\alpha t)}{\pi} \int_{0}^{f} \sigma f(w - j\alpha).\exp(jwt).dw \qquad (4.37)$$

The Gibbs oscillations, which arise when a finite number of terms of an infinite Fourier series are taken, is overcome by introducing the sigma factor given below.

$$\sigma = \frac{\sin(\pi w/f)}{(\pi w/f)} \qquad (4.38)$$

In Equation (4.37), a frequency-shift constant, α, is also included to ensure numerical stability when the

integral is evaluated digitally. The relationship between the sigma, frequency-shift constant and truncation frequency, f, has been studied extensively [26].

4.4 SIGNAL PROCESSING OF THE DESIRED SIGNALS

The second part of the simulation is concerned with the signal processing of the voltages of interest obtained in the previous sub-section. This consists of several interface programes as described below.

The output results obtained in the time domain are fed into the first interface program, which functions as a preprocessor for SPICE. It should be appreciated that, the filtering operation has been performed using SPICE. The program then produces a data file which is suitable for being directly used as a SPICE input file. SPICE is then run, it processes the information in its input file, which also includes the electrical characteristics of the band-pass filter used as part of the signal processing, and then produces an output file that is basically the filtered results.

According to the decision logic check unit, Figure (4.5), Chapter (3), the filtered voltages are next squared and integrated to give an output which is proportional to the energy content in the waveforms. There are several ways of achieving this, but the method of integration used

here is based on the "TRAPEZOIDAL RULE" which is again carried out using another standard fortran program which is the final interface program in the second part of the simulation.

By referring to Figure (4.5) and Appendix 4F, the total energy in a period of T, or the total area under the squared voltage curve from the origin to T is,

$$E = \int_0^T v^2 \, . \, dt$$

$$= t \, . \left[\frac{1}{2} \, . \, [\, (V_0)^2 + (V_n)^2 \,] + \sum_{i=1}^{n-1} (V_i)^2 \right] \qquad (4.39)$$

where

$$n = \frac{T}{t} \qquad (4.40)$$

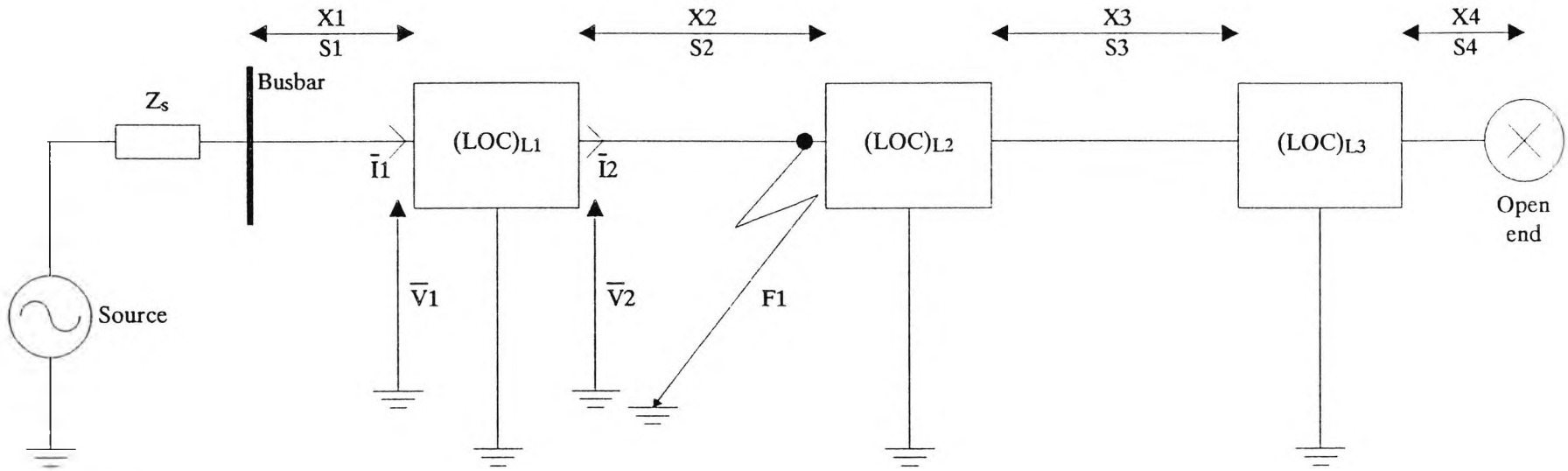

FIG(4.1), SCHEMATIC DIAGRAM OF THE SIMULATED SYSTEM PER PHASE.

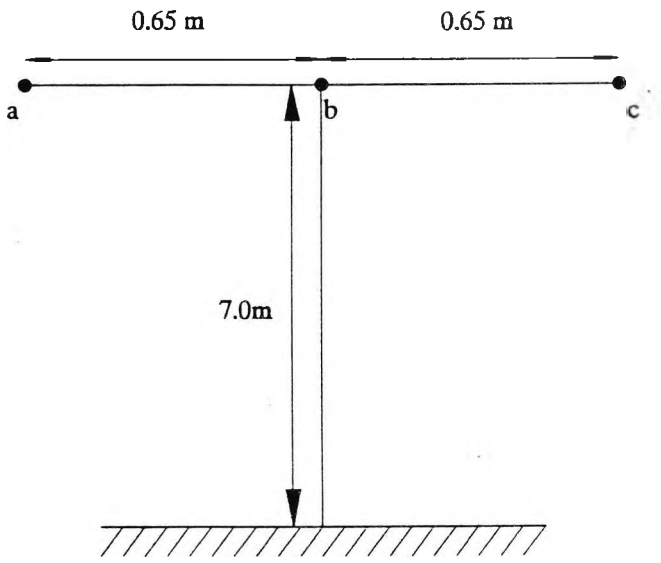

FIG(4.2), LINE CONFIGURATION.

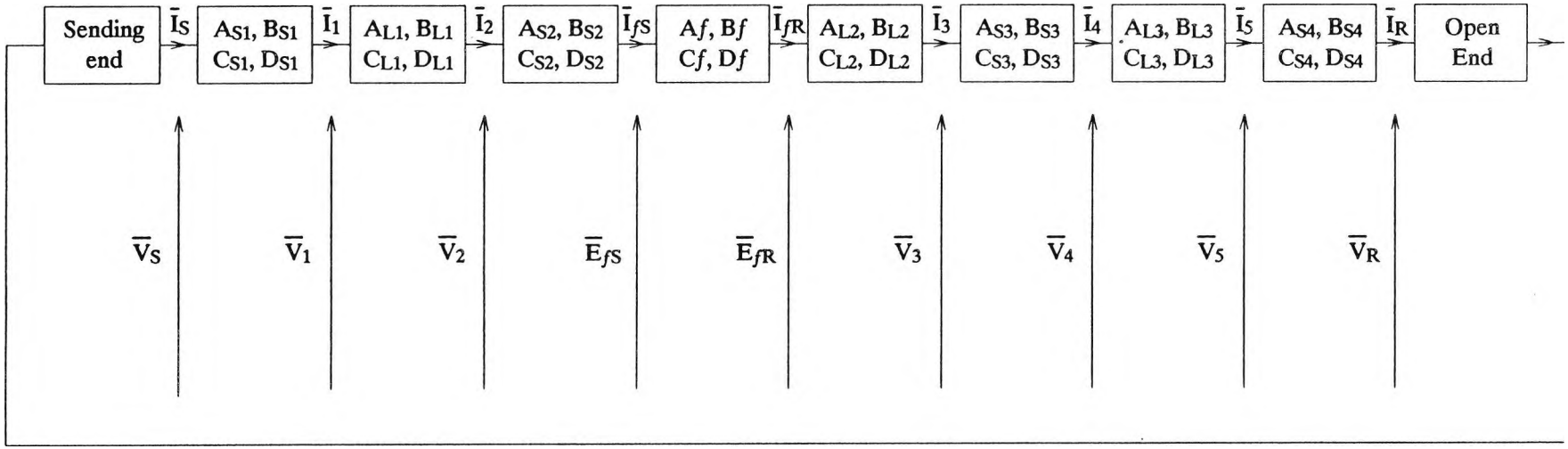

FIG(4.3), FAULT TRANSIENT MODEL OF THE SIMULATED SYSTEM.

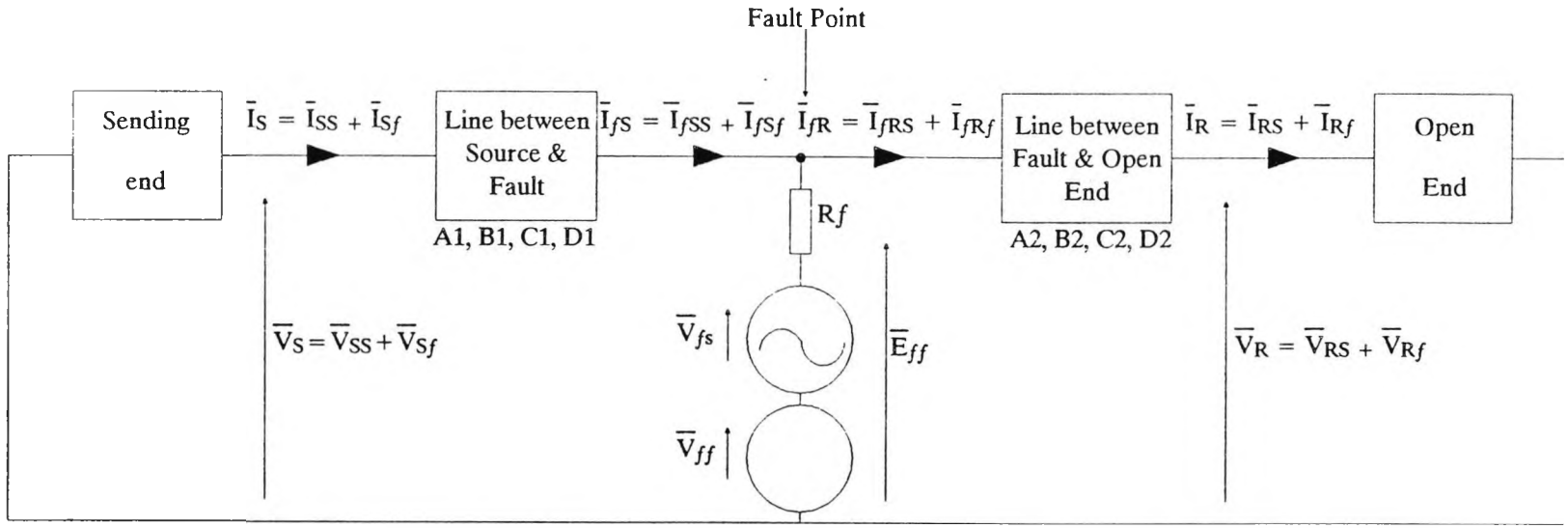

FIG(4.4), FAULT TRANSIENT MODEL UTILISING SUPERIMPOSED FAULT VOLTAGE.

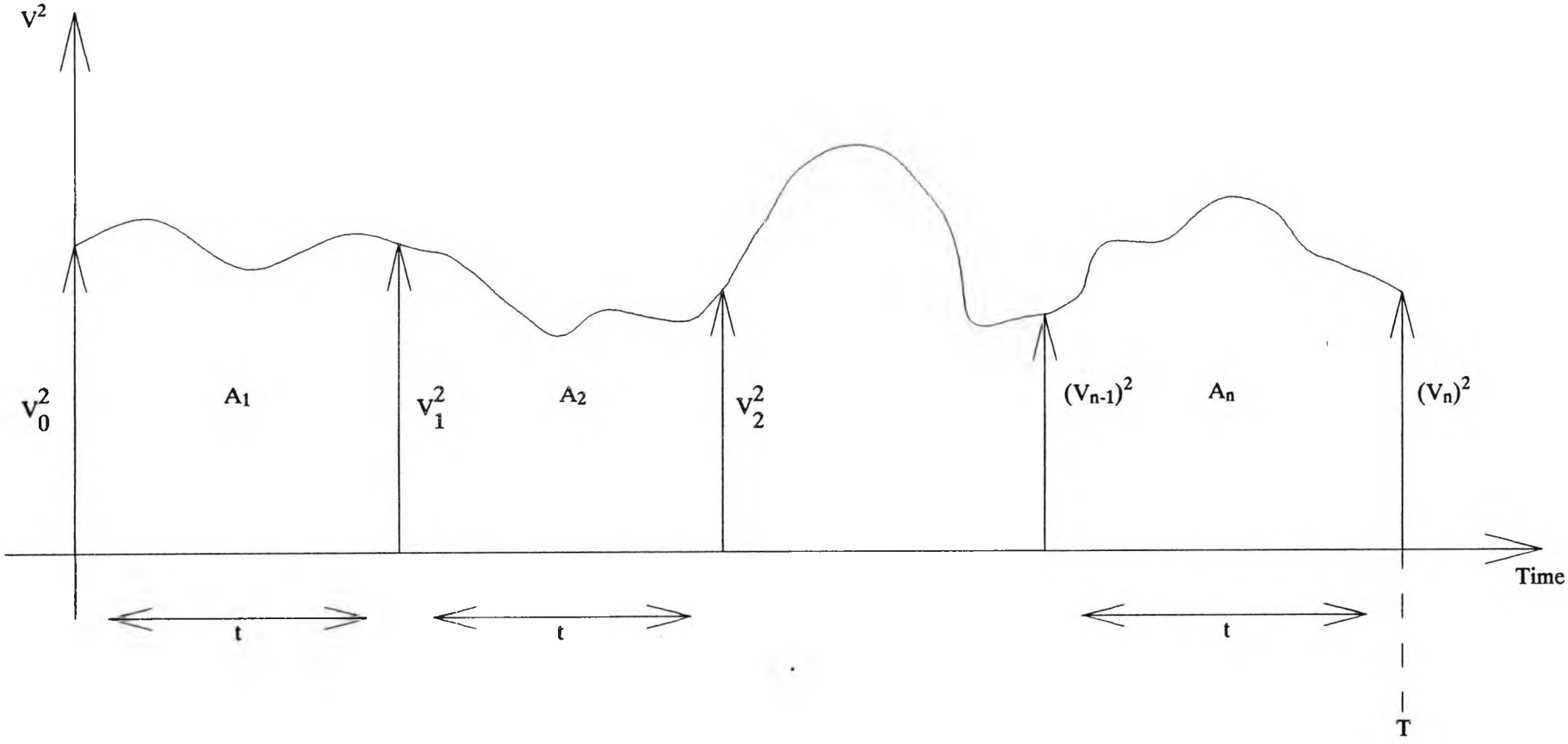

FIG(4.5), USE OF TRAPEZOIDAL RULE TO FIND AREA UNDER A CURVE.

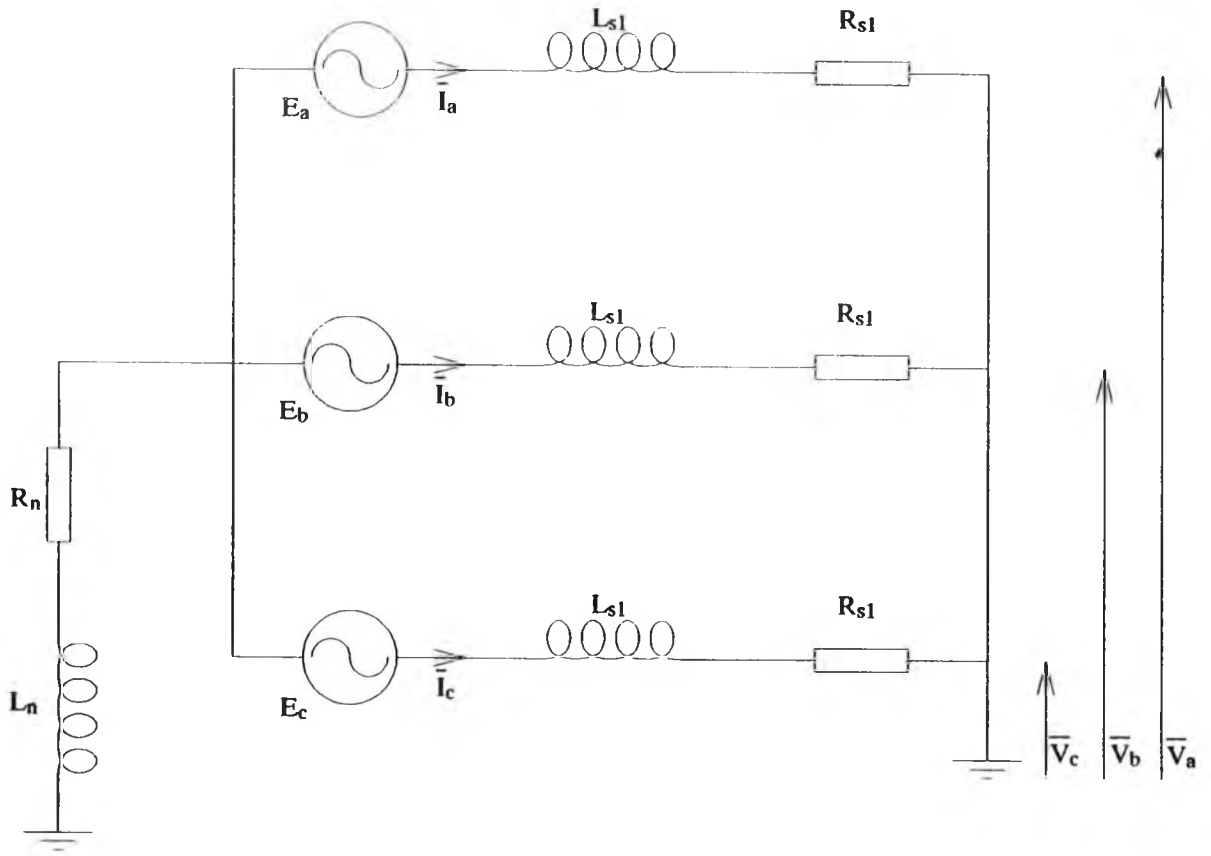

FIG(4.6), SOURCE NETWORK MODEL.

CHAPTER (5)

SENSITIVITY ANALYSIS ON DIRECTIONALITY PROPERTY OF THE NEW EQUIPMENT

5.1 INTRODUCTION

The performance of the new equipment developed has been studied using the program and the techniques described in Chapter (4). In this chapter, the simulation results illustrating the directionality property of the locator are presented. Sensitivity studies were carried to include the effect of fault resistance, fault inception angle, source capacities, fault positions and the effect of type of fault on the performance of this new equipment.

The effect of varying the bandwidth of the stack tuners and line trap circuit of each equipment and that of the bandpass filter are also discussed. Finally the means by which the discrimination margin can be maximised are provided.

5.1.1 SELECTION OF APPROPRIATE SIGNALS

The directionality property of the new fault locator is best illustrated by analysing the fault induced high frequency voltage signals received at sides X and Y of locators $(LOC)_{L1}$ and $(LOC)_{L2}$ due to an in-zone fault at point F1 in Figure (5.1). Note, this figure shows a simple

line diagram in which for a three phase line one locator is connected between each phase and earth. It should also be noted that, the signals received are the voltages across the resistors of the stack tuners employed on both sides of locators $(LOC)_{L1}$ and $(LOC)_{L2}$.

5.2 THE EFFECT OF TYPE OF FAULT

First consider a solid fault between phase (a) and earth with a fault inception angle of 90.0 degrees. Figure (5.2) shows the primary voltage signals, i.e, unfiltered voltages, received across the resistors of the stack tuners of the first locator $(LOC)_{L1}$ at side Y and its corresponding primary voltage signals at side X is shown in Figure (5.3). The filtered response of these signals, after passage through a band-pass filter, are illustrated in Figures (5.4) and (5.5) respectively.

It is clearly evident that, the energy content, E_Y in the voltage signals at side Y is at a higher level than its corresponding energy content, E_X in the voltage signals at side X of the first locator $(LOC)_{L1}$. This is shown in Figure 5.6(a) from which the signal processing network correctly determines the direction of the fault which is downstream. However, by analysing the voltage signals obtained by locator $(LOC)_{L2}$ due to the same fault at F1, it is also correctly determined that, the direction of the fault is upstream. This is shown in Figure 5.6(b), from

which it is clearly evident that, the energy content E_X in the filtered waveforms, at side X of the locator $(LOC)_{L2}$ is at a higher level than its corresponding energy level E_Y at side Y.

The corresponding waveforms for other types of faults are shown as follows:

(i) Figures 5.7(a) and 5.7(b) show the waveforms for a double phase to earth, (a-b-e).

(ii) Figures 5.8(a) and 5.8(b) show the waveforms for a three phase to earth fault, (a-b-c-e).

(iii) Figures 5.9(a) and 5.9(b) show the waveforms for a phase to phase fault, (a-b).

From Figures 5.6(a) to 5.9(b), it is clearly seen that the type of fault does not effect the directionality property of the new equipment as the signal processing network correctly distinguishes between a downstream and upstream fault regardless of its type.

5.3 THE EFFECT OF FAULT RESISTANCE

The effect of fault resistance on the directionality performance of the locator was studied by analysing the signals from the locator $(LOC)_{L1}$ due to a fault at point F1 in Figure (5.1). For a single phase (a) to earth fault with a fault resistance of 100 Ω, the voltage signals

observed across the resistors of the stack tuners of the locator $(LOC)_{L1}$ at sides Y and X are as shown in Figures (5.10) and (5.11) respectively. The corresponding waveforms showing the difference between energy content in the voltage waveforms on either side of the locator for a fault with R_f = 100 Ω and R_f = 50 Ω are shown in Figures (5.12) and (5.13) respectively.

On comparing these Figures with Figure 5.6(a) in which R_f was equal to zero it is clearly seen that, the amount of energy content in the voltage signals appearing on both sides of the locator decreases as the fault resistance R_f increases. This is basically due to the fact that, the high frequency travelling wave components on the line become progressively more damped as the fault resistance increases. There is also a reduction in the primary voltage signals as the fault resistance is increased and this can be seen by comparing Figures (5.10) and (5.11) with Figures (5.2) and (5.3) in which the fault resistance was equal to zero. Finally, Figure 5.13(a) shows the variation of the discrimination margin against the fault resistance over a range of 0Ω-100Ω. This figure clearly shows that, the discrimination margin between the energy levels on both sides of the locator is almost unaffected and does not change much by the value of the fault resistance. For this reason the signal processing network correctly distinguishes between an upstream and a downstream fault.

5.4 THE EFFECT OF FAULT INCEPTION ANGLE

In the results illustrated so far, the faults have been applied at an instant corresponding to voltage maximum in the faulty phase or phases. These are of course the worst cases from the travelling wave point of view. However, the other important extreme is reached when a fault is applied near or at zero voltage. Figures (5.14) and (5.15) show the primary voltage signals received by the locator $(LOC)_{L1}$ due to a fault at point F1 in Figure (5.1) with a fault inception angle of 5.0 degrees.

On comparing these waveforms with Figures (5.2) and (5.3), it is clearly evident that, the travelling waves are reduced. This is because there is not a large and sudden voltage change at the point of fault and the distortion is therefore extremely small. However, no matter how small the distortion is, Figure (5.16) shows that, the discrimination margin between the energy contents of voltage waveforms sampled on both sides of the locator $(LOC)_{L1}$, is still of the same order as that of the case with a fault inception angle of 90.0 degrees, previously shown in Figure 5.6(a).

The variation of the discrimination margin between 0.0 to 90.0 degrees is further illustrated in Figure 5.16(a). This clearly shows that, the energy content in

the voltage signals for a fault at 0.0 degrees is zero and that the directionality property of the new equipment is almost independent of the fault inception angle from 1 to 90 degrees.

5.5 THE EFFECT OF SOURCE CAPACITY

The directionality performance of the new equipment has been also studied under different source capacities. Figures (5.17) and (5.18) show the comparison between the energy content in the signals on both sides of the locator for short-circuit level of 150 MVA and 50 MVA respectively. Figure (5.19) shows the variation of the discrimination margin against short-circuit level from 50 MVA to 250 MVA. Although there is a reduction in the discrimination margin between the energy levels obtained from both sides of the new locator as the short-circuit level decreases, the locator however still does correctly distinguish between an upstream and a downstream fault under different source capacities.

5.6 THE EFFECT OF FAULT POSITION

The sensitivity analysis carried out on the signals received by locator $(LOC)_{L1}$ in Figure (5.1) so far, have been due to a fault placed at a point on the line very close to the locator $(LOC)_{L2}$. The effect of fault position has been studied by analysing signals observed by $(LOC)_{L1}$

due to different fault positions on the line section between $(LOC)_{L1}$ and $(LOC)_{L2}$. Figure (5.20) shows the variation of the discrimination margin against fault position. It is clearly evident that, the discrimination margin for distinguishing between upstream and downstream faults does not change much and it is almost independent of fault positions.

5.7 THE EFFECT OF VARYING THE BANDWIDTH

In the results illustrated so far, a bandwidth of 5.0 kHz for the stack tuners and line trap circuit of each locator has been used. Figure (5.21) shows that, with the centre frequency f_c kept constant at 90.0 kHz, if the bandwidth is varied between 5kHz to 10kHz, neither the discrimination margin nor the directionality of the new equipment is affected to any significant extend.

Figure (5.22) illustrates the effect of altering the bandwidth of the bandpass filter; this filter is used for processing the primary voltage signals and maximising the discrimination margin between the two sides of the locator. It should be appreciated that, all the sensitivity analyses so far, have been carried out for the minimum discrimination margin obtained with the bandpass filter tuned to a bandwidth of 1200 Hz. However, Figure (5.22) shows that, the maximum discrimination margin is obtained when the filter is tuned to the same bandwidth as

that of the stack tuners and line trap circuit of each locator, which in this case is 5.0kHz.

5.9 MAXIMISATION OF DISCRIMINATION MARGIN

The sensitivity analysis presented in previous sections are the results of using a centre frequency of 90.0kHz for both the stack tuners and line trap circuit of each locator.

However, further simulation studies have shown that, in order to maximise the discrimination margin between the energy content on both sides of the locator, a higher centre frequency of 270kHz should be used. The parameter values of the locator at centre frequency of 270kHz are outlined in Appendix 5A. Figures (5.23) and (5.24) show the corresponding voltage signals to those of Figures (5.2) and (5.3), but with the stack tuners and line trap circuit tuned to a centre frequency of 270kHz. Their corresponding filtered response after passage through a bandpass filter, tuned to the centre frequency of 270kHz, are shown in Figures (5.25) and (5.26). Finally Figure (5.27) shows the comparison between energy content in the filtered waveforms of Figures (5.25) and (5.26).

On comparing Figure (5.27) obtained at a centre frequency of 270kHz with its corresponding waveform of Figure 5.6(a) obtained at a centre frequency of 90kHz, it

is clearly evident that the discrimination margin between the energy levels on both sides of the locator has considerably increased.

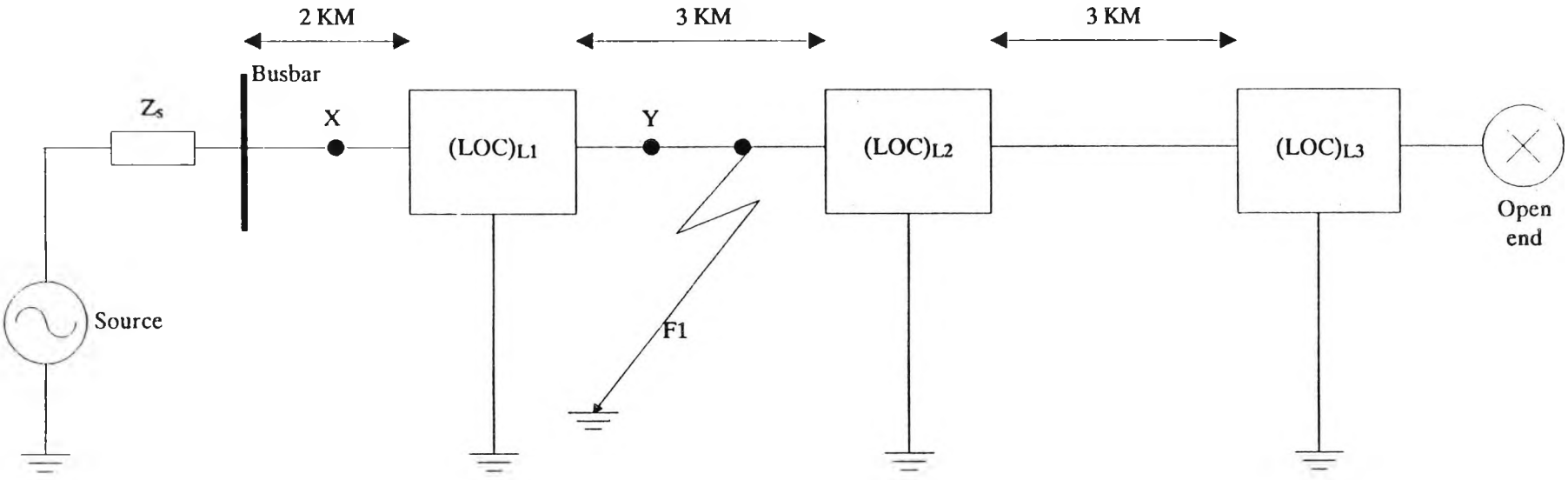

FIG (5.1), SCHEMATIC DIAGRAM OF THE SYSTEM SIMULATED PER PHASE WITH AN IN-ZONE FAULT, F1

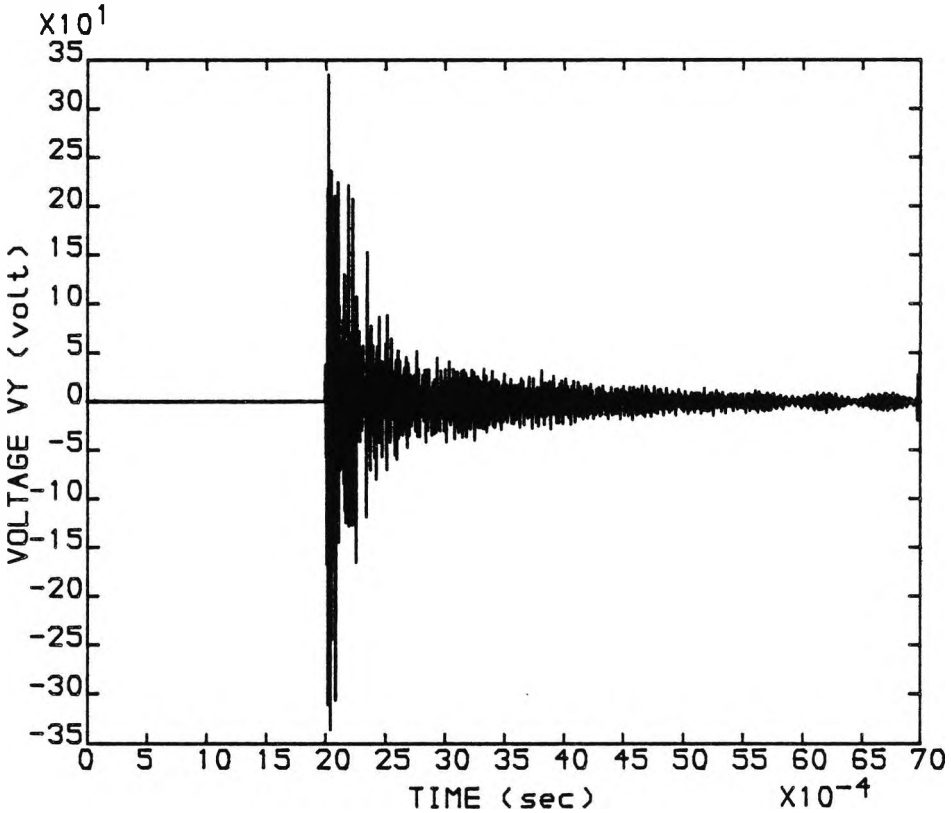

FIG(5.2). VY OF (LOC)L1 DUE TO A FAULT AT POINT F1. WITH fc = 90.0 (kHz)

SHORT-CIRCUIT LEVEL = 250 MVA

FAULT RESISTANCE = 0.0 (ohms)

TYPE OF FAULT : [a-e]

FAULT INCEPTION ANGLE = 90.0 (degrees)

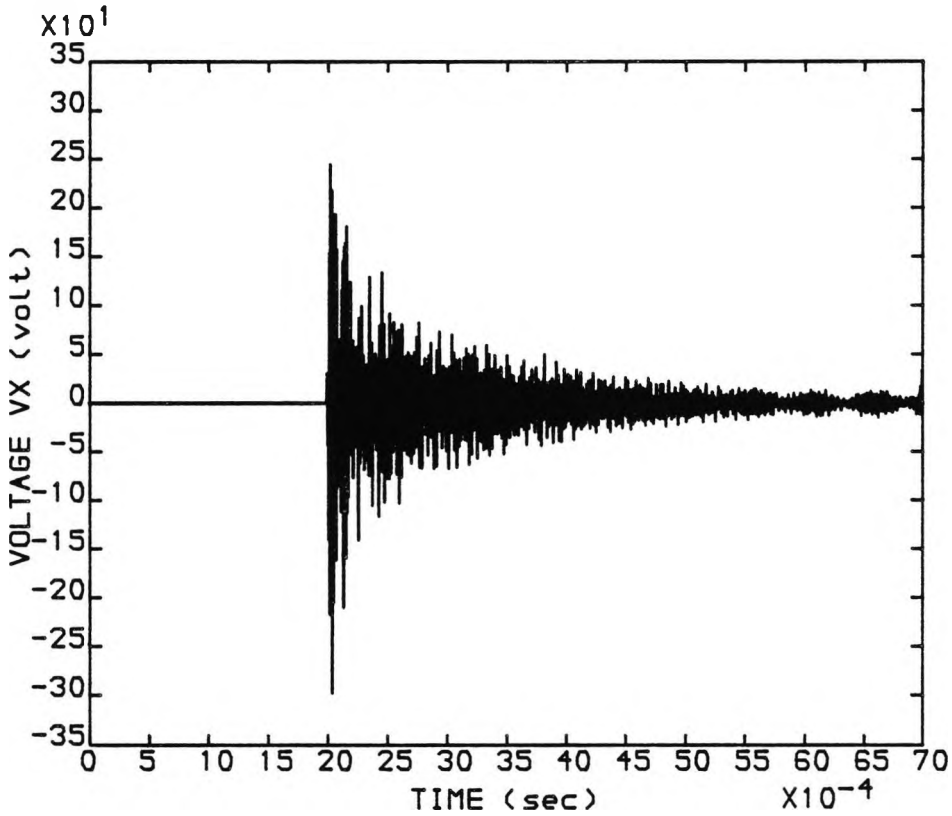

FIG(5.3). VX OF (LOC)L1 DUE TO A FAULT AT POINT F1, WITH fc = 90.0 (kHz)

SHORT-CIRCUIT LEVEL = 250 MVA

FAULT RESISTANCE = 0.0 (ohms)

TYPE OF FAULT : [a-e]

FAULT INCEPTION ANGLE = 90.0 (degrees)

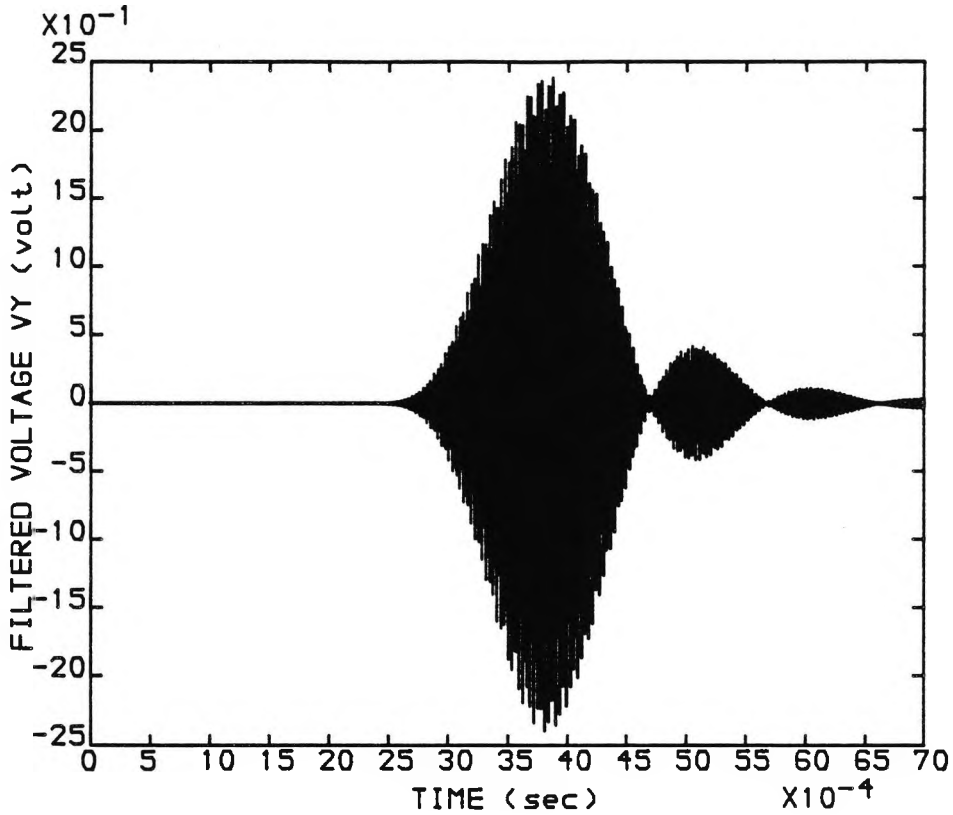

FIG(5.4). FILTERED VY OF (LOC)L1 DUE TO A FAULT AT POINT F1. WITH fc = 90.0 (kHz)

SHORT-CIRCUIT LEVEL = 250 MVA

FAULT RESISTANCE = 0.0 (ohms)

TYPE OF FAULT : [a-e]

FAULT INCEPTION ANGLE = 90.0 (degrees)

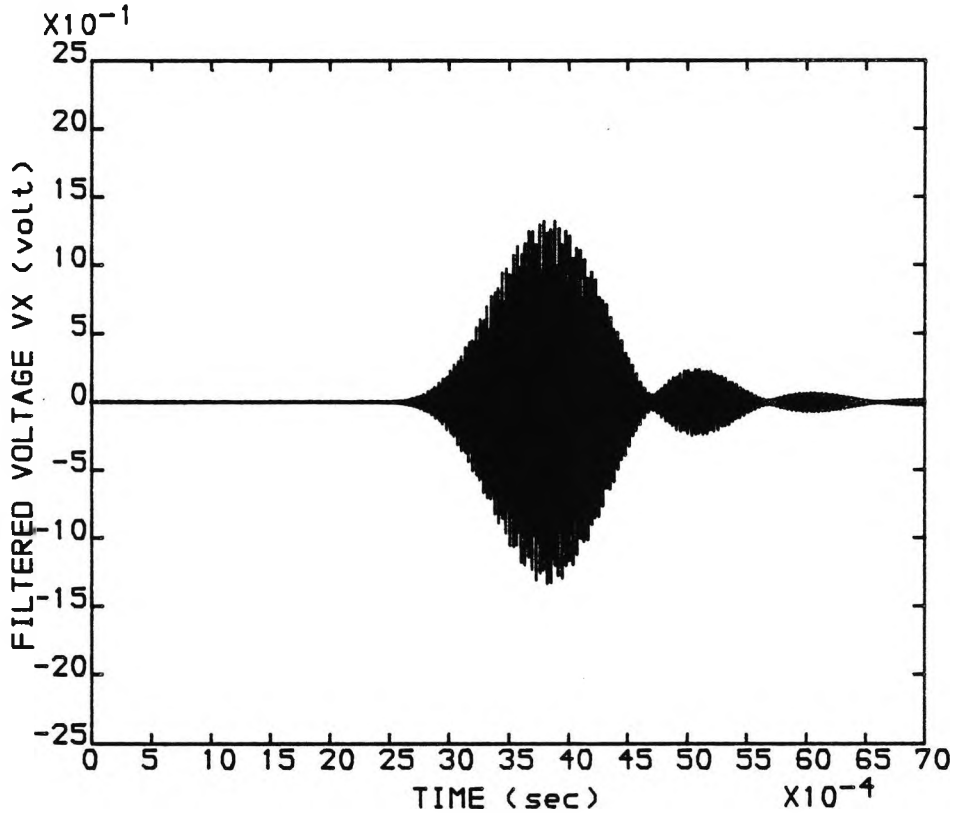

FIG(5.5). FILTERED VX OF (LOC)L1 DUE TO A FAULT AT POINT F1, WITH fc = 90.0 (kHz)

SHORT-CIRCUIT LEVEL = 250 MVA

FAULT RESISTANCE = 0.0 (ohms)

TYPE OF FAULT : [a-e]

FAULT INCEPTION ANGLE = 90.0 (degrees)

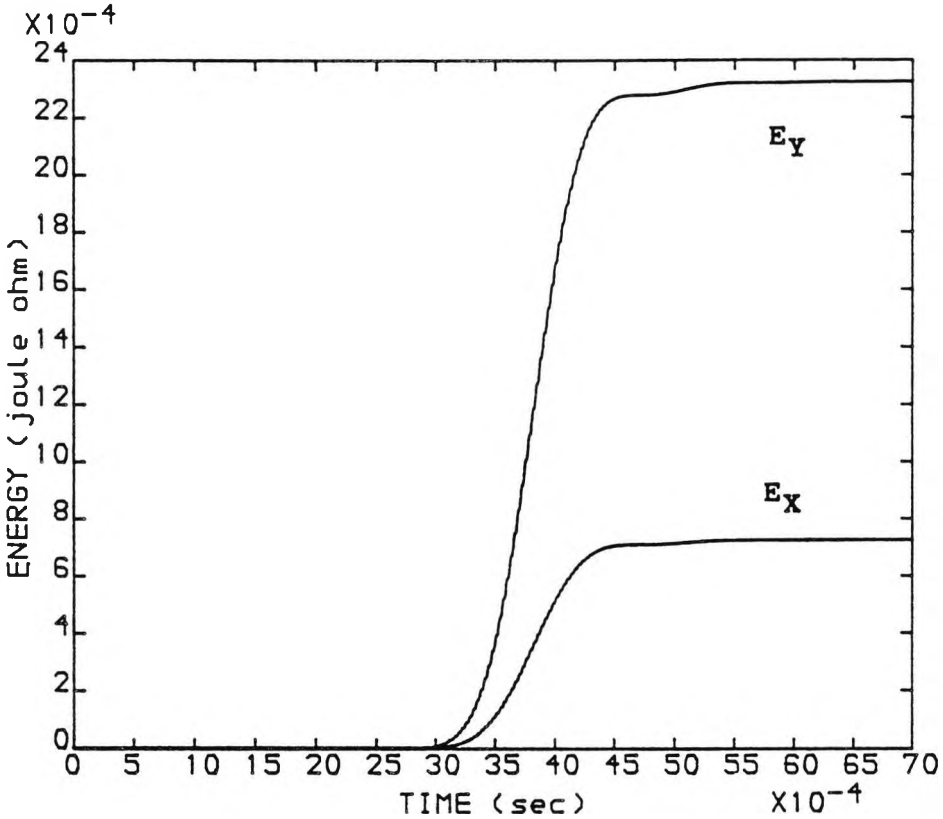

FIG 5.6(a). ENERGY COMPARISON BY (LOC) L1 DUE TO A FAULT AT POINT F1, WITH fc = 90.0 (kHz)

SHORT-CIRCUIT LEVEL = 250 MVA

FAULT RESISTANCE = 0.0 (ohms)

TYPE OF FAULT : [a-e]

FAULT INCEPTION ANGLE = 90.0 (degrees)

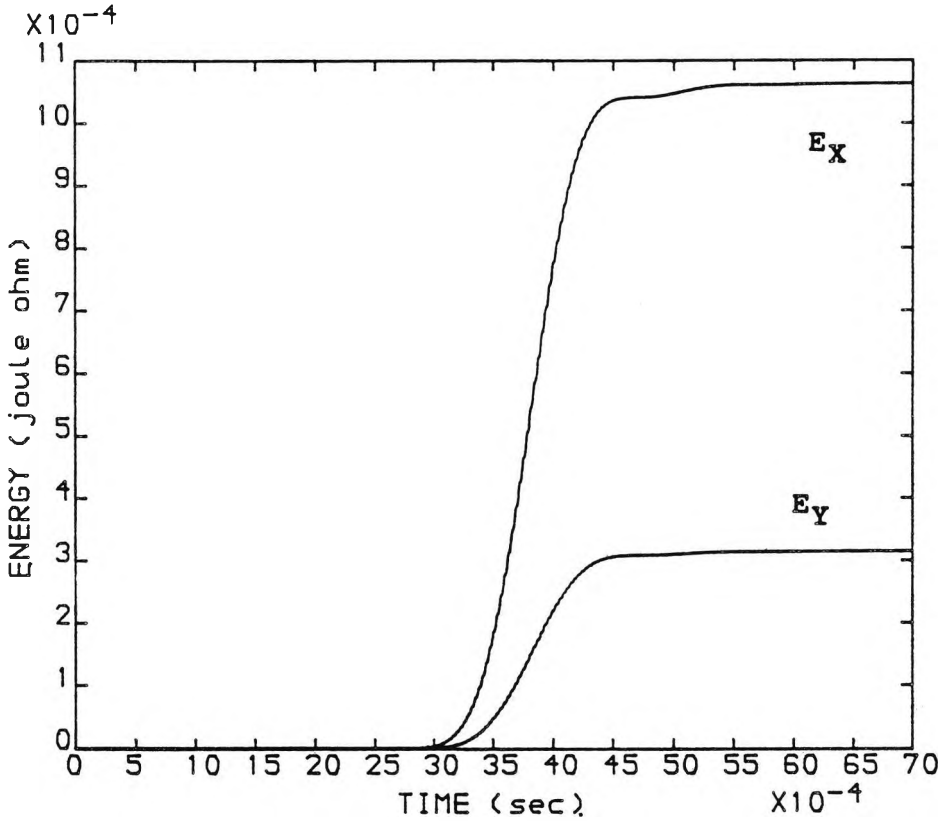

FIG 5.6(b). ENERGY COMPARISON BY (LOC)L2 DUE TO A FAULT AT POINT F1. WITH fc = 90.0 (kHz)

SHORT-CIRCUIT LEVEL = 250 MVA

FAULT RESISTANCE = 0.0 (ohms)

TYPE OF FAULT : [a-e]

FAULT INCEPTION ANGLE = 90.0 (degrees)

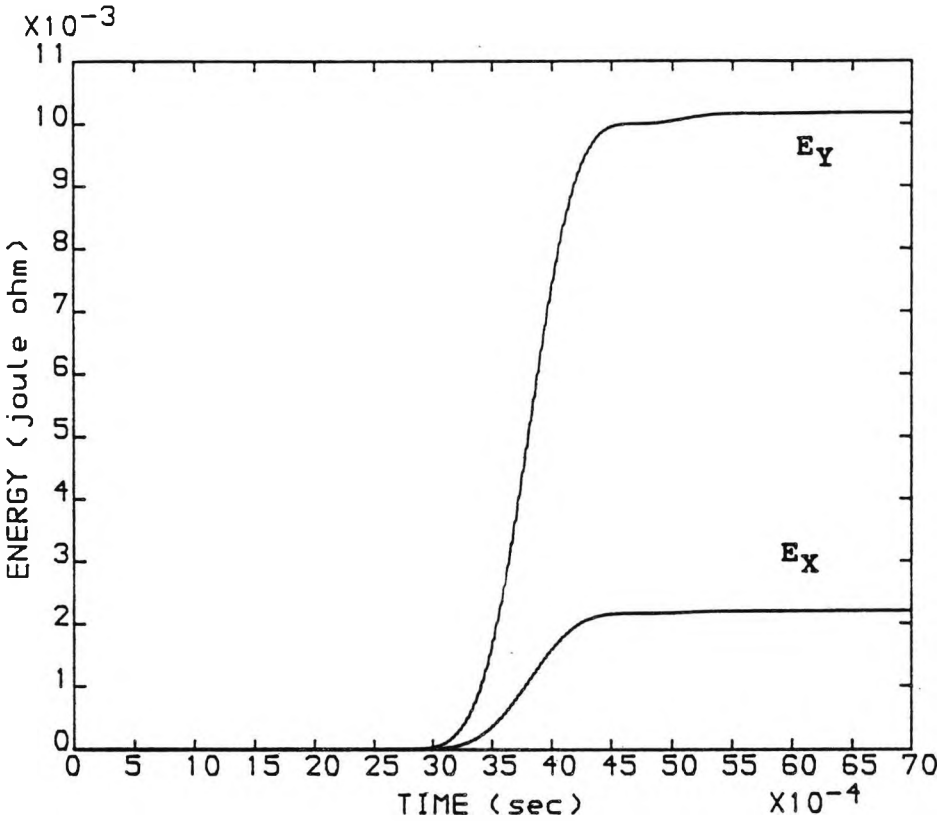

FIG 5.7 (a). ENERGY COMPARISON BY (LOC) L1 DUE TO A FAULT AT POINT F1. WITH fc = 90.0 (kHz)

SHORT-CIRCUIT LEVEL = 250 MVA

FAULT RESISTANCE = 0.0 (ohms)

TYPE OF FAULT : [a-b-e]

FAULT INCEPTION ANGLE = 90.0 (degrees)

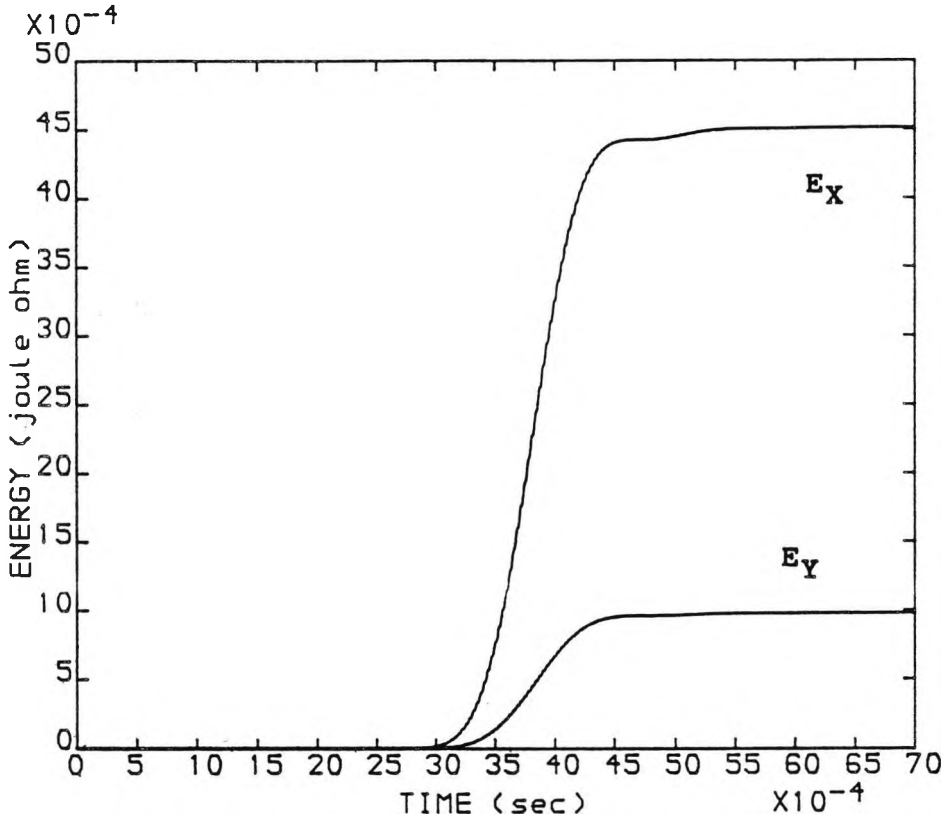

FIG 5.7(b). ENERGY COMPARISON BY (LOC) L2 DUE TO A FAULT AT POINT F1. WITH fc = 90.0 (kHz)

SHORT-CIRCUIT LEVEL = 250 MVA

FAULT RESISTANCE = 0.0 (ohms)

TYPE OF FAULT : [a-b-e]

FAULT INCEPTION ANGLE = 90.0 (degrees)

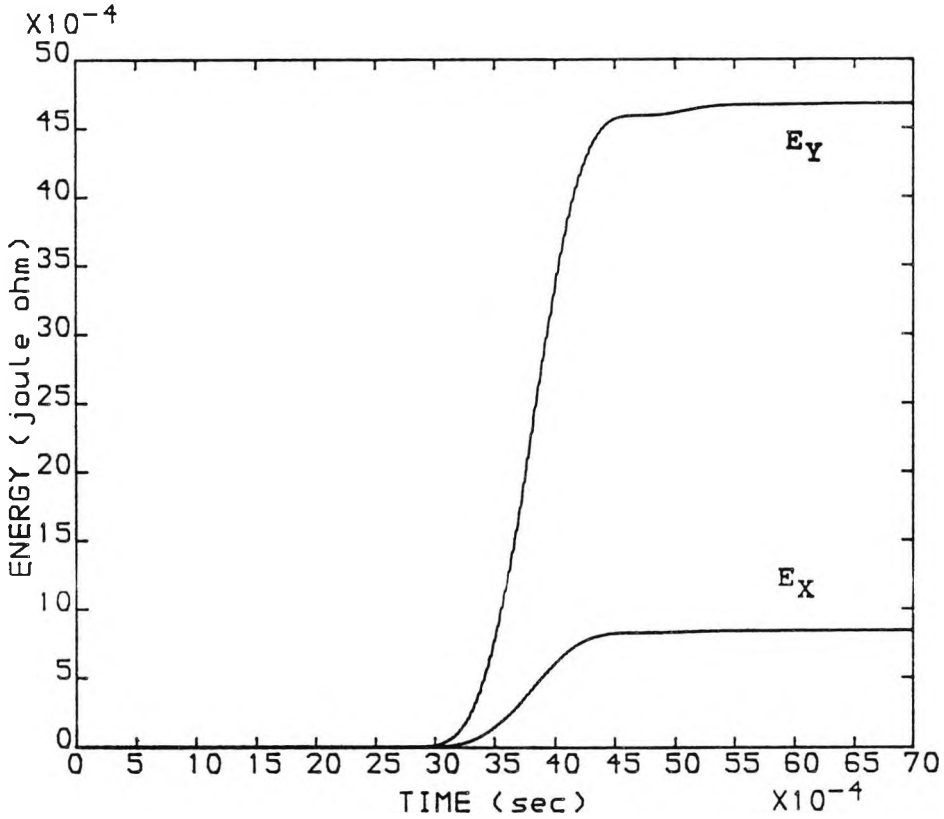

FIG 5.8(a). ENERGY COMPARISON BY (LOC) L1 DUE TO A FAULT AT POINT F1. WITH fc = 90.0 (kHz)

SHORT-CIRCUIT LEVEL = 250 MVA

FAULT RESISTANCE = 0.0 (ohms)

TYPE OF FAULT : [a-b-c-e]

FAULT INCEPTION ANGLE = 90.0 (degrees)

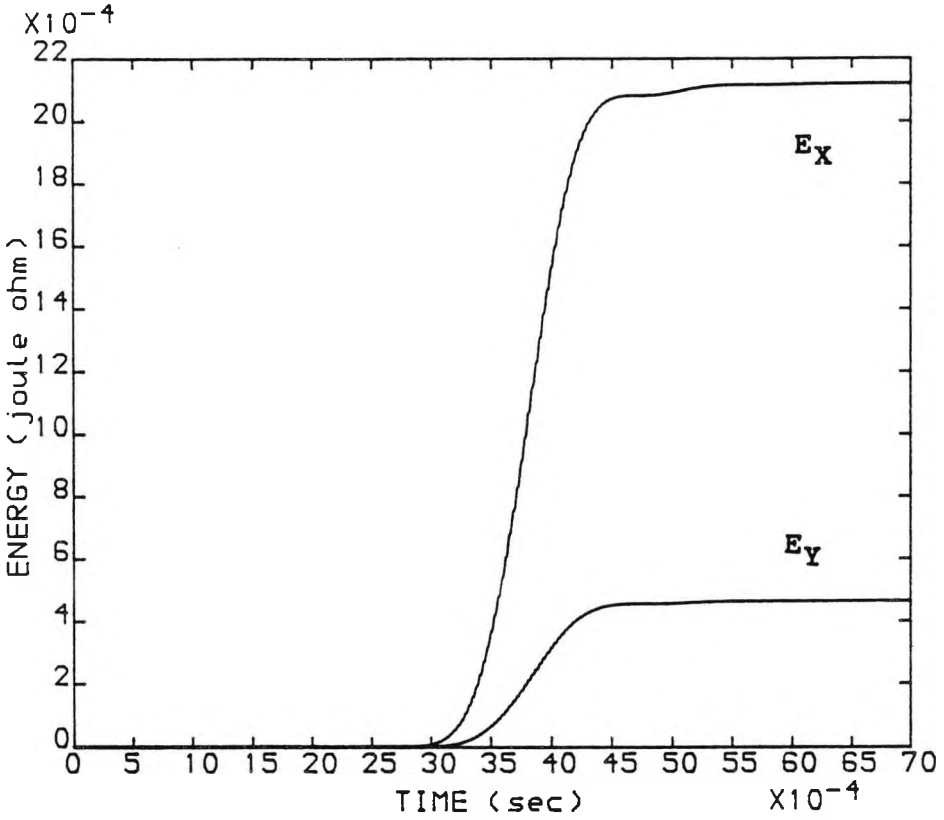

FIG 5.8(b). ENERGY COMPARISON BY (LOC) L2 DUE TO A FAULT AT POINT F1. WITH fc = 90.0 (kHz)

SHORT-CIRCUIT LEVEL = 250 MVA

FAULT RESISTANCE = 0.0 (ohms)

TYPE OF FAULT : [a-b-c-e]

FAULT INCEPTION ANGLE = 90.0 (degrees)

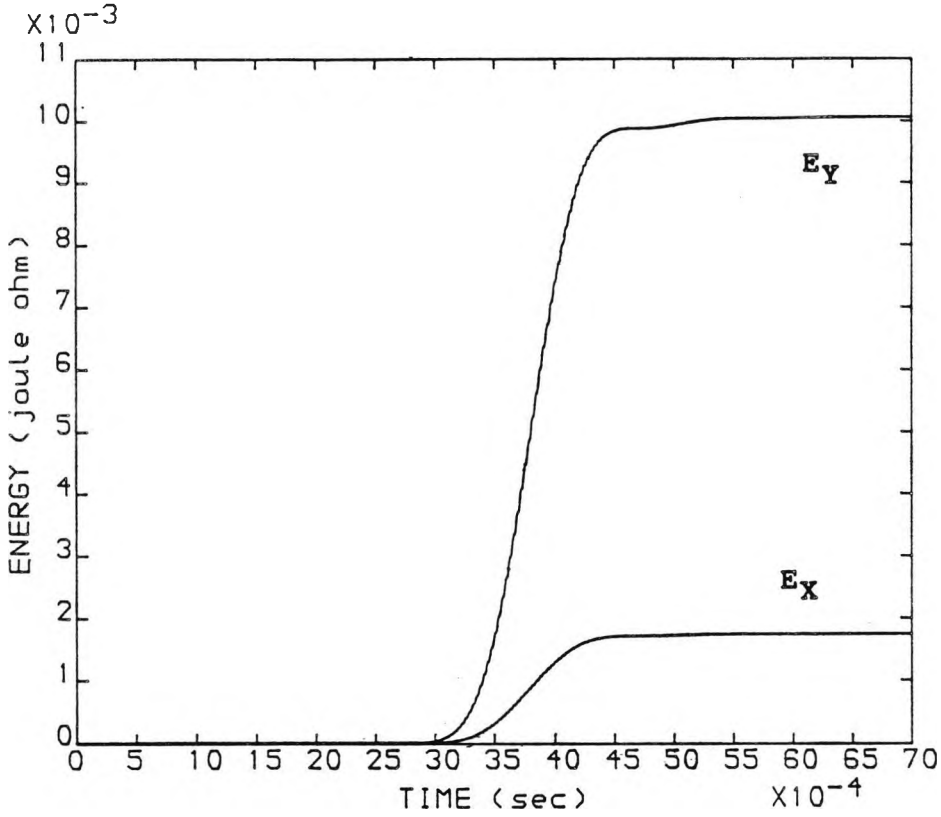

FIG 5.9(a). ENERGY COMPARISON BY (LOC) L1 DUE TO A FAULT AT POINT F1. WITH fc = 90.0 (kHz)

SHORT-CIRCUIT LEVEL = 250 MVA

FAULT RESISTANCE = 0.0 (ohms)

TYPE OF FAULT : [a-b]

FAULT INCEPTION ANGLE = 90.0 (degrees)

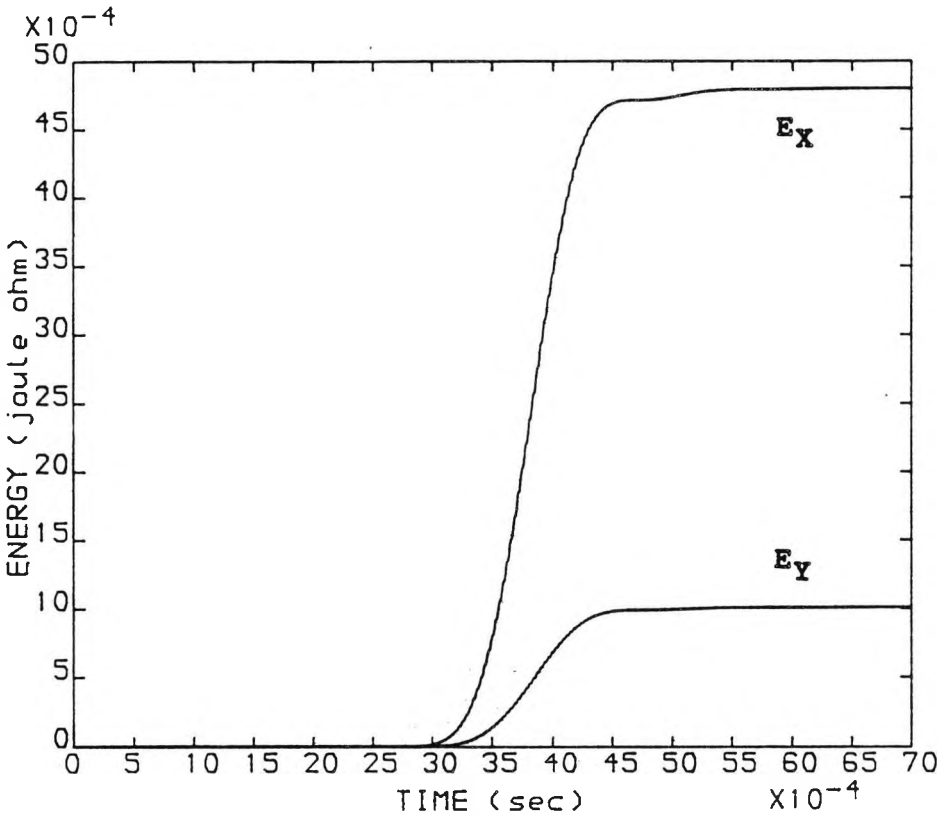

FIG 5.9(b). ENERGY COMPARISON BY (LOC) L2 DUE TO A FAULT AT POINT F1, WITH fc = 90.0 (kHz)

SHORT-CIRCUIT LEVEL = 250 MVA

FAULT RESISTANCE = 0.0 (ohms)

TYPE OF FAULT : [a-b]

FAULT INCEPTION ANGLE = 90.0 (degrees)

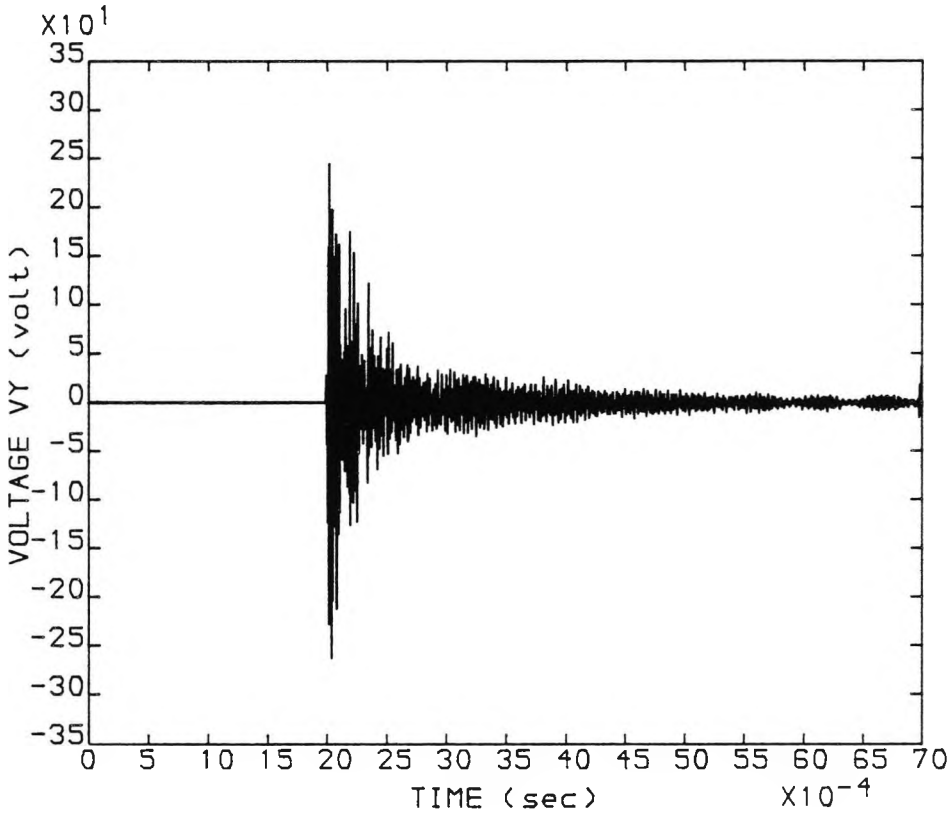

FIG(5.10). VY OF (LOC)L1 DUE TO A FAULT AT POINT F1, WITH fc = 90.0 (kHz)

SHORT-CIRCUIT LEVEL = 250 MVA

FAULT RESISTANCE = 100.0 (ohms)

TYPE OF FAULT : [a-e]

FAULT INCEPTION ANGLE = 90.0 (degrees)

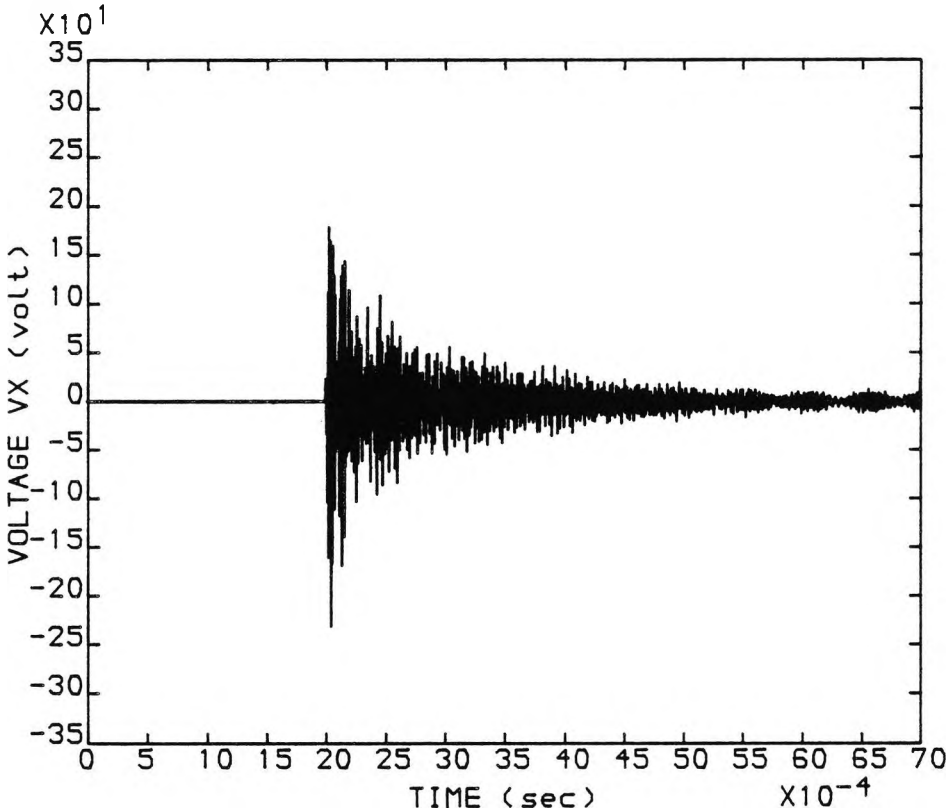

FIG(5.11). VX OF (LOC)L1 DUE TO A FAULT AT POINT F1, WITH fc = 90.0 (kHz)

SHORT-CIRCUIT LEVEL = 250 MVA

FAULT RESISTANCE = 100.0 (ohms)

TYPE OF FAULT : [a-e]

FAULT INCEPTION ANGLE = 90.0 (degrees)

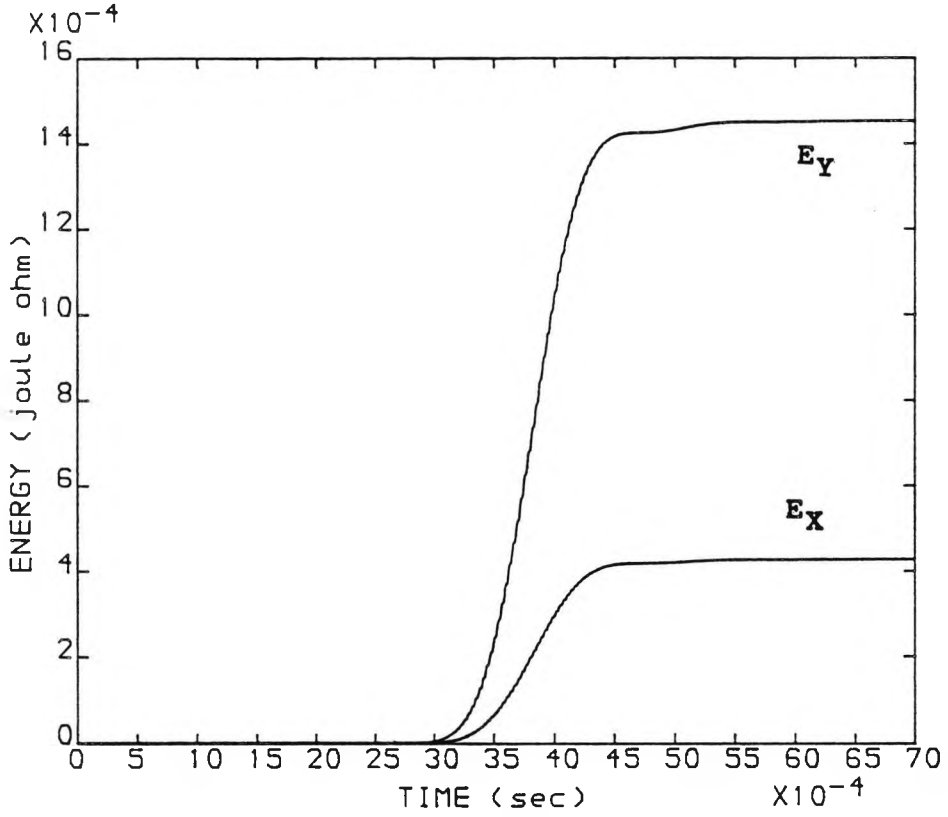

FIG (5.12). ENERGY COMPARISON BY (LOC) L1 DUE TO A FAULT AT POINT F1. WITH fc = 90.0 (kHz)

SHORT-CIRCUIT LEVEL = 250 MVA

FAULT RESISTANCE = 100.0 (ohms)

TYPE OF FAULT : [a-e]

FAULT INCEPTION ANGLE = 90.0 (degrees)

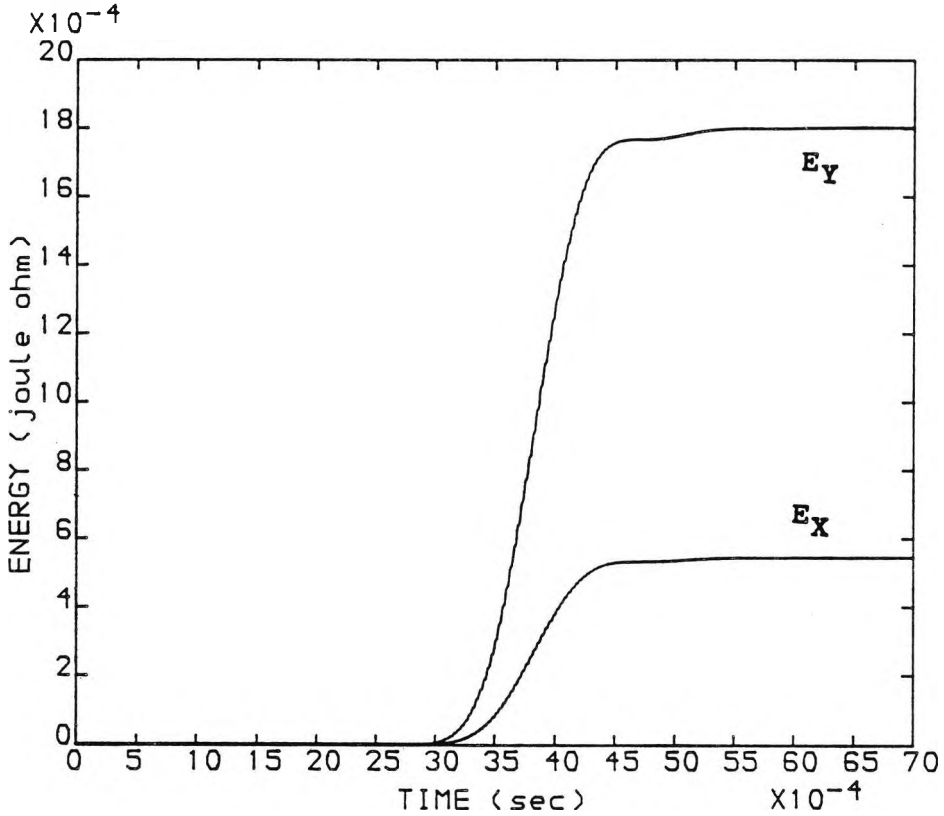

FIG (5.13). ENERGY COMPARISON BY (LOC) L1 DUE TO A FAULT AT POINT F1. WITH fc = 90.0 (kHz)

SHORT-CIRCUIT LEVEL = 250 MVA

FAULT RESISTANCE = 50.0 (ohms)

TYPE OF FAULT : [a-e]

FAULT INCEPTION ANGLE = 90.0 (degrees)

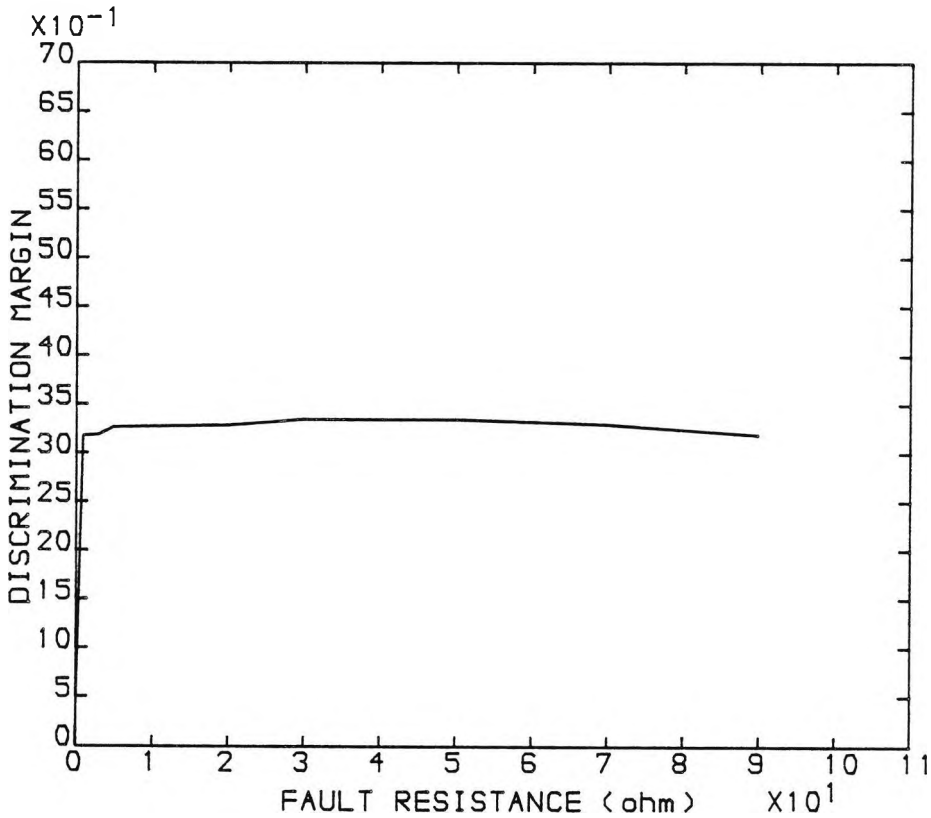

FIG 5.13(a). VARIATION OF DISCRIMINATION MARGIN AGAINST FAULT RESISTANCE

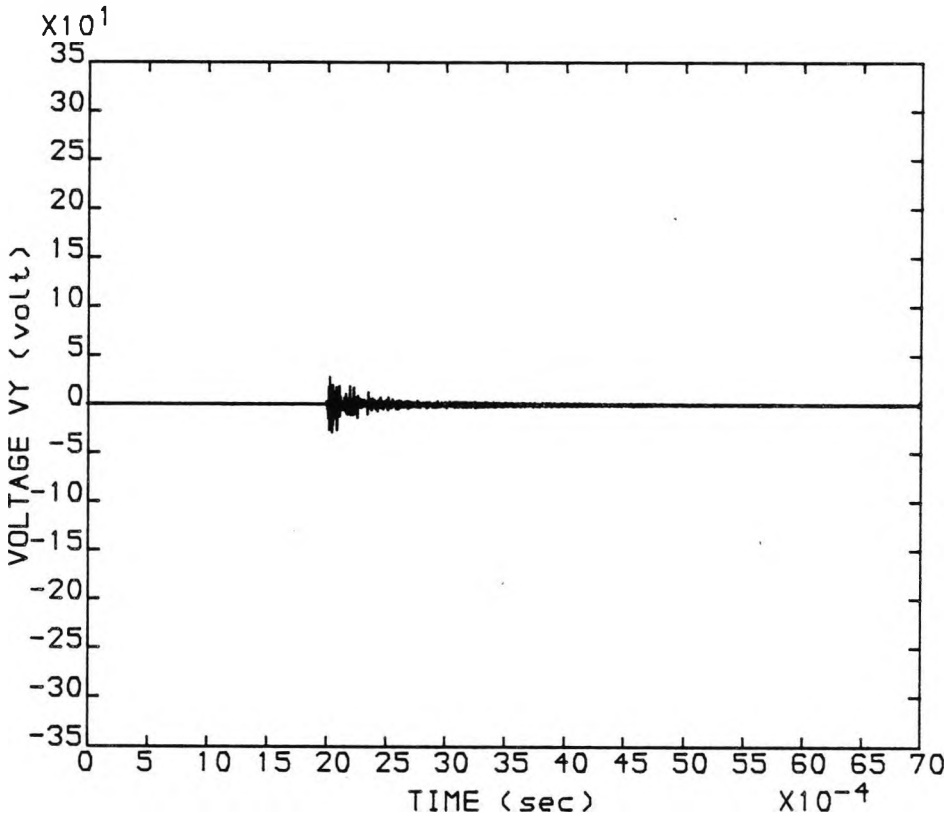

FIG(5.14), VY OF (LOC)L1 DUE TO A FAULT AT POINT F1, WITH fc = 90.0 (kHz)

SHORT-CIRCUIT LEVEL = 250 MVA

FAULT RESISTANCE = 0.0 (ohms)

TYPE OF FAULT : [a-e]

FAULT INCEPTION ANGLE = 5.0 (degrees)

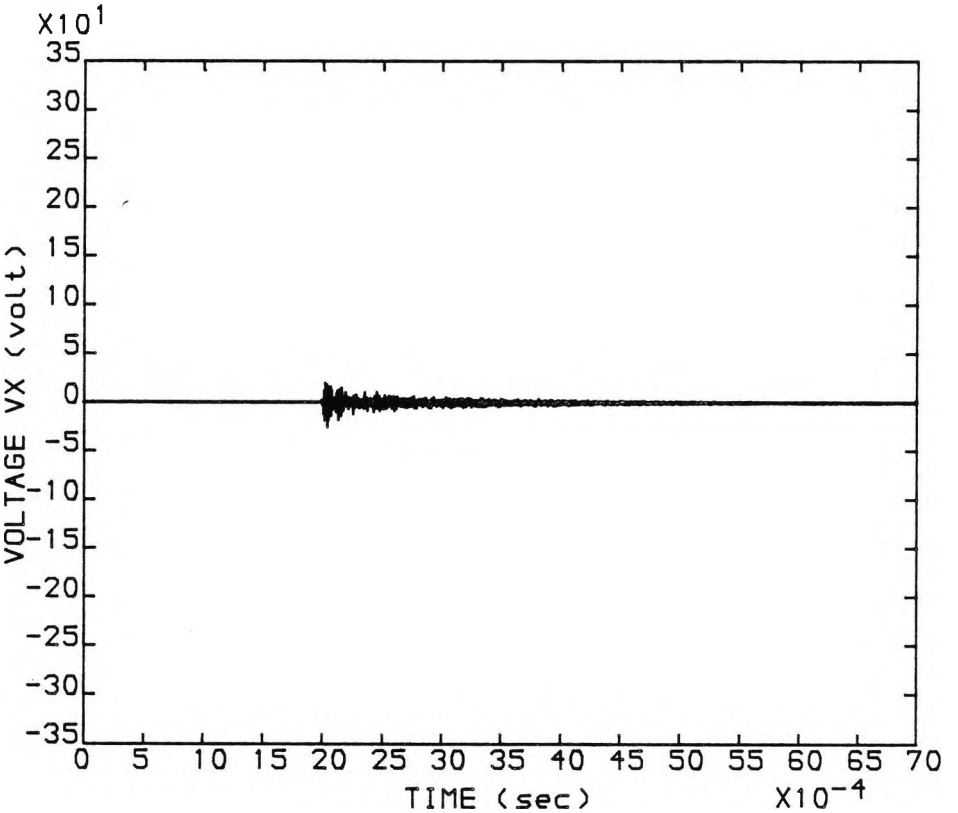

FIG(5.15), VX OF (LOC)L1 DUE TO A FAULT AT POINT F1, WITH fc = 90.0 (kHz)

SHORT-CIRCUIT LEVEL = 250 MVA

FAULT RESISTANCE = 0.0 (ohms)

TYPE OF FAULT : [a-e]

FAULT INCEPTION ANGLE = 5.0 (degrees)

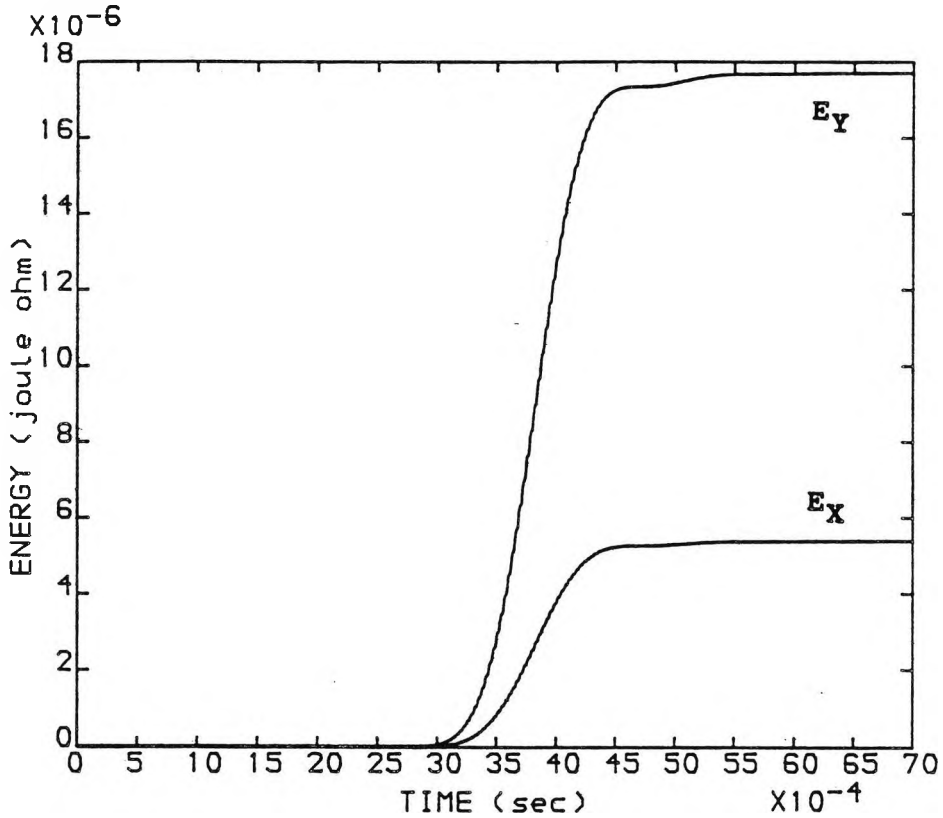

FIG (5.16). ENERGY COMPARISON BY (LOC) L1 DUE TO A FAULT AT POINT F1, WITH fc = 90.0 (kHz)

SHORT-CIRCUIT LEVEL = 250 MVA

FAULT RESISTANCE = 0.0 (ohms)

TYPE OF FAULT : [a-e]

FAULT INCEPTION ANGLE = 5.0 (degrees)

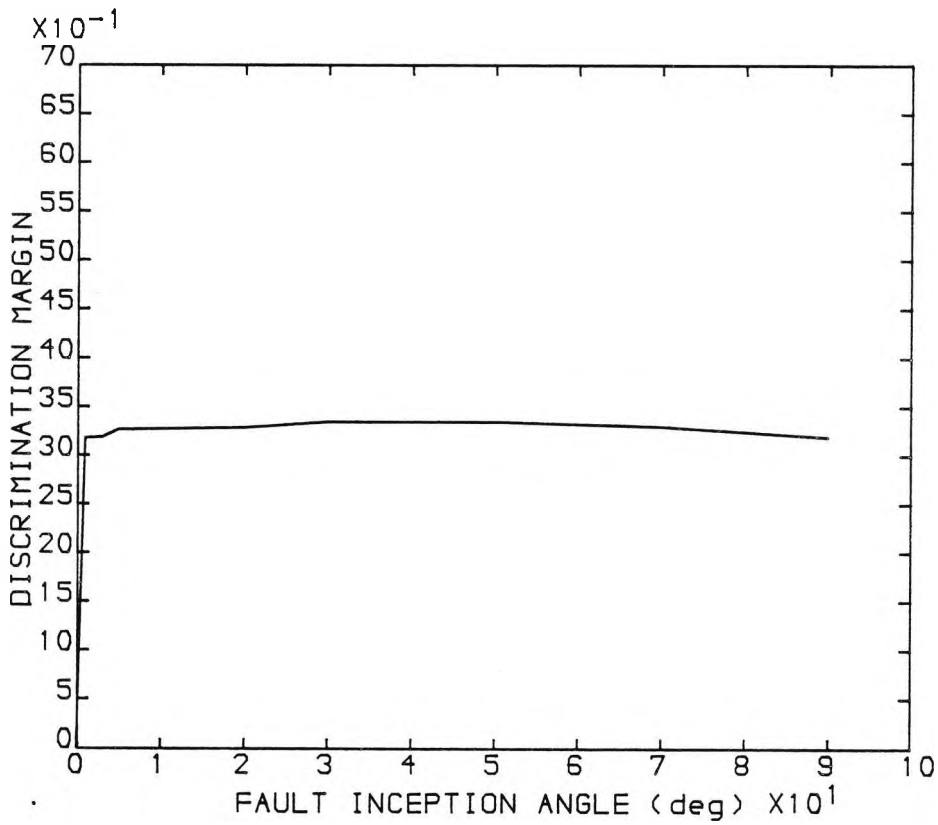

FIG 5.16(a). VARIATION OF DISCRIMINATION MARGIN AGAINST FAULT INCEPTION ANGLE

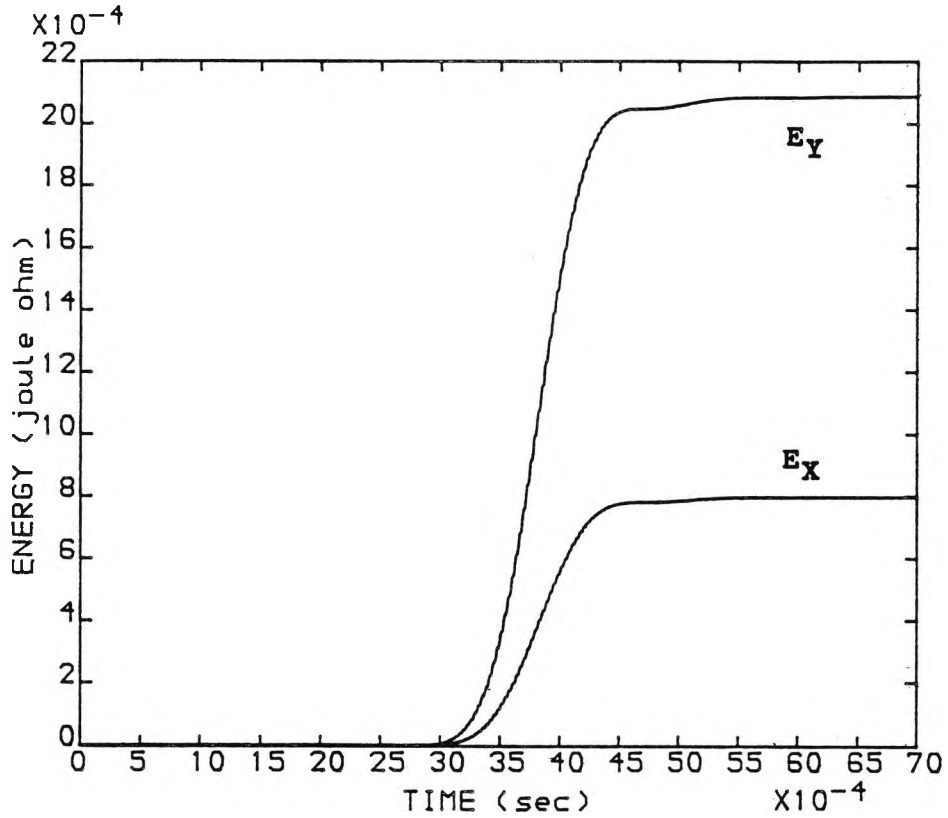

FIG (5.17). ENERGY COMPARISON BY (LOC) L1 DUE TO A FAULT AT POINT F1, WITH fc = 90.0 (kHz)

SHORT-CIRCUIT LEVEL = 150 MVA

FAULT RESISTANCE = 0.0 (ohms)

TYPE OF FAULT : [a-e]

FAULT INCEPTION ANGLE = 90.0 (degrees)

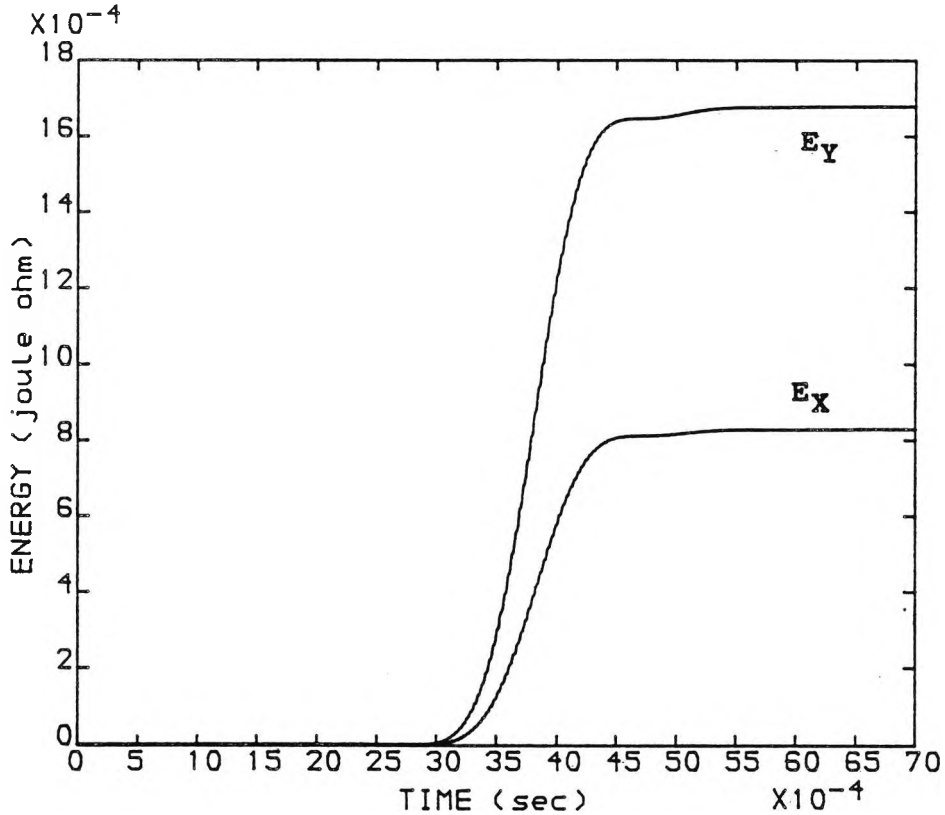

FIG (5.18). ENERGY COMPARISON BY (LOC) L1 DUE TO A FAULT AT POINT F1. WITH fc = 90.0 (kHz)

SHORT-CIRCUIT LEVEL = 50 MVA

FAULT RESISTANCE = 0.0 (ohms)

TYPE OF FAULT : [a-e]

FAULT INCEPTION ANGLE = 90.0 (degrees)

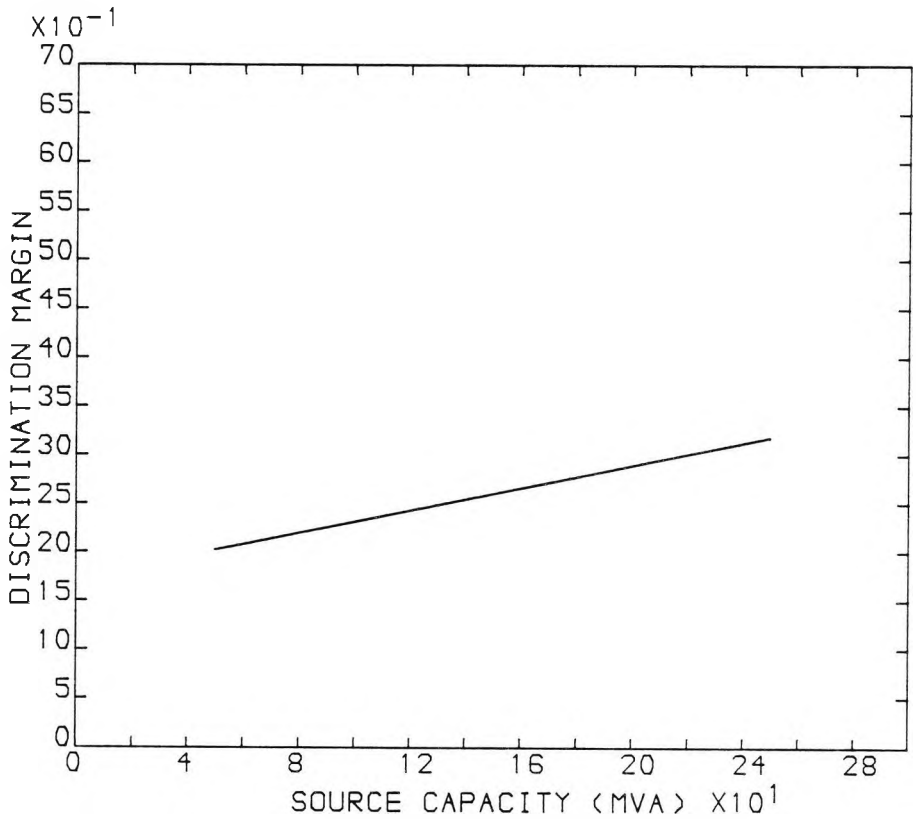

FIG (5.19), VARIATION OF DISCRIMINATION MARGIN AGAINST SOURCE CAPACITY

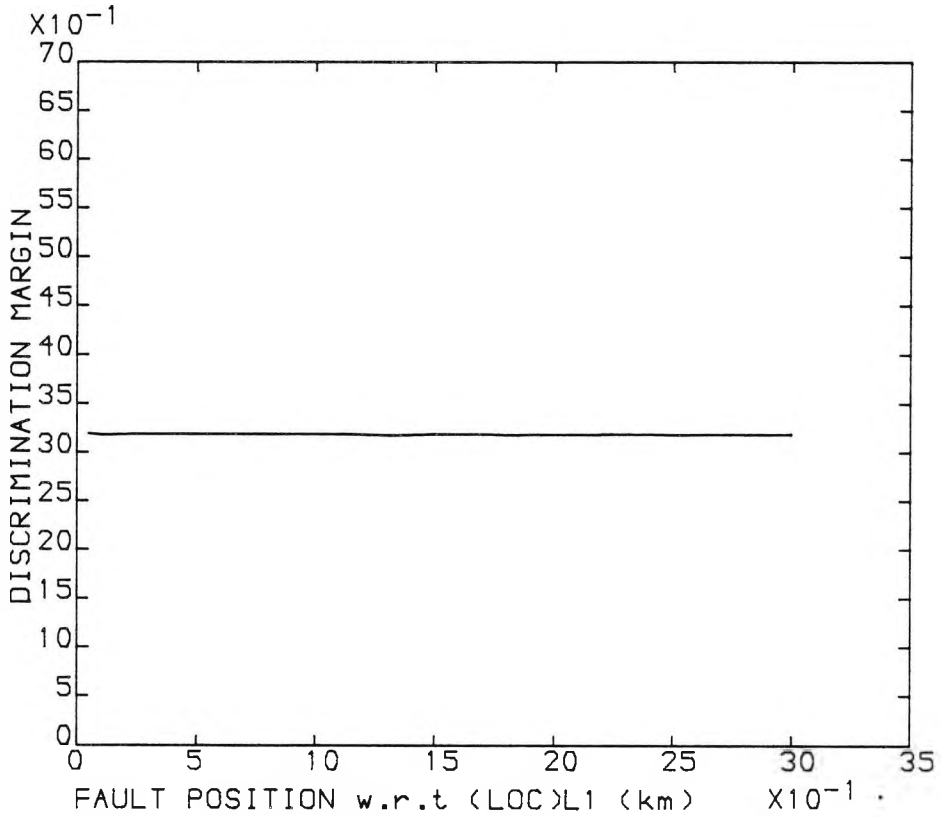

FIG (5.20), VARIATION OF DISCRIMINATION MARGIN AGAINST FAULT POSITION

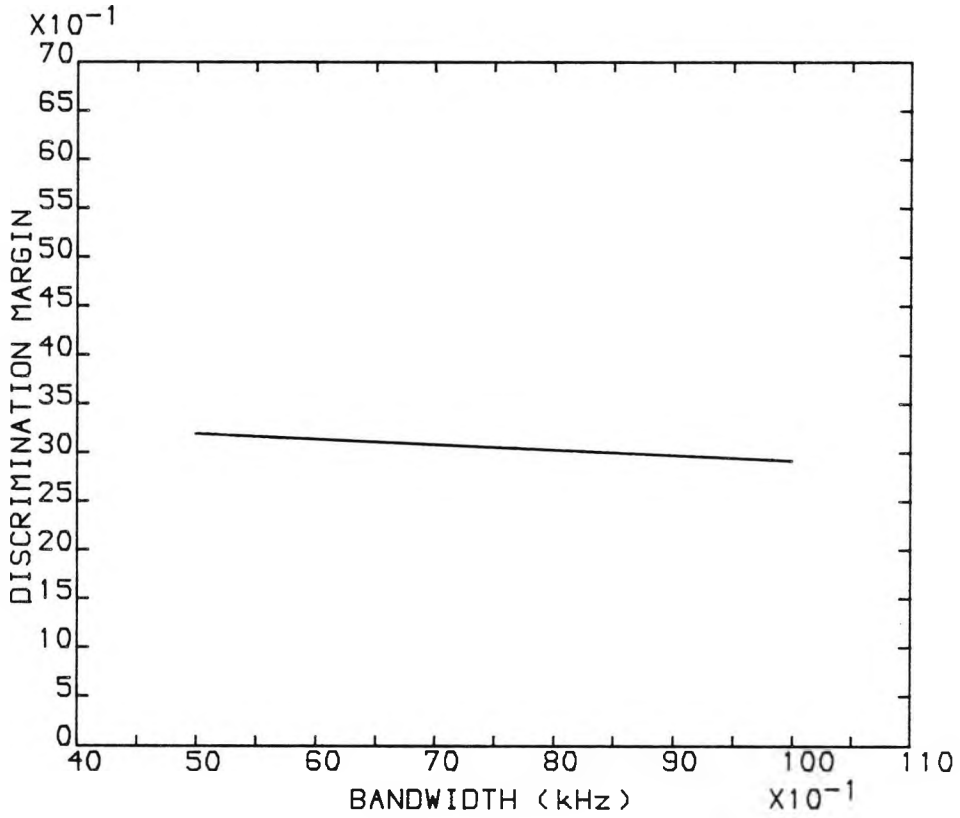

FIG (5.21). VARIATION OF DISCRIMINATION MARGIN AGAINST BANDWIDTH OF STACK TUNERS AND LINE TRAP CIRCUIT OF EACH LOCATOR

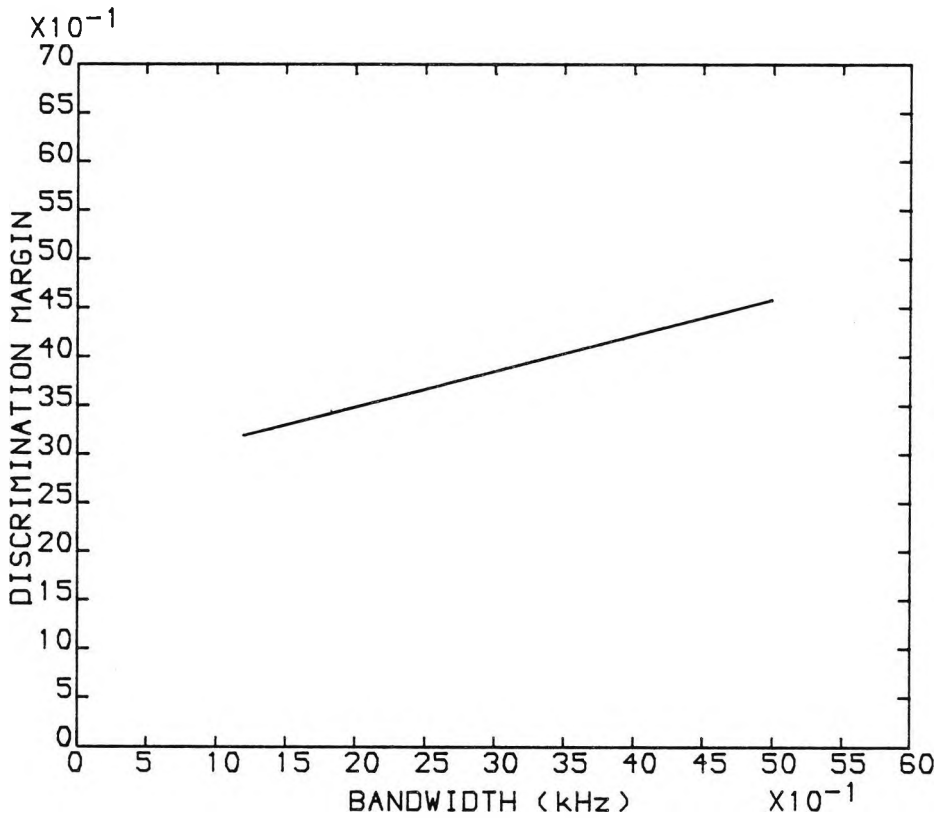

FIG (5.22). VARIATION OF DISCRIMINATION MARGIN AGAINST BANDWIDTH OF THE BANDPASS FILTER

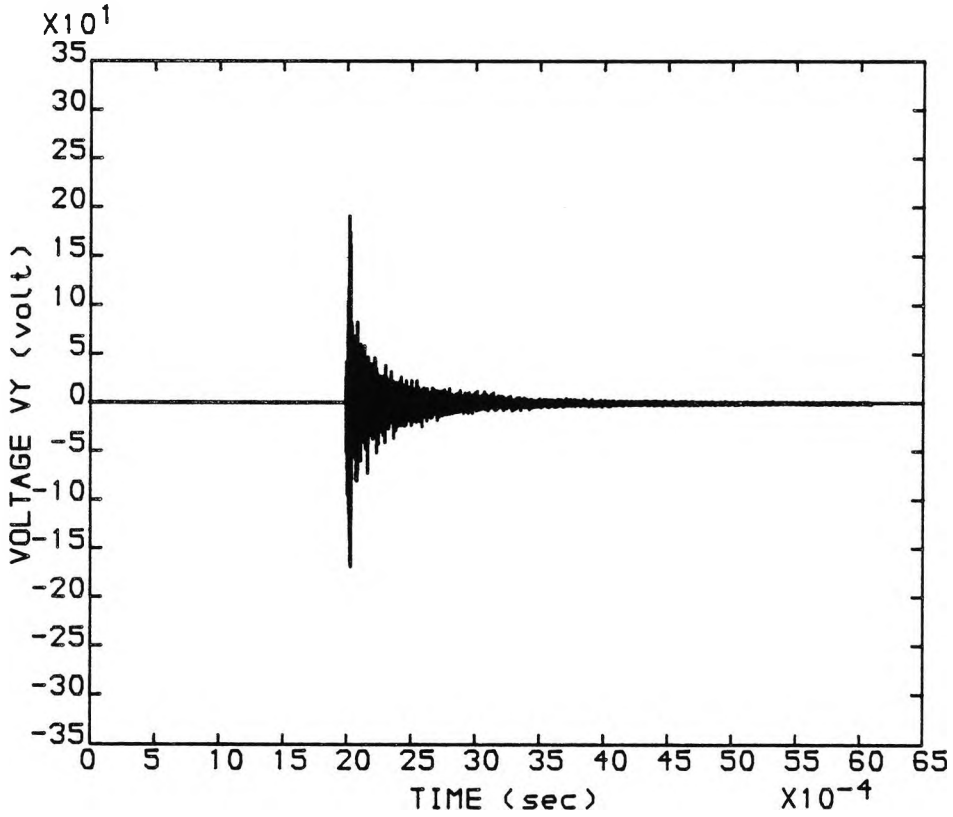

FIG(5.23), VY OF (LOC)L1 DUE TO A FAULT AT POINT F1, WITH fc = 270.0 (kHz)

SHORT-CIRCUIT LEVEL = 250 MVA

FAULT RESISTANCE = 0.0 (ohms)

TYPE OF FAULT : [a-e]

FAULT INCEPTION ANGLE = 90.0 (degrees)

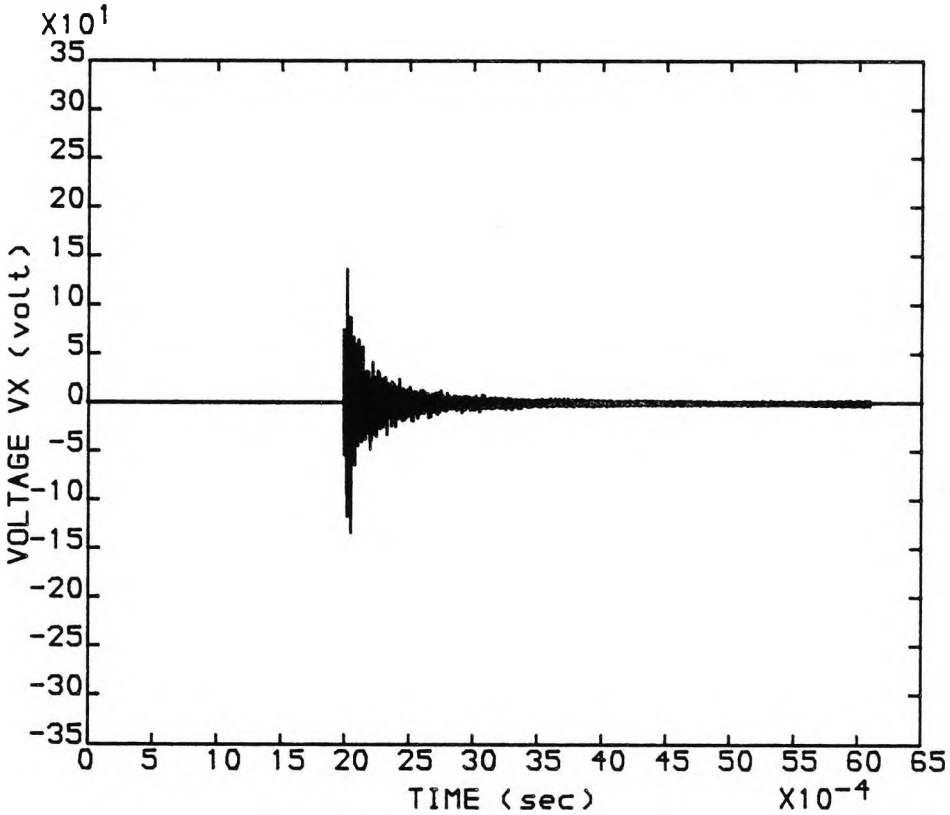

FIG(5.24). VX OF (LOC)L1 DUE TO A FAULT AT POINT F1, WITH fc = 270.0 (kHz)

SHORT-CIRCUIT LEVEL = 250 MVA

FAULT RESISTANCE = 0.0 (ohms)

TYPE OF FAULT : [a-e]

FAULT INCEPTION ANGLE = 90.0 (degrees)

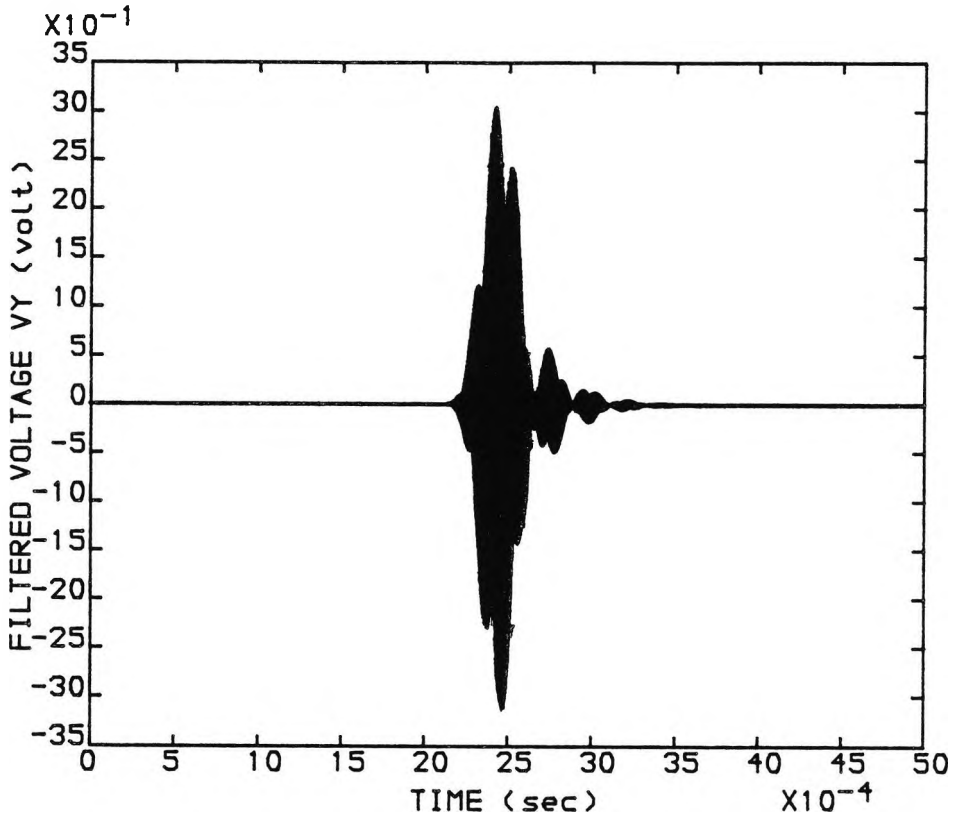

FIG(5.25), FILTERED VY OF (LOC)L1 DUE TO A FAULT AT POINT F1, WITH fc = 270.0 (kHz)

SHORT-CIRCUIT LEVEL = 250 MVA

FAULT RESISTANCE = 0.0 (ohms)

TYPE OF FAULT : [a-e]

FAULT INCEPTION ANGLE = 90.0 (degrees)

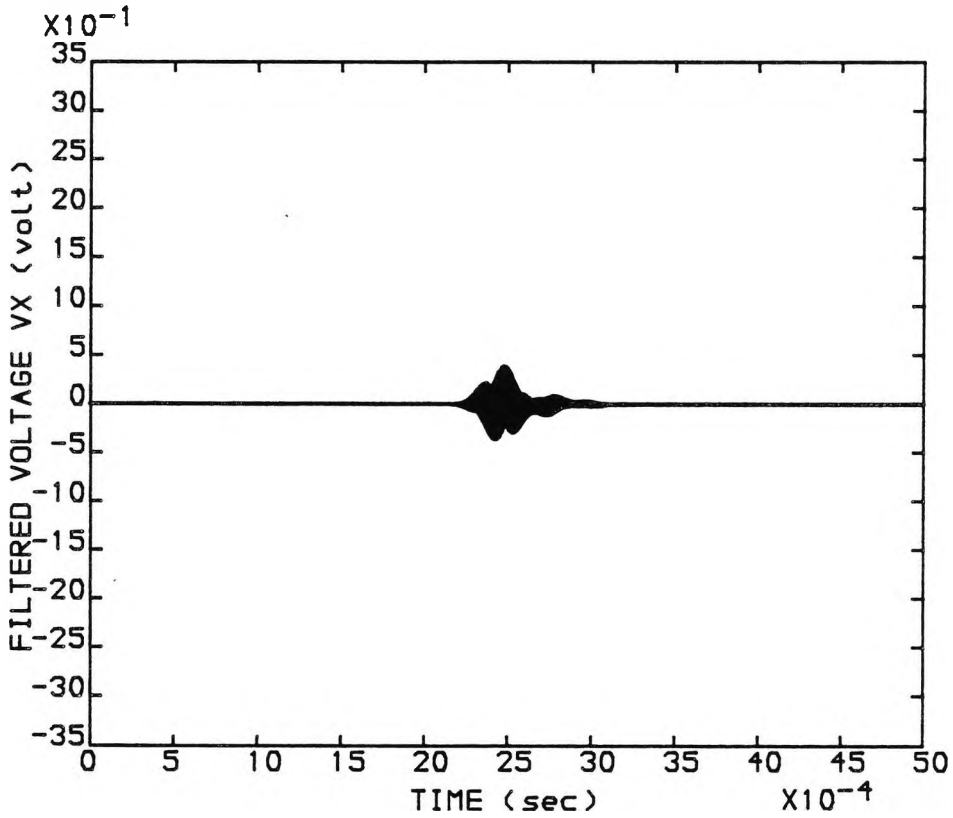

FIG(5.26), FILTERED VX OF (LOC)L1 DUE TO A FAULT AT POINT F1, WITH fc = 270.0 (kHz)

SHORT-CIRCUIT LEVEL = 250 MVA

FAULT RESISTANCE = 0.0 (ohms)

TYPE OF FAULT : [a-e]

FAULT INCEPTION ANGLE = 90.0 (degrees)

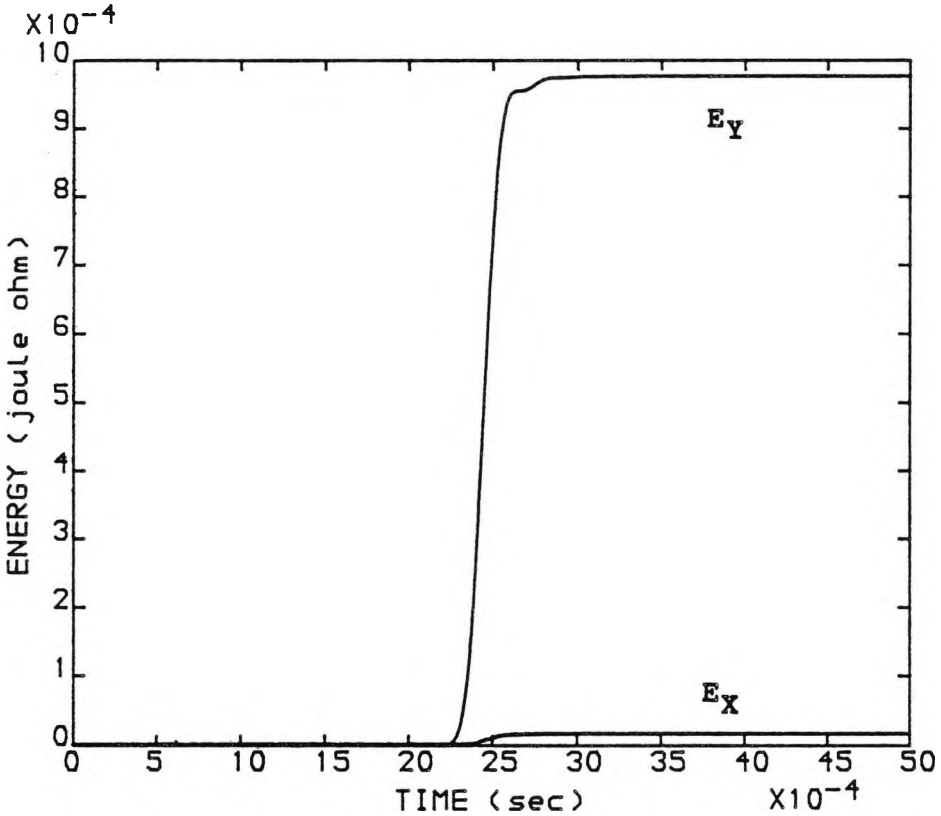

FIG (5.27). ENERGY COMPARISON BY (LOC) L1 DUE TO A FAULT AT POINT F1, WITH fc = 270.0 (kHz)

SHORT-CIRCUIT LEVEL = 250 MVA

FAULT RESISTANCE = 0.0 (ohms)

TYPE OF FAULT : [a-e]

FAULT INCEPTION ANGLE = 90.0 (degrees)

CHAPTER (6)

SENSITIVITY ANALYSIS ON FAULT LOCATING PROPERTY OF THE NEW EQUIPMENT

6.1 INTRODUCTION

The directionality property of the new directional fault locator was examined and illustrated using the sensitivity analysis performed in Chapter (5). In this chapter, further analysis and simulation results to show the capability of this new equipment to distinguish between in-zone and out-of-zone faults are presented. The results include the effect of type of fault, fault inception angle, fault resistance and the effect of source capacity on the discrimination margin existing between in-zone and out-of-zone faults.

Finally the maximisation of discrimination margin and the determination of the threshold level THL, described in Chapter (3), are discussed.

6.1.1 SELECTION OF APPROPRIATE SIGNALS

The method by which the new locator configuration distinguishes between in-zone and out-of-zone faults on a given overhead distribution system was described in Chapter (3).

The sensitivity analysis have been carried out using the signals provided by $(LOC)_{L1}$ due to two different fault positions: at points F1 and F2 close to $(LOC)_{L2}$ as shown in Figure (6.1). The fault F1, represents an in-zone fault while the fault at F2 represents an out-of-zone fault as sensed by locator $(LOC)_{L1}$. It should be appreciated that, the signals provided by $(LOC)_{L1}$, are the voltages across the resistors of the stack tuners employed on both sides of $(LOC)_{L1}$ at X and Y. Figure (6.1) shows the schematic diagram of the system under test per phase. The energy content in the filtered voltages at sides Y and X are again referred to as E_Y and E_X respectively.

6.2 THE EFFECT OF TYPE OF FAULT

As previously described, the discrimination between in-zone and out-of-zone faults is accomplished by evaluating the difference in energy levels on either side of a locator arising from different types of faults.

Figures (6.2) and (6.3) show the voltage signals appearing across the resistors of the stack tuners of locator $(LOC)_{L1}$ situated at sides Y and X respectively. The type of fault applied is a single phase to earth solid fault, (a-e) at point F2. The corresponding waveforms of Figures (6.2) and (6.3) after passage through a band-pass filter, are illustrated in Figures (6.4) and (6.5)

respectively. It is clearly seen that, the energy content in the filtered voltages are almost equal, resulting in a very small energy level difference between the two.

The energy level difference analysed by locator $(LOC)_{L1}$ due to an in-zone fault at F1 and its corresponding waveform due to an out-of-zone fault at F2 are shown in Figure (6.6). From the results, it is evident that, the energy level difference for an in-zone fault is at a much higher level than that of an out-of-zone fault.

The corresponding result of Figure (6.6) for a double phase to earth fault, (a-b-e), is shown in Figure (6.7), for a three phase to earth fault, (a-b-c-e), is shown in Figure (6.8), and finally for a phase to phase fault, (a-b), is shown in Figure (6.9). Figures (6.6) to (6.9), clearly demonstrate the capability of the new equipment to distinguish between in-zone and out-of-zone faults for different types of faults.

6.3 THE EFFECT OF FAULT RESISTANCE

Figures (6.10) and (6.11) show the voltage signals across the resistors of stack tuners of locator $(LOC)_{L1}$ at sides Y and X respectively due to a single phase to earth fault, (a-e), at F2 with a fault resistance of 50.0 Ω. The magnitude of energy level difference between these signals after having been filtered, should be at a lower level

than that of its corresponding energy level difference for a fault at F1. This is shown in Figure (6.12), from which it is clearly evident that, a sufficiently large margin does exist between the two energy level differences, in order for the locator to distinguish between in-zone and out-of-zone faults having a fault resistance of up to 50.0 Ω.

The corresponding waveforms of Figure (6.12) with a fault resistance of 100.0 Ω is shown in Figure (6.13).

6.4 THE EFFECT OF FAULT INCEPTION ANGLE

The two possible worst cases from the travelling-wave point of view, are the faults at instants corresponding to a voltage maximum and a voltage minimum, in the faulted phase or phases. So far the sensitivity analysis have been carried out, using faults occurring at a voltage maximum or at an inception angle of 90.0 degrees. The corresponding voltage signals of Figures (6.2) and (6.3) are shown in Figures (6.14) and (6.15) respectively for a fault with an inception angle of 5.0 degrees. In this case the distortion is very small, and this is due to the absence of a large and sudden voltage change at the point of fault.

Figures (6.16) and (6.17) show the comparison between the energy level differences corresponding to in-zone and

out-of-zone faults with fault inception angles of 5.0 and 45.0 degrees respectively. These together with Figure (6.6) show that the discrimination margin between the energy level differences is almost independent of the fault inception angle.

6.5 THE EFFECT OF SOURCE CAPACITY

In this section the effect of source capacity on the fault locating property of the new equipment has been investigated. Figures (6.18) and (6.19), show the comparison between the energy level differences observed by locator $(LOC)_{L1}$ due to in-zone fault at F1 and out-of-zone fault at F2 for Short-Circuit Levels of 150 MVA and 50 MVA respectively.

On comparing these with Figure (6.6) which corresponds to the case with a Short-Circuit Level of 250 MVA, it is seen that, the discrimination margin reduces as the Short-Circuit Level decreases. However, even with a Short-Circuit level of 50 MVA, the discrimination margin is adequate to enable the in-zone and out-of-zone faults to be correctly determined by the locator $(LOC)_{L1}$.

6.6 MAXIMISATION OF DISCRIMINATION MARGIN

As previously described in Chapter (5), tuning the stack tuners and the line trap circuit of the new

equipment to a centre frequency of 270 kHz, would considerably increase the discrimination margin between the energy levels obtained from the stack tuners. Consequently, this would also result in a higher discrimination margin existing between the magnitude of energy level differences due to in-zone and out-of-zone faults.

Figures (6.20) and (6.21) show the corresponding voltage signals at a centre frequency of 270 kHz to those of Figures (6.2) and (6.3) at a centre frequency of 90 kHz respectively. Figures (6.22) and (6.23) show the filtered response waveforms of Figures (6.20) and (6.21) respectively. Once more, due to the fact that, the fault is beyond locator $(LOC)_{L2}$, the difference between energy content in the filtered response waveforms is very small.

Finally Figure (6.24) illustrates the comparison between the magnitude of energy level differences due to in-zone and out-of-zone faults. This clearly shows the increase in the discrimination margin from almost 16 times at a centre frequency of 90 kHz, Figure (6.6), to almost 100 times at the centre frequency of 270 kHz.

6.7 DETERMINATION OF THE THRESHOLD LEVEL, THL

So far the results illustrated show, how the discrimination margin between in-zone and out-of-zone

faults is affected by different fault conditions. However, as previously described in Chapter (3), the operation of the new equipment and the scheme developed to produce the right trip signal for distinguishing between in-zone and out-of-zone faults, depends entirely on using a threshold level. The threshold level to be used depends on the various circuit parameters and it can be set to control the basic sensitivity to faults.

One of the major factors influencing the determination of a threshold level is the fault inception angle. It has been seen that, when a fault occurs some where near a zero crossing of the voltage, there is not a large sudden change of voltage, resulting in a very low energy level difference compared with those occurring at a voltage maximum. However, apart from this fact and as an example, from the sensitivity analysis carried out in this chapter, it is quite evident that two or even one threshold level can be defined. This can be used in order to distinguish correctly between in-zone and out-of-zone faults under different fault conditions considered. These include different types of fault and in the case of a single phase to earth fault, (a-e), different fault resistances, source capacities and fault inception angles.

Considering Figures (6.6) to (6.9), it can be seen that, the maximum energy level difference due to an out-of-zone fault corresponds to 5.0×10^{-4} Joule ohm,

(JΩ). Also the minimum energy level difference due to an in-zone fault corresponds to 16.0 x 10^{-4} JΩ. Hence it can be seen that, a threshold level within the range, 5.0 x 10^{-4} to 16.0 x 10^{-4} JΩ, could well be used so far.

Figure (6.25) shows that, a threshold level corresponding to, say 10.0 x 10^{-4} JΩ, is always exceeded by any energy level due to in-zone faults and always remains unreached by any energy level due to out-of-zone faults. Hence in-zone and out-of-zone faults can easily be distinguished.

Now consider the sensitivity analysis shown in Figures (6.10) to (6.19), due to a single phase to earth fault, (a-e), with different fault resistances, fault inception angles and source capacities. These figures show that, the highest energy level difference, 4.7 x 10^{-4} JΩ, due to an out-of-zone fault, has been obtained in a case with fault resistance of 0.0 Ω, Short-Circuit level of 50.0 MVA and fault inception angle of 90.0 degrees. Also the lowest energy level difference, 8.3 x 10^{-4} JΩ, due to an in-zone fault has been obtained in the case: Short-Circuit Level of 250.0 MVA, fault resistance of 0.0 Ω and fault inception angle of 45.0 degrees. Other in-zone and out-of-zone faults with Short-Circuit Level of 150.0 MVA or the fault resistance as high as 50.0 or 100.0 Ω, have respectively shown higher energy level differences than 8.3 x 10^{-4} JΩ and lower energy level differences than

4.7×10^{-4} JΩ.

Figure (6.26) illustrates that, a threshold level of 7.0×10^{-4} JΩ could be used to correctly distinguish between in-zone and out-of-zone single phase to earth faults, (a-e), under different fault conditions. However, the same threshold level of 7.0×10^{-4} JΩ, could also be used to distinguish between different types of in-zone and out-of-zone faults shown in Fig(6.25) as well.

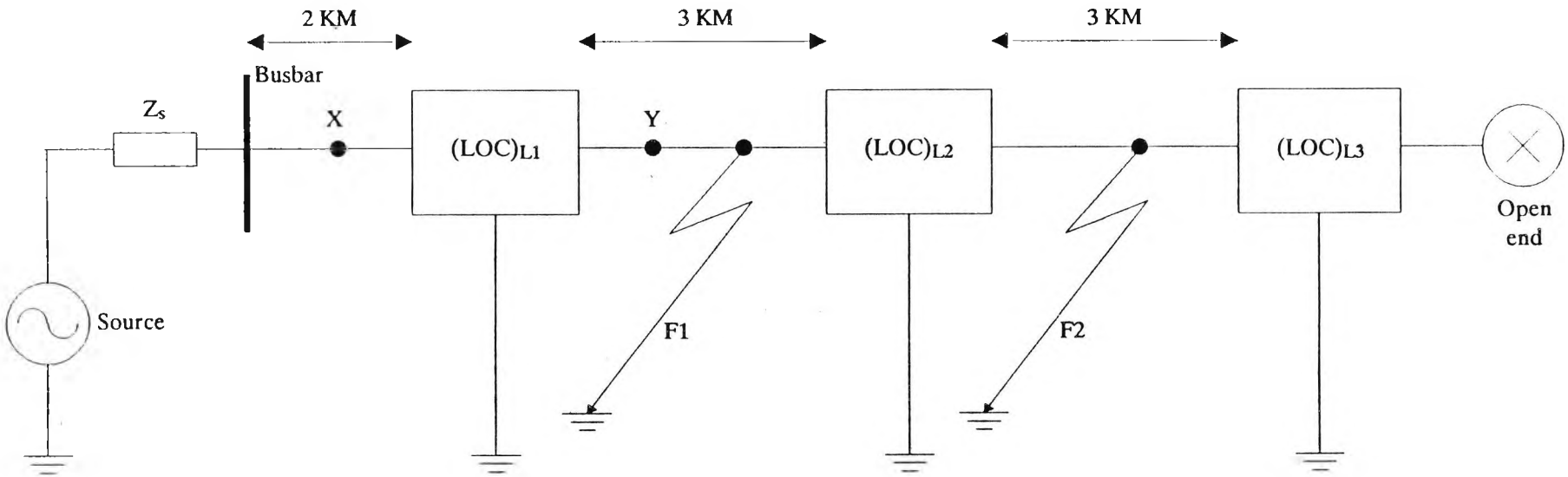

FIG (6.1), SCHEMATIC DIAGRAM OF THE SYSTEM SIMULATED PER PHASE WITH IN-ZONE FAULT, F1 AND OUT-OF-ZONE FAULT, F2

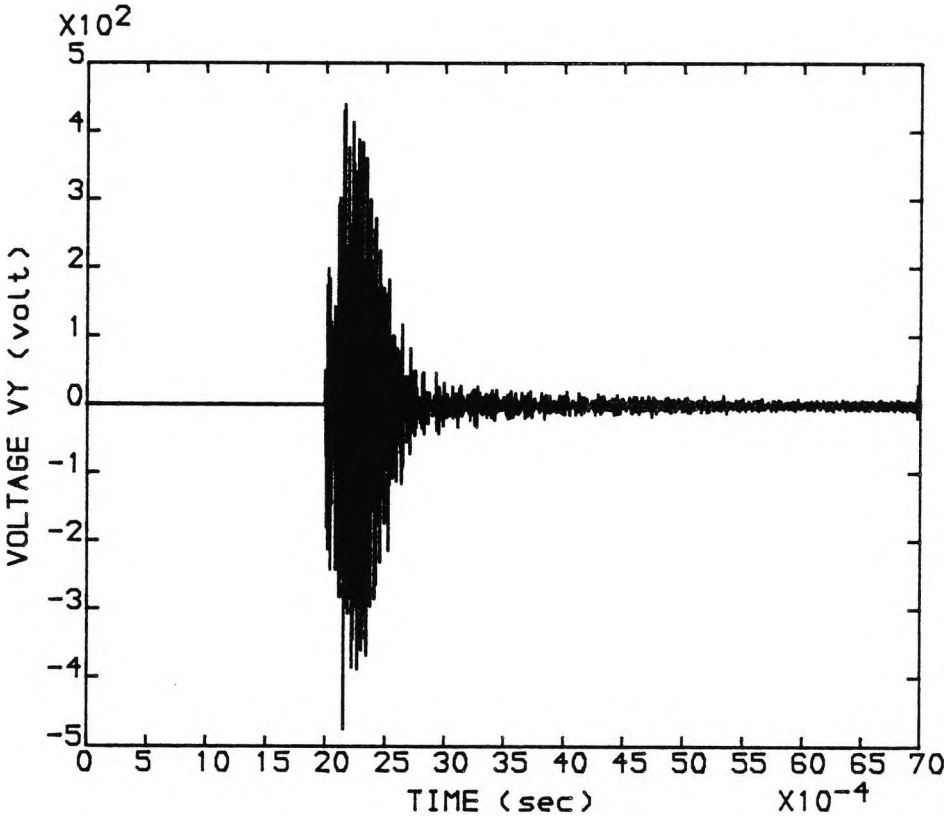

FIG (6.2). VY OF (LOC) L1 DUE TO A FAULT AT POINT F2, WITH fc = 90.0 (kHz)

SHORT-CIRCUIT LEVEL = 250 MVA

FAULT RESISTANCE = 0.0 (ohms)

TYPE OF FAULT : [a-e]

FAULT INCEPTION ANGLE = 90.0 (degrees)

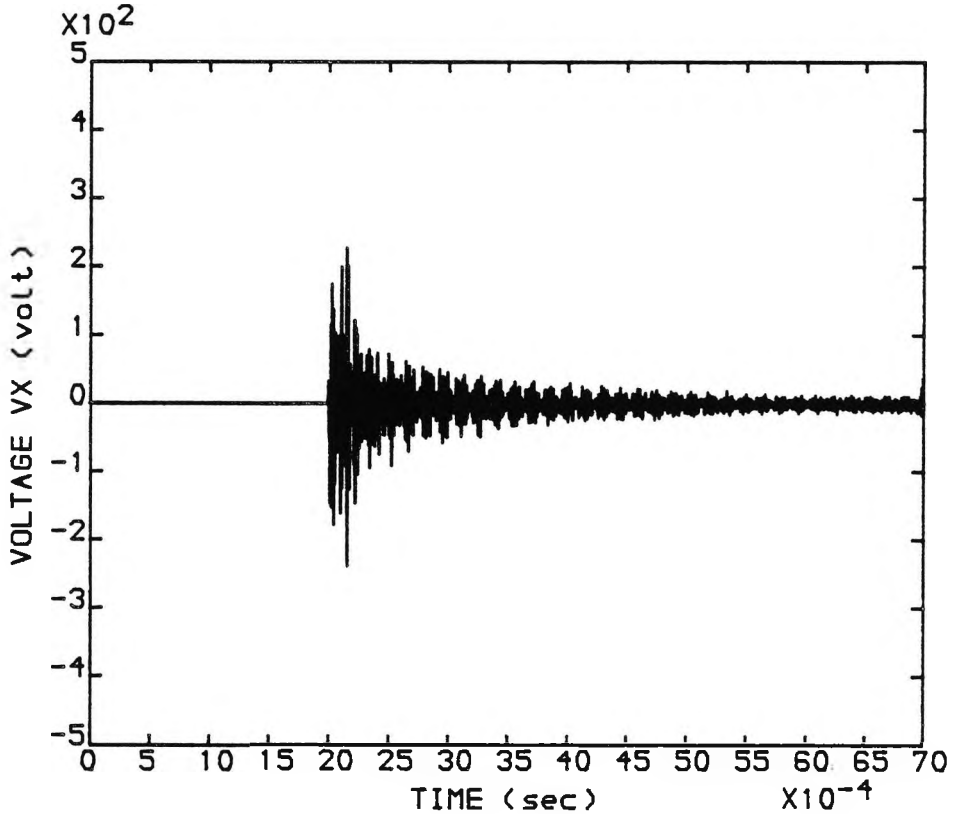

FIG (6.3). VX OF (LOC) L1 DUE TO A FAULT AT POINT F2. WITH fc = 90.0 (kHz)

SHORT-CIRCUIT LEVEL = 250 MVA

FAULT RESISTANCE = 0.0 (ohms)

TYPE OF FAULT : [a-e]

FAULT INCEPTION ANGLE = 90.0 (degrees)

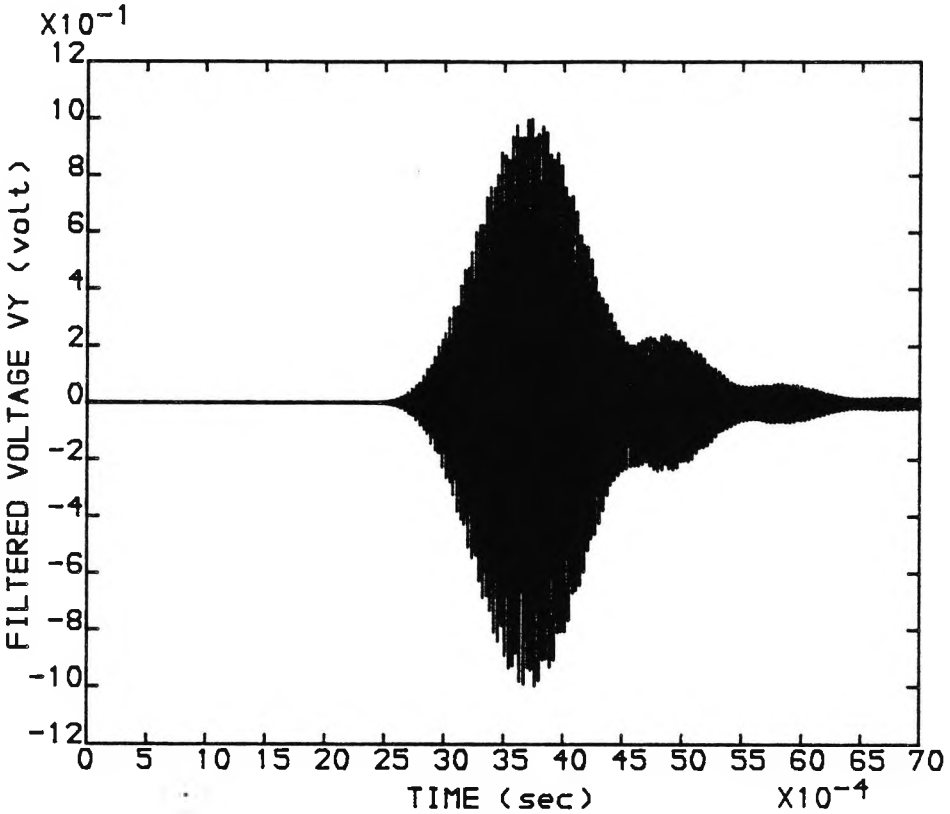

FIG (6.4). FILTERED VY OF (LOC) L1 DUE TO A FAULT AT POINT F2, WITH fc = 90.0 (kHz)

SHORT-CIRCUIT LEVEL = 250 MVA

FAULT RESISTANCE = 0.0 (ohms)

TYPE OF FAULT : [a-e]

FAULT INCEPTION ANGLE = 90.0 (degrees)

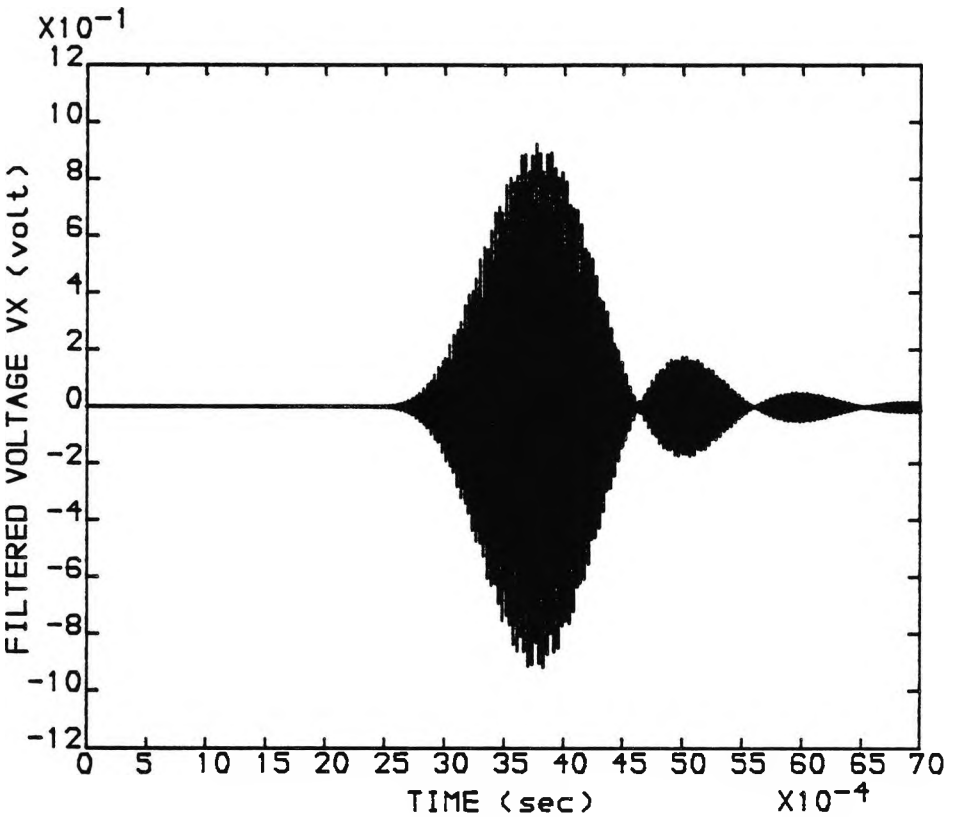

FIG (6.5). FILTERED VX OF (LOC) L1 DUE TO A FAULT AT POINT F2. WITH fc = 90.0 (kHz)

SHORT-CIRCUIT LEVEL = 250 MVA

FAULT RESISTANCE = 0.0 (ohms)

TYPE OF FAULT : [a-e]

FAULT INCEPTION ANGLE = 90.0 (degrees)

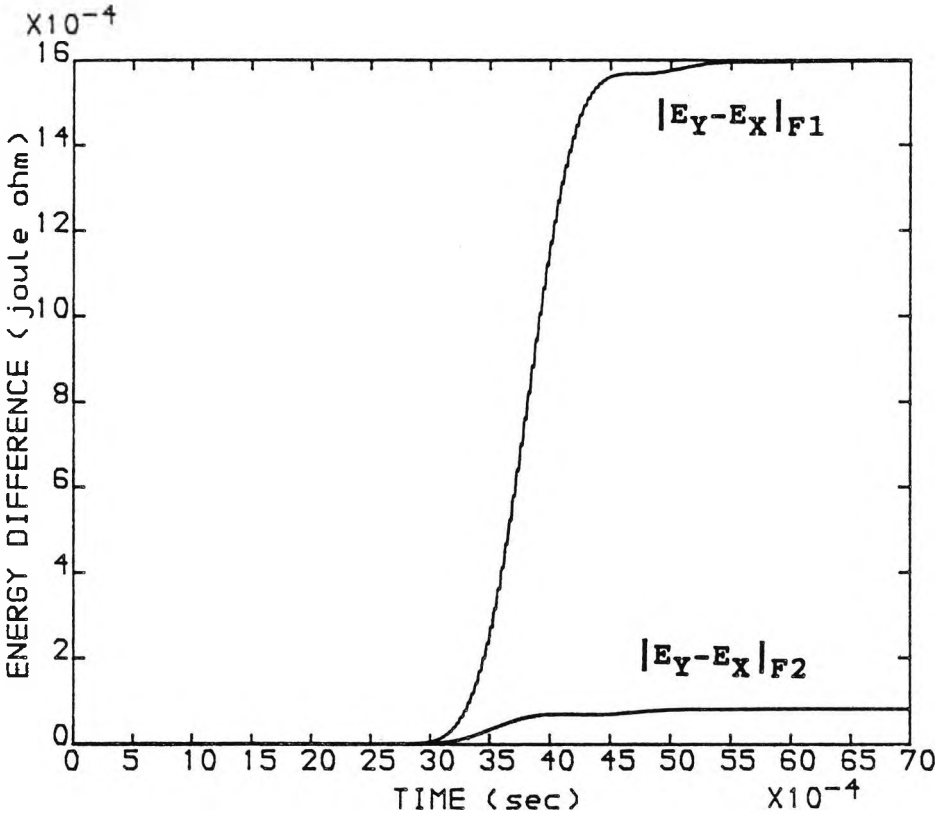

FIG (6.6), ENERGY DIFFERENCE COMPARISON BY (LOC) L1 BETWEEN IN-ZONE AND OUT-OF-ZONE FAULTS WITH fc = 90.0 (kHz)

SHORT-CIRCUIT LEVEL = 250 MVA

FAULT RESISTANCE = 0.0 (ohms)

TYPE OF FAULT : [a-e]

FAULT INCEPTION ANGLE = 90.0 (degrees)

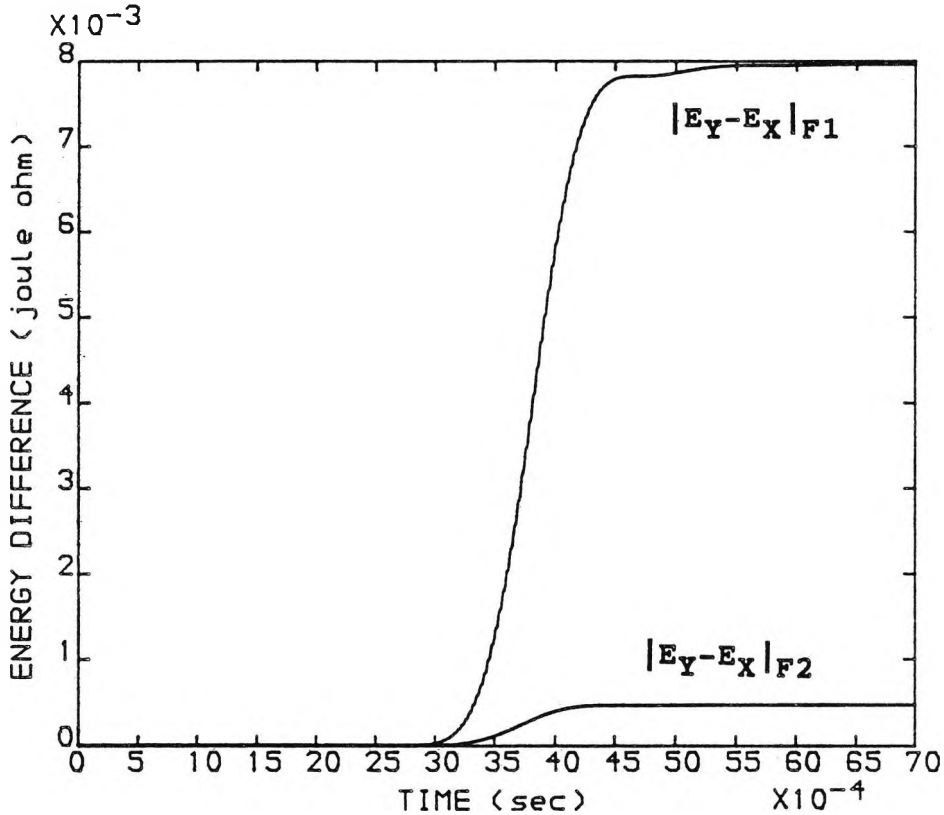

FIG (6.7). ENERGY DIFFERENCE COMPARISON BY (LOC) L1 BETWEEN IN-ZONE AND OUT-OF-ZONE FAULTS WITH fc = 90.0 (kHz)

SHORT-CIRCUIT LEVEL = 250 MVA

FAULT RESISTANCE = 0.0 (ohms)

TYPE OF FAULT : [a-b-e]

FAULT INCEPTION ANGLE = 90.0 (degrees)

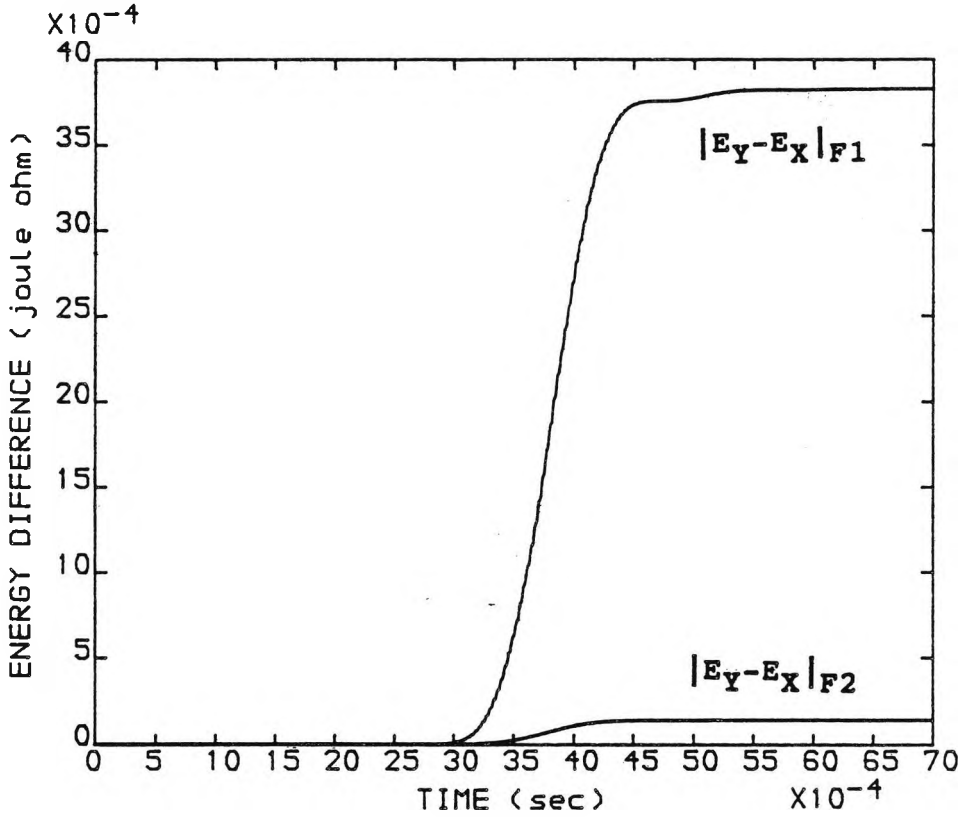

FIG (6.8). ENERGY DIFFERENCE COMPARISON BY (LOC) L1 BETWEEN IN-ZONE AND OUT-OF-ZONE FAULTS WITH fc = 90.0 (kHz)

SHORT-CIRCUIT LEVEL = 250 MVA

FAULT RESISTANCE = 0.0 (ohms)

TYPE OF FAULT : [a-b-c-e]

FAULT INCEPTION ANGLE = 90.0 (degrees)

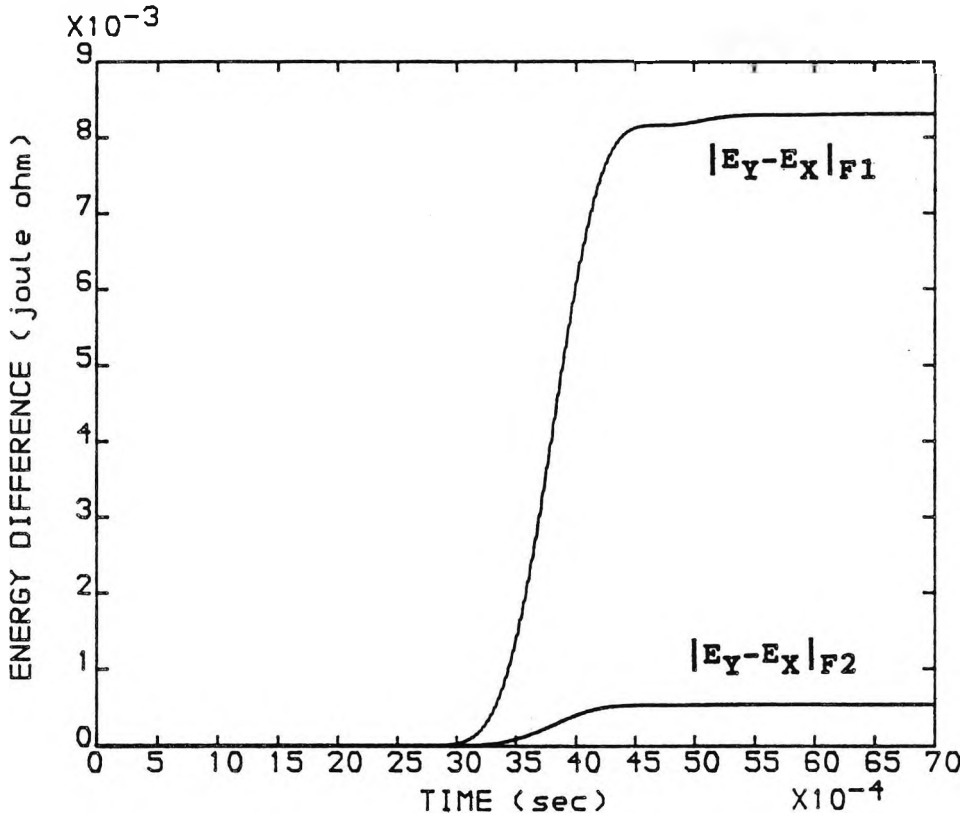

FIG (6.9). ENERGY DIFFERENCE COMPARISON BY (LOC) L1 BETWEEN IN-ZONE AND OUT-OF-ZONE FAULTS WITH fc = 90.0 (kHz)

SHORT-CIRCUIT LEVEL = 250 MVA

FAULT RESISTANCE = 0.0 (ohms)

TYPE OF FAULT : [a-b]

FAULT INCEPTION ANGLE = 90.0 (degrees)

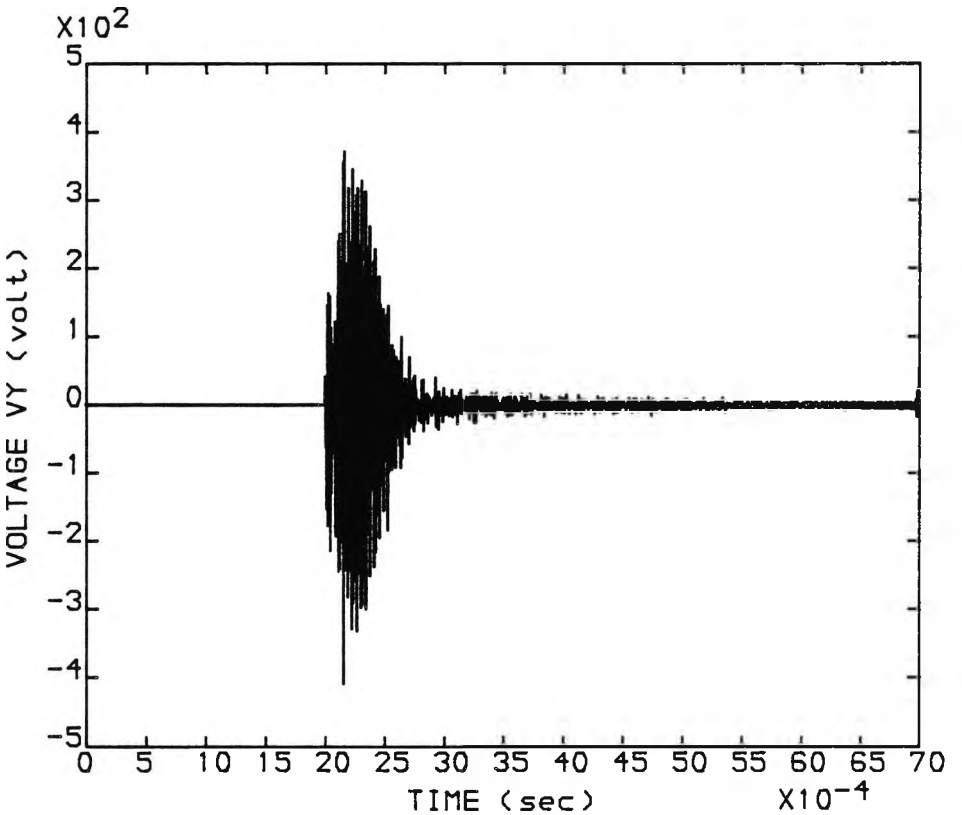

FIG (6.10). VY OF (LOC) L1 DUE TO A FAULT AT POINT F2. WITH fc = 90.0 (kHz)

SHORT-CIRCUIT LEVEL = 250 MVA

FAULT RESISTANCE = 50.0 (ohms)

TYPE OF FAULT : [a-e]

FAULT INCEPTION ANGLE = 90.0 (degrees)

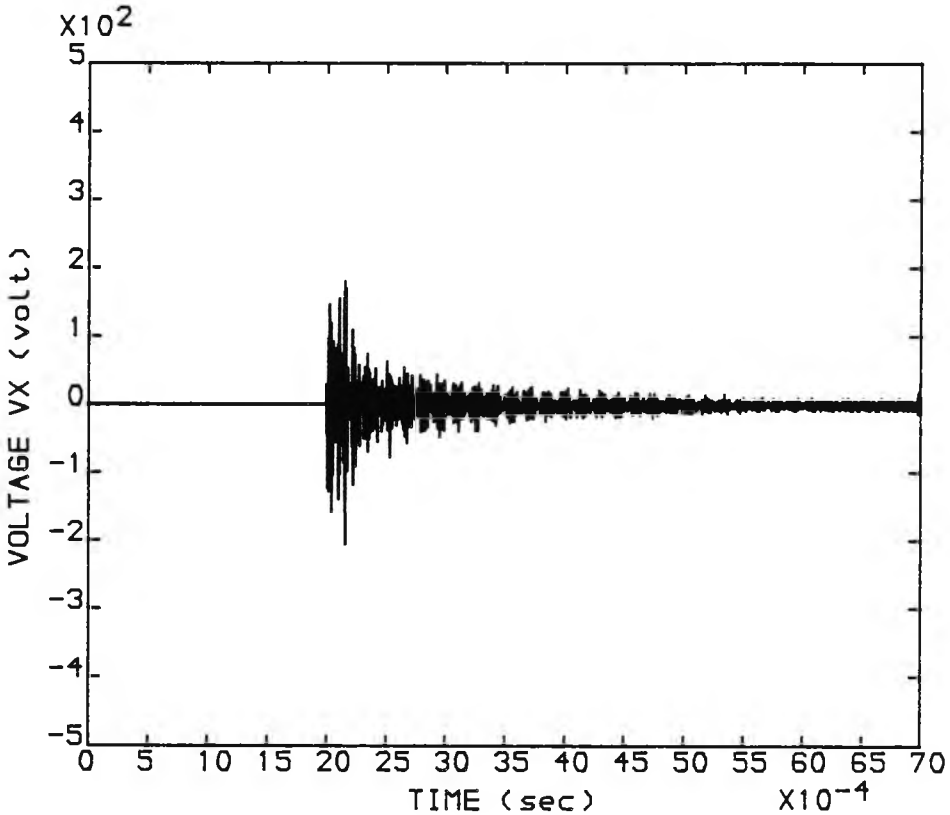

FIG (6.11). VX OF (LOC) L1 DUE TO A FAULT AT POINT F2. WITH fc = 90.0 (kHz)

SHORT-CIRCUIT LEVEL = 250 MVA

FAULT RESISTANCE = 50.0 (ohms)

TYPE OF FAULT : [a-e]

FAULT INCEPTION ANGLE = 90.0 (degrees)

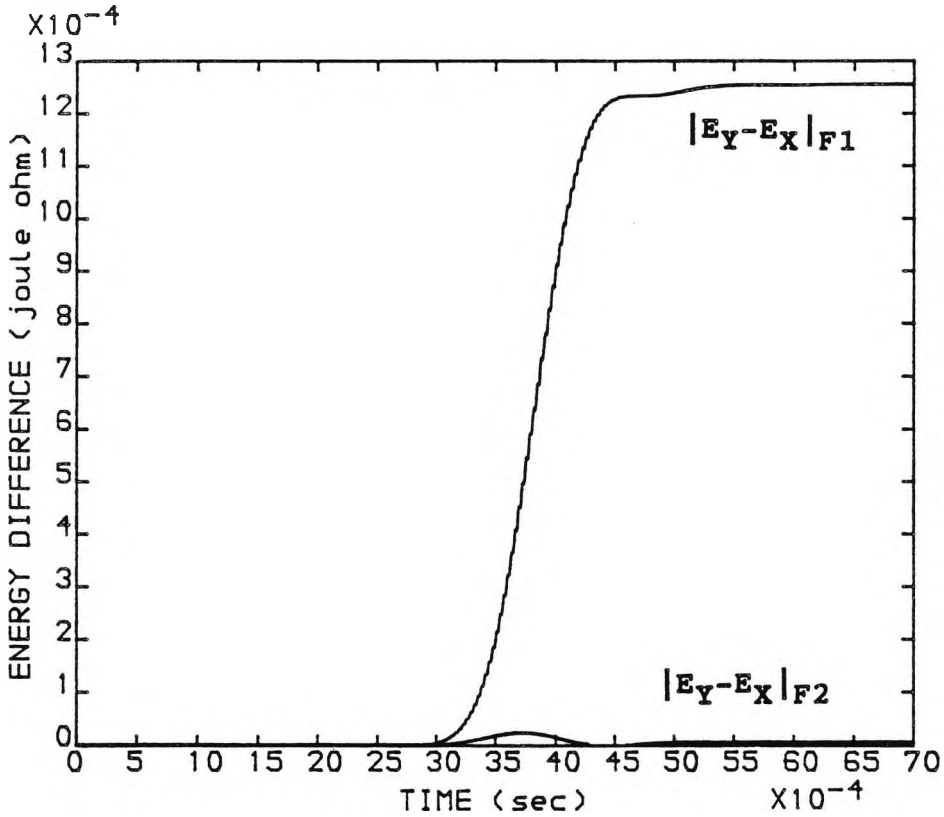

FIG (6.12). ENERGY DIFFERENCE COMPARISON BY (LOC) L1 BETWEEN IN-ZONE AND OUT-OF-ZONE FAULTS WITH fc = 90.0 (kHz)

SHORT-CIRCUIT LEVEL = 250 MVA

FAULT RESISTANCE = 50.0 (ohms)

TYPE OF FAULT : [a-e]

FAULT INCEPTION ANGLE = 90.0 (degrees)

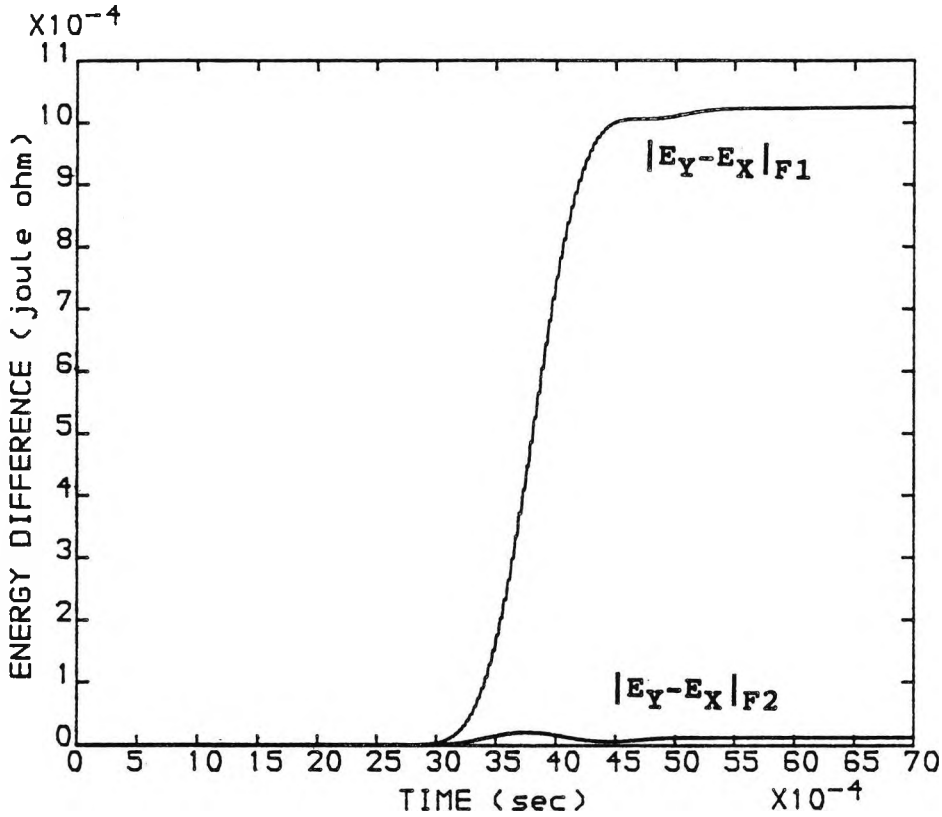

FIG (6.13), ENERGY DIFFERENCE COMPARISON BY (LOC) L1 BETWEEN IN-ZONE AND OUT-OF-ZONE FAULTS WITH fc = 90.0 (kHz)

SHORT-CIRCUIT LEVEL = 250 MVA

FAULT RESISTANCE = 100.0 (ohms)

TYPE OF FAULT : [a-e]

FAULT INCEPTION ANGLE = 90.0 (degrees)

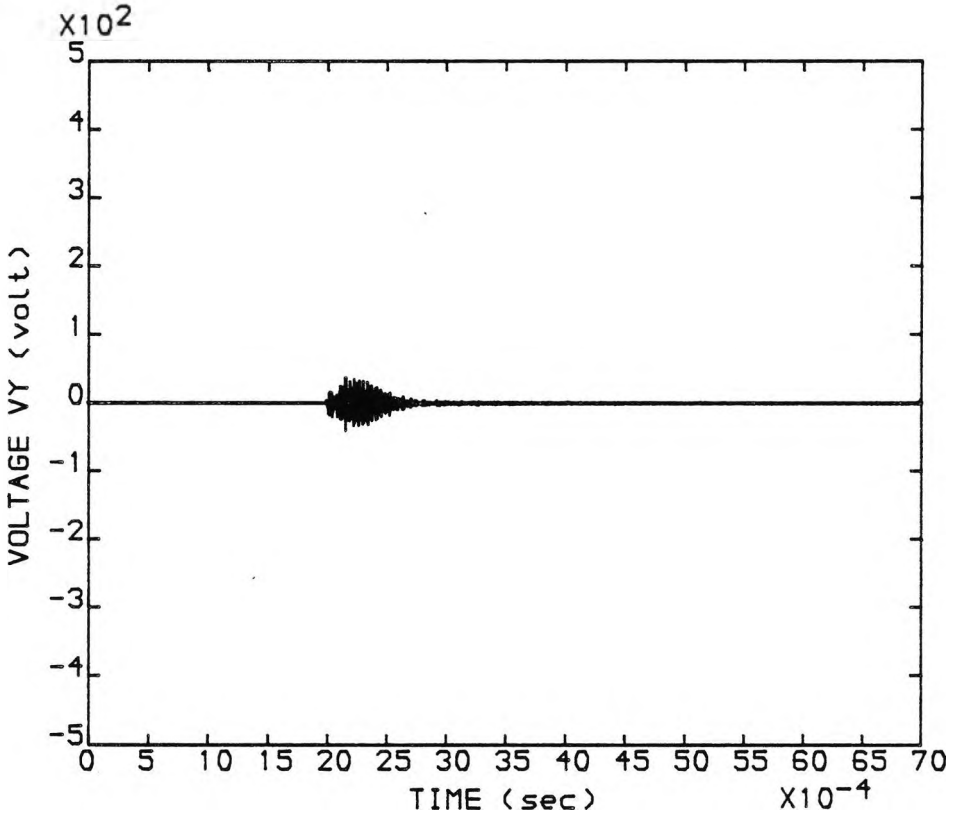

FIG (6.14). VY OF (LOC) L1 DUE TO A FAULT AT POINT F2. WITH fc = 90.0 (kHz)

SHORT-CIRCUIT LEVEL = 250 MVA

FAULT RESISTANCE = 0.0 (ohms)

TYPE OF FAULT : [a-e]

FAULT INCEPTION ANGLE = 5.0 (degrees)

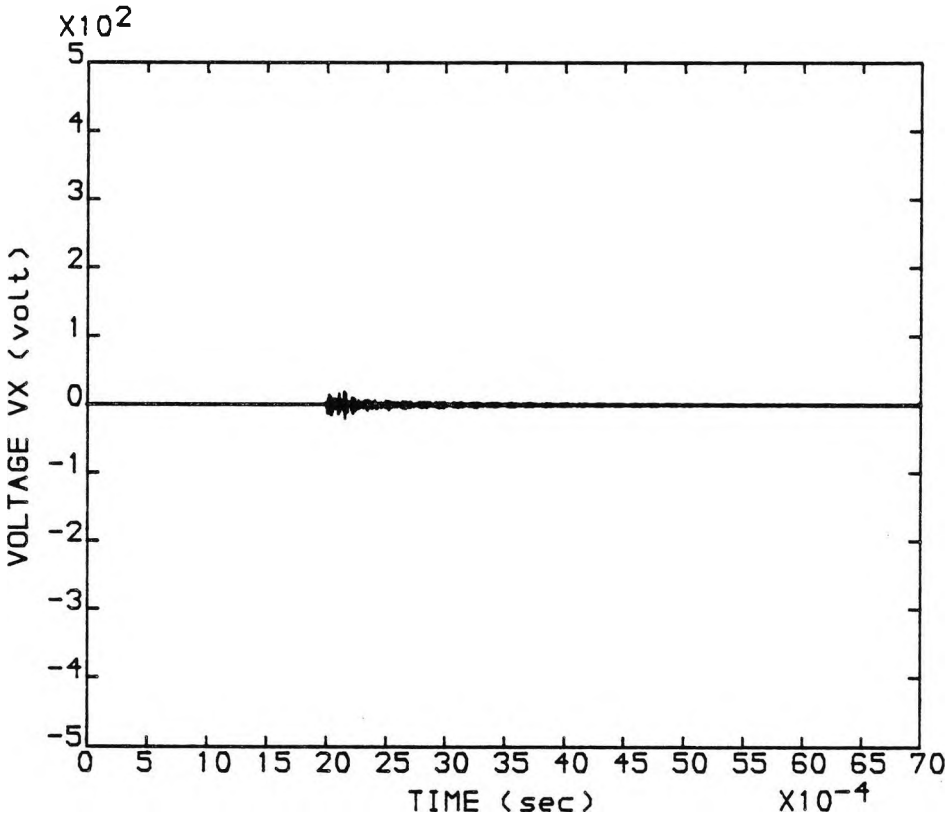

FIG (6.15), VX OF (LOC) L1 DUE TO A FAULT AT POINT F2, WITH fc = 90.0 (kHz)

SHORT-CIRCUIT LEVEL = 250 MVA

FAULT RESISTANCE = 0.0 (ohms)

TYPE OF FAULT : [a-e]

FAULT INCEPTION ANGLE = 5.0 (degrees)

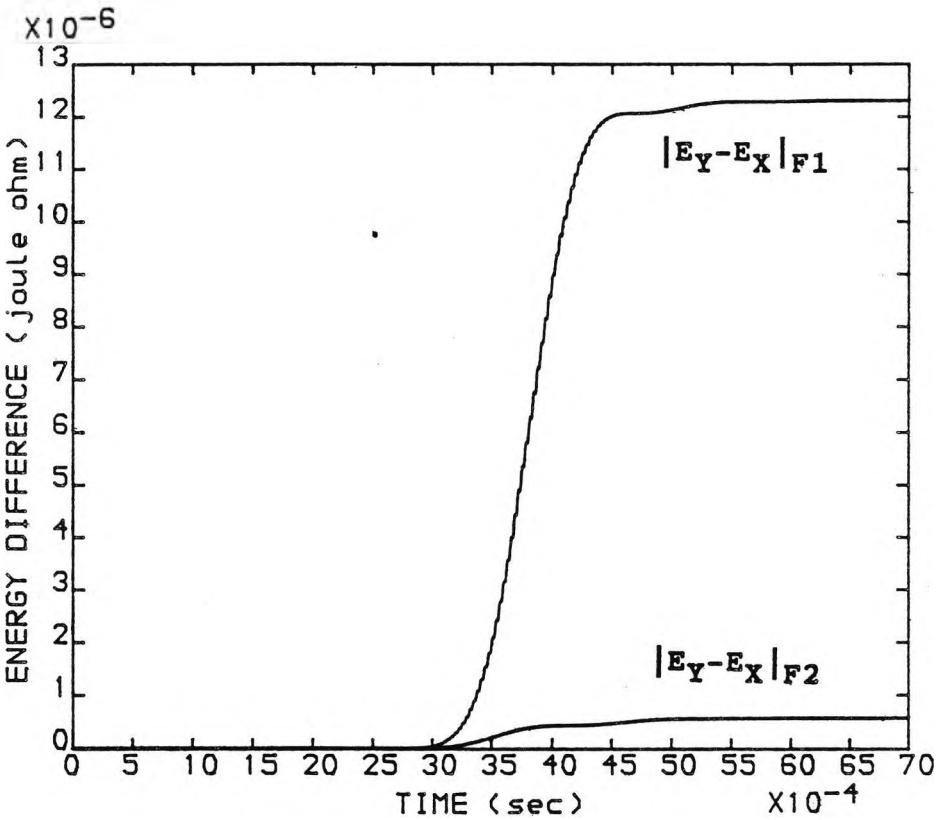

FIG (6.16). ENERGY DIFFERENCE COMPARISON BY (LOC) L1 BETWEEN IN-ZONE AND OUT-OF-ZONE FAULTS WITH fc = 90.0 (kHz)

SHORT-CIRCUIT LEVEL = 250 MVA

FAULT RESISTANCE = 0.0 (ohms)

TYPE OF FAULT : [a-e]

FAULT INCEPTION ANGLE = 5.0 (degrees)

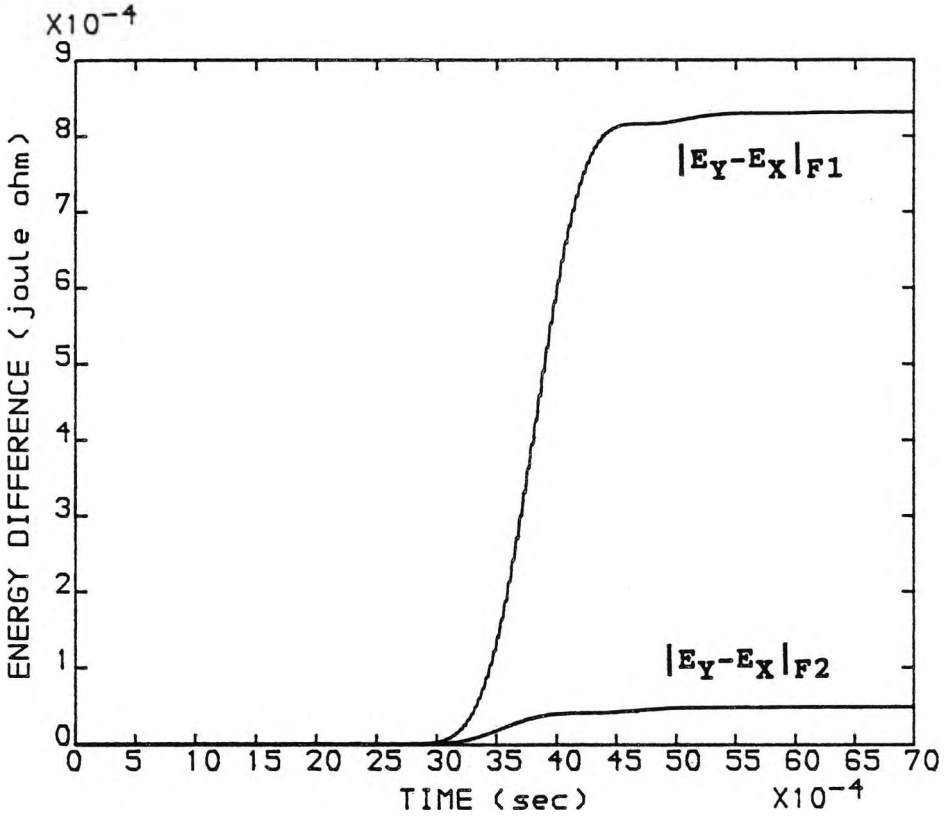

FIG (6.17). ENERGY DIFFERENCE COMPARISON BY (LOC) L1 BETWEEN IN-ZONE AND OUT-OF-ZONE FAULTS WITH fc = 90.0 (kHz)

SHORT-CIRCUIT LEVEL = 250 MVA

FAULT RESISTANCE = 0.0 (ohms)

TYPE OF FAULT : [a-e]

FAULT INCEPTION ANGLE = 45.0 (degrees)

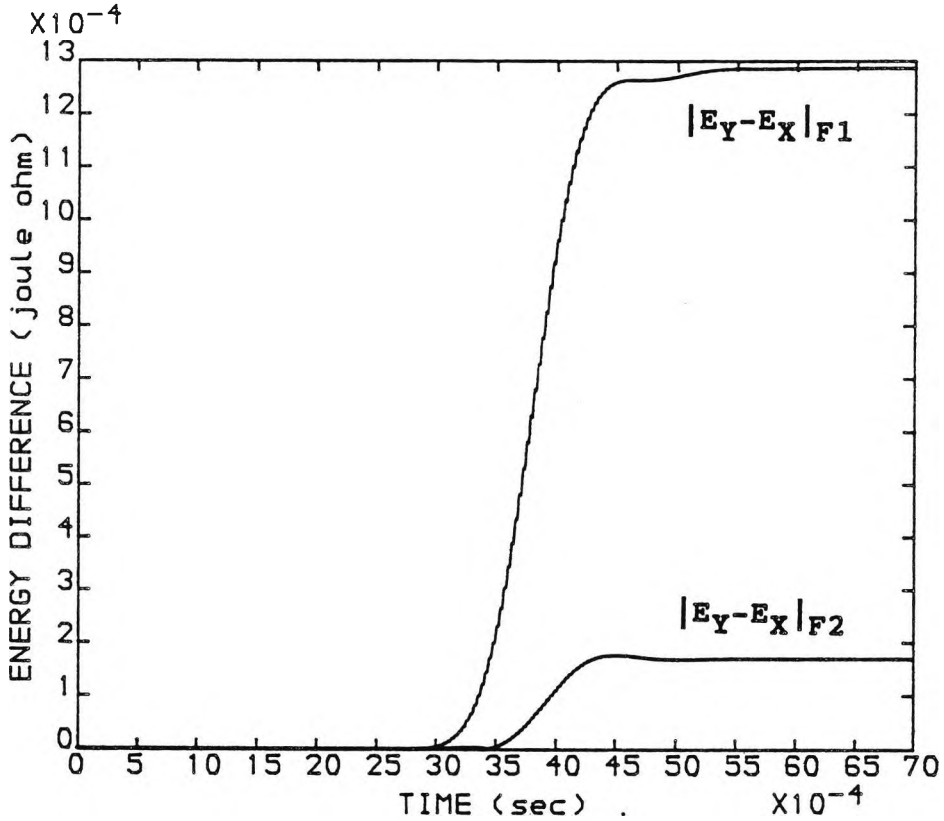

FIG (6.18). ENERGY DIFFERENCE COMPARISON BY (LOC)L1 BETWEEN IN-ZONE AND OUT-OF-ZONE FAULTS WITH fc = 90.0 (kHz)

SHORT-CIRCUIT LEVEL = 150 MVA

FAULT RESISTANCE = 0.0 (ohms)

TYPE OF FAULT : [a-e]

FAULT INCEPTION ANGLE = 90.0 (degrees)

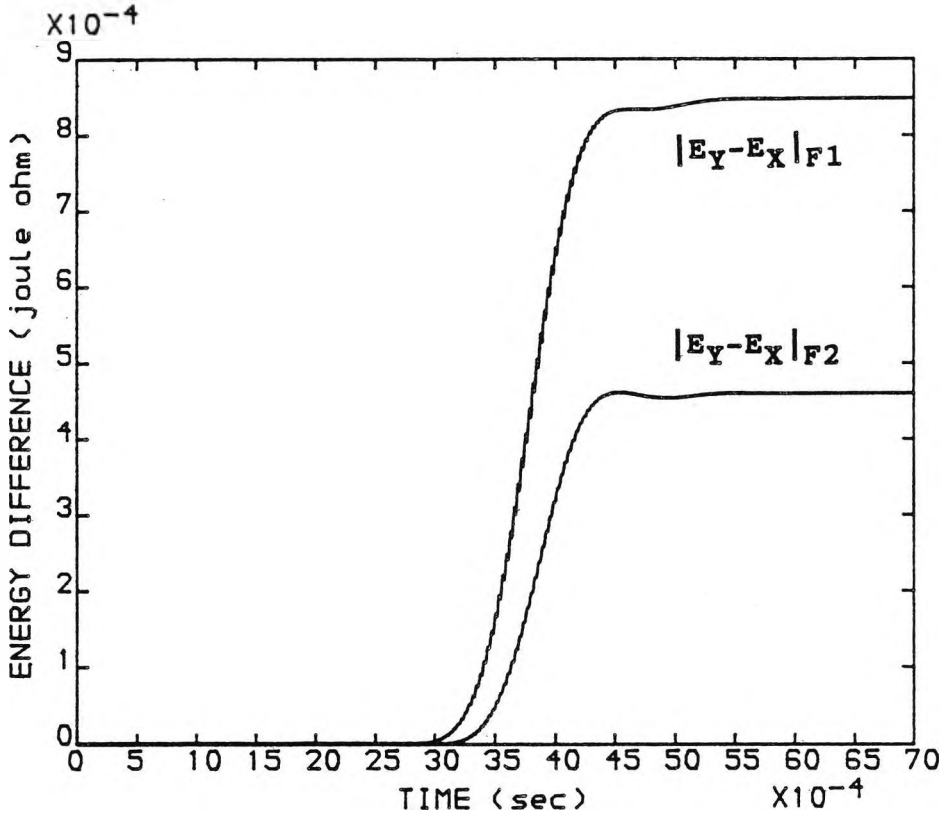

FIG (6.19). ENERGY DIFFERENCE COMPARISON BY (LOC) L1 BETWEEN IN-ZONE AND OUT-OF-ZONE FAULTS WITH fc = 90.0 (kHz)

SHORT-CIRCUIT LEVEL = 50 MVA

FAULT RESISTANCE = 0.0 (ohms)

TYPE OF FAULT : [a-e]

FAULT INCEPTION ANGLE = 90.0 (degrees)

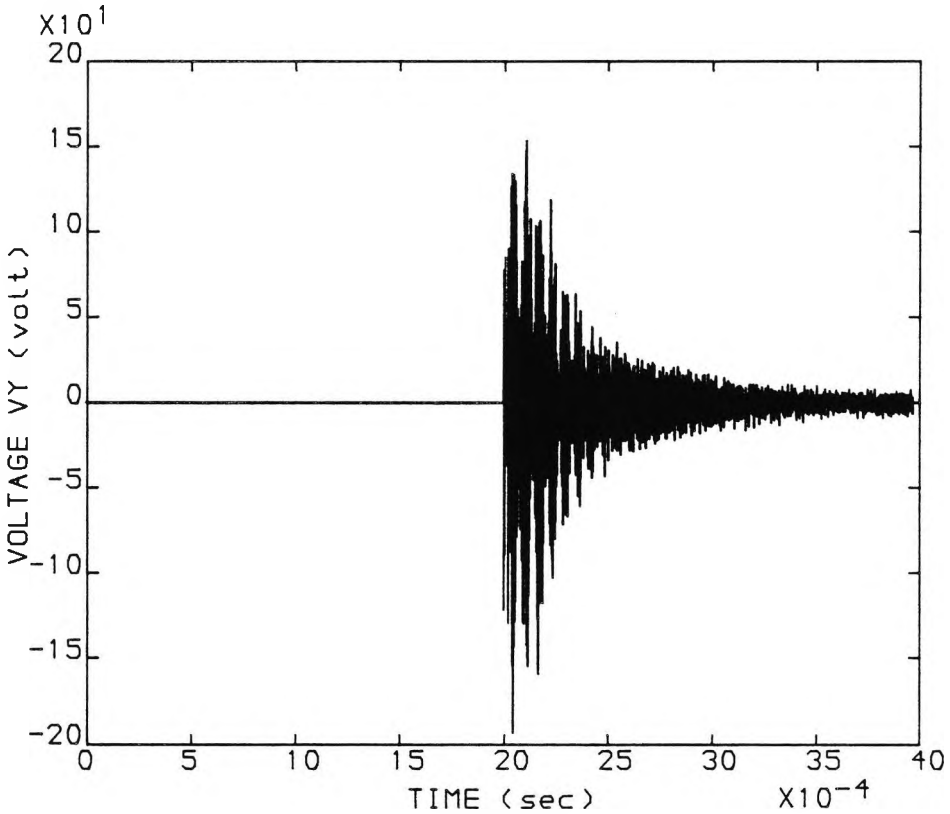

FIG (6.20), VY OF (LOC) L1 DUE TO A FAULT AT POINT F2, WITH fc = 270.0 (kHz)

SHORT-CIRCUIT LEVEL = 250 MVA

FAULT RESISTANCE = 0.0 (ohms)

TYPE OF FAULT : [a-e]

FAULT INCEPTION ANGLE = 90.0 (degrees)

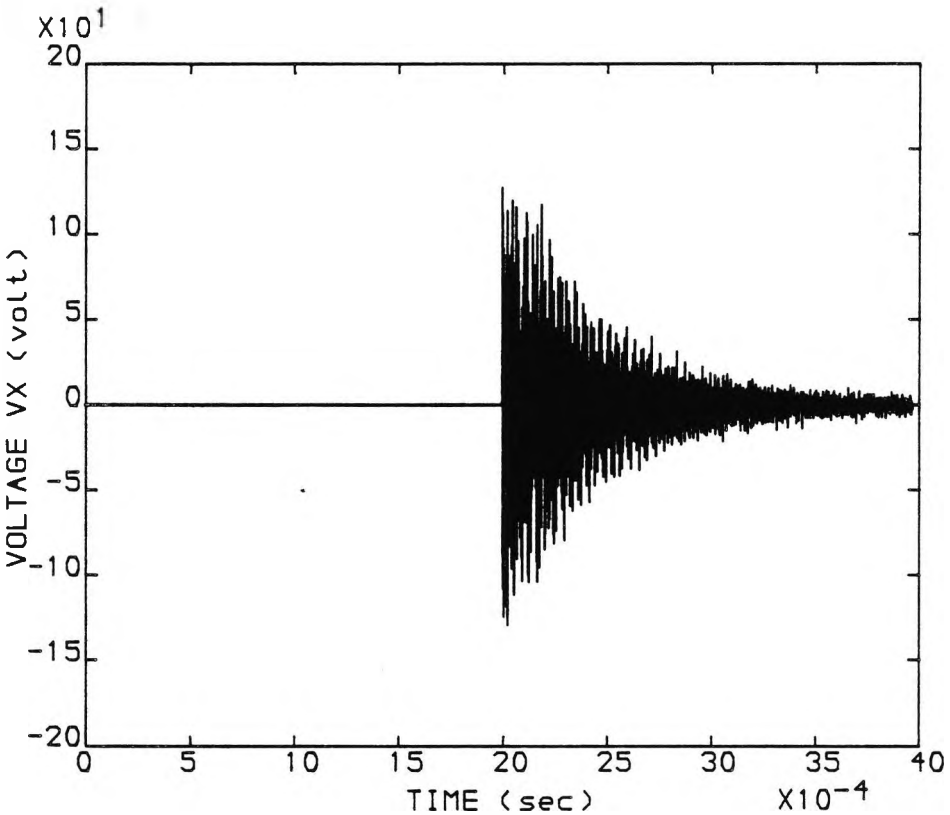

FIG (6.21), VX OF (LOC) L1 DUE TO A FAULT AT POINT F2, WITH fc = 270.0 (kHz)

SHORT-CIRCUIT LEVEL = 250 MVA

FAULT RESISTANCE = 0.0 (ohms)

TYPE OF FAULT : [a-e]

FAULT INCEPTION ANGLE = 90.0 (degrees)

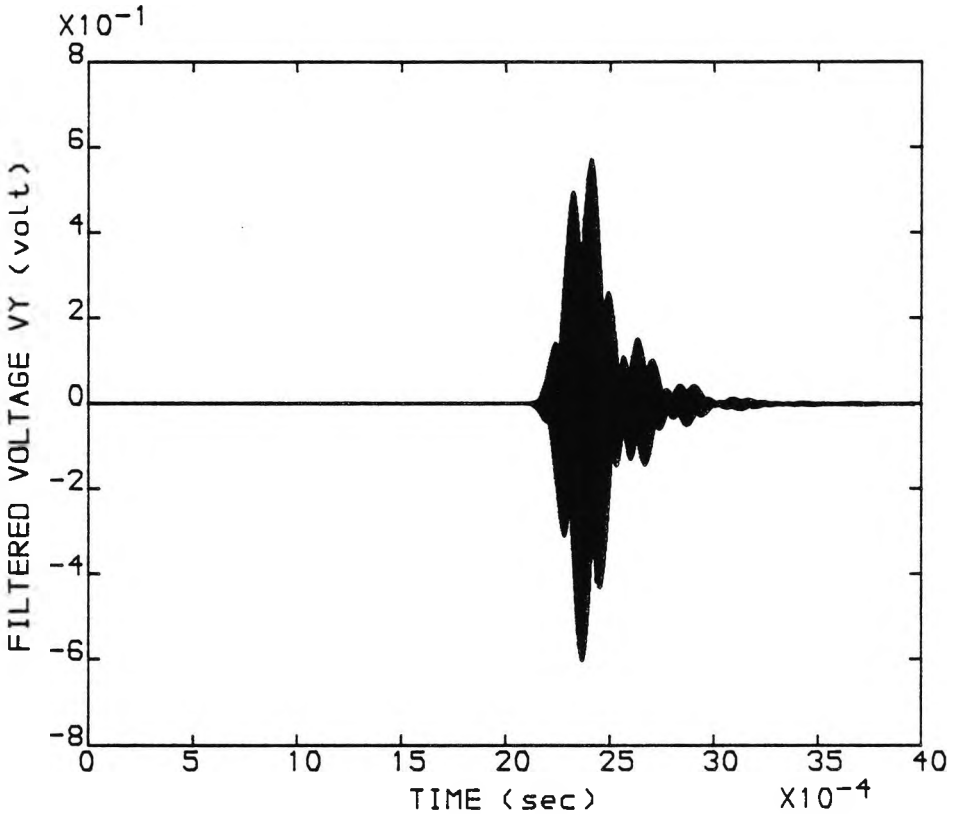

FIG (6.22), FILTERED VY OF (LOC) L1 DUE TO A FAULT AT POINT F2, WITH fc = 270.0 (kHz)

SHORT-CIRCUIT LEVEL = 250 MVA

FAULT RESISTANCE = 0.0 (ohms)

TYPE OF FAULT : [a-e]

FAULT INCEPTION ANGLE = 90.0 (degrees)

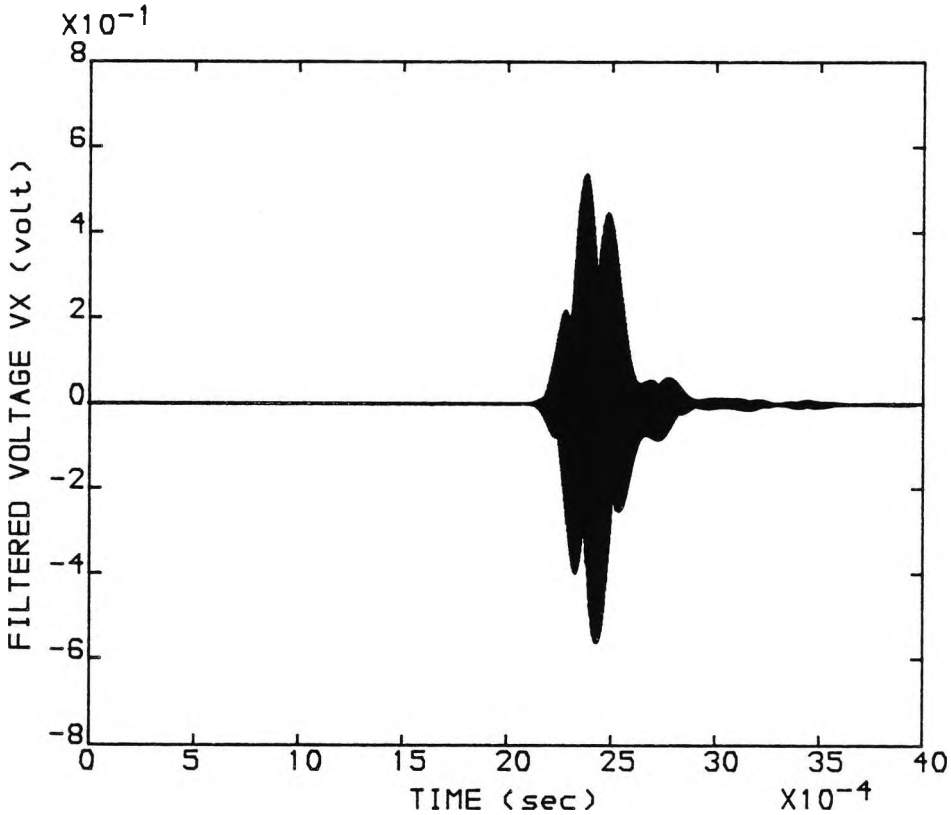

FIG (6.23). FILTERED VX OF (LOC) L1 DUE TO A FAULT AT POINT F2. WITH fc = 270.0 (kHz)

SHORT-CIRCUIT LEVEL = 250 MVA

FAULT RESISTANCE = 0.0 (ohms)

TYPE OF FAULT : [a-e]

FAULT INCEPTION ANGLE = 90.0 (degrees)

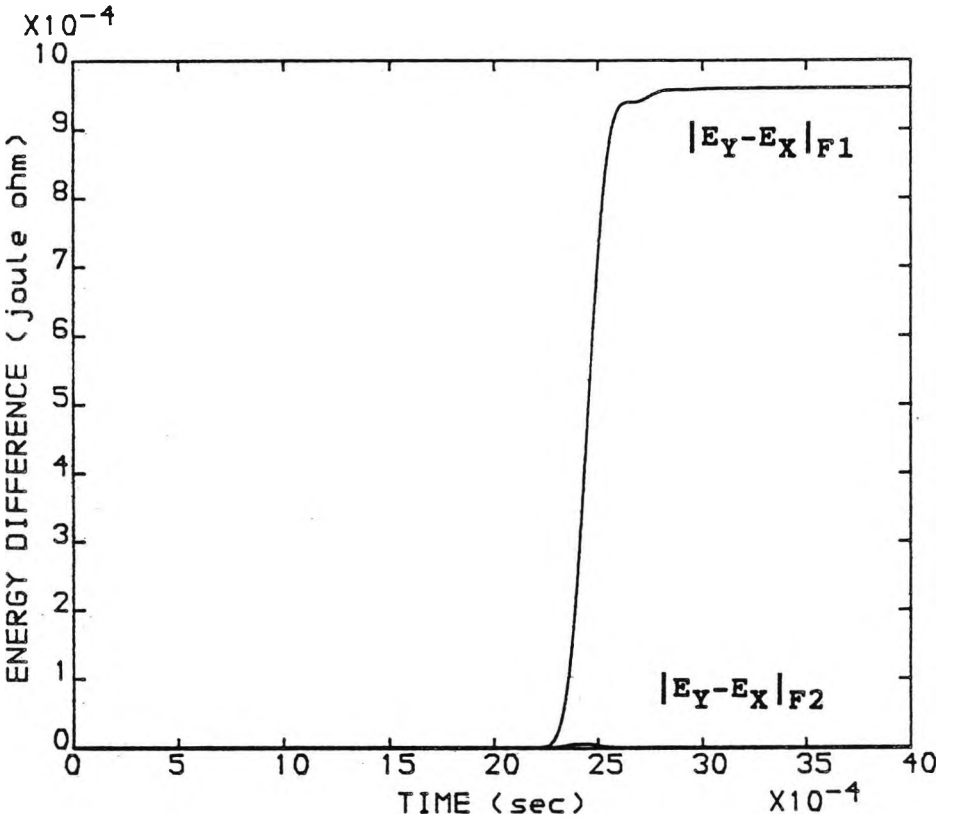

FIG (6.24). ENERGY DIFFERENCE COMPARISON BY (LOC) L1 BETWEEN IN-ZONE AND OUT-OF-ZONE FAULTS WITH fc = 270.0 (kHz)

SHORT-CIRCUIT LEVEL = 250 MVA

FAULT RESISTANCE = 0.0 (ohms)

TYPE OF FAULT : [a-e]

FAULT INCEPTION ANGLE = 90.0 (degrees)

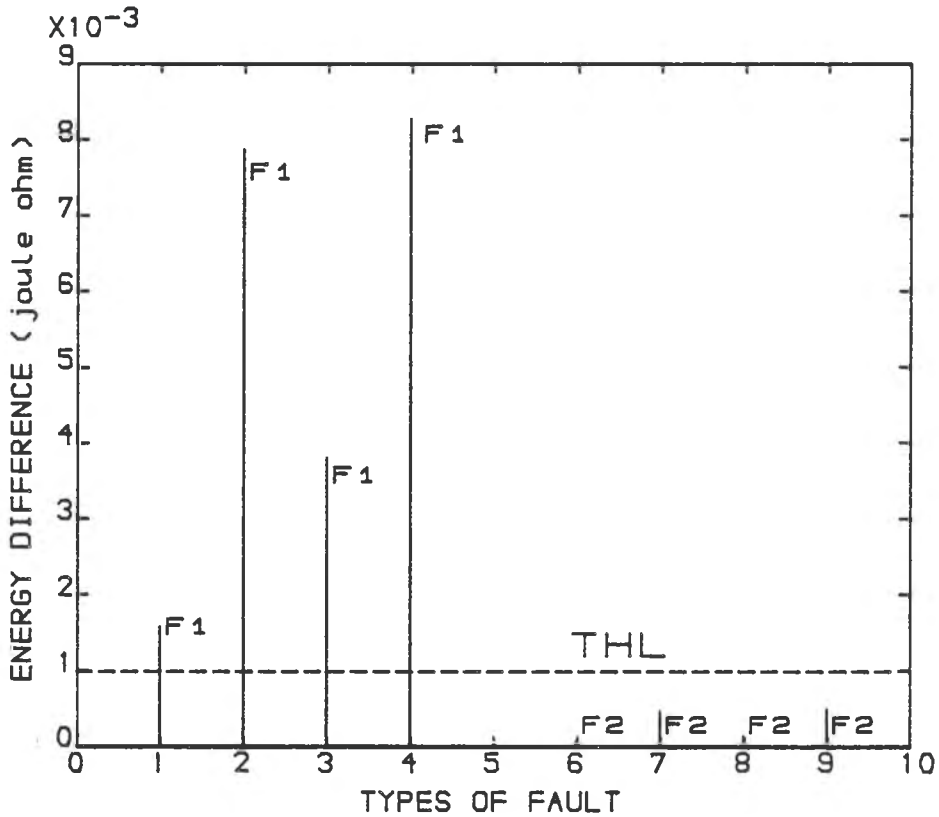

FIG (6.25). DISCRIMINATION BETWEEN IN-ZONE AND OUT-OF-ZONE FAULTS

KEY:

F1 = IN-ZONE FAULT
F2 = OUT-OF-ZONE FAULT

FAULT CONDITION:

SHORT-CIRCUIT LEVEL = 250 MVA
FAULT RESISTANCE = 0.0 (ohms)
FAULT INCEPTION ANGLE = 90.0 (degrees)

TYPE OF FAULT:

1 AND 6 = [a-e]
2 AND 7 = [a-b-e]
3 AND 8 = [a-b-c-e]
4 AND 9 = [a-b]

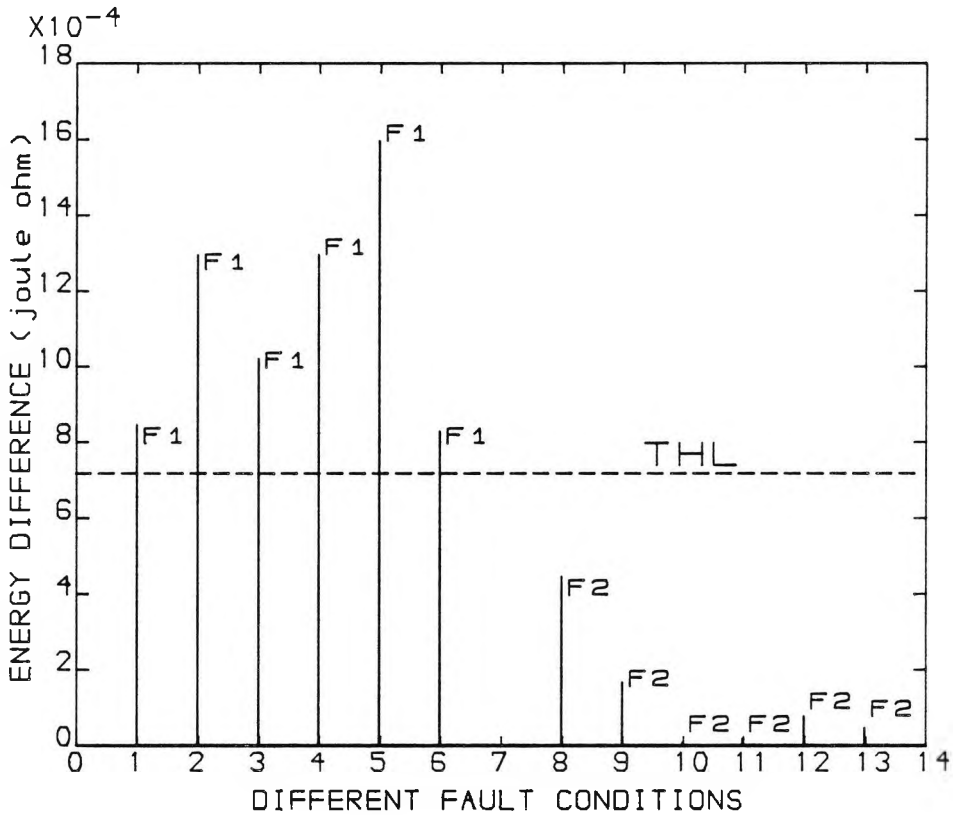

FIG (6.26), DISCRIMINATION BETWEEN IN-ZONE AND OUT-OF-ZONE FAULTS UNDER DIFFERENT FAULT CONDITIONS

KEY:

F1 = IN-ZONE FAULT
F2 = OUT-OF-ZONE FAULT
SCL = SHORT-CIRCUIT LEVEL
Rf = FAULT RESISTANCE
# = FAULT INCEPTION ANGLE

FAULT CONDITIONS:

TYPE OF FAULT: [a-e]

	SCL, (MVA)	Rf, (ohms)	#, (degrees)
1 AND 8 :	50.0	0.0	90.0
2 AND 9 :	150.0	0.0	90.0
3 AND 10:	250.0	100.0	90.0
4 AND 11:	250.0	50.0	90.0
5 AND 12:	250.0	0.0	90.0
6 AND 13:	250.0	0.0	45.0

CHAPTER (7)

SIMULATION OF AN OVERHEAD RADIAL SYSTEM USING (EMTP)

7.1 INTRODUCTION

So far developments and analysis on performance of the new equipment described here has been carried out using a simple 11kV overhead line equipped with three locators. However, in order to investigate the performance of this new equipment more realistically, an overhead radial system equipped with more locators was simulated. The Electromagnetic Transients Program known as (EMTP) and widely used for modelling power systems in order to provide adequate transient protection, was used for simulation purposes.

This chapter begins with a discussion of how the line and the new locator were simulated using EMTP, and it ends by presenting more results on back the directionality and fault locating properties of the new equipment.

7.2 ELECTROMAGNETIC TRANSIENTS PROGRAM (EMTP)

The Electromagnetic Transients Program EMTP, is a general purpose circuit simulation program capable of solving electric power networks of considerable size [32].

It provides the time responses (voltages and currents

as functions of time) of any given interconnections of resistors, inductors, capacitors, single and multiphase π-circuit, distributed and lumped-parameter lines, switches, sources and certain other elements. Inclusion of non-linear elements and capability of simulating frequency-dependent parameters are other features of the Electromagnetic Transients Program. Further, most of the algorithms used in EMTP are numerically stable and avoid the truncation errors which may accumulate from step to step.

This package is available for use on nearly all computer systems of practical interest. While most computer prgrams are developed and operate on only one brand of computer, the EMTP is distinguished by the machine translation of a Universal Transients Program File (UTPF) to most computer systems of interest [33]. Disk storage is needed for the program, data file, plot files and output files. In large measure, minimum requirements are dependent upon complexity of the program and level of usage. The output is the FORTRAN EMTP for the computer system of interest. The procedure has been tested on number of different computer systems [34].

7.2.1 EMTP SIMULATION

The Electromagnetic Transients Program EMTP, was used to simulate the overhead distribution network shown in

Figure (7.1). It is clearly seen that, the network has been equipped with five locators dividing it into several line sections. These have been modelled using distributed parameters as shown in Figure (7.2).

The exact partial differential equations governing the voltage and current on the line for N phases (conductors), are as given below.

$$\frac{-\partial V(x)}{\partial x} = [L]\,\frac{\partial I(x)}{\partial t} + [R]\,I(x) \qquad (7.1)$$

and

$$\frac{-\partial I(x)}{\partial x} = [C]\,\frac{\partial V(x)}{\partial t} \qquad (7.2)$$

Although the incremental section of line has been shown only for N=1, in general, [L], [C] and [R] are vector-matrix equations which are obtained from a line-constants program which is part of the EMTP package.

However, for a three phase assumed perfectly transposed line, instead of the associated resistance and inductance matrices having common diagonal values Z_s and common off-diagonal values Z_m, it is more convenient to use the associated zero and positive sequence values (R_o, L_o) and (R_1, L_1) respectively. This is shown below.

$$\begin{bmatrix} Z_s & Z_m & Z_m \\ Z_m & Z_s & Z_m \\ Z_m & Z_m & Z_s \end{bmatrix} \Longrightarrow \begin{bmatrix} Z_o & 0 & 0 \\ 0 & Z_1 & 0 \\ 0 & 0 & Z_1 \end{bmatrix}$$

where

$$Z_o = Z_s + 2Z_m \qquad (7.3)$$

$$Z_1 = Z_s - Z_m \qquad (7.4)$$

Similarly, the associated zero and positive sequence values Y_o and Y_1 respectively have been used instead of the associated capacitance matrix having common diagonal values Y_s and common off-diagonal values Y_m. This is shown below.

$$\begin{bmatrix} Y_s & Y_m & Y_m \\ Y_m & Y_s & Y_m \\ Y_m & Y_m & Y_s \end{bmatrix} \Longrightarrow \begin{bmatrix} Y_o & 0 & 0 \\ 0 & Y_1 & 0 \\ 0 & 0 & Y_1 \end{bmatrix}$$

where

$$Y_o = Y_s - 2Y_m \qquad (7.5)$$

$$Y_1 = Y_s + Y_m \qquad (7.6)$$

The locator parameters have been simulated using resistive values, inductive reactance and capacitive reactance, in ohms, for resistors, inductors and capacitors respectively.

7.3 SELECTION OF APPROPRIATE SIGNALS

As previously mentioned, the signals across the resistors of stack tuners situated at sides X and Y of each locator has been used for analysis. For convenience, these voltages are referred to as VX and VY respectively, followed by the number of each locator. The energy content in the filtered voltages at sides Y and X are referred to as EVX and EVY respectively, followed by the number of each locator. The two different fault positions considered are F1 and F2 as shown in Figure (7.1).

7.4 EMTP SIMULATION RESULTS

First consider a fault at F1. Figures (7.3) and (7.4) show the voltage signals $(VY_n)_{F1}$ and $(VX_n)_{F1}$ respectively. Their corresponding voltage waveforms after passage through a band-pass filter are shown in Figures (7.5) and (7.6) respectively. The comparison between energy contents $(EVY_n)_{F1}$ and $(EVX_n)_{F1}$ of filtered voltage waveforms $(VY_n)_{F1}$ and $(VX_n)_{F1}$ respectively is shown in Figure (7.7). Due to the fact that, $(EVY_n)_{F1}$ is at a higher level than $(EVX_n)_{F1}$, the locator $(LOC)_n$ determines the fault to be downstream. The corresponding energy levels of those of Figure (7.7) obtained by locator $(LOC)_{n+1}$ due to the same fault at F1 is shown in Figure (7.8). In this case, since $(EVX_{n+1})_{F1}$ is higher than $(EVY_{n+1})_{F1}$, the locator $(LOC)_{n+1}$

determines the fault to be upstream.

However, if a fault occurs at F2 as shown in Figure (7.1), due to the fact that, $(EVX_{n+1})_{F2}$ would be lower than $(EVY_{n+1})_{F2}$, the locator $(LOC)_{n+1}$ sees the fault to be downstream as shown in Figure (7.9). The behaviour of locator $(LOC)_{n+2}$ due to the fault at F2 is shown in Figure (7.10), in which case, the fault is correctly determined to be upstream.

The comparison between the magnitude of the energy level difference, $|(EVY-EVX)_n|_{F1}$ and $|(EVY-EVX)_n|_{F2}$ of locator $(LOC)_n$ due to faults at F1 and F2 respectively is shown in Figure (7.11). This clearly shows that a threshold level THL, corresponding to 5.0×10^{-2} Joule ohm, is well exceeded by $|(EVY-EVX)_n|_{F1}$ and is well above $|(EVY-EVX)_n|_{F2}$. Therefore the locator $(LOC)_n$ would determine a fault on the line section between locators $(LOC)_n$ and $(LOC)_{n+1}$ to be in-zone and a fault beyond locator $(LOC)_{n+1}$ to be out-of-zone.

Furthermore, it should be appreciated that, due to a fault at F1, only locators (LOC)n and (LOC)n+1 would experience energy level difference greater than a predefined threshold level, THL. Figure (7.12) clearly illustrates that, only energy level difference of the two locators isolating the faulty section of the line have well exceeded the THL, while that of other remote

locators, $(LOC)_{n-1}$, $(LOC)_{n-2}$ and $(LOC)_{n+2}$ are well below the THL. The corresponding energy levels to those of Figure (7.12), due to a fault at F2 is shown in Figure (7.13). This also clearly shows that a fault at F2 is only sensed by locators $(LOC)_{n+1}$ and $(LOC)_{n+2}$.

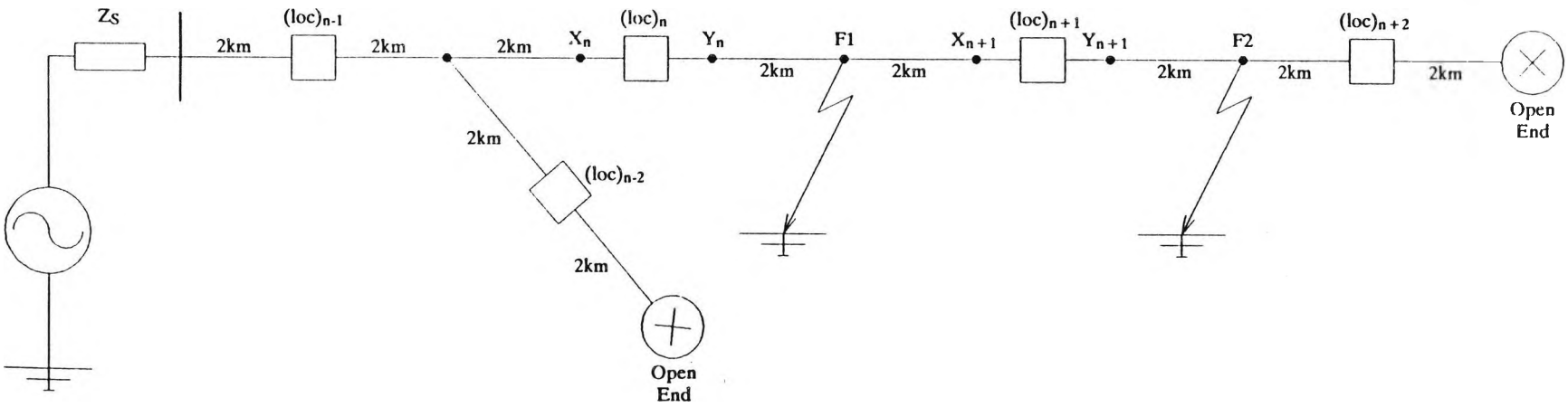

FIG (7.1), SCHEMATIC DIAGRAM OF A SIMPLE OVERHEAD RADIAL SYSTEM

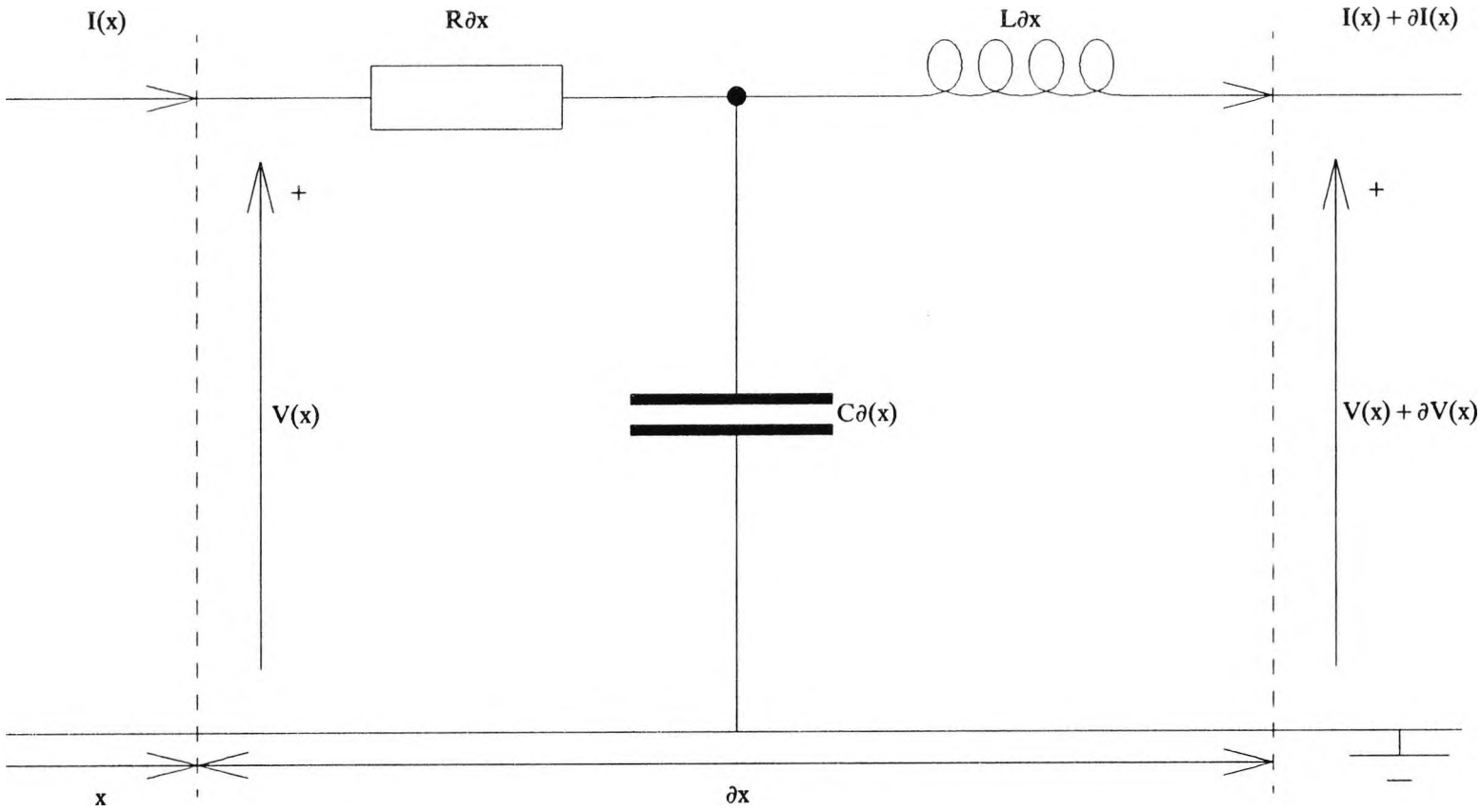

FIG (7.2), DIFFERENTIAL LINE ELEMENT

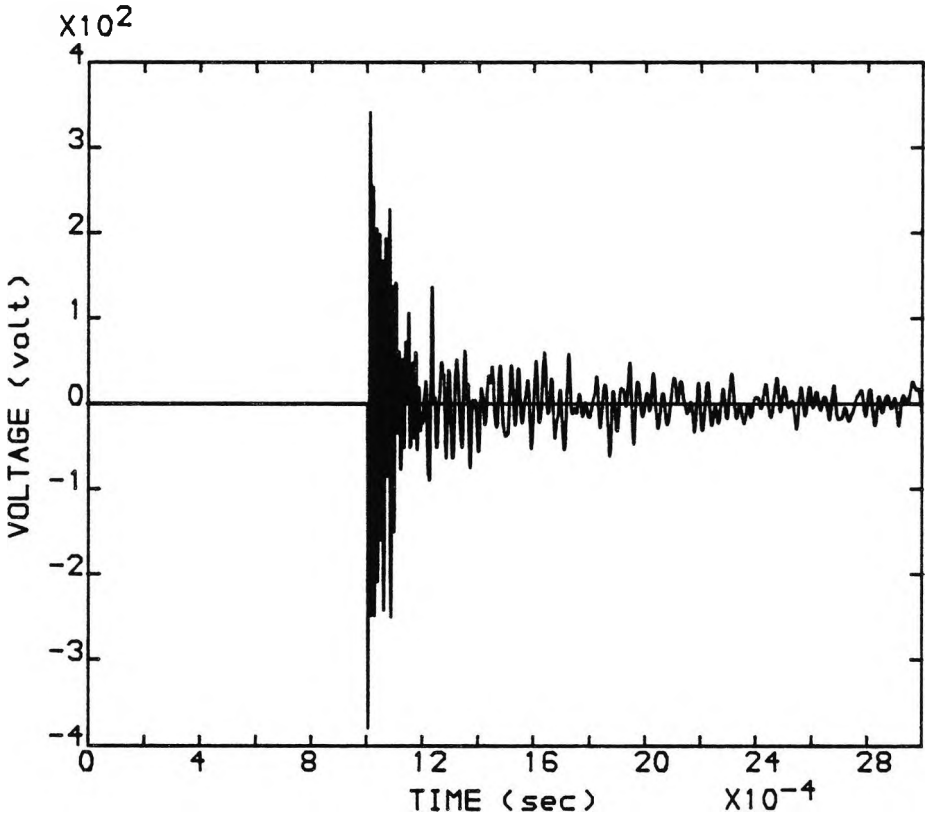

FIG (7.3). VOLTAGE SIGNAL (VYn) F1 DUE TO A FAULT AT POINT F1, WITH fc = 90.0 (kHz)

SHORT-CIRCUIT LEVEL = 250 MVA

FAULT RESISTANCE = 0.0 (ohms)

TYPE OF FAULT : [a-e]

FAULT INCEPTION ANGLE = 90.0 (degrees)

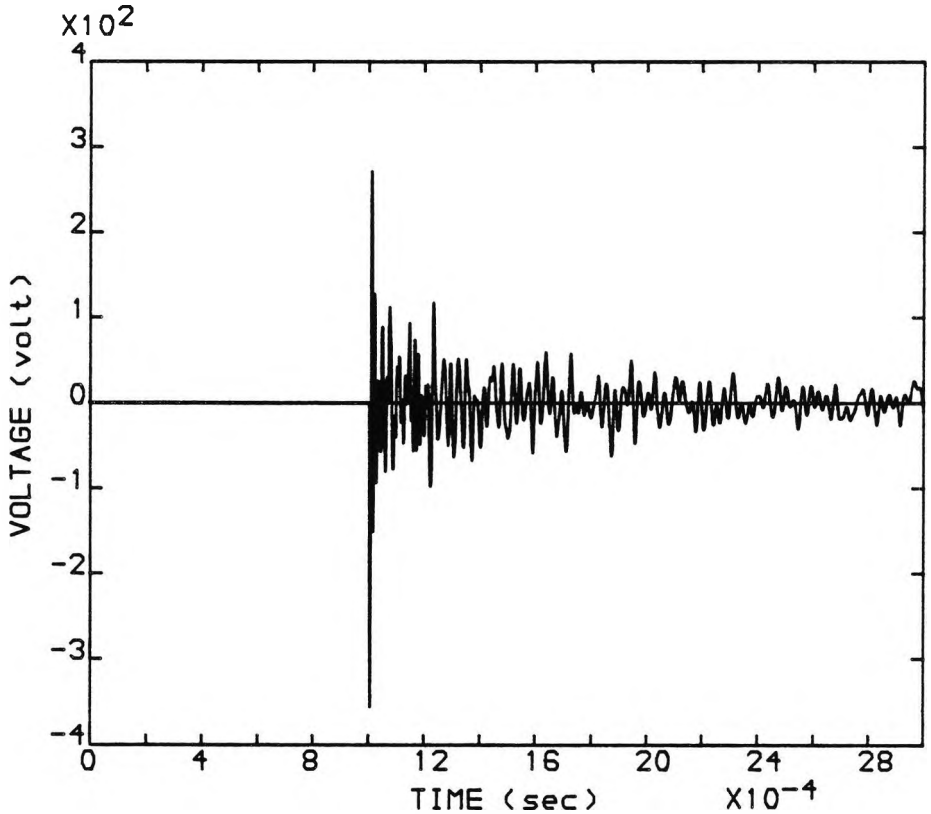

FIG (7.4). VOLTAGE SIGNAL (VXn) F1 DUE TO A FAULT AT POINT F1, WITH fc = 90.0 (kHz)

SHORT-CIRCUIT LEVEL = 250 MVA

FAULT RESISTANCE = 0.0 (ohms)

TYPE OF FAULT : [a-e]

FAULT INCEPTION ANGLE = 90.0 (degrees)

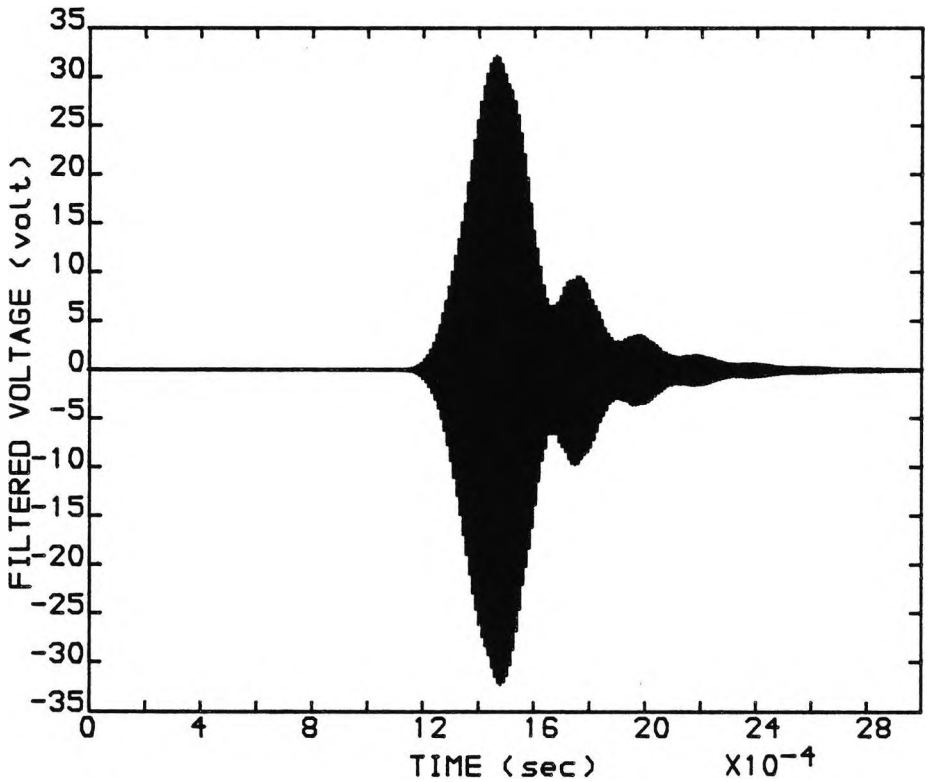

FIG (7.5). FILTERED VOLTAGE (FVYn) F1 DUE TO A FAULT AT POINT F1. WITH fc = 90.0 (kHz)

SHORT-CIRCUIT LEVEL = 250 MVA

FAULT RESISTANCE = 0.0 (ohms)

TYPE OF FAULT : [a-e]

FAULT INCEPTION ANGLE = 90.0 (degrees)

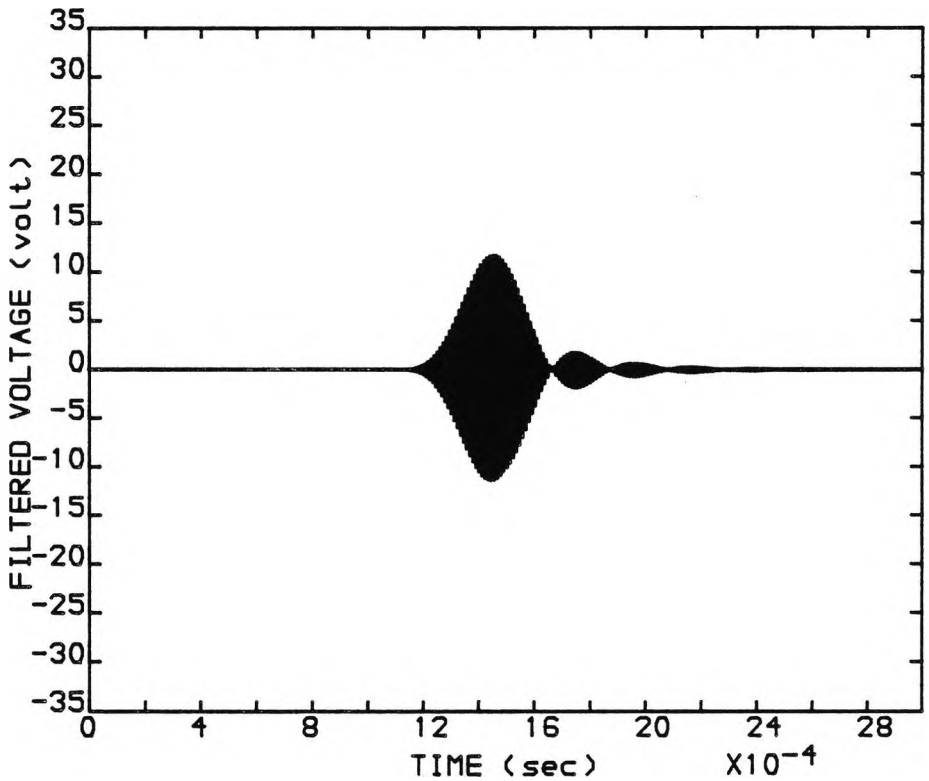

FIG (7.6). FILTERED VOLTAGE (FVXn) F1 DUE TO A FAULT AT POINT F1. WITH fc = 90.0 (kHz)

SHORT-CIRCUIT LEVEL = 250 MVA

FAULT RESISTANCE = 0.0 (ohms)

TYPE OF FAULT : [a-e]

FAULT INCEPTION ANGLE = 90.0 (degrees)

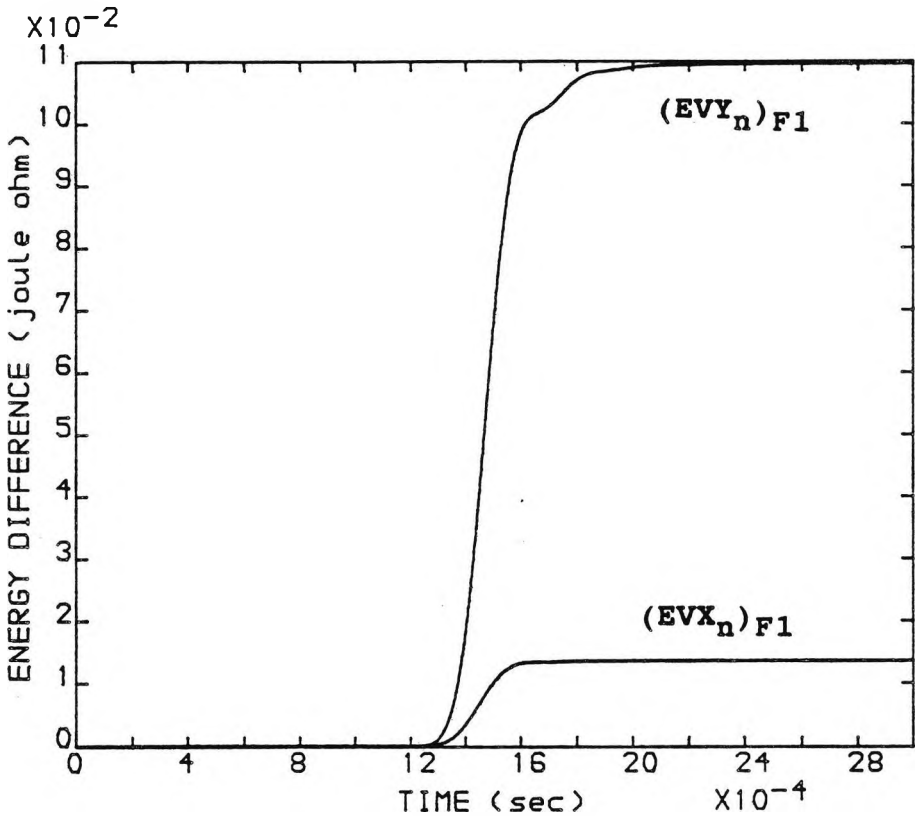

FIG (7.7). ENERGY COMPARISON BY (LOC)n DUE TO A FAULT AT POINT F1 WITH fc = 90.0 (kHz)

SHORT-CIRCUIT LEVEL = 250 MVA

FAULT RESISTANCE = 0.0 (ohms)

TYPE OF FAULT : [a-e]

FAULT INCEPTION ANGLE = 90.0 (degrees)

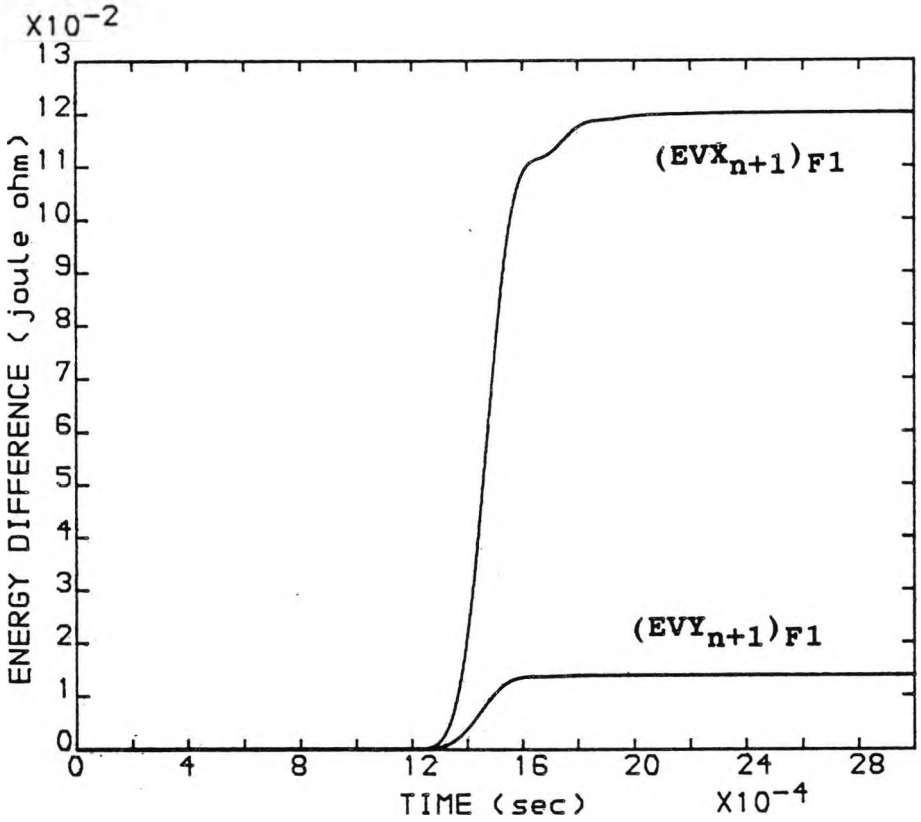

FIG (7.8). ENERGY COMPARISON BY (LOC)n+1 DUE TO A FAULT AT POINT F1 WITH fc = 90.0 (kHz)

SHORT-CIRCUIT LEVEL = 250 MVA

FAULT RESISTANCE = 0.0 (ohms)

TYPE OF FAULT : [a-e]

FAULT INCEPTION ANGLE = 90.0 (degrees)

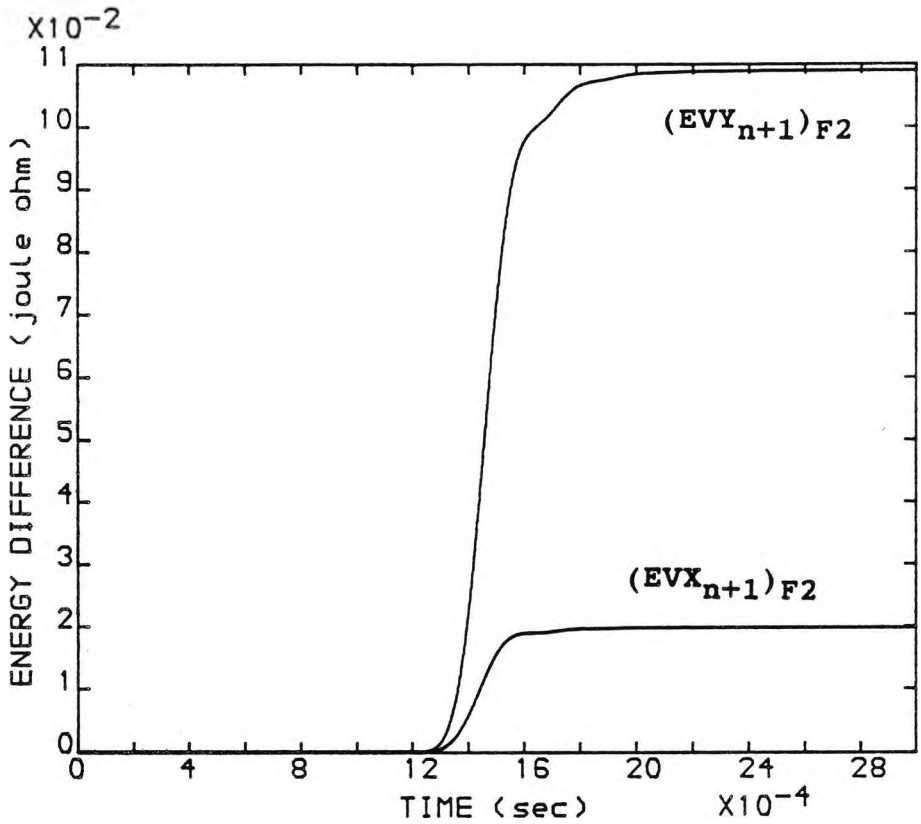

FIG (7.9). ENERGY COMPARISON BY (LOC) n+1 DUE TO A FAULT AT POINT F2 WITH fc = 90.0 (kHz)

SHORT-CIRCUIT LEVEL = 250 MVA

FAULT RESISTANCE = 0.0 (ohms)

TYPE OF FAULT : [a-e]

FAULT INCEPTION ANGLE = 90.0 (degrees)

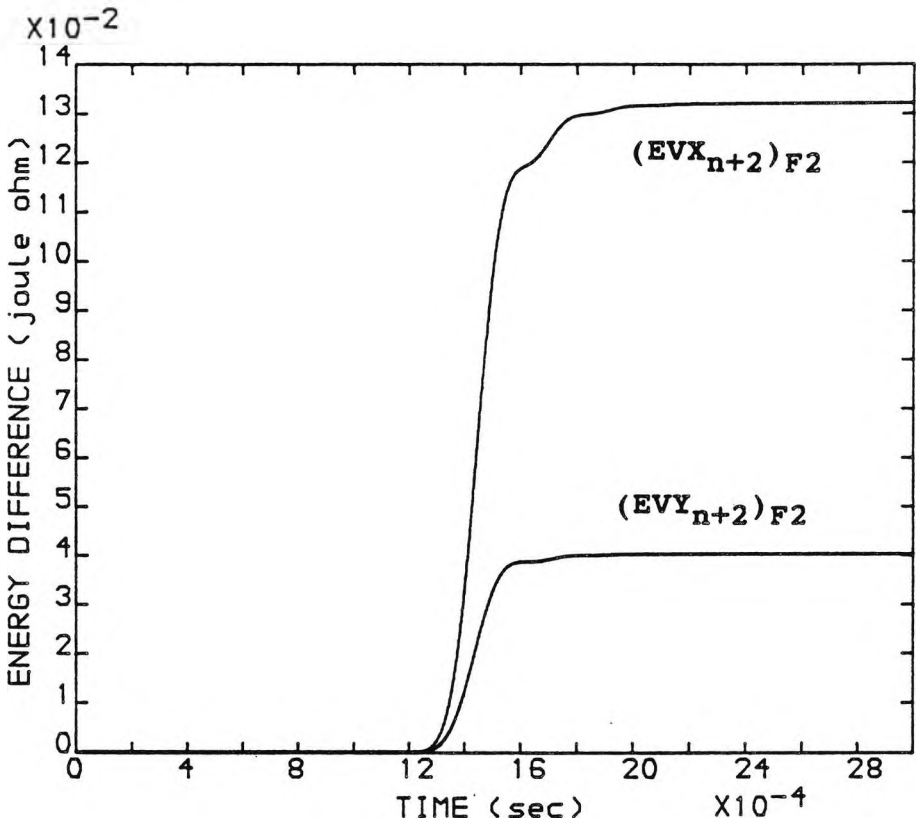

FIG (7.10). ENERGY COMPARISON BY (LOC)n+2 DUE TO A FAULT AT POINT F2 WITH fc = 90.0 (kHz)

SHORT-CIRCUIT LEVEL = 250 MVA

FAULT RESISTANCE = 0.0 (ohms)

TYPE OF FAULT : [a-e]

FAULT INCEPTION ANGLE = 90.0 (degrees)

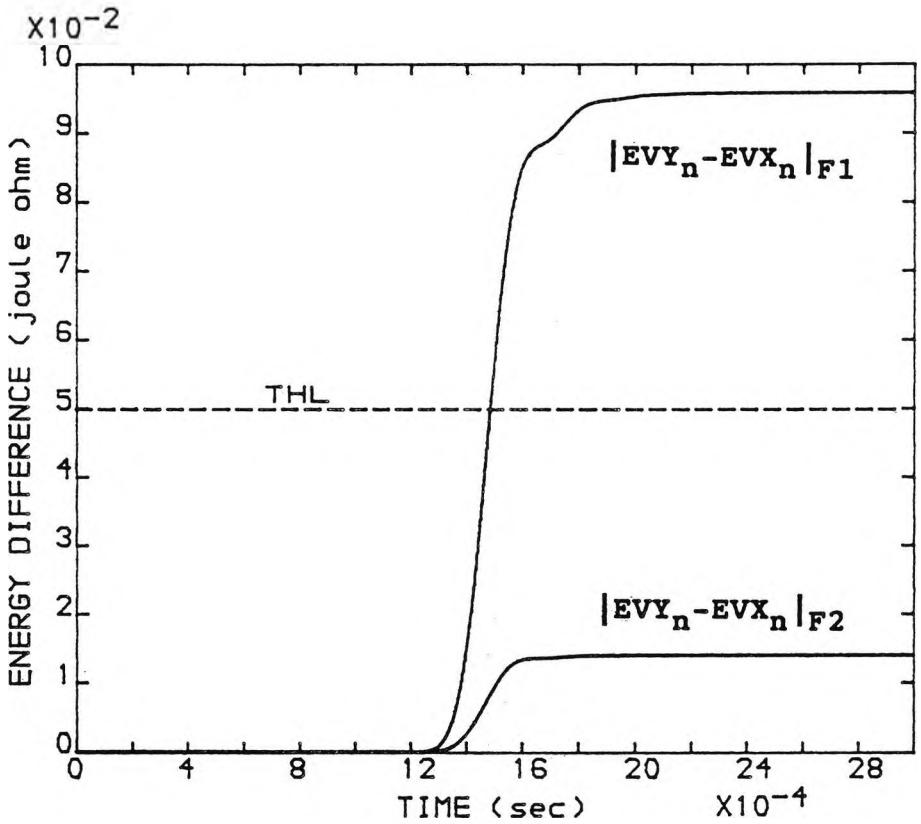

FIG (7.11). DISCRIMINATION BETWEEN FAULTS AT POINTS F1 AND F2 WITH fc = 90.0 (kHz)

SHORT-CIRCUIT LEVEL = 250 MVA

FAULT RESISTANCE = 0.0 (ohms)

TYPE OF FAULT : [a-e]

FAULT INCEPTION ANGLE = 90.0 (degrees)

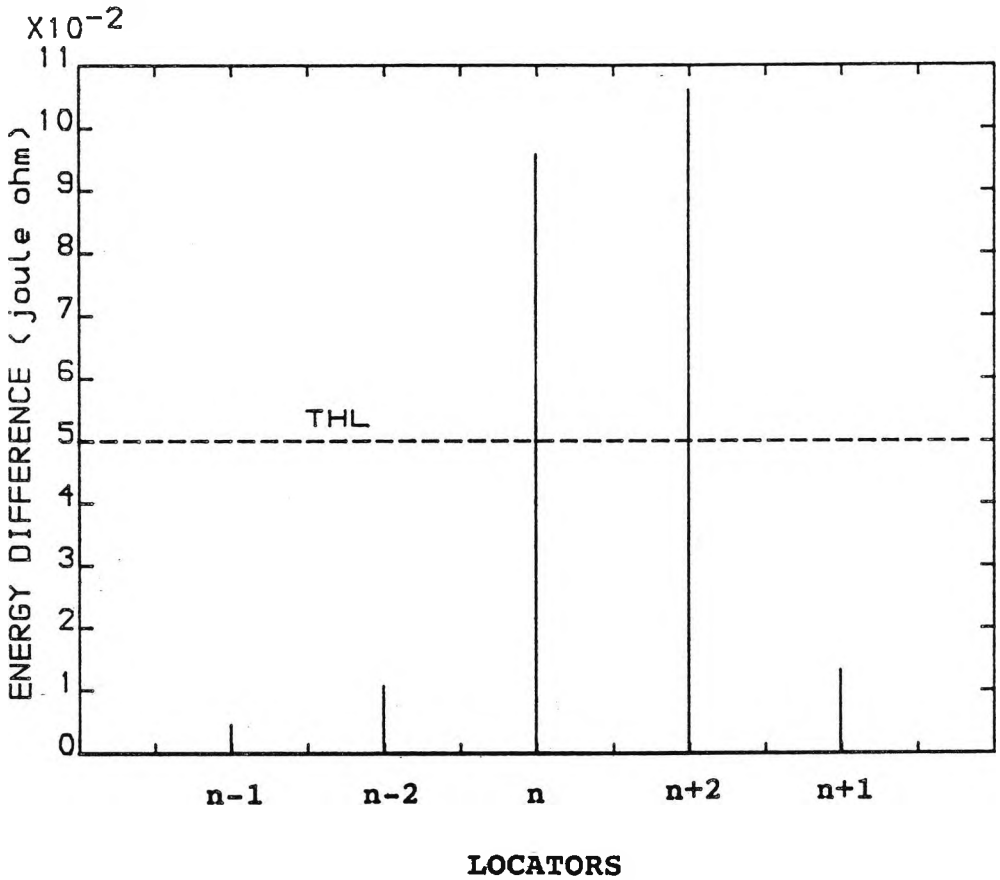

FIG (7.12). COMPARISON OF ENERGY DIFFERENCES OF LOCATORS WITH THL DUE TO A FAULT AT F1

FAULT CONDITIONS:

SHORT-CIRCUIT LEVEL = 250 MVA

FAULT RESISTANCE = 0.0 (ohms)

TYPE OF FAULT : [a-e]

FAULT INCEPTION ANGLE = 90.0 (degrees)

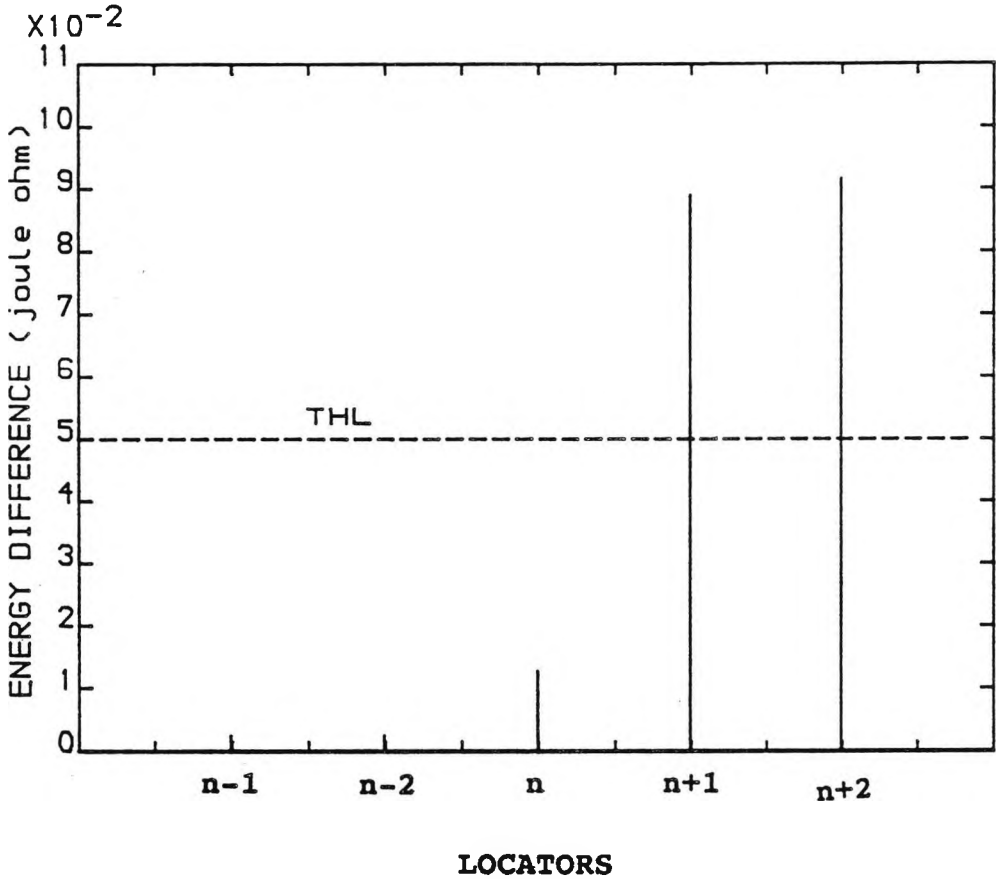

FIG (7.13). COMPARISON OF ENERGY DIFFERENCES OF LOCATORS WITH THL DUE TO A FAULT AT F2

FAULT CONDITIONS:

SHORT-CIRCUIT LEVEL = 250 MVA

FAULT RESISTANCE = 0.0 (ohms)

TYPE OF FAULT : [a-e]

FAULT INCEPTION ANGLE = 90.0 (degrees)

CHAPTER (8)

CONCLUSIONS AND FUTURE WORK

8.1 CONCLUSIONS

Utilities and equipment manufacturers have been investigating and developing automated systems for the protection of power distribution systems for over a decade. Most utilities employ reclosing relays with circuit breakers to handle transient faults. Permanent faults, however, require the location of the faulty line section, isolation and possibly a rescheduling of the network before normal power delivery may be resumed. Non-directional fault indicators are available both for short circuit and earth fault current detection. However, in interconnected networks, non-directional fault indicators become less useful and often directional fault locators are required. The work presented in this thesis, has been concerned with investigations into the design of a new directional fault locator suitable for use on overhead distribution systems operating typically at 11kV. The main features of this new protection scheme are that, not only does it determine the direction of a fault, i.e, whether a fault is upstream or downstream, but it also distinguishes between in-zone and out-of-zone faults, i.e, it identifies the faulty section of an overhead distribution system.

Development of the new equipment, using a computer

program based on a frequency domain technique, has been well described. Digital simulation of the network and the new locator, using two-port transfer matrices, has also been described in full details.

The new equipment consists of a line trap circuit and two identical stack tuners, from which information for directional fault finding and locating are provided. The operating principle of this new protection scheme, are based on the detection of high frequency components of fault generated noise and have been fully discussed in the thesis. In the past, the schemes based upon this operating principle have relied on use of a communication link to locate a fault on an overhead distribution system. However, the main advantage of this new directional fault locator is that, it does not require the presence of such a communication link. From the construction point of view, another major advantage of this new scheme is that, there is no need for any connections between the three corresponding locators each placed on one phase of a three phase system.

Voltage signals obtained from the stack tuners in each of the three phases of the system were combined together using the aerial mode combination [1, -2, 1]. This is a feature of the new scheme which successfully incorporates a cancellation method for any common mode signals from remote sources such as radio transmitters or

from sources of large r.f interference in the vicinity.

In order to increase the difference between the desired signals, a filtering processing was used. This was carried out using a narrow band-pass Butterworth filter, tuned to the same centre frequency f_c as that of the line trap circuit and stack tuners of each equipment. This part of the simulation was performed using SPICE .

The filtered response of the signals have shown to provide better results, i.e, better discrimination ratio between the two sides of the locator. However, to further increase and maximise this discrimination ratio, comparison of the energy content in the filtered response was considered. This was simply carried out by squaring and integrating the filtered signals over a period of time. As a result, a far better discrimination ratio between the corresponding signals from the two sides of the new locator network was provided, in order to correctly and safely determine the direction of a fault.

The sensitivity analysis has shown that, the new equipment does correctly determine the direction of a fault regardless of its type. The effect of fault resistance has been studied and satisfactory responses have shown that, the performance of the new equipment is almost independent of fault resistance up to 100.0 Ω.

The two extreme cases from the travelling-wave point of view, have also carefully been examined and it has been shown that, the directionality property of the new equipment is not influenced by fault inception angles between 1 to 90 degrees. Moreover, satisfactory responses have also been obtained under different source capacities, and finally it was shown that, different fault positions did not have any effect on the performance of the equipment.

Further satisfactory response with the new equipment tuned to a centre frequency of 270 kHz rather than 90 kHz, which is the frequency used throughout the project, has also been obtained. This certainly has shown that, the stack tuners and the line trap circuit of each locator could be tuned to any frequency that may not interfere with other carrier frequencies.

Further simulation results have shown that, in-zone and out-of-zone faults could best be distinguished from each other by comparing the energy level difference obtained from each locator with a predefined threshold level THL. Sensitivity analyses have shown that, the energy level difference of any locator, sensing a fault to be an in-zone one, always exceeds the threshold level. Similarly the energy level difference of any locator, sensing a fault to be out-of-zone, would never reach the threshold level THL.

Furthermore, for faults with resistance up to 100 Ω, short circuit levels as low as 50 MVA and fault inception angles down to 45 degrees, the in-zone and out-of-zone faults have been very well and correctly distinguished.

A more realistic radial overhead distribution network, incorporating more locators has also been simulated to further analyse the performance of the new locator. This has been conducted using the Electromagnetic Transients Program EMTP. This has resulted in a set of further simulation results.

From the results illustrated through out this thesis, it should be appreciated that, the new equipment and scheme can detect low level faults, which other conventional schemes have difficulties in coping with. Finally, it is hoped and planned that, this work will be the precursor to economic automatic fault detection and location.

8.2 SUGGESTIONS FOR FUTURE WORK

As previously described, the design of the new locator has been carried out, using computer simulation aids. Therefore, a major area to which a great deal of consideration should be given is the physical realisation of the parameters used to develop the new equipment.

These, in particular, include the inductor L1 in the line trap circuit and the capacitors Cs in the stack tuners of each locator, (see Figure (2.6)). Further consideration can also be given to the digital signal processing required, in order to provide a better discriminative ability for the locator for directional fault finding and locating.

It has been clearly seen that, the performance of the new equipment has only been evaluated on a simple radial overhead power distribution system. The new scheme and equipment could very well be applied to other typical arrangements for the overhead distribution networks. These include, network or grid system of distribution and parallel or loop system.

The performance of the new equipment has been evaluated for two different centre frequencies, 90.0 kHz and 270.0 kHz only. Hence further work could be carried out to optimise the design of the new locator for a range of centre frequencies and fully investigate the performance of these arrangements for a wide variety of practical fault conditions in typical overhead distribution networks mentioned above.

As previously mentioned, the operating principle of the new locator to distinguish between in-zone and out-of-zone faults, entirely depends on use of a threshold

level THL. This reference level depends on the various circuit gains and it should be set to control the basic sensitivity to faults. Therefore, determination of an optimum threshold level that can be used in all different fault conditions, is clearly an area in which further work may usefully be done. It should be mentioned that, this requires more sensitivity analyses to be carried out.

Investigations into the design of this new equipment have been carried out for an overhead distribution system operating typically at 11kV. However, further considerations regarding the application of this locator to other system voltages up to 36kV could also be looked into.

REFERENCES

[1] S.J.Balser, K.A.Clements, D.J.Lawrence, " A Micro-processor-based Technique for Detection of High Impedance Faults ", Paper No.86 WM 155-6. IEEE/PES WPM,1986

[2] M.Aucoin, J.Zeigler and B.D.Russell, " Feeder Protection and Monitoring Systems, Part I: Design, implementation and testing ", IEEE transactions on Power Apparatus and Systems, Vol. PAS-104, No. 4,April, 1985, PP.873-880.

[3] H.Calhoun,et.al., " Development and Testing of an Electro-mechanical Relay to Detect Fallen Distribution Conductors ", IEEE Transactions on Power Apparatus and Systems, Vol. PAS-101 No. 6, June 1982, PP. 1643-1648.

[4] A.G.Phadke and He Hankun, " Detection of Broken Distribution Conductors," Proceedings of IEEE Southeast Conference, Releigh, N. Carolina, Paper No. CH2161-8/85/0000-0074.

[5] H.L.Graham, A.J.Carlson, T.AGranberg, " Broken Conductor and High Impedance Fault Detection by High Frequency Impedance Monitoring ", Paper No. A-80-06406. IEEE WPM,1980.

[6] B.M.Aucion and B.D.Russell, " Distribution High Impedance Fault Detection Utilising High Frequency Current Components ", IEEE Transactions on Power Apparatus and Systems Vol. PAS-101, No. 6, June 1982, PP. 1596-1606.

[7] B.M.Aucion, B.D.Russell, " Detection of Distribution High Impedance Faults Using Burst Noise Signals Near 60 Hz", IEEE Transactions on Power Delivery, 86T&D546-6.

[8] " Detection of High Impedance Faults," EPRI Report EL-2413, Prepared by Power Technologies, Inc., June,1982.

[9] " Detection of Arcing Faults on Distribution Feeder, " EPRI Report EL-2757, Prepared by Texas A&M University, December, 1982.

[10] R.E.Lee, M.T.Bishop, " Performance Testing of the Ratio Ground Relay on a Four-Wire Distribution Feeder", IEEE Transactions on Power Apparatus and Systems, Vol.PAS-102, No.9 Sep.1983.

[11] B.Don Russell, Ram P. Chinchali, and K. Mehta, " An Arcing Fault Detection Technique Using Low Frequency Current Components - Performance Evaluation Using Recorded Field Data", IEEE Transactions on Power Delivery, Vol. 3, No. 4, October 1988.

[12] B.Don Russell, Ram P. Chinchali, " A digital Signal Processing Algorithm for Detecting Arcing Faults on Power Distribution Feeders, " IEEE Transactions on Power Delivery, Vol,4, No.1, January 1989. PP. 132-140.

[13] B.Don.Russell, Ram.P.Chinchail, C.J.Kim, "Behaviour of Low Frequency Spectra During Arcing Fault and Switching Events ", IEEE Transactions on Power Delivery, Vol.3, No.4, October 1988.

[14] CLARKE,G.J., and HORN,H.E.,"Monitoring and Protection Systems Suited to Overhead Distribution Systems", April 1985, Proceedings of The Third International Conference on Developments in Power System Protection, IEE, Pub.No.249, PP.199-203.

[15] Mike.Aucoin, "Status of High Impedance Fault Detection" IEEE Transactions on Power Apparatus and Systems, Vol.PAS-104, No.3, March 1985.

[16] J.R.Dunki-jacobs, " The Effects of Arcing Faults on Low-Voltage Systems Design " IEEE Transactions on Industry Applications, Vol. 1A-8, No. 3, May/June 1972.

[17] Redmon,J.R., and Gentz, C.H., "Effect of Distribution Automation and Control on Future Systems Configuration",IEEE Transactions on Power Apparatus and Systems, Vol PAS-100, April 1981 42-47.

[18] Chen, A.C.M. "Automated Power Distribution" IEEE Spectrum April 1982. 55-60.

[19] GALLOWAY,R.H., SHORROCKS,W.B., and WEDEPOHL,L.W. "Calculation of electrical parameters for short and long polyphase transmission lines", 1964, Proc.IEE, 111, (12), pp. 2051-2059

[20] JOHNS,A.T., and AGGRAWAL,R.K. "Digital simulation of faulted e.h.v transmission lines with particular reference to very high-speed protection", 1976, Proc, IEE, vol 123, no.4, pp.353-359

[21] WEDEPOHL,L.M., and MOHAED, S.E.T.
"Multiconductor transmission lines", 1969, Proc.IEE, 116(9), pp 1553-1563.

[22] WEDEPOHL, L.M.
"Application of matrix methods to the solution of travelling-wave phenomena in polyphase systems", 1963, Proc. IEE, 110, (12), pp.2200-2212.

[23] COX, E.H.
"Overhead-line practice", 1975, Proc. IEE, No.10R, vol.122, pp 1009-1017.

[24] BUTTERWORTH, S.
Electrical characteristics of overhead lines, The electrical research association,1954.

[25] DAY,Sylvia J., Mullinex, N., and REED, J.R.: "Developments in obtaining transient response using Fourier transforms: Gibbs phenomena and Fourier integrals", Internat. J. Elect. Engng. Educ., 1965, 3, pp. 501-506

[26] DAY,Sylvia J., Mullinex, N., and REED, J.R: " Developments in obtaining transient response using Fourier transforms: Use of the modified Fourier transform",ibid., 1966, 4, pp. 31-40

[27] S. Ramo, J. R. Whinnery, Fields and Waves in Modern Radio, 1964, John Wiley and Sons, inc.

[28] Dwight, tables of integrals, Macmillan, rev.ed., 1947; Mclachlan, Bessel functions for engineers, oxford, 1934.

[29] L, Weinberg, "Network design by use of modern synthesis techniques and tables", Proc. National Electronics Conf., vol. 12; 1956.

[30] L, Weinberg, "Additional tables for design of optimum ladder works", J. Franklin Inst, (part 1) July, (part 2) August, 1957.

[31] Power system protection, vol (3),
Edited by the Electricity Council, 1969.

[32] Alternative Transients Program,
Rule Book, Part II.

[33] W. scott Meyer, "Machine Translation of an Electromagnetic Transients Program (EMTP) Among Different Digital Computer Systems", IEEE PICA Conference Record, Vol. 10, PP. 272-277, 1977.

[34] IEEE Tutorial Course, " Digital Simulation of Electrical Transient Phenomena", A Continuing Educational Course of The Power Engineering Society, Course Text, 81 EH0173-5-PWR.

APPENDIX :2A

Skin effect: Depth of current penetration in a round cylindrical conductor.

Reference [27] shows that, the expression for the resistance of a round wire at any frequency in terms of the parameter q, which is $\sqrt{2}$ times the ratio of wire radius to depth of penetration of the current, is as given below,

$$R = \frac{R_S}{\sqrt{2}.\pi.r_o} \times \left[\frac{(\text{Ber } q \,.\, \text{Bei}' \, q) - (\text{Bei } q \,.\, \text{Ber}' \, q)}{(\text{Ber}' \, q)^2 + (\text{Bei}' \, q)^2} \right] \text{ ohms/meter} \qquad (2A.1)$$

where,

$$q = \frac{\sqrt{2}.r_o}{\delta} = \frac{\sqrt{2}.r_o.\sqrt{f}}{0.066} \qquad (2A.2)$$

The Ber and Bei functions are the real and imaginary parts of the value of J_o, the Bessel function of the first kind of order zero, for complex arguments, according to the relation given below:

$$J_o\left(\frac{q}{\sqrt{j}}\right) = \text{Ber } q + j \text{ Bei } q \qquad (2A.3)$$

where q is real and $j = \sqrt{-1}$

and

$$\text{Ber}'q + j \text{ Bei}' q = \frac{d}{dq} [\text{ Ber } q + j \text{ Bei } q] \qquad (2A.4)$$

The functions Ber q, Bei' q, Bei q and Ber' q are tabulated in many references,[28].

In Equation (2A.1),

R_s = Surface resistivity

$$= \left[\frac{\pi . f . \mu}{\tau} \right]^{\frac{1}{2}} \Omega \qquad (2A.5)$$

where,

f = Frequency (Hz)

and for the copper wire,

μ = Permeability = $4\pi \times 10^{-7}$ (H/m)

τ = Conductivity = 5.8×10^{7} (Ω/m)

and

r_o = Radius of wire = 5.0×10^{-3} (m)

However, at a frequency of 100 kHz, the ratio of (r_o/δ) is greater than 5.5, in which case, the following high frequency approximation for resistance may be used,[27].

$$R_{h.f} = \frac{\left[\frac{\pi.f.\mu}{\tau}\right]^{\frac{1}{2}}}{2.\pi.r_o} \text{ ohms/meter} \qquad (2A.6)$$

This gives, for a 20.0m long wire, a resistance of 0.05 Ω which is negligibly small.

APPENDIX: 2B

The bandwidth of the line trap circuit is taken as the frequency difference between the two points at which its magnitude frequency response is 0.707 times the maximum value. This bandwidth was found to be 5000 Hz as given below.

$$(\Theta f)_{Trap} = (f_2 - f_1)_{Trap} = 5000 \text{ Hz} \qquad (2B.1)$$

where,

f_2 = Upper cut-off frequency

and

f_1 = Lower cut-off frequency

The bandwidth of each stack tuner is also equal to 5000 Hz and, since it is a simple L-C-R series tuned circuit, it is calculated using the equation given below.

$$(\Theta f)_{Stack\ tuner} = \frac{RP1}{2\pi LP1} = \frac{RP2}{2\pi LP2}$$

$$= (f_2 - f_1)_{S1} = (f_2 - f_1)_{S2}$$

$$= 5000 \text{ Hz} \qquad (2B.2)$$

where S1 and S2 correspond to stack tuners 1 and 2 respectively. Note that, RP1 = RP2 and LP1 = LP2.

The cut-off frequencies f_2 and f_1 are the frequencies at which the attenuation is -3dB. Therefore,

$$f_2 = f_c + \frac{5000}{2} = 92.5 \text{ kHz} \qquad (2B.3)$$

and

$$f_1 = f_c - \frac{5000}{2} = 87.5 \text{ kHz} \qquad (2B.4)$$

APPENDIX: 2C

The parameter values of the locator at centre frequency of 90.0 kHz are as given below.

LINE TRAP CIRCUIT

L1 = 0.1 mH

Rc = 0.05 Ω

C1 = 31.27 nF

Rd = 2.0 Ω

L2 = 3.183 mH

C2 = 982.46 pF

R1 = 10.0 KΩ

STACK TUNER , S1

LP1 = 15.91 mH

Cs = 196.55 pF

RP1 = 500.0 Ω

STACK TUNER , S2

LP2 = 15.91 mH

Cs = 196.55 pF

RP2 = 500.0 Ω

APPENDIX: 2D

For the stack tuner, S1, as illustrated in Figure (2.8), it is true to say that,

$$V1 = V_{s1} \qquad (2D.1)$$

and

$$I1 = (V_{s1} / ZP) + I_{s1} \qquad (2D.2)$$

$$I1 = V_{s1} \cdot YP + I_{s1} \qquad (2D.3)$$

where $YP = \frac{1}{ZP}$ = Admittance of stack tuners.

re-writing Equations (2D.1) and (2D.3) in the matrix notation, gives:

$$\begin{bmatrix} V1 \\ I1 \end{bmatrix} = \begin{bmatrix} 1 & 0 \\ YP & 1 \end{bmatrix} \begin{bmatrix} V_{s1} \\ I_{s1} \end{bmatrix} \qquad (2D.4)$$

for the line trap circuit, Zs, as illustrated in Figure (2.8), it is true to say that,

$$V_{s1} = V_{s2} + Zs.I_{s2} \qquad (2D.5)$$

and

$$I_{s1} = I_{s2} \qquad (2D.6)$$

therefore

$$\begin{bmatrix} V_{s1} \\ I_{s1} \end{bmatrix} = \begin{bmatrix} 1 & Zs \\ 0 & 1 \end{bmatrix} \begin{bmatrix} V_{s2} \\ I_{s2} \end{bmatrix} \qquad (2D.7)$$

where Zs is the impedance of the line trap circuit.

Similarly for stack tuner, S2, we have

$$V_{s2} = V2 \qquad (2D.8)$$

$$I_{s2} = (V_{s2} / ZP) + I2 \qquad (2D.9)$$

$$= V2 \; . \; YP + I2 \qquad (2D.10)$$

which could be written in the matrix form:

$$\begin{bmatrix} V_{s2} \\ I_{s2} \end{bmatrix} = \begin{bmatrix} 1 & 0 \\ YP & 1 \end{bmatrix} \begin{bmatrix} V2 \\ I2 \end{bmatrix} \qquad (2D.11)$$

Eliminating the column matrices including V_{s2}, I_{s2}, V_{s1} and I_{s1} in Equations (2D.4), (2D.7) and (2D.11), we have

$$\begin{bmatrix} V1 \\ I1 \end{bmatrix} = \begin{bmatrix} 1 & 0 \\ YP & 1 \end{bmatrix} \begin{bmatrix} 1 & Zs \\ 0 & 1 \end{bmatrix} \begin{bmatrix} 1 & 0 \\ YP & 1 \end{bmatrix} \begin{bmatrix} V2 \\ I2 \end{bmatrix} \qquad (2D.12)$$

Equation (2D.12) can be re-written into the form:

$$\begin{bmatrix} V1 \\ I1 \end{bmatrix} = \begin{bmatrix} A & B \\ C & D \end{bmatrix} \begin{bmatrix} V2 \\ I2 \end{bmatrix} \qquad (2D.13)$$

$$X = Y \cdot Z$$

In Equation (2D.13), X and Z take the form of a (6 x 1) matrix and Y takes the form of a (6 x 6) matrix when representing the locators on all three phases as shown in Figure (2.9). These are given below.

$$\begin{bmatrix} V1 \\ I1 \end{bmatrix} = \begin{bmatrix} V1_a \\ V1_b \\ V1_c \\ I1_a \\ I1_b \\ I1_c \end{bmatrix} \qquad (2D.14)$$

and

$$\begin{bmatrix} V2 \\ I2 \end{bmatrix} = \begin{bmatrix} V2_a \\ V2_b \\ V2_c \\ I2_a \\ I2_b \\ I2_c \end{bmatrix} \qquad (2D.15)$$

The A, B, C and D elements of matrix Y in Equation (2D.13) are as given below.

$$A = \left[U \right] + \left[Zs \right]\left[YP \right] = \begin{bmatrix} A_a & 0 & 0 \\ 0 & A_b & 0 \\ 0 & 0 & A_c \end{bmatrix} \qquad (2D.16)$$

where $A_a = A_b = A_c$

and

$$B = \left[Zs \right] = \begin{bmatrix} B_a & 0 & 0 \\ 0 & B_b & 0 \\ 0 & 0 & B_c \end{bmatrix} \qquad (2D.17)$$

where $B_a = B_b = B_c$

and

$$C = 2.\left[YP \right] + \left[Zs \right]\left[YP \right]^2 = \begin{bmatrix} C_a & 0 & 0 \\ 0 & C_b & 0 \\ 0 & 0 & C_c \end{bmatrix} \qquad (2D.18)$$

where $C_a = C_b = C_c$

and

$$D = \left[U \right] + \left[Zs \right]\left[YP \right] = \begin{bmatrix} D_a & 0 & 0 \\ 0 & D_b & 0 \\ 0 & 0 & D_c \end{bmatrix} \qquad (2D.19)$$

where $D_a = D_b = D_c$

Also in Equations (2D.16) to (2D.19),

$$\left[U \right] = \begin{bmatrix} 1 & 0 & 0 \\ 0 & 1 & 0 \\ 0 & 0 & 1 \end{bmatrix} \qquad (2D.20)$$

and

$$\left[Zs \right] = \begin{bmatrix} ZT(jw) & 0 & 0 \\ 0 & ZT(jw) & 0 \\ 0 & 0 & ZT(jw) \end{bmatrix} \qquad (2D.21)$$

where ZT(jw) is given by Equation (2D.22),

$$ZT(jw) = \frac{Z1(jw) \cdot Z2(jw) \cdot Z3(jw)}{[Z1(jw) \cdot Z2(jw)] + [Z1(jw) + Z2(jw)] \cdot Z3(jw)} \ \Omega \qquad (2D.22)$$

and from Figure (2.4),

$$Z1(jw) = Rc + jwL1 \ \Omega \qquad (2D.23)$$

$$Z2(jw) = Rd + 1/jwC1 \ \Omega \qquad (2D.24)$$

and

$$Z3(jw) = R1 + jwL2 + 1/jwC2 \ \Omega \qquad (2D.25)$$

and finally,

$$\begin{bmatrix} YP \end{bmatrix} = \begin{bmatrix} YS(jw) & 0 & 0 \\ 0 & YS(jw) & 0 \\ 0 & 0 & YS(jw) \end{bmatrix} \qquad (2D.26)$$

where

$$YS(jw) = \frac{1}{RP1 + jwLP1 + \dfrac{1}{jwCs}} \qquad (2D.27)$$

Note that,

RP1 = RP2 and LP1 = LP2

Finally re-arranging Equation (2D.13) to represent all three locators on all three phases with no mutual effect between them as shown in Figure (2.9), the Equation (2D.28) is obtained.

$$\begin{bmatrix} V1_a \\ V1_b \\ V1_c \\ I1_a \\ I1_b \\ I1_c \end{bmatrix} = \begin{bmatrix} A_a & 0 & 0 & B_a & 0 & 0 \\ 0 & A_b & 0 & 0 & B_b & 0 \\ 0 & 0 & A_c & 0 & 0 & B_c \\ C_a & 0 & 0 & D_a & 0 & 0 \\ 0 & C_b & 0 & 0 & D_b & 0 \\ 0 & 0 & C_c & 0 & 0 & D_c \end{bmatrix} \begin{bmatrix} V2_a \\ V2_b \\ V2_c \\ I2_a \\ I2_b \\ I2_c \end{bmatrix} \qquad (2D.28)$$

APPENDIX: 2E

The effective impedance of stack tuners, at centre frequency f_c matches the surge impedance of the line as shown in Figure (2.10). Therefore, it is true to say that at f_c,

$$RP1 = RP2 = \frac{Ro}{2} \qquad (2E.1)$$

therefore,

$$VY = I.\ (\ ZT + \frac{Ro}{2}\ ) \qquad (2E.2)$$

and

$$VX = I.(\ \frac{Ro}{2}\ ) \qquad (2E.3)$$

where,

I = Current through ZT

and

ZT = Total impedance of the line trap circuit at centre frequency f_c

$$= X.Ro \qquad (2E.4)$$

where

Ro = Surge impedance of the line.

therefore,

$$\frac{VX}{VY} = \frac{I.(Ro/2)}{I.(ZT + Ro/2)} \qquad (2E.5)$$

putting Equation (2E.4) in (2E.5), the following equation is obtained.

$$\frac{VX}{VY} = \frac{1}{(2X + 1)} \qquad (2E.6)$$

APPENDIX: 3A

The following is the list of the elements values of the band-pass filter used in the decision logic check circuit of Figure (3.5).

$R1 = 1000.0\ (\Omega)$

$L1 = 0.4606 \times 10^{-1}\ (H)$

$C1 = 0.6789 \times 10^{-10}\ (F)$

$L2 = 0.2358 \times 10^{-4}\ (H)$

$C2 = 0.1326 \times 10^{-6}\ (F)$

$L3 = 0.2032\ (H)$

$C3 = 0.1539 \times 10^{-10}\ (F)$

$L4 = 0.1255 \times 10^{-4}\ (H)$

$C4 = 0.2493 \times 10^{-6}\ (F)$

$L5 = 0.2653\ (H)$

$C5 = 0.1179 \times 10^{-10}\ (F)$

$L6 = 0.1255 \times 10^{-4}\ (H)$

$C6 = 0.2493 \times 10^{-6}\ (F)$

$L7 = 0.2032\ (H)$

$C7 = 0.1539 \times 10^{-10}\ (F)$

$L8 = 0.2358 \times 10^{-4}$ (H)

$C8 = 0.1326 \times 10^{-6}$ (F)

$L9 = 0.4606 \times 10^{-1}$ (H)

$C9 = 0.6789 \times 10^{-10}$ (F)

$R_n = 1000.0$ (Ω)

-3dB Bandwidth = 1200 (Hz)

Centre frequency = 90.0 (KHz)

APPENDIX: 4A

The line data for simulation of the network used in Figure (4.1) of this Chapter are listed below.

1 LINE DATA

NC = Number of conductors = 3.0

(XX) = Spacing between conductors = 0.65 (m)

(H) = Distance between each conductor and ground = 7.0 (m)

LPQ = Total length of line = 10.0 (Km)

PL1 = Distance between the source and locator $(LOC)_{L1}$ = 2.0 (Km)

L1L2 = Distance between locator $(LOC)_{L1}$ and Locator $(LOC)_{L2}$ = 3.0 (Km)

L2L3 = Distance between locator $(LOC)_{L2}$ and locator $(LOC)_{L3}$ = 3.0 (Km)

L3Q = Distance between locator L3 and the open end of the line

CR = Conductor radius = 0.126156 (inches)

RC = The natural resistance of each conductor at power frequency = 0.543816 (Ω/Km)

XC = The natural reactance of each conductor at power frequency = 0.339975 (Ω/Km)

Z_{s1} = Positive phase sequence impedance (PPS) = Z_{se} - Z_{mu} = 0.541 + j0.64 (Ω/Km)

Z_{s2} = Negative phase sequence impedance (NPS) = Z_{se} - Z_{mu} = 0.541 + j0.64 (Ω/Km)

Z_{so} = Zero phase sequence impedance (ZPS) = Z_{se} + $2Z_{mu}$ = 0.688 + j2.02 (Ω/Km)

2 SOURCE DATA

V_{LL} = System voltage = 11.0 (kV)

VAP = short-circuit-level at source = 0.25 (GVA)

QR = X/R ratio at source = 30.0

LNP = Z_{so}/Z_{s1} ratio at source = 1.0

APPENDIX: 4B

It should be noted that, before the fault, the sending end and receiving end currents and voltages are related by Equation (4B.1).

$$\begin{bmatrix} \bar{V}_{SS} \\ \bar{I}_{SS} \end{bmatrix} = \begin{bmatrix} A_s & B_s \\ C_s & D_s \end{bmatrix} \begin{bmatrix} \bar{V}_{RS} \\ \bar{I}_{RS} \end{bmatrix} \qquad (4B.1)$$

but due to the open end,

$$\bar{I}_{RS} = 0 \qquad (4B.2)$$

and

$$\begin{bmatrix} A_s & B_s \\ C_s & D_s \end{bmatrix} = \begin{bmatrix} A1 & B1 \\ C1 & D1 \end{bmatrix} \begin{bmatrix} A2 & B2 \\ C2 & D2 \end{bmatrix} \qquad (4B.3)$$

from Equations (4B.1) and (4B.2),

$$\bar{V}_{SS} = A_s . \bar{V}_{RS} \qquad (4B.4)$$

therefore,

$$\bar{V}_{RS} = A_s^{-1} . \bar{V}_{SS} \qquad (4B.5)$$

The vector $\bar{V}_{fs}$ is evaluated using Equation (4B.6).

$$\begin{bmatrix} \bar{V}_{fs} \\ \bar{I}_{fS} \end{bmatrix} = \begin{bmatrix} A2 & B2 \\ C2 & D2 \end{bmatrix} \begin{bmatrix} \bar{V}_{RS} \\ 0 \end{bmatrix} \qquad (4B.6)$$

therefore,

$$\bar{V}_{fs} = A2.\bar{V}_{RS} \qquad (4B.7)$$

putting Equation (4B.5) in (4B.7) yields,

$$\bar{V}_{fs} = A2.A_s^{-1}.\bar{V}_{SS} \qquad (4B.8)$$

where from Equation (4B.3),

$$A_s = \left[A1.A2 + B1.C2 \right] \qquad (4B.9)$$

APPENDIX: 4C

The voltages and currents at the sending end source and the point of fault on Figure (4.4), assuming homogeneous line sections, are related to each other as given in Equation (4C.1).

$$\begin{bmatrix} \bar{E}_{ff} \\ -\bar{I}_{fSf} \end{bmatrix} = \begin{bmatrix} A1 & B1 \\ C1 & D1 \end{bmatrix} \begin{bmatrix} \bar{V}_{Sf} \\ -\bar{I}_{Sf} \end{bmatrix} \qquad (4C.1)$$

therefore, from Equation (4C.1),

$$\bar{E}_{ff} = A1.\bar{V}_{Sf} - B1.\bar{I}_{Sf} \qquad (4C.2)$$

and

$$-\bar{I}_{fSf} = C1.\bar{V}_{Sf} - D1.\bar{I}_{Sf} \qquad (4C.3)$$

the voltage and current at the sending end are related to the source impedance by Equation (4C.4).

$$\bar{V}_{Sf} = -Z_{SS}.\bar{I}_{Sf} \qquad (4C.4)$$

hence,

$$\bar{I}_{Sf} = -Z_{SS}^{-1}.\bar{V}_{Sf} \qquad (4C.5)$$

putting Equation (4C.5) in (4C.2), gives

$$\bar{E}_{ff} = A1.\bar{V}_{Sf} + B1.Z_{SS}^{-1}.\bar{V}_{Sf} \qquad (4C.6)$$

and substituting Equation (4C.5) in Equation (4C.3),

yields

$$-\bar{I}_{fSf} = C1.\bar{V}_{Sf} + D1.Z_{SS}^{-1}.\bar{V}_{Sf} \qquad (4C.7)$$

from Equation (4C.6),

$$\bar{E}_{ff} = \left[A1 + B1.Z_{SS}^{-1} \right] . \bar{V}_{Sf} \qquad (4C.8)$$

and from Equation (4C.7),

$$-\bar{I}_{fSf} = \left[C1 + D1.Z_{SS}^{-1} \right] . \bar{V}_{Sf} \qquad (4C.9)$$

therefore from Equation (4C.9),

$$\bar{V}_{Sf} = -\left[C1 + D1.Z_{SS}^{-1} \right]^{-1} . \bar{I}_{fSf} \qquad (4C.10)$$

putting Equation (4C.10) in Equation (4C.8), gives,

$$\bar{E}_{ff} = -\left[A1 + B1.Z_{SS}^{-1} \right] \left[C1 + D1.Z_{SS}^{-1} \right]^{-1} . \bar{I}_{fSf} \qquad (4C.11)$$

Now the voltages and currents at the point of fault and the receiving end are related by the Equation (4C.12).

$$\begin{bmatrix} \bar{E}_{ff} \\ \bar{I}_{fRf} \end{bmatrix} = \begin{bmatrix} A2 & B2 \\ C2 & D2 \end{bmatrix} \begin{bmatrix} \bar{V}_{Rf} \\ \bar{I}_{Rf} \end{bmatrix} \qquad (4C.12)$$

where,

$$\bar{I}_{Rf} = 0$$

from Equation (4C.12),

$$\bar{E}_{ff} = A2.\bar{V}_{Rf} \qquad (4C.13)$$

and

$$\bar{I}_{fRf} = C2.\bar{V}_{Rf} \qquad (4C.14)$$

from which,

$$\bar{V}_{Rf} = C2^{-1}.\bar{I}_{fRf} \qquad (4C.15)$$

Equation (4C.15) in (4C.13), gives

$$\bar{E}_{ff} = A2.C2^{-1}.\bar{I}_{fRf} \qquad (4C.16)$$

now from Equation (4C.11),

$$\bar{I}_{fSf} = -\left[C1 + D1.Z_{SS}^{-1} \right] \left[A1 + B1.Z_{SS}^{-1} \right]^{-1} . \bar{E}_{ff} \qquad (4C.17)$$

and from Equation (4C.16),

$$\bar{I}_{fRf} = C2.A2^{-1}.\bar{E}_{ff} \qquad (4C.18)$$

The vector of transposed superimposed voltages from each conductor to earth, $\bar{E}_{ff}$ is obtained from Equation (4C.19) given below.

$$\bar{E}_{ff} = \bar{V}_{ff} + Rf \; . \left[\bar{I}_{fSf} - \bar{I}_{fRf} \right] \qquad (4C.19)$$

where Rf is a diagonal matrix of the required value of fault resistance in each phase as given below,

$$Rf = \begin{bmatrix} Rf & 0 & 0 \\ 0 & Rf & 0 \\ 0 & 0 & Rf \end{bmatrix} \qquad (4C.20)$$

Equations (4C.17) and (4C.18), give,

$$\left[\bar{I}_{fSf} - \bar{I}_{fRf} \right] = - \left[\left[C1 + D1.Z_{SS}^{-1} \right] . \left[A1 + B1.Z_{SS}^{-1} \right]^{-1} + \left[C2.A2^{-1} \right] \right] . \bar{E}_{ff} \qquad (4C.21)$$

This can be re-written as Equation (4C.22) for simplicity,

$$\left[\bar{I}_{fSf} - \bar{I}_{fRf} \right] = - \left[M \right] . \bar{E}_{ff} \qquad (4C.22)$$

therefore,

$$\bar{E}_{ff} = - \left[M \right]^{-1} \left[\bar{I}_{fSf} - \bar{I}_{fRf} \right] \qquad (4C.23)$$

Putting Equation (4C.19) in (4C.23), yields,

$$\bar{V}_{ff} + Rf.\left[\bar{I}_{fSf} - \bar{I}_{fRf} \right] = - \left[M \right]^{-1} . \left[\bar{I}_{fSf} - \bar{I}_{fRf} \right] \quad (4C.24)$$

from which,

$$\bar{V}_{ff} = - \left[\left[M \right]^{-1} + Rf \right] \left[\bar{I}_{fSf} - \bar{I}_{fRf} \right] \quad (4C.25)$$

where,

$$\left[M \right] = \left[\left[C1 + D1.Z_{SS}^{-1} \right] \left[A1 + B1.Z_{SS}^{-1} \right]^{-1} + \left[C2.A2^{-1} \right] \right] \quad (4C.26)$$

APPENDIX: 4D

The simulation of the source network has been carried out using the simplified model of Figure (4.6), as outlined below.

$$\bar{V}_a = \bar{I}_a \cdot Z_{s1} + (\bar{I}_a + \bar{I}_b + \bar{I}_c) \cdot Z_n$$

$$= \bar{I}_a \cdot (Z_{s1} + Z_n) + (\bar{I}_b + \bar{I}_c) \cdot Z_n \qquad (4D.1)$$

where the positive phase sequence source impedance Z_{s1} is given by Equation (4D.2),

$$Z_{s1} = R_{s1} + jwL_{s1} \qquad (4D.2)$$

and the neutral source impedance Z_n is given by Equation (4D.3),

$$Z_n = R_n + jwL_n \qquad (4D.3)$$

similarly,

$$\bar{V}_b = \bar{I}_b \cdot (Z_{s1} + Z_n) + (\bar{I}_a + \bar{I}_c) \cdot Z_n \qquad (4D.4)$$

and

$$\bar{V}_c = \bar{I}_c \cdot (Z_{s1} + Z_n) + (\bar{I}_b + \bar{I}_a) \cdot Z_n \qquad (4D.5)$$

in matrix form,

$$\begin{bmatrix} \bar{V}_a \\ \bar{V}_b \\ \bar{V}_c \end{bmatrix} = \begin{bmatrix} Z_{se} & Z_{mu} & Z_{se} \\ Z_{mu} & Z_{se} & Z_{mu} \\ Z_{mu} & Z_{mu} & Z_{se} \end{bmatrix} \begin{bmatrix} \bar{I}_a \\ \bar{I}_b \\ \bar{I}_c \end{bmatrix}$$

$$= \begin{bmatrix} Z_{SS} \end{bmatrix} \begin{bmatrix} \bar{I}_a \\ \bar{I}_b \\ \bar{I}_c \end{bmatrix} \qquad (4D.6)$$

where

$$Z_{se} = (Z_{s1} + Z_n) \qquad (4D.7)$$

and

$$Z_{mu} = Z_n = \frac{1}{3} (Z_{so} - Z_{s1}) \qquad (4D.8)$$

The self impedance Z_{se} and mutual impedance Z_{mu} are calculated as follows.

$$SCL = \sqrt{3} \cdot |I_{sc}| . |V_L| \qquad Eqn(4D.9)$$

where SCL is the Short-Circuit level , $|V_L|$ is the nominal supply voltage and $|I_{sc}|$ is the short circuit current.

From Equation (4D.9),

$$|I_{sc}| = \frac{|V_L|}{\sqrt{3} \cdot |Z_{s1}|} \qquad (4D.10)$$

therefore

$$SCL = \frac{|V_L|^2}{|Z_{s1}|}$$

from which

$$|Z_{s1}| = \frac{|V_L|^2}{SCL} \qquad (4D.11)$$

also

$$Z_{s1} = R_{s1} + jX_{s1}$$

$$= R_{s1} \cdot \left(1 + j \frac{X_{s1}}{R_{s1}} \right) \qquad (4D.12)$$

where R_{s1} and X_{s1} are the positive phase sequence source resistance and inductance respectively.

The neutral source impedance Z_n is obtained using the equation given below.

$$Z_n = \frac{1}{3} \cdot (Z_{so} - Z_{s1})$$

$$= \frac{Z_{s1}}{3} \cdot \left(\frac{Z_{so}}{Z_{s1}} - 1 \right) \qquad (4D.13)$$

Therefore, knowing the parameters such as (SCL), short-circuit-level, (X/R) ratio, (Z_{so}/Z_{s1}) ratio and the system voltage V_L, the source network impedance, Z_{SS} can be calculated.

APPENDIX: 4E

The voltages and currents at the sending end are related to the fault point variables by Equation (4E.1).

$$\begin{bmatrix} \bar{V}_{Sf} \\ \bar{I}_{Sf} \end{bmatrix} = \begin{bmatrix} A1 & B1 \\ C1 & D1 \end{bmatrix} \begin{bmatrix} \bar{E}_{ff} \\ \bar{I}_{fSf} \end{bmatrix} \qquad (4E.1)$$

From Equation (4E.1),

$$\bar{V}_{Sf} = A1.\bar{E}_{ff} + B1.\bar{I}_{fSf} \qquad (4E.2)$$

and

$$\bar{I}_{Sf} = C1.\bar{E}_{ff} + D1.\bar{I}_{fSf} \qquad (4E.3)$$

Equation (4C.17) from Appendix 4C in (4E.2), yields,

$$\bar{V}_{Sf} = \left[A1 - B1.\left[C1 + D1.Z_{SS}^{-1} \right] . \left[A1 + B1.Z_{SS}^{-1} \right]^{-1} \right] . \bar{E}_{ff} \qquad (4E.4)$$

Equation (4C.17) from Appendix 4C in Equation (4E.3), gives,

$$\bar{I}_{Sf} = \left[C1 - D1.\left[C1 + D1.Z_{SS}^{-1} \right] . \left[A1 + B1.Z_{SS}^{-1} \right]^{-1} \right] . \bar{E}_{ff} \qquad (4E.5)$$

also the voltages and currents at sending end are related to the right hand side variables of the first locator in Figure (4.1) by Equation (4E.6).

$$\begin{bmatrix} \bar{V}_{Sf} \\ \bar{I}_{Sf} \end{bmatrix} = \begin{bmatrix} A_{S1} & B_{S1} \\ C_{S1} & D_{S1} \end{bmatrix} \begin{bmatrix} \bar{V}1 \\ \bar{I}1 \end{bmatrix} \qquad (4E.6)$$

from above equation,

$$\bar{V}_{Sf} = A_{S1}.\bar{V}1 + B_{S1}.\bar{I}1 \qquad (4E.7)$$

and

$$\bar{I}_{Sf} = C_{S1}.\bar{V}1 + D_{S1}.\bar{I}1 \qquad (4E.8)$$

from Equation (4E.7),

$$\bar{I}1 = B_{S1}^{-1} . \left[\bar{V}_{Sf} - A_{S1}.\bar{V}1 \right] \qquad (4E.9)$$

and from Equation (4C.8),

$$\bar{V}1 = C_{S1}^{-1} \cdot \left[\bar{I}_{Sf} - D_{S1} \cdot \bar{I}1 \right] \qquad (4E.10)$$

putting Equation (4E.9) in Equation (4E.10),yields,

$$\bar{V}1 = \left[U - C_{S1}^{-1} \cdot D_{S1} \cdot B_{S1}^{-1} \cdot A_{S1} \right]^{-1} \cdot C_{S1}^{-1} \cdot \bar{I}_{Sf} - \left[U - C_{S1}^{-1} \cdot D_{S1} \cdot B_{S1}^{-1} \cdot A_{S1} \right]^{-1} \cdot \left[C_{S1}^{-1} \cdot D_{S1} \cdot B_{S1}^{-1} \right] \cdot \bar{V}_{Sf} \qquad (4E.11)$$

where U is a unity (3 x 3) matrix as given below,

$$U = \begin{bmatrix} 1 & 0 & 0 \\ 0 & 1 & 0 \\ 0 & 0 & 1 \end{bmatrix} \qquad (4E.12)$$

APPENDIX: 4F

By referring to Figure (4.5) and, the total energy in a period of T, or the total area under the squared voltage curve from the origin to T is,

$$E = \int_0^T V^2 \, . \, dt$$

$$= A_1 + A_2 + \ldots + A_n \qquad (4F.1)$$

where

$$A_1 = \frac{t}{2} \, . \, \left((V_0)^2 + (V_1)^2 \right)$$

$$A_2 = \frac{t}{2} \, . \, \left((V_1)^2 + (V_2)^2 \right)$$

$$\vdots$$

$$A_n = \frac{t}{2} \, . \, \left((V_{n-1})^2 + (V_n)^2 \right)$$

The sum of all the areas calculated in this way, would result in a general form representing the total area or the energy as given below.

$$E = t \cdot \left[\frac{1}{2} \cdot \left[(V_0)^2 + (V_n)^2 \right] + \sum_{i=1}^{n-1} (V_i)^2 \right]$$

(4F.2)

where

$$n = \frac{T}{t} \qquad \text{(4F.3)}$$

APPENDIX: 5A

The parameter values of the locator at centre frequency of 270.0 kHz are as given below.

LINE TRAP CIRCUIT

L1 = 0.1 mH

Rc = 0.05 Ω

C1 = 3.474 nF

Rd = 20.0 Ω

L2 = 3.183 mH

C2 = 109.26 pF

R1 = 10.0 KΩ

STACK TUNER , S1

LP1 = 15.91 mH

Cs = 21.839 pF

RP1 = 500.0 Ω

STACK TUNER , S2

LP2 = 15.91 mH

Cs = 21.839 pF

RP2 = 500.0 Ω

PUBLISHED PAPERS

[1] M. EL-HAMI, A.T. JOHNS, L.L. LAI, D.J. DARUVALA, " An investigation into a new technique for discriminating between in-zone and out-of-zone faults on overhead power distribution networks", accepted for presentation at The 25th Universities' Power Engineering Conference, (UPEC), 1990, Aberdeen.

[2] A.T. JOHNS, M. EL-HAMI, D.J. DARUVALA, " Investigations into a new directional fault locator for overhead distribution systems", Proceedings of the 24th Universities' Power Engineering Conference, (UPEC), Sept. 1989, Belfast, pp, 25-28.

[3] D.J. DARUVALA, A.T. JOHNS, M. EL-HAMI, " Modelling of a simple fault detector/protection system in SPICE", Proceedings of the 24th Universities' Power Engineering Conference, (UPEC), Sept. 1989, Belfast, pp, 77-80.

The following paper has been accepted for presentation at The 25th Universities' Power Engineering Conference, (UPEC), 1990, Aberdeen.

AN INVESTIGATION INTO A NEW TECHNIQUE FOR DISCRIMINATING BETWEEN IN-ZONE AND OUT-OF-ZONE FAULTS ON OVERHEAD POWER DISTRIBUTION NETWORKS

M. EL-HAMI A.T. JOHNS L.L. LAI D.J. DARUVALA

ELECTRICAL POWER AND ENERGY SYSTEMS RESEARCH CENTRE
CITY UNIVERSITY, LONDON, U.K.

ABSTRACT

The problems associated with detection, location and clearing of faults on overhead power distribution systems are of high importance. Immediate detection and isolation of faulted distribution feeders reduce the time required for locating faults and restoration of supplies.

This paper investigates a new technique for fault location on overhead distribution networks using a new fault locator. The technique is based upon detecting fault induced high frequency components introduced on the line due to a fault. The Electromagnetic Transients Program (EMTP), has been used to simulate a simple 11kV radial system and the results show that the scheme is feasible.

INTRODUCTION

Overhead power distribution systems can be damaged or disrupted in many ways by faults. Most utilities employ reclosing relays with circuit breakers to handle transient faults. Permanent faults, however require a location of the faulty line section, isolation and possibly rescheduling of the network before normal power delivery may be resumed.

Reference [1] describes a method of fault detection and location on overhead lines using a new sensor. Investigations into the design of a new directional fault locator for use on overhead lines operating typically at 11kV have also been reported recently [2]. The operating principle of this new device and scheme are based upon detection of fault induced high frequency components on the line.

With appropriate signal processing of the fault generated signals, the usefulness of this new scheme has been extended and, in addition to being directional, it is now capable of distinguishing between in-zone and out-of-zone faults on overhead power distribution networks.

THE NEW PROPOSED TECHNIQUE

Figure 1 shows the schematic diagram of a simple overhead radial system equipped with the new locators per phase. It is clearly seen that the new devices are inserted at convenient intervals and at strategic points, dividing the network into several zones. Figure 2 shows a locator which consists of two stack tuners and a line trap circuit, all of which are tuned to the same bandwidth and centre frequency f_c. With the arrangement shown in figure 2, each locator determines:

a) Whether or not the fault is in one of the zones adjacent to that locator, or is in a zone beyond the next locator.

b) Whether the fault is upstream or downstream.

The capability of the new device to determine the direction of a fault has been described in reference [2]. It shows that the attenuation of the locator within a narrow band of frequencies around f_c is $1/(2P + 1)$, where P is the ratio of the effective impedance of the line trap circuit Z_T to the effective impedance of stack tuners which is equal to the surge impedance of the line, Ro.

To understand the principle of the scheme, a section of the network in figure 1 is redrawn as shown in figure 3. At the centre frequency, f_c, the line trap circuit has an effective impedance of Z_T and each stack tuner has an effective impedance equal to the surge impedance of the line Ro. If a fault occurs at F2, all the high frequency components generated by this fault in a narrow band of frequencies around f_c (in-band signals) will be attenuated by the locator $(LOC)_{n+1}$. Consequently, the output voltages $(VX_{n+1})_{F2}$ and $(VY_{n+1})_{F2}$ would have the relationship given below.

$$(VY_{n+1})_{F2} \approx (2P + 1) \cdot (VX_{n+1})_{F2} \quad \text{Equ (1)}$$

The locator $(LOC)_{n+1}$ thus reduces the in-band signals impressed on the line by the fault. However, on comparing the voltages, $(VX_n)_{F2}$ and $(VY_n)_{F2}$ received by locator $(LOC)_n$ due to the same fault at F2, a different relationship is given below:

$$(VY_n)_{F2} \approx (VX_n)_{F2} \quad \text{Equ(2)}$$

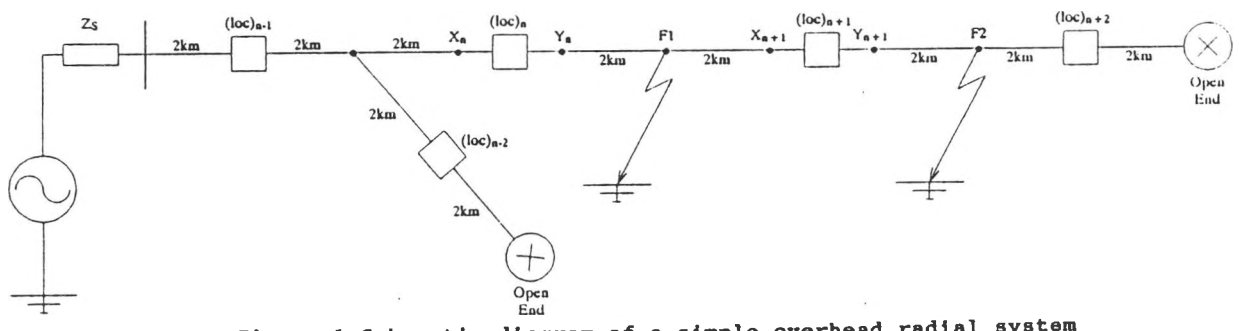

Figure 1 Schematic diagram of a simple overhead radial system

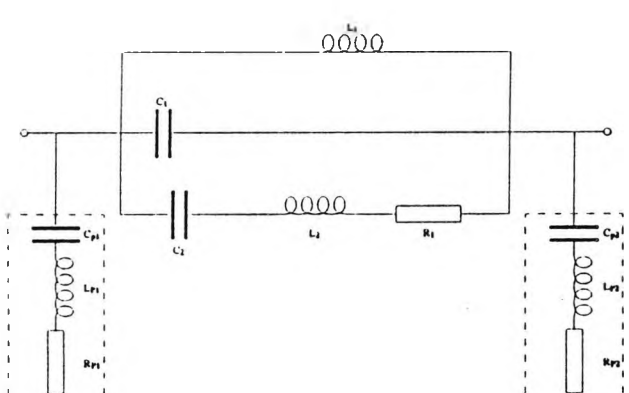

Figure 2 Locator arrangement

This is due to the fact that, the in-band signals have already been attenuated by the locator $(LOC)_{n+1}$, which is closest to the fault.

If a fault occurs at F1, the in-band noise is detected by both locators $(LOC)_n$ and $(LOC)_{n+1}$ and therefore the following equations are valid,

$$(VY_n)_{F1} \approx (2P + 1) \cdot (VX_n)_{F1} \qquad \text{Equ(3)}$$

$$(VX_{n+1})_{F1} \approx (2P + 1) \cdot (VY_{n+1})_{F1} \qquad \text{Equ(4)}$$

Figure 4 shows that, the three-phase output voltages across the resistors of the stack tuners are added together using the combination [1 -2 1] to form a composite voltage. This voltage is then passed through a narrow band pass filter with a centre frequency f_c. The filtered voltage is then squared and integrated with respect to time, according to the equation given below:

$$E = \int_0^t V^2 \, dt \qquad \text{Equ(5)}$$

And E is the energy extracted from the filtered voltage over the time t.

From equations (1), (3) and (4), it can be seen that if EVX_C and EVY_C are the energies extracted from the filtered voltages across the resistors of stack tuners situated at sides X and Y of the closest locator to a fault respectively, it should be appreciated that for a downstream fault,

$$EVY_C > EVX_C \qquad \text{Equ(6)}$$

similarly for an upstream fault,

$$EVY_C < EVX_C \qquad \text{Equ(7)}$$

The direction decision logic check, shown in figure 4, thus determines the fault direction by producing high or low logic signal outputs, V_{DD} and V_{DU} according to the direction of the fault.

From equation (2), it is evident that, if EVY_A and EVX_A are the energies extracted from the voltage waveforms across the resistors of stack tuners situated at sides Y and X of any locator placed beyond the closest locator to a fault respectively, for both downstream and upstream faults the following relationship exists.

$$EVY_A \approx EVX_A \qquad \text{Equ(8)}$$

From equations (6) to (8) it can be seen that, for both downstream and upstream faults it is true to say that,

$$E_C > E_A \qquad \text{Equ(9)}$$

where,

$$E_C = | EVY_C - EVX_C | \qquad \text{Equ(10)}$$

$$E_A = | EVY_A - EVX_A | \qquad \text{Equ(11)}$$

Therefore to distinguish between in-zone and out-of-zone faults, the magnitude of the energy level difference E_{Loc}, between the two sides of any locator can be compared with a predefined threshold level, THL. For an in-zone fault,

$$E_{Loc} > THL$$

and for an out-of-zone fault,

$$E_{Loc} < THL$$

Figure 4 shows that both the outputs of the directional logic check and the level detectors are fed into the fault zone decision logic, which would decide whether or not to produce a trip signal.

SIMULATION RESULTS

To demonstrate the capability of the new device and scheme to distinguish between in-zone and out-of-zone faults, voltage signals received by locator $(LOC)_n$ due to faults at F1 and F2, as shown in figure 3, are analysed. The line data as detailed in [3] and values for system parameters are given in the Appendix. Figures 5 and 6 show the voltage signals VY_n and VX_n of locator $(LOC)_n$ due to an in-zone fault at F1. Their corresponding voltage waveforms FVY_n and FVX_n, after passage through a band-pass filter, are shown in figures 7 and 8 respectively. It shows that the energy

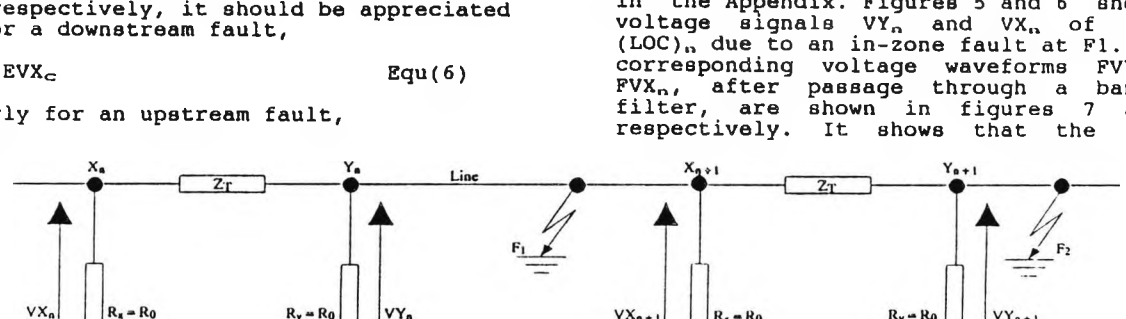

Figure 3 Equivalent circuits of locators $(Loc)_n$ and $(Loc)_{n+1}$ at centre frequency f_c

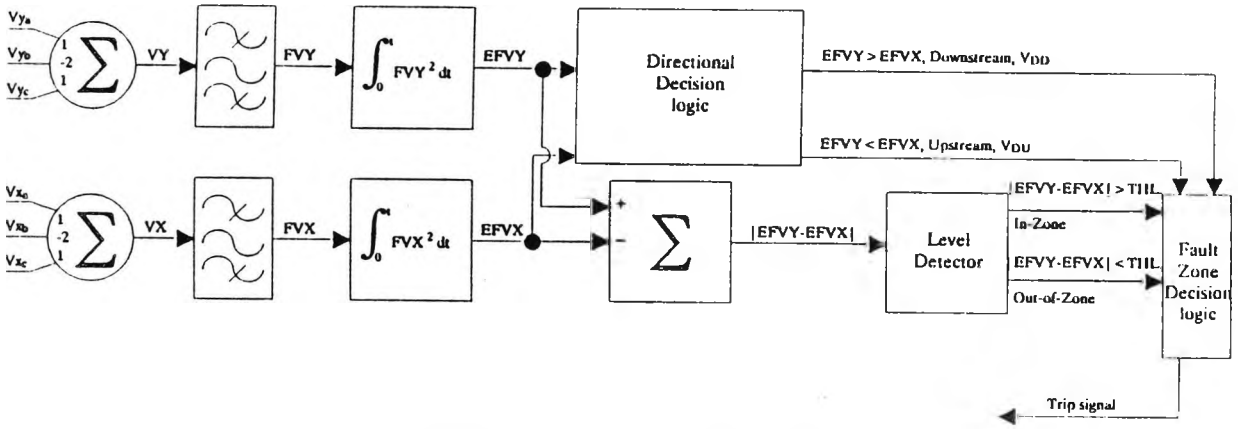

Figure 4 Decision logic scheme

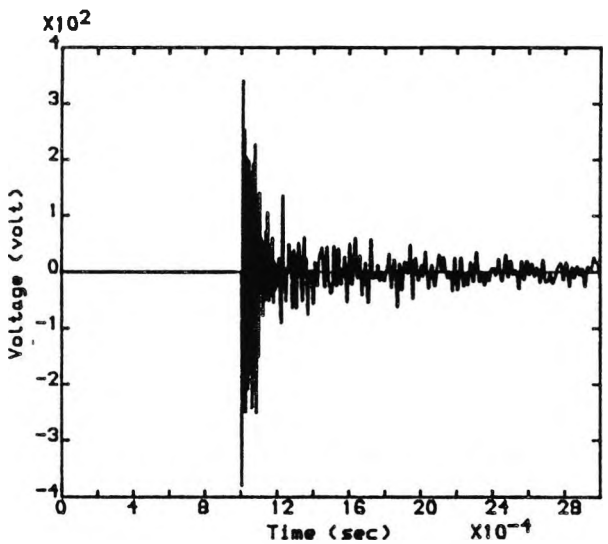

Figure 5 Voltage across resistor R_{P2} of locator $(Loc)_n$

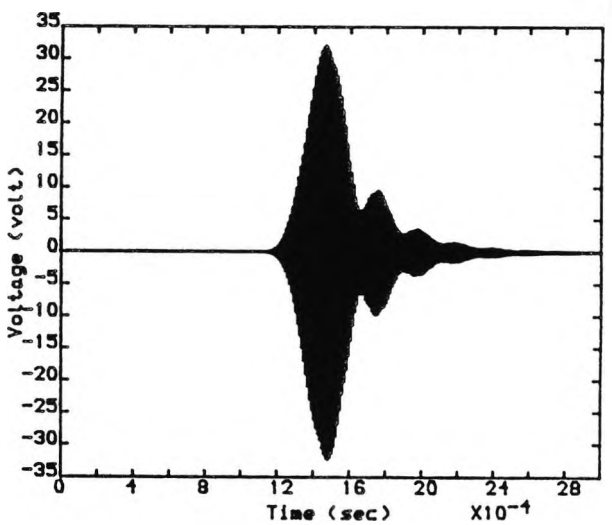

Figure 7 Filtered voltage across resistor R_{P2} of locator $(Loc)_n$

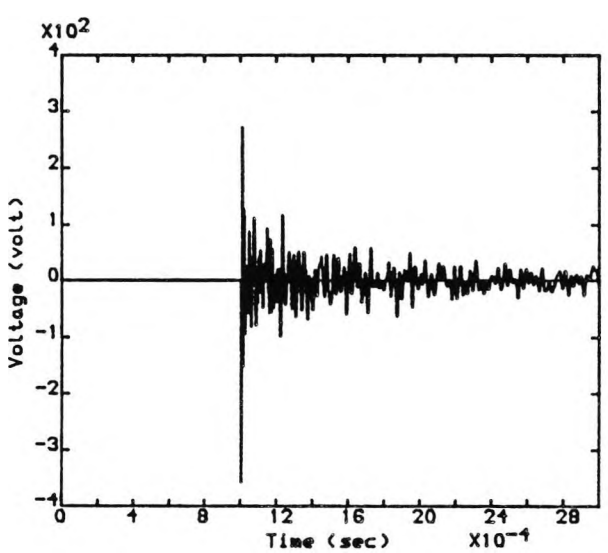

Figure 6 Voltage across resistor R_{P1} of locator $(Loc)_n$

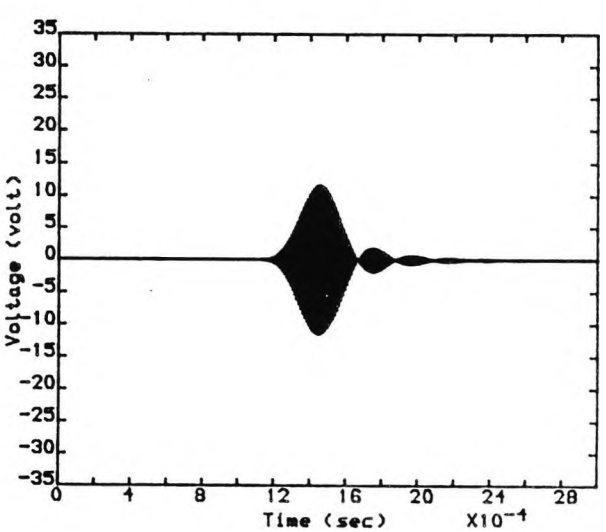

Figure 8 Filtered voltage across resistor R_{P1} of locator $(Loc)_n$

content in FVY_n, according to equation (5), is greater than the energy content in FVX_n. Figure 9 shows a comparison of the magnitude of the difference between energy contents in FVY_n and FVX_n due to in-zone and out-of-zone faults with a threshold level THL, however, the determination of this level is not without the scope of the present paper. It is clear that locator $(LOC)_n$ receives a higher or lower energy level difference than THL depends on whether it is an in-zone or an out-of-zone fault respectively.

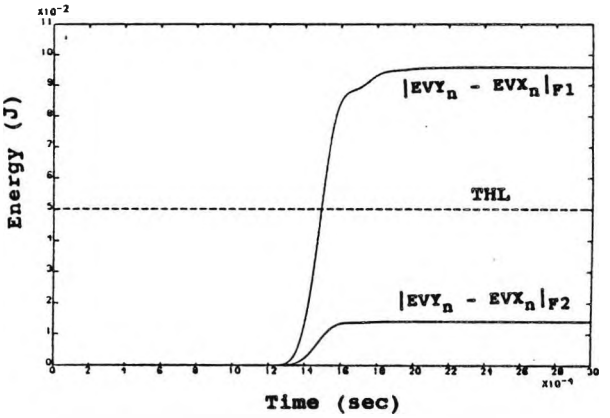

Figure 9 Comparison of energy level difference for in-zone and out-of-zone faults

Furthermore, figure 10 shows that, due to a fault at F1, the threshold level THL, is exceeded by energy levels difference in locators $(LOC)_n$ and $(LOC)_{n+1}$ but not in locators $(LOC)_{n-1}$, $(LOC)_{n-2}$ and $(LOC)_{n+2}$.

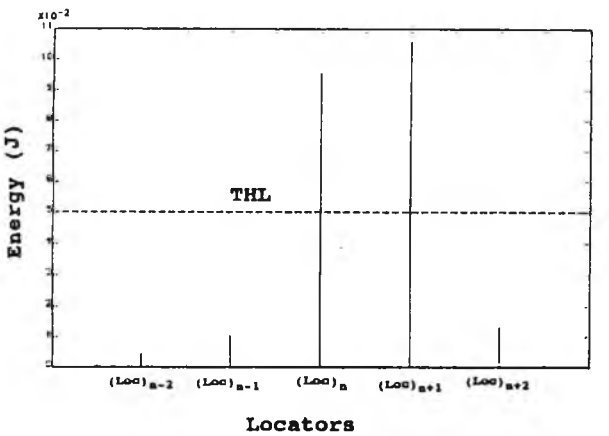

Figure 10 Energy level difference of locators

CONCLUSIONS

A new directional fault locator has been designed for use on overhead power distribution systems operating typically at 11kV . The operating principle of the new device and scheme, which is based upon detection of fault generated high frequency components on the line, has been described. This paper also describes a new technique to distinguish between in-zone and out-of-zone faults. The advantage of the new scheme over other conventional schemes is that, the presence of a communication link to locate the faulty section of the line is not required. This scheme can detect low level faults but the conventional schemes have difficulties coping with these situations.

REFERENCES

1. Clarke, G.J., and Horn, H.E., April 1985, "Monitoring and protection systems suited to overhead distribution systems", Proceedings of the Third International Conference on Developments in Power System Protection, IEE, Pub. No. 249, 199-203.

2. Johns, A.T., El-Hami, M. and Daruvala, D.J., Sept 1989, "Investigations into a new directional fault locator for overhead distribution systems", Proceedings of the 24th Universities Power Engineering Conference, (UPEC), Belfast, 25-28.

3. Cox, E.H., 1975, "Overhead-line practice", ProcIEE, No.10R, Vol 122, 1009-1017.

ACKNOWLEDGEMENTS

The authors wish to thank the British Technology Group, (BTG), London, for their support and City University, London, for the provision of facilities for this research.

APPENDIX

The line is horizontally constructed with no earth wire and the values for the line and system parameters are as shown below:

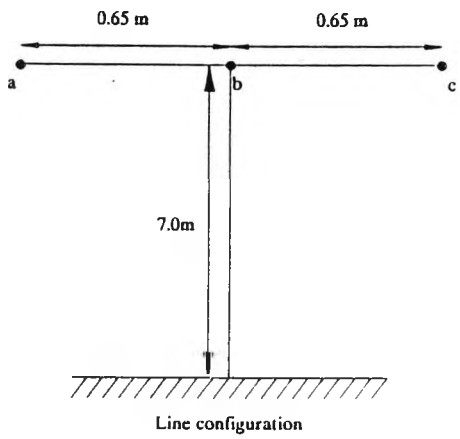

Line configuration

Line positive phase sequence impedance = 0.541 + j0.64 Ω/km
Line negative phase sequence impedance = 0.541 + j0.64 Ω/km
Line zero phase sequence impedance = 0.688 + j2.02 Ω/km
Source short circuit level = 250 MVA
X/R ratio at source = 30
Zso/Zsl ratio at source = 1
System voltage = 11 kV

The following two papers have been presented at The 24th Universities' Power Engineering Conference, (UPEC), 1989, Belfast.

INVESTIGATIONS INTO A NEW DIRECTIONAL FAULT LOCATOR FOR OVERHEAD DISTRIBUTION SYSTEMS

A.T. JOHNS M. EL-HAMI D.J. DARUVALA

CITY UNIVERSITY, LONDON, UK.

ABSTRACT

The necessity for further developments of protection for overhead distribution systems is still of a high degree, particularly in areas with interconnected networks.
This paper investigates a new directional fault locator which is being designed for use in overhead distribution networks. The scheme used utilizes fault generated noise. At first, the arrangement and operating function of this new locator is discussed and then the means by which information is provided for directional fault finding is explained. Finally simulation results, illustrating the operation of this device in a simple 11kV rural feeder situation is given.

INTRODUCTION

Over the years, rural distribution networks have been extended by a considerable amount and the increasing complexity of these networks therefore demands higher performance of protection and better control equipment.
In areas with interconnected networks, a directional fault locator is often required. When a fault occurs on a power distribution system a wideband of noise will be impressed on the line at the point of fault. The scheme used here is based upon detecting the fault-induced high frequency components on the line. The proposed technique also makes use of polymeric materials technology [3]. The new directional fault locators investigated here are inserted at strategic points and convenient intervals along an overhead distribution system to observe high frequency components due to a fault and provide information for directional fault finding.
The device is particularly useful for locating faults in overhead distribution systems operating at typically 11kV.

ARRANGEMENT AND OPERATING PRINCIPLE OF THE LOCATOR

The arrangement of the locator is shown in Fig(1), where a stack tuner is employed on each side of a line trap circuit. From Fig(1), it can be seen that each stack tuner is fitted with an isolation transformer. With this arrangment, each stack tuner has a very high impedance at 50Hz and an effective impedance which matches the line surge impedance R_o at the centre frequency f_o to which each is tuned. The line trap circuit, which is nominally tuned to the same centre frequency f_c, operates as a virtual short circuit at 50 Hz in order not to disturb the steady state performance of the system and has an effective impedance equal to Z_T at f_c.
It should be appreciated that the stack tuner capacitors Cs, can be of the concentric type and separated from the h.v conductors by a suitable insulating dielectric, e.g, polymeric insulating materials. Extra elements are added together to construct the circuit as shown in Fig(1). This locator is placed between each phase of a three phase system and earth.
To describe the basic operating principle of this locator, its per phase equivalent circuit at the centre frequency f_c is shown in Fig(2); the impedance of the locator matches the line surge or characteristic impedance (R_o) on both sides. If a fault occurs at F, a wideband noise is generated and impressed on the line at F. All the high frequency components which are in a narrow band of frequencies around f_c, will be greatly attenuated by this locator. It will be seen that the in-band signal level at point X is approximately (1/(2X+1)) times the in-band signal level that is impressed at the point Y of the locator, (for a particular trap and stack tuner parameters as outlined in Appendix B), i.e,

$$V_x/V_y = 1/(2X+1) \qquad \text{Eqn(1)}$$

The voltages V_x and V_y are reproduced on the secondary of the transformers T_2 and T_1 as V_{ox} and V_{oy} respectively. The relationship given in Eqn(1) also applies to voltages V_{ox} and V_{oy}.
The three output voltages for the three phases from the secondary of the isolation transformers are then fed into a summation circuit (Figure 3), where they are added together using the Aerial mode component of propagation [1,-2,1]. This combination is particularly convenient because it causes any common mode signals induced in the power line from a remote source to be cancelled.
The summation circuit produces outputs SV_y and SV_x which are then fed into a narrow band pass filter which is tuned to the same centre frequency f_c to which the locator is tuned. The filter only passes those signals within its band width and produces output signals FSV_y and FSV_x. It can be seen from Fig(3) that, FSV_y and FSV_x are fed into a directional decision logic check which effectively checks the difference between the energy stored in those signal components and produces EV_x and EV_y. Thus if EV_x-EV_y is a positive quantity the fault is downstream, and if EV_x-EV_y is a negative quantity the fault is upstream.

SIMULATION RESULTS

Figure (4) shows the case of a number of locators of the type shown in Fig(1) inserted at convenient points along an overhead distribution feeder with an open end. Note, Fig(4) is a simple line diagram in which for a three phase line one locator is connected between each phase and earth. Line data [6,7] is given in appendix B. The simulation was carried out using an accurate program based on the methods and techniques given in references [1,2,4,5]. The simulation results were analysed on both sides of the locators L1 and L2 due to a fault at F. The output voltages across the resistors of the stack tuners at point Y and X are shown in Figures (5) and (6) respectively. The first quarter of a cycle of their corresponding waveforms after passage through a band pass filter of the same centre frequency f_c as the locator are shown in Figures (7) and (8).
The results show that the signals received at point X are greatly attenuated by the

locator. Fig 9(a) shows the discriminating signals for the upstream fault indicated by locator L1, and the corresponding discriminating signal for a downstream fault as seen and indicated by locator L2 in Fig (4), is shown in Fig 9(b).

CONCLUSION

In this paper, the principle of a new directional fault locator, which is being designed for use in overhead distribution systems is outlined. The arrangement and the operating function of this new device has been explained together with the basis upon which directional fault finding is achieved. Preliminary results show the potential of the device as a new directional fault locator.

ACKNOWLEDEGMENTS

The authors would like to thank The British Technology Group (BTG) for their support and the City University, London, for the provision of facilities for this research. The authors also acknowledege with thanks the assistance of Dr L L Lai.

APPENDIX: A

Refering to the circuit of Fig(2) where R_x and R_y match the line surge impedance R_o, it is true to say that,

$$R_x = R_y = R_o/2$$
$$V_y = I.(Z_T + R_o/2)$$

and $V_x = I.(R_o/2)$

where I = Current through Z_T

and Z_T = Total impedance of the line trap circuit at centre frequency f_o $= X.R_o$

therefore,

$$\frac{V_x}{V_y} = \frac{I.(R_o/2)}{I.(Z_T + R_o/2)}$$

so,

$$\frac{V_x}{V_y} = \frac{1}{(2X + 1)}$$

APPENDIX: B

The line under simulation is a horizontally constructed 11kV line with no earth wire as shown below;

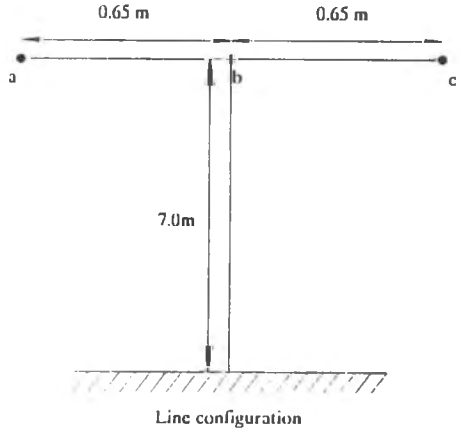

Line configuration

Line length = 10 km
Line positive phase sequence
impedance = 0.541 + j0.46 Ω/km
Line negative phase sequence
impedance = 0.541 + j0.46 Ω/km
Line zero phase sequence
impedance = 0.688 + j1.84 Ω/km
Source, short-circuit level = 250 MVA

REFERENCES

1-GALLOWAY,R.H., SHORROCKS,W.B., and WEDEPOHL,L.W.
"Calculation of electrical parameters for short and long polyphase transmission lines", 1964, Proc.IEE, 111, (12), pp. 2051-2059

2-JOHNS,A.T., and AGGRAWAL,R.K.
"Digital simulation of faulted e.h.v transmission lines with particular reference to very high-speed protection", 1976, Proc, IEE, vol 123, no.4, pp.353-359

3-CLARKE,G.J., and HORN,H.E.
"Monitoring and protection systems suited to overhead distribution systems", April 1985, Proceedings of the third international conference on developments in power system protection, IEE, Pub. No. 249, pp. 199-203

4-WEDEPOHL,L.M., and MOHAED, S.E.T.
"Multiconductor transmission lines", 1969, Proc.IEE, 116(9), pp 1553-1563.

5-WEDEPOHL, L.M.
"Application of matrix methods to the solution of travelling-wave phenomena in polyphase systems", 1963, Proc. IEE, 110, (12), pp.2200-2212.

6-COX, E.H.
"Overhead-line practice", 1975, Proc. IEE, No.10R, vol.122, pp 1009-1017.

7-BUTTERWORTH, S.
Electrical characteristics of overhead lines, The electrical research association,1954.

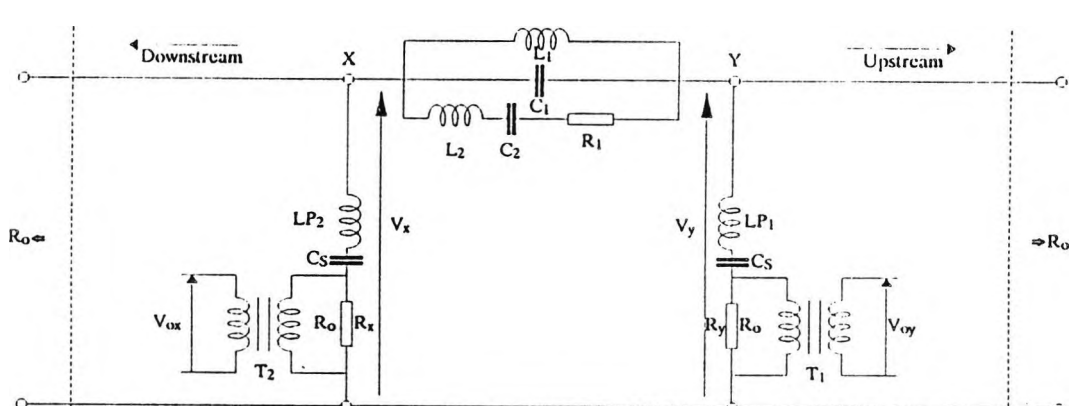

Fig (1), The arrangement of the locator

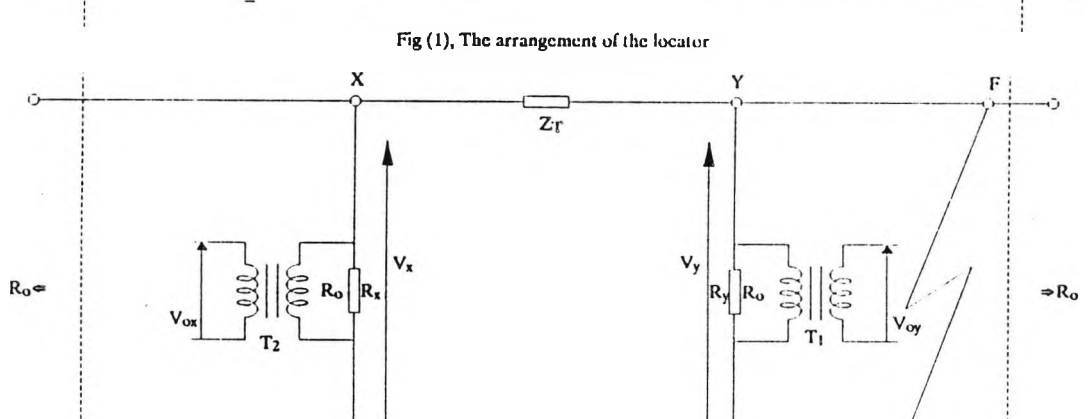

Fig (2), The equivalent circuit of the locator at center frequency f_c

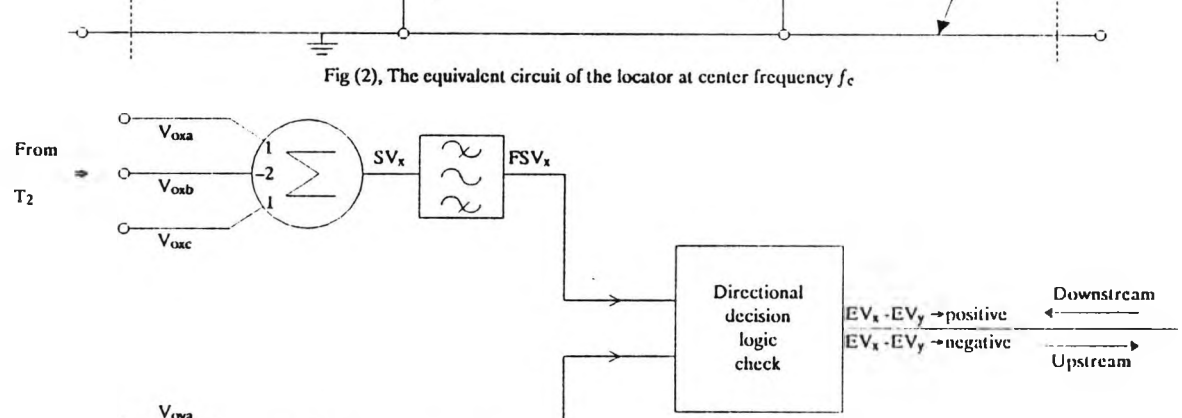

Fig (3), Decision making representation

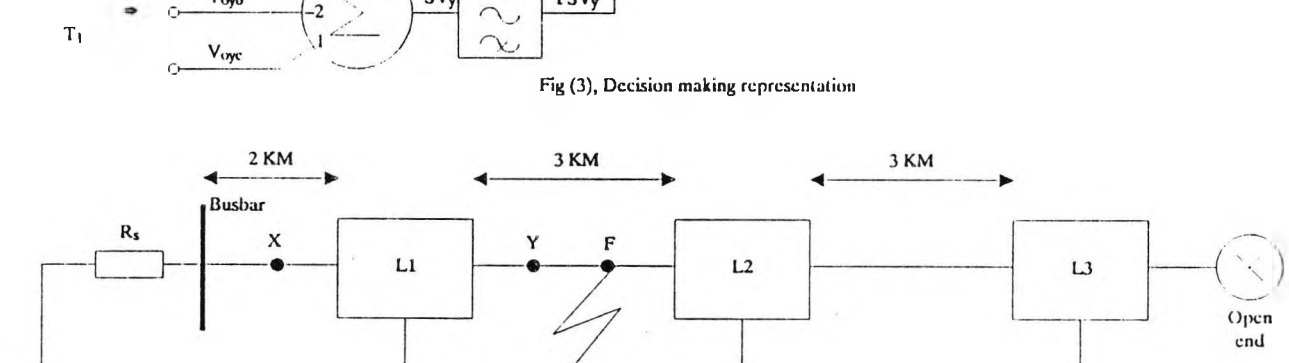

Fig (4), Schematic diagram of the system under test per phase

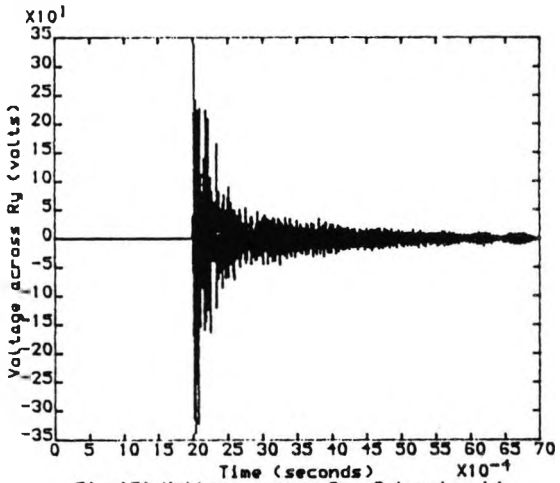

Fig (5) Voltage across Ry of locator L1.

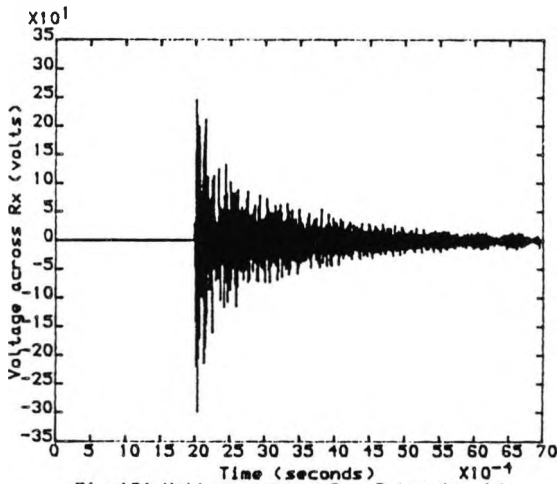

Fig (6) Voltage across Rx of locator L1.

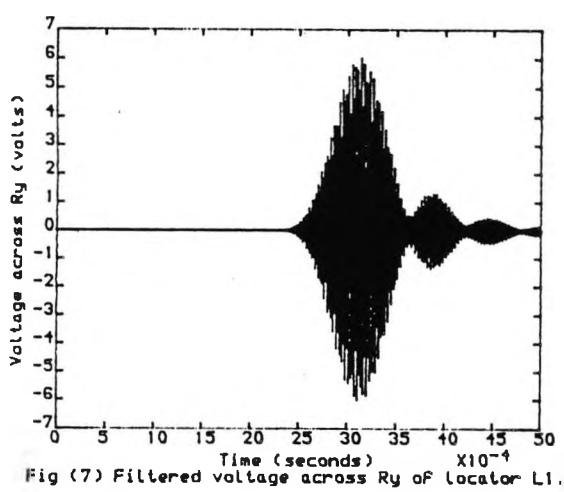

Fig (7) Filtered voltage across Ry of locator L1.

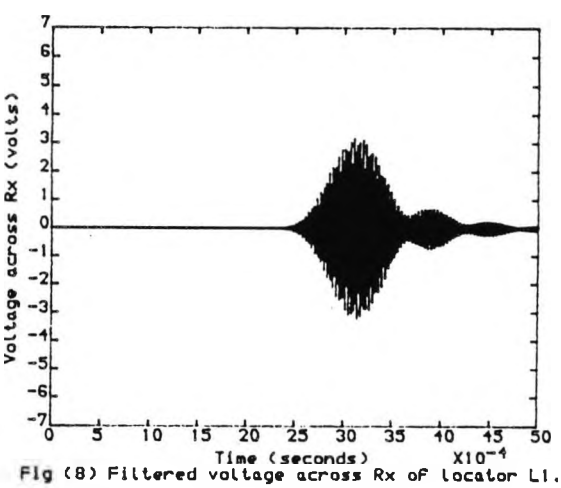

Fig (8) Filtered voltage across Rx of locator L1.

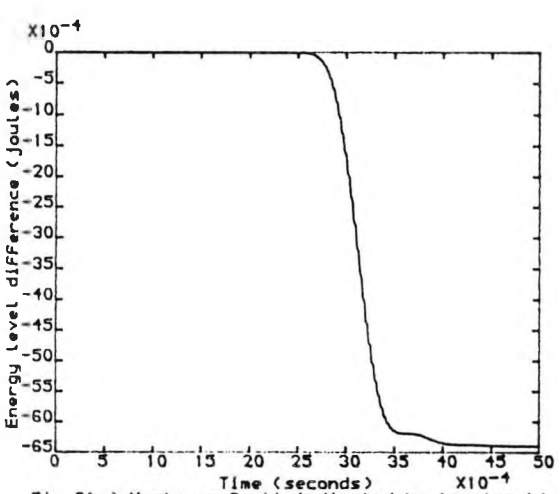

Fig 9(a) Upstream Fault indicated by locator L1.

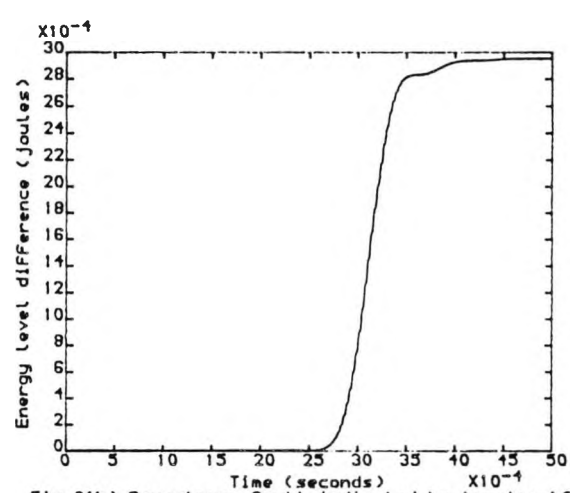

Fig 9(b) Downstream Fault indicated by locator L2.

Modelling of a simple fault detection/protection system in SPICE

D.J. DARUVALA A.T. JOHNS M. EL-HAMI

POWER AND ENERGY SYSTEMS RESEARCH GROUP,
CITY UNIVERSITY, LONDON, U.K.

ABSTRACT

This paper discusses the considerations which are involved in modelling, in SPICE, a directional fault locator in an overhead distribution system. It is explained how switched fault non-linearities may be modelled using multi-dimensional dependent sources which are available in SPICE-2. Finally, the use of this approach for fault simulations on a typical simple system is discussed.

1. INTRODUCTION

SPICE is the industry standard work-horse for the simulation of electronic circuits; its use for the simulation of power transmission systems is less well documented. A directional fault location scheme has been described by the authors [1], in another paper, at this conference. When producing the software for the simulation of this protection scheme, several options were studied. One of these options involved the study of modelling, in a single SPICE program, the power transmission line together with the associated electronic signal processing circuits.
In this paper the models used for individual parts of the system are discussed first and then an assessment of using this approach is given.

2 BRIEF DESCRIPTION OF THE FAULT DETECTION SCHEME TO BE SIMULATED

When a fault occurs on a power transmission line, a transient wave-form propagates from that disturbance. The frequency spectrum of this transient depends upon the type of disturbance.
In the scheme, discussed in this paper, fault-locators were inserted at convenient and strategic intervals in the line, thereby dividing the line into zones. Their function is to:

(i) impede the flow of fault induced high frequency transient noise signals across zone boundaries without offering any resistance to the flow of full-load current at power frequencies,
(ii) allow the extraction of these high frequency transient signals for further signal processing, with a view to determining:
  (a) whether the fault is upstream or downstream,
  (b) whether it is in-zone or out of zone.

This is best explained by considering the schematic representation shown in Figure 1. When a fault, F, occurs in the length of line between locators L_n and $L_{(n+1)}$. The fault induced noise signals should be easily detectable at sections XX and YY but should be below the detection level threshold at sections WW and ZZ; the presence of wave-traps in the two locators would assist in providing this discrimination. The main purpose of the simulation would be to optimize network configurations and component values to maximize this discrimination.

3. MODELLING OF A POWER SYSTEM FAULT DETECTION SCHEME USING SPICE

It was felt that a full study of a 3-conductor, 3-phase system would be an unnecessary complication and that reliable information could be gleaned from the study of a single phase system. This assumption is readily justified on the basis that any multi-conductor system can be decomposed into a number of un-coupled single-phase equivalent circuits by using the theory of natural modes developed by Wedepohl [2]. The new locators use signals that correspond closely to, at least, one Aerial mode of propagation and the results of a study of a single-phase equivalent using Aerial mode components, therefore, provides a realistic indication of performance of the new locators.
In developing the SPICE model for the complete single-phase system the task was subdivided into two parts:

(i) the modelling of a power transmission line and the modelling of a fault
(ii) the design of fault-locator networks to optimize element values with a view to maximizing the:
  (a) attenuation of the passage of the transient signal from one zone to the next,
  (b) extraction of the information contained in the transient signal. These will be discussed in turn.

4 MODELLING OF A 2-WIRE LINE IN SPICE

A length of lossy transmission line may be modelled in SPICE in two ways [3], [4]:

(i) the line may be considered to be lossless and all its losses lumped into a single resistance in series with it,
(ii) the line may be represented as a number of identical T-sections in cascade.

4.1 Lumped losses in series with a length of lossless distributed line model

A length of lossy line is represented by a lumped resistance in series with a length of distributed lossless line as shown in Figure 2.
Version 2 of SPICE contains a built-in model of a lossless line which is described to the program by a single statement of the form:

Txxx n_1 n_2 n_3 n_4 Z_0 T_D

where Txxx is the identifier for the lossless transmission line element, n_1 and n_2 are nodes at port 1, and n_3 and n_4 are the nodes at port 2. Z_0 is the characteristic impedance of the line and T_D is the transmission delay:

$$Z_0 = \sqrt{(L/C)} \quad \text{and} \quad v = \sqrt{(LC)}^{-1},$$

and $T_D = l\sqrt{(LC)}$,

where v is the velocity of propagation, and, L and C are the inductance and the capacitance per unit length of the line, and l is the length of the line.
Consequently, using this approach it is possible to dramatically reduce the total node count. However, one should be aware that SPICE uses a transient time-step which

is less than ½ the minimum transmission delay. Hence very long run times can result when short transmission lines are represented in this way; the shorter the line the smaller the propagation delay, and when this time interval is small relative to the analysis time frame, inordinately long run times can result.

4.2 Modelling of a lossy power transmission line using a number of T-sections in cascade

Alternatively, a number of T-sections in cascade can be used to model the transmission line. Typical element values/100 m length of an 11 kV 3-wire distribution line are shown in Figure 3. A fairly good approximation, to the true electrical performance of the line, can be obtained by using, at least, 10 such T-sections/electrical wavelength at the highest frequency of interest.
The resulting network representation of the line will have a large number of circuit nodes; a network comprising n T-sections in cascade has 2(2n + 1) nodes.
In the cascade arrangement of the T-networks shown, between each pair of shunt capacitors, there are two R's and two L's in series and a total of five nodes. By lumping together the two resistors and the two inductors into single elements of value 2R and 2L respectively, the node count is reduced by two for each pair of T-sections. If this is done for all but the first and the last sections, and if the latter are modified appropriately then the total number of nodes in the cascade could be reduced from 2(2n + 1) to 2(n + 1); for large values of n the reduction in the total number of nodes would be quite significant.

5. MODELLING OF ARCS IN SPICE

The well-known Warrington [5] formula:

$$R_f = (28700\ l_0)I^{-1.4} \quad \text{ohms}$$

gives a simple model for a primary arc. In the above equation l_0 is the length of the arc and is in metres and I is the r.m.s. value of the primary fault current.
Johns and Al-Rawi [6] have expressed the view that as far as secondary arcing phenomena is concerned "it is extremely difficult, if not impossible, to model such arcs in all their complexities, and that for computational purposes it is convenient to use the piecewise linear approximation of a typical long arc cyclogram as shown by the broken line in Figure 4." They further state that if I_p denotes the peak value of the secondary arc current and V_p denotes the constant voltage parameter, then V_p is a function of I_p as shown in Figure 4, where Maikopar [7], by collating the results of many investigations, has deduced that the relationship:

$$V_p = 75(I_p)^{-0.4} \quad \text{(volts/m)}$$

is valid for values of I_p in the range:

$$1\ A < I_p < 55\ A.$$

The curves shown in Figure 4 display hysteresis but zero striking and extinguishing voltages. This is a reasonable assumption because the voltage across the arc falls to zero when voltage reversals occur and during such voltage reversals the current remains at zero for relatively short times. Consequently, it can be reasonably assumed that the arc can be re-established without an appreciable re-striking voltage. The hysteresis present in the characteristic can be removed to simplify the model further as shown in Figure 5.

5.1 Modelling the simple arc model of Figure 5 in SPICE

A series combination of voltage dependent non-linear resistor and a switch, placed across the line, can be used for realizing the characteristic shown in Figure 7.
Neither the model for a switch nor for a voltage dependent non linear resistor exists in SPICE-2, yet a series combination of these two components can be modelled using a two dimensional voltage dependent current source as explained in the next section.

5.2 Modelling of a switched non-linear resistor

Multidimensional, non-linear, dependent current and voltage sources are available in SPICE-2. A two dimensional voltage controlled current source is shown schematically in Figure 6, where I_w is given by:

$$I_w = k_0 + k_1V_{34} + k_2V_{56} + k_3V_{34}^2 + k_4V_{34}V_{56} + k_5V_{56}^2 + k_6V_{34}^3 + k_7V_{34}^2V_{56} + k_8V_{34}V_{56}^2 + \ldots \quad \ldots\ldots\ldots\ldots(1)$$

and in a SPICE program such a source would be represented by the statement:

$G_n\ n_1\ n_2$ POLY(2) $n_3\ n_4\ n_5\ n_6\ k_0\ k_1\ k_2\ k_3 \ldots\ldots\ k_n$

To make the current source, shown in Figure 6, simulate a non-linear resistor, the following three steps need to be taken:

(i) make the node n_3 coincide with the node n_1 and the node n_4 coincide with the node n_2.

(ii) In the polynomial, given by equation (1), make all coefficients zero, except those of the terms $V_{34}V_{56}$, $V_{34}^2V_{56}$, $V_{34}^3V_{56}$ .... etc.; ie. only the terms k_4, k_8 ..... will be non-zero.

(iii) allow the voltage V_{56} to switch between only two values: 0V and 1V.

This arrangement is shown schematically in Figure 7, where I_w is given by:

$$I_w = kV_{12} + k'V_{12}^2 + k''V_{12}^3 + \ldots \quad \ldots(2)$$

when $V_{56} = 1$;
and $I_w = 0$, when $V_{56} = 0$,
and since in equation (2) the value of the current source I_w is a function of the voltage across itself, the arrangement shown behaves like the switched non-linear conductance, shown schematically in Figure 8.

6 FAULT SIMULATIONS ON A TYPICAL SIMPLE SYSTEM

The models described above were used to simulate a simple protection scheme incorporating two locators in a distribution line of total length 4 km as shown in Figure 9.
The line was modelled as a cascade of T-sections where each T-section is like the one shown in Figure 3. The locator networks were similar in design to the type described by Johns, El-Hami and Daruvala in Figure 1 of their paper at this conference [1]. The whole system including the locator network and the associated signal processing circuits were simulated using a single SPICE program. Substantial use was made of the subcircuit facility of SPICE and the resulting program was quite compact. The overall performance was, however, disappointing. Problems with convergence were encountered on several occasions; these problems are endemic in the public domain versions of SPICE; there are ways of overcoming them and these procedures

are now well-known. However, constantly having to grapple with such problems can be very time consuming.

7 CONCLUSION

It is quite feasible to use the procedures outlined in this paper to simulate, entirely in SPICE, simple fault detection/protection systems and the programs which result can be quite compact and elegant. However, as mentioned above, difficulties were frequently encountered when running these programs using version 2G.5 of SPICE. Work is in progress to determine if these difficulties persist under HSPICE; HSPICE is now available under the UGC/DTI initiative.
To complete the picture, it ought to be mentioned that the results obtained by Johns, El-Hami and Daruvala [1] were obtained by using a suite of interfaced programs. The use of SPICE was relegated to the role it is most suited for: an indispensable aid for the design of signal processing integrated circuits. The line and the locator networks were analysed in the frequency domain and the time domain values were obtained via the FFT algorithm. The PWL independent source function (of SPICE) was used as a vehicle to feed these values to the SPICE program. High quality, hard copy graphical output was obtained by using Gino based routines as a post-processor to SPICE. Interfaces between the different parts were written in fortran and/or C. The whole package has been successfully run in shell under a unix operating system and in DCL (Dec command language) with a VMS operating system. This suite of programs is described in a paper which is being prepared for publication.

8 ACKNOWLEDGEMENTS

The authors would like to thank the British Technology Group (BTG) for their support and the City University, London, for the provision of facilities for this research.

REFERENCES

[1] A.T. Johns, M. El-Hami and D.J. Daruvala, "Investigation of a new Directional Fault Locator for Overhead Distribution Systems", UPEC 1989.

[2] L.M. Wedepohl, "Application of matrix methods to the solution of travelling-wave phenomena in polyphase systems", Proc. IEE, vol.110, no. 12, p.2200-2212. (Dec. 1963).

[3] S.E. Suzzman-Fort and J.C. Hartman, "SPICE implementation of lossy transmission line and Schottky Diode Models", I.E.E.E. Trans., vol.MTT-36, p.153-156, Jan. 1988.

[4] A.J. Gruodis, "Transient analysis of uniform resistive transmission lines in a homogeneous medium", IBM J. of Res. & Dev., vol. 23, no. 6, p. 675-681. Nov. 1979.

[5] A.R. Van. C. Warrington, "Reactance relays negligibly affected by arc impedance", Electrical World, vol.98, p.502-505, 1931.

[6] A.T. Johns and A.M. Al-Rawi, "Digital simulation of EHV systems under secondary arcing conditions associated with single pole autoreclosure", IEE Proceedings, vol. 129, pt. C, no. 2, p. 49-58. (March 1982)

[7] A.S. Maikopar, "The quenching of an open arc", Electrichestvo, 1960, no.4, p. 64-69.

[8] L.W. Nagel, " SPICE 2: A computer program to simulate semiconductor circuits", Memorandum no. ERL-M520, 9 May 1975. Electronics Research Laboratory, University of California, Berkeley. 94720.

[9] A. Vladimirescu, K. Zhang, A.R. Newton, D.O. Pederson, A. Sangiovanni-Vincentelli, "SPICE Version 2G Users' Guide", Dept. EECS, Univ. of California, Berkeley, 1981.

APPENDIX

A note on SPICE

Very briefly SPICE works as follows [8]:
The network information which is contained in a SPICE input program is first converted into a set of simultaneous non-linear differential equations. Numerical integration is then used to convert these equations to non-linear algebraic equations. These equations are then solved by iterative matrix techniques. The entire network is represented by a single matrix and a constant time step is used. The smallest time constant in the circuit determines the size of the time-step that is used. The iterative process does not always lead to convergence and this is a major shortcoming of Berkeley SPICE. Proprietary forms of SPICE such as HSPICE, MSPICE, PSPICE claim to have overcome this problem in varying degrees.
Version 2G.5 of SPICE [9] is available under the UGC/DTI initiative. From discussions at recent SPICE users' group meetings it is clear that this version is still extensively used in preference to later versions of Berkeley SPICE which are now generally available.
The lossy line model, discussed in this paper is based on the Gruodis model [4] which takes into account the losses which arise due to the skin effect and hence represents the power transmission line more faithfully than models which represent lossy lines as a cascade of lumped RC sections as is done in SPICE 3A7, the latter model being more appropriate for representing lossy distributed structures on semiconductor substrates. SPICE 3A7 was released from Berkeley not so long ago and 3B.. versions have become available since then. The source code for SPICE-2 is in Fortran whereas for SPICE-3 it is in C.
In addition to the model for a lossy line SPICE-3 incorporates models for a switch, and for GaAs MESFET's; these models are not available in SPICE-2. Conversely, some useful facilities which are found in SPICE-2 are absent from SPICE-3. For instance, multidimensional dependent current and voltage sources were not available in the version of SPICE-3 used the authors. Finally, there are still some nasty bugs in SPICE-3 which are gradually being eliminated with the periodic appearance of updates.

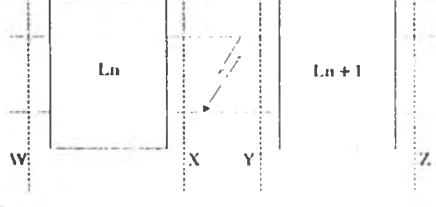

Figure 1 Schematic representation of the fault detection scheme.

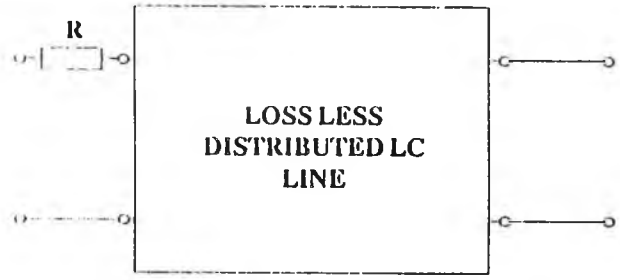

Fig (2) Lossless distributed LC line

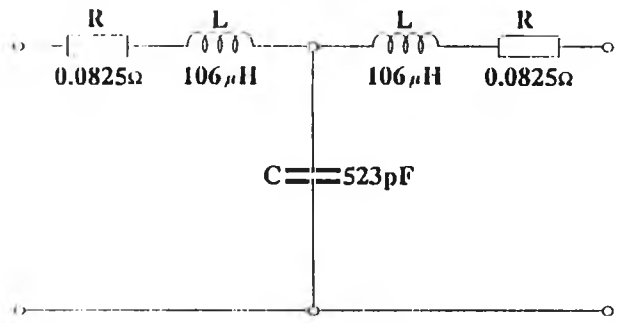

Fig (3) A T-section representing 100m length of a typical 11kV line

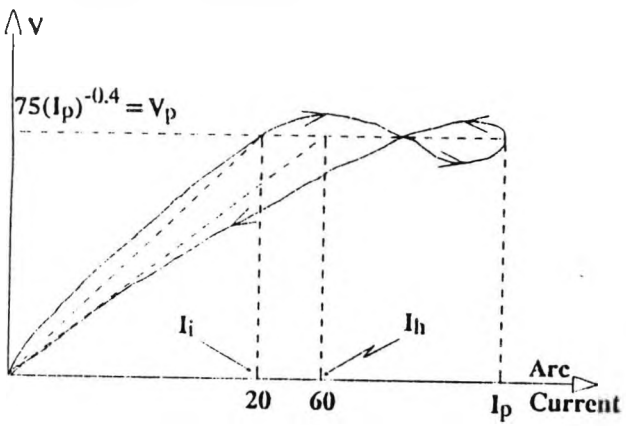

Fig (4) Typical long arc cyclogram

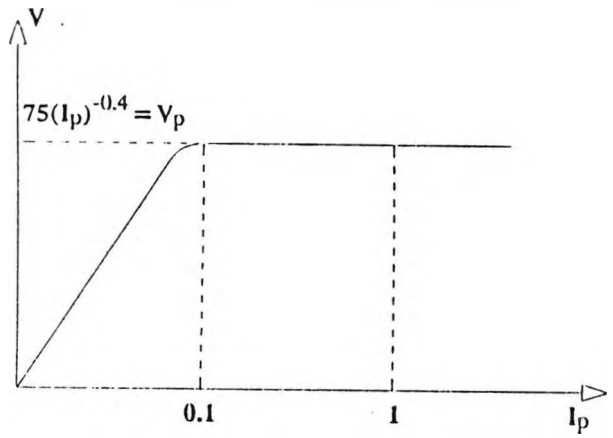

Fig (5) Piecewise linear approximation of an arc cyclogram

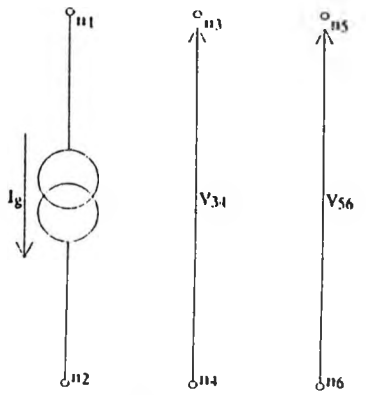

Fig (6) A 2-dimentional voltage controlled current source

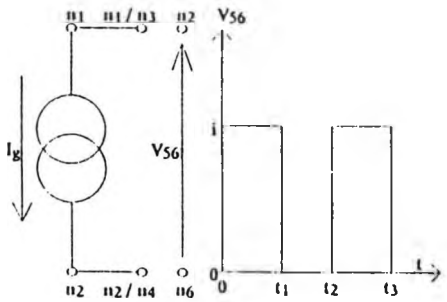

Fig (7) Model for switched non-linear resistance shown in fig (8)

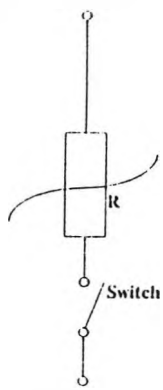

Fig (8)

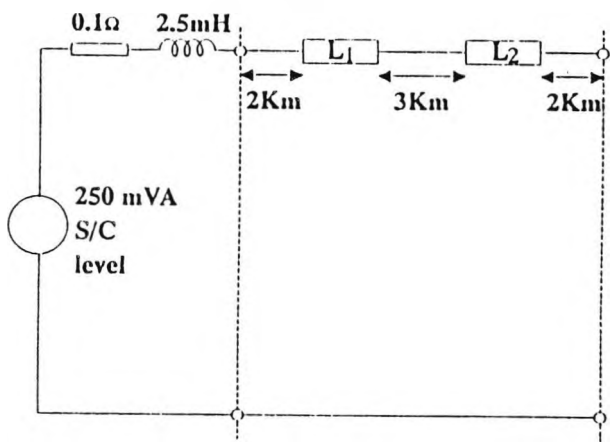

Fig (9) Schematic diagram of a simple protection scheme